ISSN 1948-0210 (online)

World Journal of *Stem Cells*

World J Stem Cells 2023 August 26; 15(8): 781-875

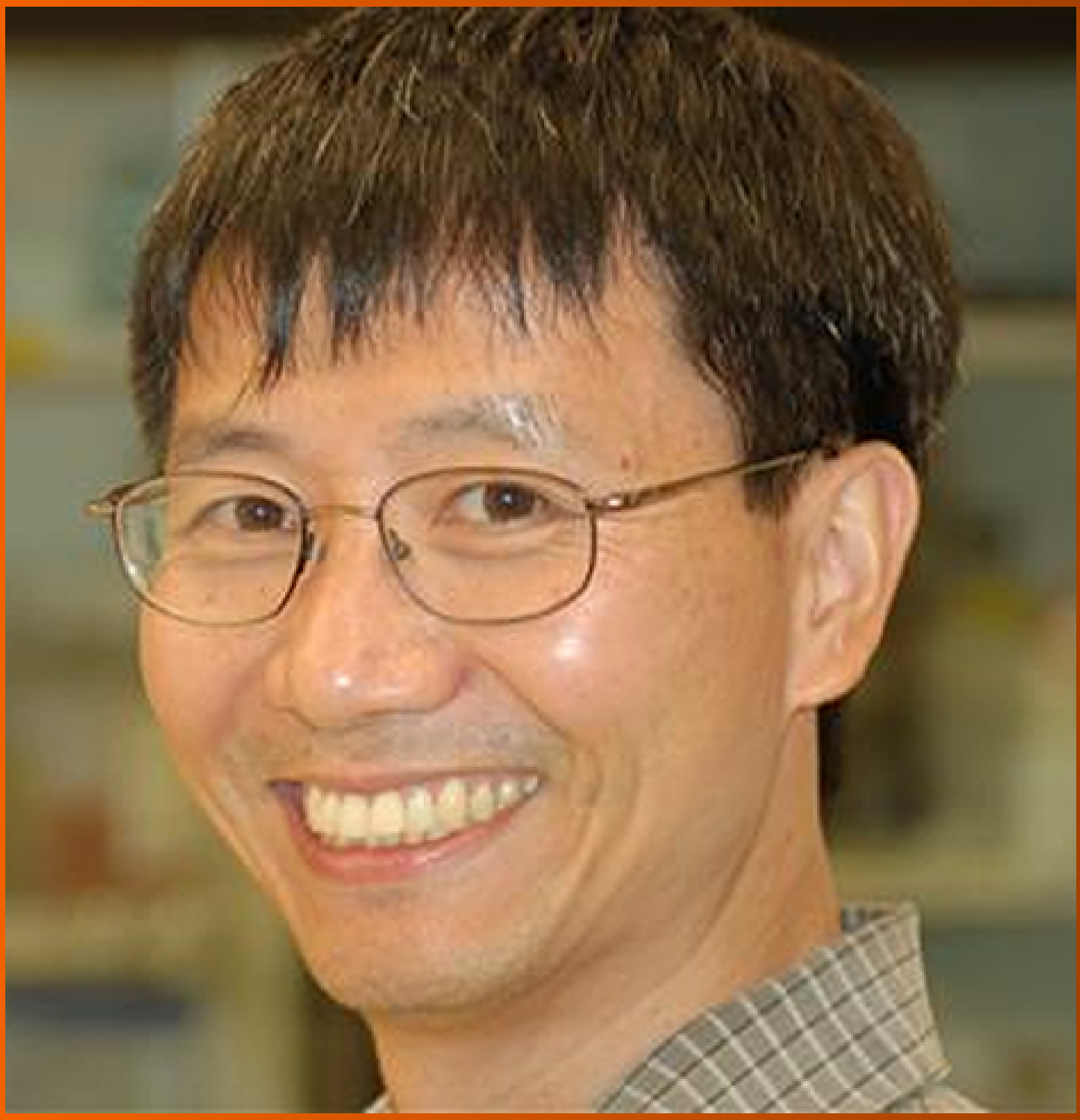

Published by Baishideng Publishing Group Inc

World Journal of Stem Cells

Contents

Monthly Volume 15 Number 8 August 26, 2023

EDITORIAL

ORIGINAL ARTICLE

Basic Study

META-ANALYSIS

World Journal of Stem Cells

Monthly Volume 15 Number 8 August 26, 2023

Contents

ABOUT COVER

Editor-in-Chief of *World Journal of Stem Cells*, Shengwen Calvin Li, BSc, MPhil, PhD, EIC, FRSM, FRSB, Children's Hospital of Orange County Children's Research Institute, Children's Hospital of Orange County, University of California-Irvine School of Medicine, Orange, CA 92868-3874, United States. shengwel@hs.uci.edu

AIMS AND SCOPE

The primary aim of *World Journal of Stem Cells* (*WJSC*, *World J Stem Cells*) is to provide scholars and readers from various fields of stem cells with a platform to publish high-quality basic and clinical research articles and communicate their research findings online. *WJSC* publishes articles reporting research results obtained in the field of stem cell biology and regenerative medicine, related to the wide range of stem cells including embryonic stem cells, germline stem cells, tissue-specific stem cells, adult stem cells, mesenchymal stromal cells, induced pluripotent stem cells, embryonal carcinoma stem cells, hemangioblasts, lymphoid progenitor cells, *etc*.

INDEXING/ABSTRACTING

The *WJSC* is now abstracted and indexed in Science Citation Index Expanded (SCIE, also known as SciSearch®), Journal Citation Reports/Science Edition, PubMed, PubMed Central, Scopus, Biological Abstracts, BIOSIS Previews, Reference Citation Analysis, China National Knowledge Infrastructure, China Science and Technology Journal Database, and Superstar Journals Database. The 2023 Edition of Journal Citation Reports® cites the 2022 impact factor (IF) for *WJSC* as 4.1; IF without journal self cites: 3.9; 5-year IF: 4.5; Journal Citation Indicator: 0.53; Ranking: 15 among 29 journals in cell and tissue engineering; Quartile category: Q3; Ranking: 99 among 191 journals in cell biology; and Quartile category: Q3. The *WJSC*'s CiteScore for 2022 is 8.0 and Scopus CiteScore rank 2022: Histology is 9/57; Genetics is 68/325; Genetics (clinical) is 19/90; Molecular Biology is 119/380; Cell Biology is 95/274.

RESPONSIBLE EDITORS FOR THIS ISSUE

Production Editor: *Xiang-Di Zhang*; **Production Department Director:** *Xu Guo*; **Editorial Office Director:** *Jia-Ru Fan*.

NAME OF JOURNAL
World Journal of Stem Cells

ISSN
ISSN 1948-0210 (online)

LAUNCH DATE
December 31, 2009

FREQUENCY
Monthly

EDITORS-IN-CHIEF
Shengwen Calvin Li, Carlo Ventura

EDITORIAL BOARD MEMBERS
https://www.wjgnet.com/1948-0210/editorialboard.htm

PUBLICATION DATE
August 26, 2023

COPYRIGHT
© 2023 Baishideng Publishing Group Inc

INSTRUCTIONS TO AUTHORS
https://www.wjgnet.com/bpg/gerinfo/204

GUIDELINES FOR ETHICS DOCUMENTS
https://www.wjgnet.com/bpg/GerInfo/287

GUIDELINES FOR NON-NATIVE SPEAKERS OF ENGLISH
https://www.wjgnet.com/bpg/gerinfo/240

PUBLICATION ETHICS
https://www.wjgnet.com/bpg/GerInfo/288

PUBLICATION MISCONDUCT
https://www.wjgnet.com/bpg/gerinfo/208

ARTICLE PROCESSING CHARGE
https://www.wjgnet.com/bpg/gerinfo/242

STEPS FOR SUBMITTING MANUSCRIPTS
https://www.wjgnet.com/bpg/GerInfo/239

ONLINE SUBMISSION
https://www.f6publishing.com

© 2023 Baishideng Publishing Group Inc. All rights reserved. 7041 Koll Center Parkway, Suite 160, Pleasanton, CA 94566, USA
E-mail: bpgoffice@wjgnet.com https://www.wjgnet.com

World Journal of Stem Cells

Submit a Manuscript: https://www.f6publishing.com

World J Stem Cells 2023 August 26; 15(8): 781-786

DOI: 10.4252/wjsc.v15.i8.781

ISSN 1948-0210 (online)

EDITORIAL

Mastering the craft: Creating an insightful and widely-cited literature review

Shengwen Calvin Li

Specialty type: Medicine, general and internal

Provenance and peer review: Invited article; Externally peer reviewed.

Peer-review model: Single blind

Peer-review report's scientific quality classification

Grade A (Excellent): 0
Grade B (Very good): B, B
Grade C (Good): 0
Grade D (Fair): 0
Grade E (Poor): 0

P-Reviewer: Gica N, Romania; Kode JA, India

Received: August 8, 2023
Peer-review started: August 9, 2023
First decision: August 14, 2023
Revised: August 22, 2023
Accepted: August 23, 2023
Article in press: August 23, 2023
Published online: August 26, 2023

Shengwen Calvin Li, Neuro-oncology and Stem Cell Research Laboratory, Children's Hospital of Orange County, Department of Neurology, University of California-Irvine School of Medicine, Orange, CA 92868-3874, United States

Corresponding author: Shengwen Calvin Li, MPhil, PhD, Academic Editor, Academic Research, Adjunct Professor, Professor, Research Scientist, Senior Editor, Senior Scientist, Vice Editor-in-Chief, Neuro-oncology and Stem Cell Research Laboratory, Children's Hospital of Orange County, Department of Neurology, University of California-Irvine School of Medicine, 455 South Main Street, Orange, CA 92868-3874, United States. shengwel@uci.edu

Abstract

The art of constructing an insightful literature review manuscript has witnessed an exemplar in the work of Oz *et al* (2023), wherein concept progression harmoniously merges with figures and tables. Reflecting on retrospective data science, it is evident that well-cited articles can wield a transformative influence on the Journal Citation Reports Impact Factor score, as exemplified by Robert Weinberg's landmark on cancer (Hanahan and Weinberg, 2011). Here, we aim to spotlight a commendable contribution by Tuba Oz, Ajeet Kaushik, and Małgorzata Kujawska in this issue while pivoting towards identifying the hallmarks of a subpar literature review-elements that hinder rather than promote advancement. The hurdles and roadblocks encountered within subpar literature reviews are multifold. Anticipation of emerging trends, identification of challenges, and exploration of solutions remain conspicuously absent. Original Contributions fail to surface amidst the vast sea of pre-existing literature, with noticeable gaps amplified by the lack of illustrative figures and tables. The manuscript, at times, assumes a skeletal form, reflecting an attempt to accommodate an excess of references, leading to convoluted sentences laden with citations. In contrast, a potent solution lies in adopting a comprehensive approach. A nuanced and critical evaluation of sources can culminate in a robust discussion, surpassing the mere summarization of conclusions drawn by others. This approach, often dismissed, holds the potential to elevate clarity, coherence, and logical flow, ultimately inviting engaged readership and coveted citations. The critical necessity of integrating visionary insights is underscored and achieved through a rigorous analysis of pivotal concepts and innovative ideas. Examples can be harnessed to elucidate the application of these solutions. We advocate a paradigm shift, urging literature review writers to embrace the readers' perspective. A literature review's purpose extends beyond providing a comprehensive panorama; it should illuminate avenues for concept development

within a specific field of interest. By achieving this balance, literature reviews stand to captivate a devoted readership, paving the way for manuscripts that are both widely read and frequently cited. The pathway forward requires a fusion of astute analysis and visionary insights, shaping the future of literature review composition.

Key Words: Literature review; Concept progression; Data science; Journal Citation Reports Impact Factor; Original contributions; Comprehensive approach; Clarity and coherence; Visionary insights; Reader engagement; Concept development

©The Author(s) 2023. Published by Baishideng Publishing Group Inc. All rights reserved.

Core Tip: This manuscript highlights a remarkable literature review, demonstrating a seamless fusion of concept progression with figures and tables. Reflecting on data science, it reveals how influential articles can impact the Journal Citation Report Impact Factor. We focus on identifying elements hindering effective literature reviews. Key challenges include absent trend anticipation, gaps in original contributions, and skeletal content. To address this, we propose a comprehensive approach involving critical evaluation, fostering clarity, coherence, and reader engagement. Integration of visionary insights and examples further enhances the impact, emphasizing the importance of concept development and paving the way for influential literature reviews.

Citation: Li SC. Mastering the craft: Creating an insightful and widely-cited literature review. *World J Stem Cells* 2023; 15(8): 781-786
URL: https://www.wjgnet.com/1948-0210/full/v15/i8/781.htm
DOI: https://dx.doi.org/10.4252/wjsc.v15.i8.781

INTRODUCTION

As an editor-in-chief and academic editor, I have not read an insightful literature review until now[1], which came with concept progression well illustrated in figures and tables. Second, retrospective data science revealed a few well-cited articles elevated a Journal Citation Reports Impact Factor score tremendously, *e.g.*, the hallmarks of Cancer by Robert Weinberg, accumulating 69346 citations[2]. Thus, I would like to point out a good one in this issue by Tuba Oz, Ajeet Kaushik, and Małgorzata Kujawska, which might help extrapolate some elements from their writing. However, rather than talk about good elements, I wanted to illustrate the list of inferior elements: The elements that construct a sub-standard literature review, as my conviction was that spotting roadblocks and putting forth measures to tackle those help take success to a higher level.

HURDLES AND ROADBLOCKS

The manuscript text lacked anticipation of any trends, failed to identify or provide answers to particular challenges or problems, and did not identify any leading problems or exceptional opportunities in the sub-field. Given the abundance of existing literature in the field, no original contributions were apparent in the content. Additionally, there seemed to be general gaps in the material, particularly evident in the absence of figures and tables.

Certain sections of the text appeared to be very sketchy, giving the impression that the manuscript was significantly cut down to include over 100 references, and specific sentences crowded cited up to 10 references in one phrase without details on what was about each reference. Instead of merely describing conclusions drawn by other authors, *i.e.*, regurgitating the known facts and data, the authors did not propose their insightful themes based on updating the article by engaging in a more thorough analysis of key concepts and ideas to explore uncharted water, by asking new questions and offering innovative speculations.

The final obstacle in our pursuit was intricately related to the meticulous referencing of the primary data articles. It went beyond the straightforward act of merely acknowledging the sources; it encompassed the intricate task of accurately framing distinct data sets and explicitly attributing terminologies to their original sources. This presented a distinct challenge: The emergence of crowd-group-article citing, where up to seven citations were amalgamated within a single sentence or even a solitary phrase.

CIRCUMVENTING HURDLES IN THE ROAD LEADS TO WELL-READ AND FREQUENTLY-CITED MANUSCRIPTS IN A LITERATURE REVIEW

This flush-out thinking would involve drawing on a range of relevant sources to produce a detailed and insightful discussion. Such critical analysis would be preferable to the alternative of simply summarizing the conclusions drawn by

others. If addressed, all the above elements, particularly the visionary element, might lead to better clarity, coherence, and logical flow, which earns readership and citations. I could illustrate how to overcome these hurdles with examples. My conviction: Advancements in literature review manuscripts require vision, foresight, assiduity, tenacity, determination, and the unwavering courage to go where others fear and hesitate. Why not? Why not consider the unimaginable? It is often claimed that success comprises 99% hard work and 1% inspiration: Both are essential, and neither is a minus.

"Imagination is far more important than knowledge". These profound words, which sprang from the mind of a genius named Albert Einstein, reverberate through the halls of time, lighting a flame of inspiration that guides us beyond the limitations of what we know. Einstein tells us that the power of imagination is the lighthouse that lights up new horizons, which is a crucial point to remember in a society where facts and data often take center stage.

Consider the following: Every spectacular discovery, every extraordinary creation, and every creative leap began in the limitless world of the human imagination. Knowledge provides us with the instruments to comprehend, but imagination gives us the wings to transcend. Such a wing's power propels us sky-high to bird-view unexplored territory and invites us to dance on the edge of the known while welcoming us to embrace the mysteries that lie beyond.

Then there are inquiries, which are unassuming yet powerful forces that propel forward-growth. "Asking questions is more important than knowledge", remarked Albert Einstein. How accurately this is said! The very act of questioning, of attempting to understand the complexities of the cosmos, is a declaration of both our intrinsic curiosity and our unyielding willpower to learn more. Questions kindle the flame of discovery, taking us down roads we've never traveled before and opening the door to worlds we would never have imagined were possible.

Imagine a world in which people simply accepted what they already knew without any attempt to learn more or to satisfy their natural curiosity. In such a world, there would be no development or invention, and people would just sit about doing nothing productive. But we are not content to live in that reality because we are driven by an insatiable appetite to learn more, to understand better, and to elevate ourselves beyond the confines of the present. This hunger compels us to seek out new information and new perspectives.

The words of Albert Einstein are a tribute to the reality that knowledge is a basis but that imagination and inquiry are the wings that propel us to new heights. Knowledge is a foundation. Therefore, let us not be afraid to fantasize beyond the bounds of what is already known. Let us use the power of imagination to conceive of worlds that have not yet been seen and possibilities that have not yet been investigated. And let us never stop asking questions; for by doing so, we create the path for a future that is brighter, bolder, and bursting with the grandeur of human potential. Let us never stop asking questions.

Along the line of referencing, the challenge was not only ensuring accurate citations but also preserving the content's clarity and flow. The risk of overwhelming the reader with an excess of citations was ever-present, demanding a judicious selection process. Each citation had to be carefully evaluated for its relevance and its ability to enhance the understanding of the topic under discussion. Navigating this obstacle required a delicate balance between comprehensive acknowledgment and maintaining the coherence of the narrative. It necessitated the establishment of a coherent thread that seamlessly interwove the multitude of sources while upholding the integrity of the information presented. The complexity lay in recognizing that each citation represented a distinct facet of the overarching concept, contributing a unique perspective to the discourse. It necessitated precision in language, strategic distribution of citations, and a steadfast commitment to maintaining clarity. This intricate dance between referencing and readability was a testament to our dedication to scholarly rigor while delivering information in a manner that was accessible and engaging to our audience. Through this process, we not only conquered the hurdle of crowd-group citing but also upheld the standards of meticulous scholarship in our work.

THE EXAMPLES

The first classical example is the literature review "the hallmarks of Cancer" by Robert Weinberg and his collaborator Douglas Hanahan. They proposed six elements, including maintaining proliferative signaling, evading growth inhibitory signals, resisting programmed cell death, facilitating perpetual replication potential, inducing the formation of new blood vessels (angiogenesis), and triggering processes of cellular invasion and metastasis as the hallmarks of cancer in 2010[3], earning 41039 citations. Two underlying causes are fundamental to acquiring these hallmark traits: Genomic instability, which drives the rapid accumulation of genetic variants, and inflammation, which supports several hallmark activities. Beyond the boundaries of the cancer cells themselves, tumors add another level of complexity due to the presence of a group of cells that, on the surface, appear normal but are actually recruited to help the tumor develop its distinctive traits. This environment is known as the "tumor microenvironment". It is hoped that acknowledging these concepts' broad applicability would substantially impact the development of cutting-edge methods for battling human cancer.

Over the past ten years, there has been a remarkable surge of innovation in our understanding of fundamental concepts beyond the original six-element hallmarks. This period of intellectual evolution has unveiled a pair of promising new frontiers that hold the key to widespread applicability. These cutting-edge developments, akin to beacons illuminating uncharted territory, encompass the manipulation of energy metabolism and the art of outwitting the immune system's defenses, resulting in eight hallmarks of Cancer by Robert Weinberg, accumulating 69346 citations[2].

The canvas of knowledge has been enriched by an exciting brushstroke, as reprogramming the intricate dance of energy within cells emerges as a captivating endeavor. Imagine orchestrating a symphony within the microscopic realm, fine-tuning the metabolic pathways that govern life's essence as spatiotemporal regulation[4]. This spatial omics biology endeavor promises not only to enhance our ability to engineer solutions to a spectrum of challenges but also to unlock the potential for revitalizing weary cells, paving the way for novel therapies and rejuvenation.

In parallel, we witness a daring expedition into the realm of immune evasion-a pursuit that mirrors the cunning strategies of spies and adventurers. Just as an artful rogue slips through the clutches of pursuers, scientists are unraveling the enigmatic mechanisms that allow specific cells to evade the immune system's watchful eye, in particular, Carl June's invention of chimeric antigen receptor T cells immunotherapy (5702 citations)[5] in a designer fashion[6]. This tantalizing avenue opens avenues to fortifying our defenses against diseases, enabling medical interventions to bypass the barricades that often hinder treatment progress.

Together, these eight emergent pillars of insight symbolize a profound transformation in our comprehension of cancer's intricate dance. They beckon us to a landscape where creativity interlaces with knowledge, inviting us to craft innovative solutions, reinvigorate cellular vitality, and conquer challenges once deemed insurmountable. As we embark on this exhilarating voyage of discovery, the horizons of possibility stretch ever wider, promising a future enriched by the fusion of imagination and scientific achievement. All of the above visional elements earned 69346 citations, much higher than their previous 2000's article, which had 41039 citations on August 7, 2023, reflecting the conceptual development that attracts the increased readership.

The second example of a highly specialized and small domain is my own research to illustrate some visional elements by proposing new terminologies. We applied a new method that has been well used (1207 citations)[7]. We presented two new terminologies, the caveolin scaffolding domain (CSD) (969 citations)[8] and the CSD binding motif (CBM) (1129 citations)[9]. Both CSD and CBM have been well studied, which led to assistance to therapeutic development like albumin-bound (nab) paclitaxel (nab-paclitaxel; Abraxane), a $2.9 billion platform of cancer drug delivery by Patrick Soon-Shiong[10]. They further found that elevated levels of CAV1/2 expression are linked to poorer disease-free survival (DFS) and overall survival (OS) outcomes among individuals treated with paclitaxel. In contrast, among patients treated with nab-paclitaxel, heightened CAV1/2 expression appears to correlate with improved pathologic complete response rates while not imposing a significant negative impact on DFS or OS when compared to individuals with lower CAV1/2 expression levels[11]. This example manifested the conceptual development that prompted therapeutic development, followed by clinical validations.

The third approach is to propose a broad application of an envisioned technology. We hypothesized that "Hunting down the dominating subclone of cancer stem cells as a potential new therapeutic target in multiple myeloma: An artificial intelligence perspective" (16 citations)[12]. We also postulated "A biological global positioning system (bGPS): Considerations for tracking stem cell behaviors in the whole body", with eight elements to fulfill stem cell therapies (74 citations)[13]. Specifically, in response to monitoring the detrimental effects of stem cell therapies, we have outlined an all-encompassing bGPS designed to monitor the trajectory of transplanted stem cells. This system incorporates eight essential components, each meticulously tailored to ensure the efficacy of stem cell transplantation (SCT). These components encompass the following: (1) Sensitivity for single cell detection; (2) real-time positioning; (3) an inducible system; (4) retractable; (5) targeted and durable; (6) monitoring cell fate; (7) compliant with the FDA GMP guidelines for clinical applications; and (8) quantification capacity. By integrating these eight critical attributes, our proposed biological GPS not only addresses the aforementioned challenges but also provides a comprehensive framework for effectively tracking and assessing the transplanted stem cells during SCT. This holistic approach underscores our commitment to establishing a robust and clinically compliant solution that ensures the success of stem cell transplantation and holds the potential to enhance the field of regenerative medicine significantly. Future experimentation is needed to achieve the predictions.

The final approach could be to point out that some limitations exist in the current trend of studies. We pointed out that "Cancer genomic research at the crossroads: Realizing the changing genetic landscape as intratumoral spatial and temporal heterogeneity becomes a confounding factor" (44 citations)[14], thereby conjuring up hope for improvements through identifying potentials and challenges (76 citations)[15]. The manuscript led to sum up with specific solutions, such as "Control dominating subclones for managing cancer progression and posttreatment recurrence by subclonal switchboard signal: Implication for new therapies"-a key to two Nature articles and related column of "News & View" on the issue (28 citations)[16]. All of these thoughtful articles prompted the spatial and temporal intervention strategies of various diseases with the integration of machine learning models[17].

THE METRICS

We want to emphasize that while journal impact factors matter less, the impact of being cited does. An insightful remark during a prestigious award presentation caught attention: Physicists with 2000 citations or more fall within the top 1% globally. This figure corresponds to around 210 citations annually over a decade. Interestingly, citation thresholds vary by field, and approximately 44% of published manuscripts remain uncited. Strikingly, almost half of published manuscripts go uncited, and just a single citation places a manuscript near the upper half. Accumulating 10 citations elevates an article into the top quartile while surpassing 100 citations propels a paper to the top 1.8%. The crucial takeaway is that the average number of citations per manuscript tends to remain below 10 (Refer the details to Scott D. Weingart, MD: https://Lucbeaulieu.com/2015/11/19/how-many-citations-are-actually-a-lot-of-citations/) and (https://renaissance.stonybrookmedicine.edu/emergencymedicine/faculty/Weingart).

The database Thomson Reuters Web of Science's average number of citations per article published in scientific journals is as follows (URL: Web of Science Core Collection-Clarivate) using algorithms[18] and based on 4 million authors and 26 million scientific papers that span 15 years and 118 scientific disciplines[19] (Table 1).

Table 1 Average number of citations per article

Disciplines	Citations
Life sciences and medicine	6 to 30 citations
Physical sciences and engineering	5 to 20 citations
Social sciences	5 to 15 citations
Humanities, including literature, history, and philosophy	1 to 5 citations

CONCLUSION

In summary, authors should keep the readers' perspective in mind: Why did they come to read a literature review? A literature review should shed new light on concept development in a particular field. Not only does it offer a comprehensive snapshot of an area of interest, but it also provides promising directions for exploring questions. Both are essential; neither is minor to drum up an enthusiastic readership, leading to well-read and frequently-cited manuscripts in a literature review.

FOOTNOTES

Author contributions: Li SC analyzed the data, wrote the manuscript, and approved the final manuscript.

Conflict-of-interest statement: Li SC declared no conflict-of-interest.

Open-Access: This article is an open-access article that was selected by an in-house editor and fully peer-reviewed by external reviewers. It is distributed in accordance with the Creative Commons Attribution NonCommercial (CC BY-NC 4.0) license, which permits others to distribute, remix, adapt, build upon this work non-commercially, and license their derivative works on different terms, provided the original work is properly cited and the use is non-commercial. See: https://creativecommons.org/Licenses/by-nc/4.0/

Country/Territory of origin: United States

ORCID number: Shengwen Calvin Li 0000-0002-9699-9204.

S-Editor: Chen YL
L-Editor: A
P-Editor: Chen YL

REFERENCES

1 **Oz T**, Kaushik A, Kujawska M. Neural stem cells for Parkinson's disease management: Challenges, nanobased support, and prospects. *World J Stem Cells* 2023; **15**: 687-700 [PMID: 37545757 DOI: 10.4252/wjsc.v15.i7.687]
2 **Hanahan D**, Weinberg RA. Hallmarks of cancer: the next generation. *Cell* 2011; **144**: 646-674 [PMID: 21376230 DOI: 10.1016/j.cell.2011.02.013]
3 **Hanahan D**, Weinberg RA. The hallmarks of cancer. *Cell* 2000; **100**: 57-70 [PMID: 10647931 DOI: 10.1016/S0092-8674(00)81683-9]
4 **Li SC**, Kabeer MH. Spatiotemporal switching signals for cancer stem cell activation in pediatric origins of adulthood cancer: Towards a watch-and-wait lifetime strategy for cancer treatment. *World J Stem Cells* 2018; **10**: 15-22 [PMID: 29531638 DOI: 10.4252/wjsc.v10.i2.15]
5 **Maude SL**, Frey N, Shaw PA, Aplenc R, Barrett DM, Bunin NJ, Chew A, Gonzalez VE, Zheng Z, Lacey SF, Mahnke YD, Melenhorst JJ, Rheingold SR, Shen A, Teachey DT, Levine BL, June CH, Porter DL, Grupp SA. Chimeric antigen receptor T cells for sustained remissions in leukemia. *N Engl J Med* 2014; **371**: 1507-1517 [PMID: 25317870 DOI: 10.1056/NEJMoa1407222]
6 **Li SC**, Kabeer M. Designer Immunotherapy Specific for Cancer. *J Cell Sci Ther* 2013; **4**: 1 [DOI: 10.4172/2157-7013.1000e116]
7 **Song KS**, Li Shengwen, Okamoto T, Quilliam LA, Sargiacomo M, Lisanti MP. Co-purification and direct interaction of Ras with caveolin, an integral membrane protein of caveolae microdomains. Detergent-free purification of caveolae microdomains. *J Biol Chem* 1996; **271**: 9690-9697 [PMID: 8621645 DOI: 10.1074/jbc.271.16.9690]
8 **Li S**, Couet J, Lisanti MP. Src tyrosine kinases, Galpha subunits, and H-Ras share a common membrane-anchored scaffolding protein, caveolin. Caveolin binding negatively regulates the auto-activation of Src tyrosine kinases. *J Biol Chem* 1996; **271**: 29182-29190 [PMID: 8910575 DOI: 10.1074/jbc.271.46.29182]
9 **Couet J**, Li S, Okamoto T, Ikezu T, Lisanti MP. Identification of peptide and protein ligands for the caveolin-scaffolding domain. Implications for the interaction of caveolin with caveolae-associated proteins. *J Biol Chem* 1997; **272**: 6525-6533 [PMID: 9045678 DOI: 10.1074/jbc.272.10.6525]
10 **Hawkins MJ**, Soon-Shiong P, Desai N. Protein nanoparticles as drug carriers in clinical medicine. *Adv Drug Deliv Rev* 2008; **60**: 876-885 [PMID: 18423779 DOI: 10.1016/j.addr.2007.08.044]
11 **Williams TM**, Schneeweiss A, Jackisch C, Shen C, Weber KE, Fasching PA, Denkert C, Furlanetto J, Heinmöller E, Schmatloch S, Karn T,

Szeto CW, van Mackelenbergh MT, Nekljudova V, Stickeler E, Soon-Shiong P, Schem C, Mairinger T, Müller V, Marme F, Untch M, Loibl S. Caveolin gene expression predicts clinical outcomes for early-stage HER2-negative breast cancer treated with paclitaxel-based chemotherapy in the GeparSepto trial. *Clin Cancer Res* 2023 [PMID: 37432976 DOI: 10.1158/1078-0432.CCR-23-0362]

12 **Lee LX**, Li SC. Hunting down the dominating subclone of cancer stem cells as a potential new therapeutic target in multiple myeloma: An artificial intelligence perspective. *World J Stem Cells* 2020; **12**: 706-720 [PMID: 32952853 DOI: 10.4252/wjsc.v12.i8.706]

13 **Li SC**, Tachiki LM, Luo J, Dethlefs BA, Chen Z, Loudon WG. A biological global positioning system: considerations for tracking stem cell behaviors in the whole body. *Stem Cell Rev Rep* 2010; **6**: 317-333 [PMID: 20237964 DOI: 10.1007/s12015-010-9130-9]

14 **Li SC**, Tachiki LM, Kabeer MH, Dethlefs BA, Anthony MJ, Loudon WG. Cancer genomic research at the crossroads: realizing the changing genetic landscape as intratumoral spatial and temporal heterogeneity becomes a confounding factor. *Cancer Cell Int* 2014; **14**: 115 [PMID: 25411563 DOI: 10.1186/s12935-014-0115-7]

15 **Li SC**, Wang L, Jiang H, Acevedo J, Chang AC, Loudon WG. Stem cell engineering for treatment of heart diseases: potentials and challenges. *Cell Biol Int* 2009; **33**: 255-267 [PMID: 19084605 DOI: 10.1016/j.cellbi.2008.11.009]

16 **Li SC**, Lee KL, Luo J. Control dominating subclones for managing cancer progression and posttreatment recurrence by subclonal switchboard signal: implication for new therapies. *Stem Cells Dev* 2012; **21**: 503-506 [PMID: 21933025 DOI: 10.1089/scd.2011.0267]

17 **Li X**, Wang X, Huang R, Stucky A, Chen X, Sun L, Wen Q, Zeng Y, Fletcher H, Wang C, Xu Y, Cao H, Sun F, Li SC, Zhang X, Zhong JF. The Machine-Learning-Mediated Interface of Microbiome and Genetic Risk Stratification in Neuroblastoma Reveals Molecular Pathways Related to Patient Survival. *Cancers (Basel)* 2022; **14** [PMID: 35740540 DOI: 10.3390/cancers14122874]

18 **Patience GS**, Patience CA, Blais B, Bertrand F. Citation analysis of scientific categories. *Heliyon* 2017; **3**: e00300 [PMID: 28560354 DOI: 10.1016/j.heliyon.2017.e00300]

19 **Nielsen MW**, Andersen JP. Global citation inequality is on the rise. *Proc Natl Acad Sci U S A* 2021; **118** [PMID: 33558230 DOI: 10.1073/pnas.2012208118]

World Journal of Stem Cells

Submit a Manuscript: https://www.f6publishing.com

World J Stem Cells 2023 August 26; 15(8): 787-806

DOI: 10.4252/wjsc.v15.i8.787

ISSN 1948-0210 (online)

ORIGINAL ARTICLE

Basic Study

Interferon-gamma and tumor necrosis factor-alpha synergistically enhance the immunosuppressive capacity of human umbilical-cord-derived mesenchymal stem cells by increasing PD-L1 expression

Zhuo Chen, Meng-Wei Yao, Zhi-Lin Shen, Shi-Dan Li, Wei Xing, Wei Guo, Zhan Li, Xiao-Feng Wu, Luo-Quan Ao, Wen-Yong Lu, Qi-Zhou Lian, Xiang Xu, Xiang Ao

Specialty type: Cell biology

Provenance and peer review: Unsolicited article; Externally peer reviewed.

Peer-review model: Single blind

Peer-review report's scientific quality classification

Grade A (Excellent): 0
Grade B (Very good): B, B
Grade C (Good): 0
Grade D (Fair): 0
Grade E (Poor): 0

P-Reviewer: Gallone A, Italy; Maurya DK, India

Received: March 13, 2023
Peer-review started: March 13, 2023
First decision: June 6, 2023
Revised: June 20, 2023
Accepted: July 24, 2023
Article in press: July 24, 2023
Published online: August 26, 2023

Zhuo Chen, Meng-Wei Yao, Zhi-Lin Shen, Wei Xing, Wei Guo, Zhan Li, Xiao-Feng Wu, Luo-Quan Ao, Xiang Xu, Xiang Ao, Department of Stem Cell & Regenerative Medicine, State Key Laboratory of Trauma, Burn and Combined Injury, Daping Hospital, Army Medical University, Chongqing 400042, China

Zhuo Chen, College of Basic Medical Sciences, Army Medical University, Chongqing 400038, China

Shi-Dan Li, Department of Orthopedics, Daping Hospital, Army Medical University, Chongqing 400042, China

Wen-Yong Lu, Department of Hepatobiliary Surgery, The First Affiliated Hospital of Wenzhou Medical University, The South of Shangcai Village, Wenzhou 325005, Zhejiang Province, China

Qi-Zhou Lian, Department of Medicine, Li Ka Shing Faculty of Medicine, The University of Hong Kong, Hong Kong 999077, China

Xiang Ao, Department of Orthopedics, 953 Hospital of PLA Army, Shigatse Branch of Xinqiao Hospital, Army Medical University, Shigatse 857000, Tibet Autonomous Region, China

Corresponding author: Xiang Ao, PhD, Researcher, Department of Stem Cell & Regenerative Medicine, State Key Laboratory of Trauma, Burn and Combined Injury, Daping Hospital, Army Medical University, Changjiang Road, Yuzhong District, Chongqing 40042, China.
ax_syd@163.com

Abstract

BACKGROUND

The immunosuppressive capacity of mesenchymal stem cells (MSCs) is dependent on the "license" of several proinflammatory factors to express immunosuppressive factors such as programmed cell death 1 ligand 1 (PD-L1), which determines the clinical therapeutic efficacy of MSCs for inflammatory or immune diseases. In MSCs, interferon-gamma (IFN-γ) is a key inducer of PD-L1 expression, which is synergistically enhanced by tumor necrosis factor-alpha (TNF-α); however, the underlying mechanism is unclear.

AIM
To reveal the mechanism of pretreated MSCs express high PD-L1 and explore the application of pretreated MSCs in ulcerative colitis.

METHODS
We assessed PD-L1 expression in human umbilical-cord-derived MSCs (hUC-MSCs) induced by IFN-γ and TNF-α, alone or in combination. Additionally, we performed signal pathway inhibitor experiments as well as RNA interference experiments to elucidate the molecular mechanism by which IFN-γ alone or in combination with TNF-α induces PD-L1 expression. Moreover, we used luciferase reporter gene experiments to verify the binding sites of the transcription factors of each signal transduction pathway to the targeted gene promoters. Finally, we evaluated the immunosuppressive capacity of hUC-MSCs treated with IFN-γ and TNF-α in both an *in vitro* mixed lymphocyte culture assay, and *in vivo* in mice with dextran sulfate sodium-induced acute colitis.

RESULTS
Our results suggest that IFN-γ induction alone upregulates PD-L1 expression in hUC-MSCs while TNF-α alone does not, and that the co-induction of IFN-γ and TNF-α promotes higher expression of PD-L1. IFN-γ induces hUC-MSCs to express PD-L1, in which IFN-γ activates the JAK/STAT1 signaling pathway, up-regulates the expression of the interferon regulatory factor 1 (IRF1) transcription factor, promotes the binding of IRF1 and the PD-L1 gene promoter, and finally promotes PD-L1 mRNA. Although TNF-α alone did not induce PD-L1 expression in hUC-MSCs, the addition of TNF-α significantly enhanced IFN-γ-induced JAK/STAT1/IRF1 activation. TNF-α up-regulated IFN-γ receptor expression through activation of the nuclear factor kappa-B signaling pathway, which significantly enhanced IFN-γ signaling. Finally, co-induced hUC-MSCs have a stronger inhibitory effect on lymphocyte proliferation, and significantly ameliorate weight loss, mucosal damage, inflammatory cell infiltration, and up-regulation of inflammatory factors in colitis mice.

CONCLUSION
Overall, our results suggest that IFN-γ and TNF-α enhance both the immunosuppressive ability of hUC-MSCs and their efficacy in ulcerative colitis by synergistically inducing high expression of PD-L1.

Key Words: Human umbilical-cord-derived mesenchymal stem cells; Programmed cell death 1 ligand 1; Immunomodulation; Interferon-gamma; Tumor necrosis factor-alpha; Ulcerative colitis

©The Author(s) 2023. Published by Baishideng Publishing Group Inc. All rights reserved.

Core Tip: Our study showed that interferon-gamma (IFN-γ) and tumor necrosis factor-alpha (TNF-α) significantly induced programmed cell death protein 1 ligand 1 (PD-L1) expression in human umbilical-cord-mesenchymal stem cells (hUC-MSCs), and pretreated hUC-MSCs exhibited stronger immunomodulatory capacity. Signaling pathway analysis showed that TNF-α up-regulated IFN-γ receptor expression in hUC-MSCs through nuclear factor kappa-B pathway, and then promoted IFN-γ -mediated activation of JAK/STAT1/interferon regulatory factor 1 pathway and PD-L1 expression. In ulcerative colitis mice, hUC-MSCs pretreated with IFN-γ and TNF-α exhibited stronger immunosuppressive ability through high expression of PD-L1, effectively inhibited the inflammation in the colon of mice.

Citation: Chen Z, Yao MW, Shen ZL, Li SD, Xing W, Guo W, Li Z, Wu XF, Ao LQ, Lu WY, Lian QZ, Xu X, Ao X. Interferon-gamma and tumor necrosis factor-alpha synergistically enhance the immunosuppressive capacity of human umbilical-cord-derived mesenchymal stem cells by increasing PD-L1 expression. *World J Stem Cells* 2023; 15(8): 787-806
URL: https://www.wjgnet.com/1948-0210/full/v15/i8/787.htm
DOI: https://dx.doi.org/10.4252/wjsc.v15.i8.787

INTRODUCTION

Mesenchymal stem cells (MSCs) are multipotent adult stem cells present in multiple tissues, including the umbilical cord, bone marrow, and fat tissue. MSCs can self-renew by dividing and differentiating into multiple tissues, including bone, cartilage, muscle, fat cells, and connective tissue[1]. In addition, MSCs have a strong immunomodulatory capacity, exerting both anti-inflammatory and pro-inflammatory effects[2]. Owing to their immunosuppressive function, MSCs are widely used to treat various inflammatory and autoimmune diseases, including inflammatory bowel disease, rheumatoid arthritis, pulmonary fibrosis, and systemic sclerosis[3-6]. However, the current clinical efficacy of MSCs transplantation (MSCT) is highly variable among individuals, even for the same autoimmune disease[7]. In general, the immunosuppressive function of MSCs depends on the licensing of the proinflammatory factor-mediated immunological microenvironment[8,9]. The individual differences in the clinical efficacy of MSCT might be explained by the substantial individual

variations in the pro-inflammatory factor-mediated immunological microenvironment at different stages of disease development in patients with inflammatory or autoimmune diseases. Therefore, to improve the therapeutic efficacy of MSCT in these diseases, there is an urgent need to explore the licensing mechanism of the immunosuppressive function of MSCs and to establish an optimal strategy for inducing and maintaining immunosuppressive MSCs.

It is currently believed that immunosuppressive MSCs induced by pro-inflammatory factors inhibit the activity of various immune cells by secreting many soluble immunosuppressive factors, such as indoleamine 2,3-dioxygenase (IDO). They also express many immunosuppressive receptors, such as programmed cell death 1 ligand 1 (PD-L1), which functions in a cell-to-cell contact manner[10,11]. Programmed cell death 1 (PD-1) is an immune-inhibitory receptor expressed in activated T cells, which binds to PD-L1 and can inhibit proliferation, induce apoptosis, and restore the subgroup balance of T cells[12]. PD-1/PD-L1 are important immune checkpoint molecules that play a pivotal role in tumor immune escape[13]. Emerging evidence suggests that PD-1/PD-L1 dysfunction is also involved in the immune hyperactivity observed in multiple autoimmune and inflammatory diseases[14,15]. Additionally, PD-L1 plays an important role in the immunosuppressive capacity of MSCs, inhibiting the activation of the immune response in a variety of ways. This includes reducing the release of inflammatory factors, the proliferation and activation of T cells, and the Th17-mediated autoimmune response, as well as augmenting the generation of regulatory T cells (Tregs)[15-17]. Therefore, to improve the therapeutic efficacy of MSCs for inflammatory or autoimmune related diseases, there is an urgent need to clarify the regulatory mechanism of PD-L1 expression in MSCs and to establish an optimal strategy for inducing and maintaining this expression.

Interferon-gamma (IFN-γ) alone has been suggested to upregulate PD-L1 expression in MSCs at low levels, although the specific mechanism remains unclear[18]. It is also unclear whether a combination of proinflammatory factors can synergistically enhance PD-L1 expression in MSCs and their immunosuppressive function. Notably, researchers have recently demonstrated that the immunosuppressive capacity of MSCs depends on stimulation by IFN-γ, and the effect can be amplified further by cytokines, such as tumor necrosis factor-α (TNF-α)[4,19]. In addition, Li *et al*[20] recently reported that TNF-α can enhance the IFN-γ-induced PD-L1 expression in hepatocellular carcinoma cells. Such findings suggest that TNF-α could also enhance IFN-γ-induced PD-L1 expression in MSCs. In the present study, we first confirmed that IFN-γ induced human-umbilical-cord-MSCs (hUC-MSCs) express PD-L1 through the JAK/STAT1/IRF1 pathway. Second, we observed that TNF-α synergistically enhanced PD-L1 expression induced by IFN-γ in hUC-MSCs. TNF-α also upregulated IFN-γ receptor 1 (IFNGR1) expression through the nuclear factor kappa-B (NF-κB) signaling pathway to promote IFN-γ/IFNGR/STAT1/ interferon regulatory factor 1 (IRF1)/PD-L1 signaling axis activation. Finally, based on an *in vitro* lymphocyte mixing experiment and an *in vivo* dextran sulfate sodium (DSS)-induced acute colitis mouse model, we found an optimal strategy of enhancing the immunosuppressive capacity of hUC-MSCs by licensing with IFN-γ and TNF-α. The results not only elucidate the specific molecular mechanism by which the IFN-γ and TNF-α combination enhances the immunosuppressive function of MSCs, but also provide a theoretical basis for improving the therapeutic efficacy of MSCT in future clinical applications.

MATERIALS AND METHODS

Culture and treatment of hUC-MSCs

All hUC-MSCs were provided by the FuMei Stem Cell Biotechnology Company (Chongqing, China). The hUC-MSCs used in the present study were identified by flow cytometry and three-lineage differentiation culture. The results showed that the hUC-MSCs had the correct molecular phenotype and three-lineage differentiation potential (Supplementary Figure 1). All hUC-MSCs used in the experiment were derived from passages 3 to 7. hUC-MSCs were cultured and stimulated in serum-free medium (LONZA). To measure the induction of PD-L1 expression, hUC-MSCs were incubated with human IFN-γ, TNF-α or both (Peprotech, United States). After 4 h of culture, the cells were harvested for mRNA expression analysis using quantitative real-time PCR (qRT-PCR). After 24 h of culture, they were harvested for protein expression analysis by western blot or flow cytometry.

Quantitative Real-time PCR

Total RNA was extracted from hUC-MSCs using Trizol (Sigma, T9424), and reverse transcribed into cDNA using HiScript® II Q RT SuperMix for qRT-PCR (+gDNA wiper) (Vazyme, China). The qRT-PCR assay was performed using ChamQ Universal SYBR qRT-PCR Master Mix (Vazyme, China). All qRT-PCR experiments were independently repeated three times. All primer sequences used for qRT-PCR are listed in Supplementary Table 1.

Flow cytometry

The hUC-MSCs were prepared as single-cell suspensions and stained for 30 min at room temperature. PD-L1-FITC antibody (BD Pharmingen, 558065), IFNGR1-PE antibody (BD Pharmingen, 558937), FITC isotype control antibody (BD Pharmingen, 555742), or PE isotype control antibody (BD Pharmingen, 555749) were used to quantify the expression of PD-L1 or IFNGR1 in hUC-MSCs. CD29-PE antibody (BD Pharmingen, 555443), CD34-PE antibody (BD Pharmingen, 555822), CD44-PE antibody (BD Pharmingen, 555479), CD45-PE antibody (BD Pharmingen, 555483), CD73-PE antibody (BD Pharmingen, 550257), CD90-PE antibody (BD Pharmingen, 555596), and CD105-PE antibody (BD Pharmingen, 560839) were used to identify hUC-MSCs. Our gating strategy was to select active hUC-MSCs groups. Flow cytometry was performed using a NovoCyte flow cytometer (ACEA Biosciences).

Western blot analysis

Western blot assay was performed to observe changes in relative protein content. Whole cell proteins were extracted from cells using radioimmunoprecipitation assay strong lysate (Beyotime Biotechnology, P0013). The cell lysates from each sample were separated by sodium dodecyl sulfate-polyacrylamide gel electrophoresis and transferred onto polyvinylidene fluoride (PVDF) membranes. The PVDF membranes were blocked with 5% skim milk in TBST for 60 min, incubated with primary antibodies and then with secondary antibodies conjugated with horseradish peroxidase (HRP), and developed using a chemiluminescence HRP substrate (Millipore, WBKLS0100). The primary antibodies used were PD-L1, IFNGR1, JAK1, p-JAK1, JAK2, p-JAK2, STAT1, p-STAT1, IRF1, IKKα, IKKβ, p-IKKα/β, IKBα, p-IKBα, p65, p-p65, and β-tubulin (1:1000, CST). The secondary antibodies were goat anti-rabbit IgG and goat anti-mouse IgG (1:10000, CST).

Signaling inhibition assay

To investigate the signaling pathways activated by IFN-γ or TNF-α in hUC-MSCs, we used the reagents: Ruxolitinib (10 μM) and BAY11-7082 (10 μM) (Selleckchem). After 30 min of pretreatment with the inhibitors, hUC-MSCs were co-cultured with IFN-γ, TNF-α, or IFN-γ plus TNF-α for 4 h or 24 h. The cells were collected for further investigation. The control cells were treated with these cytokines and DMSO.

Small interfering RNA assay

To identify the key pathway molecules involved in the inducible expression of PD-L1 or IFNGR1, a specific Small interfering RNA (siRNA) assay was performed. The siRNA synthesized by RiboBio Company (Guangzhou, China) have proven effective and were thus used in the siRNA assay (Supplementary Figure 2). The siRNAs were transfected into hUC-MSCs using Lipofectamine RNAiMAX transfection reagent (Life Technologies, United States) according to the manufacturer's protocol. After 24 h of transfection, the hUC-MSCs were treated with cytokines for 4 h or 24 h. They were then harvested and subjected to qRT-PCR analysis or western blot.

Gene promoter activity assay

Vector plasmids, IRF1 promoter plasmids, p65 promoter plasmids, PD-L1 promoter plasmids, IFNGR1 promoter plasmids, PD-L1 promoter point mutation plasmids, and IFNGR1 promoter point mutation plasmids were purchased from OBiO Technology (Shanghai). 293T cells were cultured in plates and transfected with the plasmids by DNA transfection reagent (NEOFECT, China) according to the manufacturers' instructions. Fluorescence intensity was determined using a Dual Luciferase Reporter Gene Assay Kit (Beyotime) according to the manufacturer's instructions.

Cell proliferation assay

Cell proliferation was analyzed using the Cell Counting Kit-8 (CCK-8) assay. The hUC-MSCs were plated in six-well plates (1×10^5 cells per well) and cultured for 24 h. Subsequently, the CCK-8 reagent (Beyotime Biotechnology, China) was added to each well, according to the manufacturer's instructions. The absorbance of each well at 450 nm was measured using an ELX808 microplate reader (Biotek, United States).

Cell apoptosis assay

Apoptotic hUC-MSCs were detected using the Annexin V-FITC/PI Apoptosis Detection Kit and Annexin V-APC/PI Apoptosis Detection Kit (KeyGEN BioTECH, China). The hUC-MSCs were plated in six-well plates (1×10^5 cells per well) and cultured for the indicated time. After TNF-α stimulation for 24 h, all hUC-MSCs were stained by Annexin V and PI, according to the manufacturer's instructions. Afterward, the cells were evaluated using the NovoCyte flow cytometer. The percentage of apoptotic hUC-MSCs was determined by the sum of Annexin V positive cells.

IFNGR1 overexpression assay

IFNGR1-overexpressing lentiviruses were purchased from Shanghai OBiO Technology. The lentivirus infection procedures were modified from a previously published protocol[21]. After IFNGR1-overexpressed hUC-MSCs were successfully constructed using IFNGR1-overexpressing lentivirus, we used small interfering RNA (siRNA) to interfere with the p65 expression in cells. PD-L1 mRNA expression was detected by qRT-PCR assays after induction by IFN-γ or TNF-α for 4 h.

PBMCs isolation and proliferation assays

Peripheral blood samples were obtained from healthy donors. Peripheral blood mononuclear cells (PBMCs) were isolated using a human peripheral blood lymphocyte separation tube (Dakewe, China), activated by monoclonal anti-human CD3 antibody (Acro, United States), and stained with 10 mmol/L 5-(and-6)-carboxyfluorescein diacetate succinimidyl ester (CFSE, Beyotime, China). CFSE-labeled PBMCs (1×10^6 cells/well) were co-incubated with hUC-MSCs at a ratio of 10:1 in the presence of 100 IU/mL IL2. After co-culturing for 3 d, the proliferation of PBMCs was analyzed using flow cytometry.

DSS-induced colitis and treatment

C57BL/6J mice were purchased from the Weitong Lihua Experimental Animal Technology Company (China). The animal protocol was designed to minimize pain or discomfort to the animals. The animals were acclimatized to laboratory conditions (23 °C, 12 h/12 h light/dark, 50% humidity, ad libitum access to food and water) for 2 wk prior to experimentation. Mice were randomly assigned to six experimental groups: WT, DSS, DSS + MSCs, DSS + IT-MSCs (IT-MSCs: hUC-MSCs treated with IFN-γ and TNF-α), DSS + IT-MSCs + iso antibody, and IT-MSCs + PD-L1 antibody (atezol-

izumab, Selleck). In the DSS, DSS + MSCs, DSS + IT-MSCs, DSS + IT-MSCs + iso antibody, and IT-MSCs + PD-L1 antibody groups, acute colitis was induced in mice by the addition of 4% (w/v) DSS (40 kDa, MP Biomedicals) to the drinking water for 7 d, until euthanasia. The WT group received drinking water only. All mice were weighed daily. On day 3, mice from the DSS + MSCs, DSS + IT-MSCs, DSS + IT-MSCs + iso antibody, and IT-MSCs + PD-L1 antibody groups were transfused with 1 × 10^6 hUC-MSCs *via* the tail vein, and the other mice were transfused with equal amounts of saline *via* the tail vein. Mice in the IT-MSCs group were transfused *via* the tail vein with 1 × 10^6 hUC-MSCs previously treated with IFN-γ and TNF-α for 24 h. The hUC-MSCs of the DSS + IT-MSCs + iso antibody group and the DSS + IT-MSCs+PD-L1 antibody group were treated with IFN-γ, TNF-α, isotype antibody or PD-L1 antibody for 24 h. After seven days of induction, the mice were sacrificed by cervical dislocation, and their colons were collected.

Colon histopathology analysis

For histological analysis, colon samples were fixed with 4% paraformaldehyde (Beyotime, P0099) for 24 h and embedded in paraffin for hematoxylin and eosin staining, as previously described[22]. We evaluated the histopathological scores of colon tissue using a combination of inflammatory cell infiltration and epithelial damage to the colon[22].

Colon immunohistochemistry analysis

Immunohistochemistry was performed on paraffin embedded sections of colon samples. The sections were incubated with anti-CD4 (Abcam, 1:1000) or anti-CD11b (Abcam, 1:4000) at 4 °C overnight and with anti-rabbit IgG and HRP-linked antibody (CST, 1:50) for 60 min. Immunoreactivity was analyzed with a microscope (Olympus CKX31). The total number of CD4 or CD11b positive cells in each of four nonadjacent fields of view was counted per colon sample.

Myeloperoxidase activity assay

We performed a myeloperoxidase (MPO) activity assay to determine the number of neutrophils in the colon tissue. The MPO activity kit was purchased from Jiancheng (Nanjing, China, A044-1-1). We determined the level of MPO activity in the colon tissue following the protocol recommended by the manufacturer. The absorbance of each well was evaluated using an ELX808 microplate reader.

Enzyme linked immunosorbent assay

The concentrations of TNF-α, IFN-γ, and IL-6 secreted by mice with acute colitis were determined by enzyme linked immunosorbent assay (ELISA). The TNF-α, IFN-γ, and IL-6 ELISA kits were purchased from Boster (Wuhan, Hubei Province, China), and were used according to the manufacturer's instructions. The absorbance of each well was evaluated using an ELX808 microplate reader.

Statistical analysis

The results are shown as mean ± SD. Statistical analyses were performed using GraphPad Prism v8.4.2 (GraphPad Software Inc., San Diego, CA, United States). Student's unpaired t-test and one-way analysis of Variance were used to determine significant differences between groups. Statistical significance was set at $P < 0.05$.

RESULTS

IFN-γ induced the expression of PD-L1 in the hUC-MSCs

IFN-γ induces MSCs to express PD-L1, which exerts an immunosuppressive effect. In the present study, we further investigated the effect of IFN-γ on PD-L1 expression in hUC-MSCs. And hUC-MSCs were treated with either different concentrations of IFN-γ or fixed concentrations of IFN-γ for different time periods. PD-L1 expression in hUC-MSCs was detected using qRT-PCR, western blot, and flow cytometry. After treating hUC-MSCs with variable concentrations of IFN-γ for 24 h, the results showed that when the concentration of IFN-γ was 20 ng/mL, PD-L1 expression increased significantly; it was the highest under 100 ng/mL IFN-γ (Figure 1A-C). Moreover, PD-L1 mRNA expression induced by 20 ng/mL IFN-γ began to increase 2 h after stimulation, and was the highest at 4 h (Figure 1D). The total and membrane protein levels of PD-L1 in hUC-MSCs peaked at 24 h (Figure 1E and F). Based on the results above, we used 20 ng/mL IFN-γ stimulation for 4 h for follow-up qRT-PCR experiments, and 20 ng/mL IFN-γ stimulation for 24 h for western blot or flow cytometry experiments. The results confirmed that IFN-γ induced PD-L1 expression in hUC-MSCs.

IFN-γ upregulated PD-L1 expression through the JAK/STAT1/IRF1 pathway in hUC-MSCs

A previous study showed that IFN-γ increased PD-L1 expression in tumor cells by activating the JAK/STAT/IRF1 pathway[23]. To confirm this finding, we performed signaling inhibition and siRNA interference experiments. We found that ruxolitinib (10 μM), a JAK/STAT signaling pathway inhibitor, significantly reduced IFN-γ-induced PD-L1 mRNA expression (Figure 2A; Supplementary Figure 3A). The results of western blot and flow cytometry showed that ruxolitinib also significantly reduced the levels of IFN-γ-induced PD-L1 membrane protein and total protein (Figure 2B and C). The results suggest that IFN-γ could induce PD-L1 expression through the JAK/STAT pathway in hUC-MSCs.

To further confirm that the JAK/STAT pathway mediates the IFN-γ-induced effect on hUC-MSCs expressing PD-L1, we analyzed the total protein and the phosphorylation levels of key proteins in the JAK/STAT signaling pathway in hUC-MSCs. Western blot results showed that IFN-γ promoted JAK1/2 phosphorylation, STAT1 phosphorylation, IRF1 expression, and PD-L1 expression, while ruxolitinib reversed all these effects (Figure 2C). To confirm the findings, we

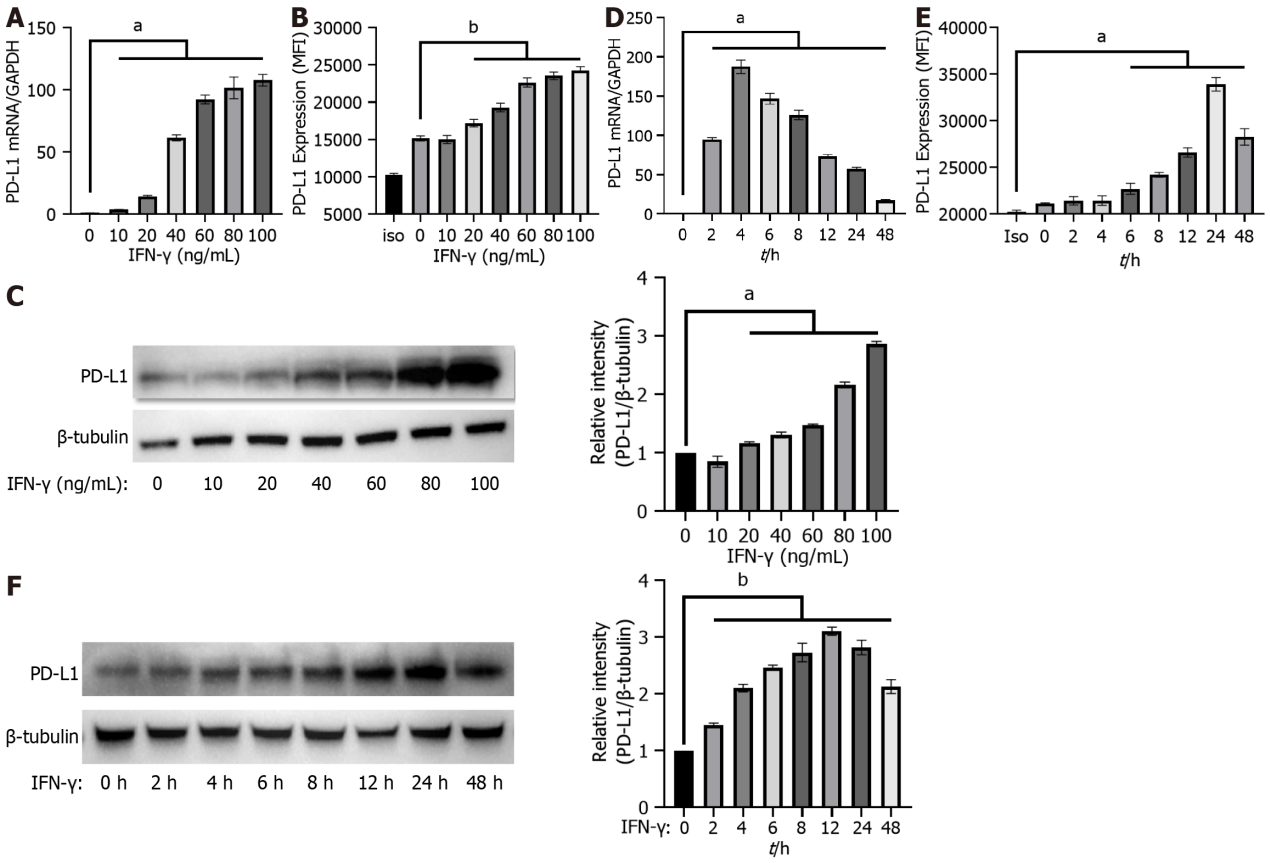

DOI: 10.4252/wjsc.v15.i8.787 **Copyright** ©The Author(s) 2023.

Figure 1 Interferon-gamma induced the expression of programmed cell death protein 1 ligand 1 in human umbilical-cord-mesenchymal stem cells. A-C: Programmed cell death protein 1 ligand 1 (PD-L1) expression was measured by quantitative real-time PCR (qRT-PCR), flow cytometry, and western blot in human umbilical-cord-mesenchymal stem cells (hUC-MSCs) treated with 0, 10, 20, 40, 60, 80 or 100 ng/mL interferon-gamma (IFN-γ) for 24 h; D-F: PD-L1 expression was measured by qRT-PCR, flow cytometry, and western blot in hUC-MSCs treated with 20 ng/mL IFN-γ for 0, 2, 4, 6, 8, 12, 24 or 48 h. Data were represented as mean ± SEM of $n = 3$. Iso: Isotype; C: Control; $^{a}P < 0.01$; $^{b}P < 0.001$. IFN-γ: Interferon-gamma; PD-L1: Programmed cell death protein 1 ligand 1.

performed an siRNA interference assay using the effective siRNAs for JAK1/2, STAT1/2/3, and IRF1/9, and observed that the siRNAs remarkably inhibited the PD-L1 expression induced by IFN-γ (Figure 2D). The results indicate that IFN-γ induced PD-L1 expression in hUC-MSCs *via* the JAK/STAT1/IRF1 pathway.

IRF1 is a key transcription factor in the JAK/STAT pathway. We constructed a dual-luciferase reporter system to confirm that IRF1 binds to the PD-L1 promoter to promote PD-L1 mRNA expression. In 293T cells, relative luciferase activity was weak when transfected with IRF1 or the PD-L1 promoter plasmid; it was the strongest when the two were co-transfected (Figure 2E). We then predicted the potential binding sites of the proximal part of the PD-L1 gene to IRF1 and identified the five most likely binding sites. Point mutant plasmids were constructed at the five binding sites to assess luciferase reporter activity. We co-transfected a WT-PD-L1 promoter plasmid and five IRF1 binding site mutant PD-L1 promoter plasmids into 293T cells with an IRF1 promoter plasmid and a Renilla luciferase plasmid. We measured the relative luciferase activity 24 h after transfection (Figure 2F). The locations of the binding sites in the PD-L1 promoter are shown in Figure 2G. According to the results, mutations at sites 4 or 5 reduced IFN-γ-induced PD-L1 promoter activity, with site 4 having the greatest effect (Figure 2F). These findings indicate that IFN-γ activated the JAK/STAT pathway in hUC-MSCs and induced IRF1 expression; IRF1, in turn, bound to the PD-L1 promoter, thereby promoting PD-L1 transcription.

TNF-α synergistically enhanced IFN-γ-induced PD-L1 expression in hUC-MSCs

As mentioned above, the mechanism by which TNF-α synergistically enhances IFN-γ-induced PD-L1 expression has not been elucidated. To study the effect of TNF-α alone or in combination with IFN-γ on PD-L1 expression in hUC-MSCs, we performed the following experiments. First, hUC-MSCs were stimulated with seven different concentrations of TNF-α (0 ng/mL, 10 ng/mL, 20 ng/mL, 40 ng/mL, 60 ng/mL, 80 ng/mL, and 100 ng/mL) for 24 h, or with the experimentally designed highest concentration (100 ng/mL) of TNF-α for different time periods (0 h, 2 h, 4 h, 6 h, 12 h, 24 h, and 48 h). Subsequently, the membrane expression of PD-L1 was detected by flow cytometry. Our results demonstrated that TNF-α stimulation alone did not affect PD-L1 expression in hUC-MSCs (Figure 3A and B).

Subsequently, to analyze the effect of TNF-α on hUC-MSCs viability, the proliferation and apoptosis of hUC-MSCs treated with TNF-α was tested using cell proliferation and apoptosis assays. We found that TNF-α had no effect on the proliferation or apoptosis of hUC-MSCs (Figure 3C and D). We then studied the effect of combined treatment with IFN-γ

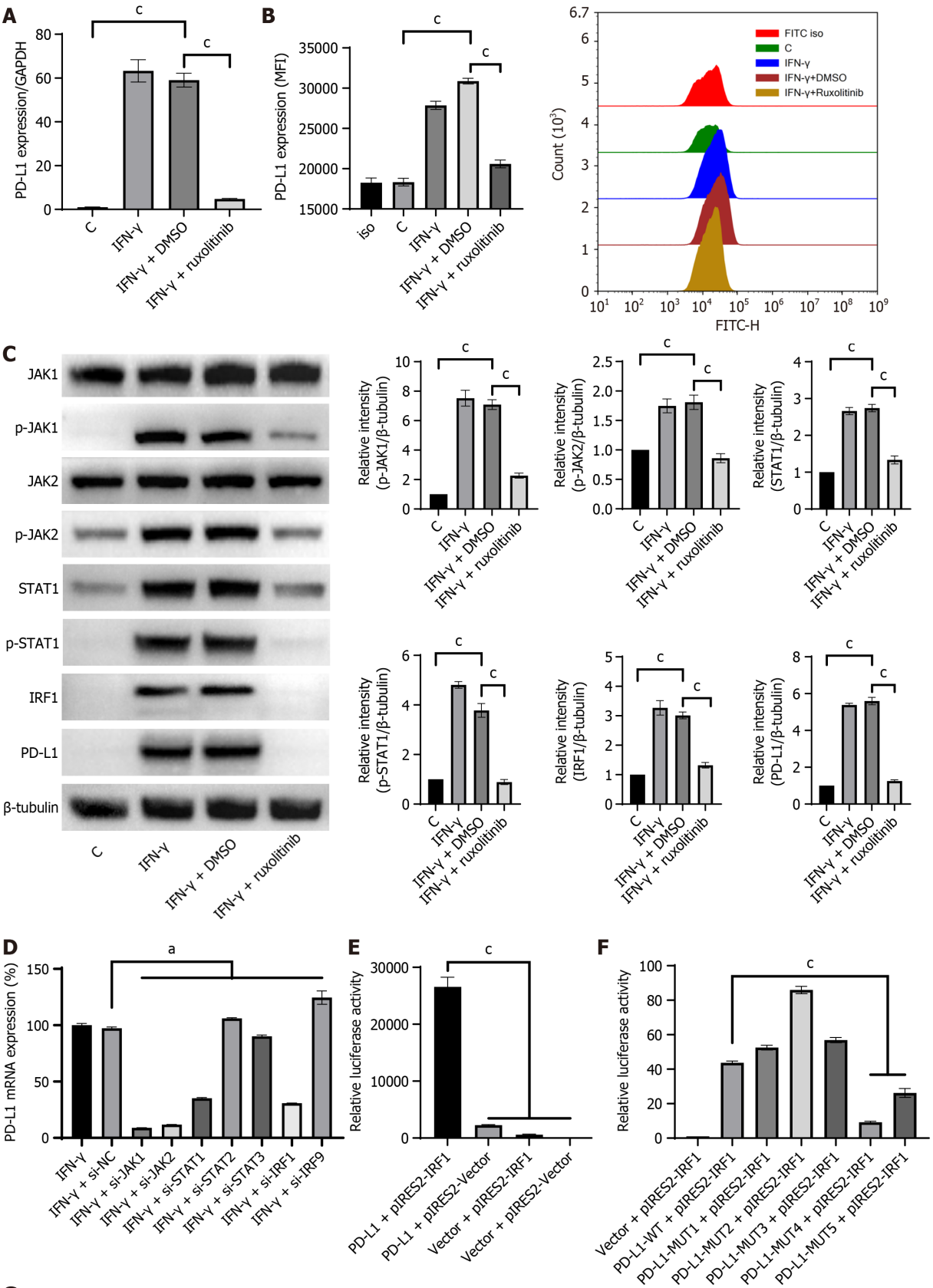

G
site 1: -951 ttagaaaaagagaaaaaaaag- 930
site 2: -615 agtttcattatg- 603
site 3: -508 aaaaaccaaagc- 496
site 4: -213 gacatgtttcactttctgtttcatttc- 186
site 5: -151 atacctaaactgaaagcttcc- 130

DOI: 10.4252/wjsc.v15.i8.787 **Copyright** ©The Author(s) 2023.

Figure 2 Interferon-gamma upregulated programmed cell death protein 1 ligand 1 expression *via* the JAK/STAT1/ interferon regulatory

factor 1 pathway in human umbilical-cord-mesenchymal stem cells. A: Programmed cell death protein 1 ligand 1 (PD-L1) expression was quantified by quantitative real-time PCR (qRT-PCR) in human umbilical-cord-mesenchymal stem cells (hUC-MSCs) treated with a combination of IFN-γ with or without the JAK inhibitor ruxolitinib (10 μM) for 4 h; B: PD-L1 expression was quantified by flow cytometry in hUC-MSCs treated with a combination of IFN-γ with or without ruxolitinib (10 M) for 24 h; C: Activation of the JAK/STAT/interferon regulatory factor 1 (IRF1) pathway and PD-L1 expression were analyzed by western blot in hUC-MSCs treated with IFN-γ (20 ng/mL) with or without ruxolitinib (10 M) for 24 h; D: The PD-L1 expression was quantified by qRT-PCR in hUC-MSCs transfected with siRNA against JAK1, JAK2, STAT1, STAT2, STAT3, IRF1, or IRF9 and subsequently treated with IFN-γ for 4 h. The expression of PD-L1 in hUC-MSCs of the IFN-γ + si-NC (negative control) group was used as the standard (100%); E: PGL4.10-PD-L1 promoter, pIRES2-IRF1, and Renilla luciferase plasmids were transfected together or separately into 293T cells. Cells were lysed 24 h after transfection and luciferase activity was measured; F: pIRES2-IRF1 plasmid and Renilla luciferase plasmid were transfected into 293T cells with the PGL4.10-PD-L1 promoter plasmid or IRF1 binding site mutant PGL4.10-PD-L1 promoter plasmids. Cells were lysed 24 h after transfection and luciferase activity was measured; G: Predicted binding sites of IRF1 on the PD-L1 promoter. Data were represented as mean ± SEM of n = 3. C: Control; Iso: Isotype; $^{a}P < 0.01$; $^{c}P < 0.0001$. IFN-γ: Interferon-gamma; PD-L1: Programmed cell death protein 1 ligand 1.

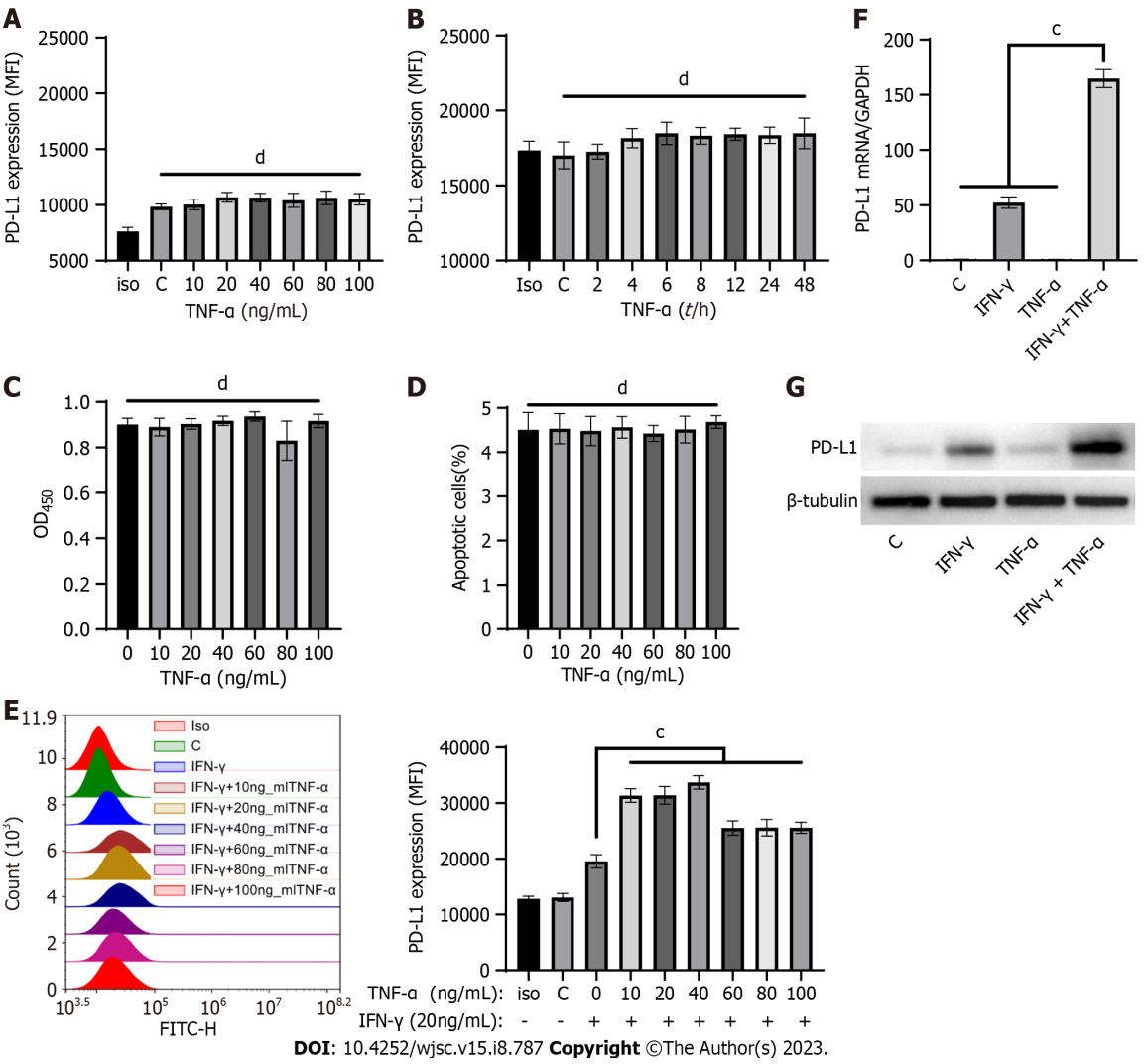

DOI: 10.4252/wjsc.v15.i8.787 **Copyright** ©The Author(s) 2023.

Figure 3 Tumor necrosis factor-alpha synergistically enhanced interferon-gamma-induced programmed cell death protein 1 ligand 1 expression in human umbilical-cord-mesenchymal stem cells. A: Programmed cell death protein 1 ligand 1 (PD-L1) expression was measured by flow cytometry in human umbilical-cord-mesenchymal stem cells (hUC-MSCs) treated with 0, 10, 20, 40, 60, 80 or 100 ng/mL tumor necrosis factor-alpha (TNF-α) for 24 h; B: PD-L1 expression was measured by flow cytometry in hUC-MSCs treated with 100 ng/mL TNF-α for 0, 2, 4, 6, 8, 12, 24, or 48 h; C: Proliferation was measured by CCK8 in hUC-MSCs treated with 0, 10, 20, 40, 60, 80 or 100 ng/mL of TNF-α for 24 h; D: Apoptotic hUC-MSCs were measured by flow cytometry in hUC-MSCs treated with 0, 10, 20, 40, 60, 80 or 100 ng/mL TNF-α for 24 h. The histogram shows the quantification results pertaining to the percentage of apoptotic cells (Annexin V^{+} cells) in each group; E: PD-L1 expression was quantified by flow cytometry in hUC-MSCs after 24 h of incubation with IFN-γ (20 ng/mL) and 0, 10, 20, 40, 60, 80 or 100 ng/mL TNF-α; F: PD-L1 expression was measured by quantitative real-time PCR in hUC-MSCs treated with IFN-γ (20 ng/mL), TNF-α (10 ng/mL), or a combination of IFN-γ (20 ng/mL) and TNF-α (10 ng/mL) for 4 h; G: PD-L1 expression was analyzed by western blot in hUC-MSCs treated with IFN-γ (20 ng/mL), TNF-α (10 ng/mL), or a combination of IFN-γ (20 ng/mL) and TNF-α (10 ng/mL) for 24 h. Data were represented as mean ± SEM of n = 3. C: Control; Iso: Isotype; $^{b}P < 0.001$; $^{c}P < 0.0001$; $^{d}P > 0.05$. IFN-γ: Interferon-gamma; PD-L1: Programmed cell death protein 1 ligand 1; TNF-α: Tumor necrosis factor-alpha.

and TNF-α on PD-L1 expression in hUC-MSCs. We stimulated hUC-MSCs with 20 ng/mL IFN-γ and different concentrations of TNF-α (0 ng/mL, 10 ng/mL, 20 ng/mL, 40 ng/mL, 60 ng/mL, 80 ng/mL, and 100 ng/mL) and detected PD-L1 expression using flow cytometry. The results showed that 10 ng/mL TNF-α enhanced IFN-γ-induced PD-L1 expression significantly; however, the enhanced effect of TNF-α did not appear to be concentration-dependent (Figure 3E). Furthermore, qRT-PCR and western blot results showed that the mRNA and total protein levels of PD-L1 increased significantly when hUC-MSCs were simultaneously stimulated with 20 ng/mL IFN-γ and 10 ng/mL TNF-α when compared with IFN-γ or TNF-α alone (Figure 3F and G). Based on the results, 10 ng/mL TNF-α was used in follow-up experiments. In addition, we investigated the effects of IFN-γ (20 ng/mL) or TNF-α (10 ng/mL) stimulation individually or in combination on the proliferation or apoptosis of hUC-MSCs. Our results showed that the stimuli were unable to exert any effect on apoptosis or proliferation of hUC-MSCs at the current concentrations (Supplementary Figure 3B and C). The findings suggest that TNF-α alone had no effect on PD-L1 expression; however, TNF-α could synergistically increase IFN-γ-induced PD-L1 expression in hUC-MSCs.

TNF-α improved PD-L1 expression by promoting the activation of JAK/STAT1/IRF1 pathway induced by IFN-γ

As previous studies have demonstrated that IFN-γ induces hUC-MSCs to express PD-L1 through the JAK/STAT1/IRF1 pathway and TNF-α induces various downstream biological effects through activation of the NF-κB pathway[24], we explored the molecular mechanism by which TNF-α enhances IFN-γ-induced PD-L1 expression using signaling inhibition experiments. We treated hUC-MSCs with ruxolitinib and the NF-κB inhibitor BAY11-7082, and then detected PD-L1 mRNA levels after combined treatment with IFN-γ and TNF-α for 4 h. Our results showed that both BAY11-7082 and ruxolitinib inhibited PD-L1 expression induced by a combination of IFN-γ and TNF-α (Figure 4A). Ruxolitinib displayed a stronger inhibitory effect, almost completely inhibiting the induction of PD-L1 mRNA expression, while BAY11-7082 only partially inhibited the expression (Figure 4A). Flow cytometry and western blot assays also showed that ruxolitinib completely inhibited PD-L1 protein expression in hUC-MSCs treated with IFN-γ and TNF-α (Figure 4B and C). Furthermore, we performed an siRNA interference assay using STAT1 siRNA and IRF1 siRNA. The siRNA against STAT1 and IRF1 decreased PD-L1 expression induced by IFN-γ or TNF-α in hUC-MSCs (Figure 4D and E). The results indicated that PD-L1 gene transcription is also induced through the JAK/STAT1/IRF1 pathway when stimulated by IFN-γ and TNF-α.

To investigate whether TNF-α affects the activation of the JAK/STAT1/IRF1 pathway, we analyzed the activation of the JAK/STAT1/IRF1 pathway in hUC-MSCs treated with IFN-γ and TNF-α. The results showed that the activation level of the JAK/STAT1/IRF1 pathway was significantly higher following stimulation with IFN-γ and TNF-α (Figure 4F). Additionally, ruxolitinib significantly reduced the phosphorylation levels of JAK1/2 and STAT1, as well as the expression levels of IRF1 and PD-L1, in hUC-MSCs induced by IFN-γ and TNF-α (Figure 4C). The results revealed that the activation of the JAK/STAT1/IRF1 pathway was significantly stronger when co-stimulated with IFN-γ and TNF-α, thus leading to higher PD-L1 expression.

TNF-α synergistically amplified IFN-γ-induced JAK/STAT1/IRF1 signaling activation by upregulating NF-κB-mediated IFNGR1 expression

IFNGR1/2 acts as the membrane receptor of IFN-γ and transmits an activation initiation signal to the JAK/STAT1/IRF1 pathway, which is the key player in PD-L1 expression[23]. We speculated that the higher activation level of the JAK/STAT1/IRF1 pathway might be caused by TNF-α induced IFNGR1/2 expression. As predicted, TNF-α upregulated the expression of IFNGR1 mRNA and protein and the expression of IFNGR2 mRNA (Figure 5A-C). Notably, since no effective anti-IFNGR2 antibody is available, only IFNGR1 expression was detected in western blot experiments. Additionally, the siRNA for IFNGR1/2 decreased PD-L1 mRNA and protein expression in hUC-MSCs induced by IFN-γ and TNF-α (Figure 5D-F). Furthermore, western blot results showed that IFNGR1 siRNA reduced JAK1/2 and STAT1 phosphorylation, as well as IRF1 expression (Figure 5F). The results suggest that TNF-α amplifies the IFN-γ-induced activation of the JAK/STAT1/IRF1 pathway by upregulating IFNGR1/2 expression.

The NF-κB pathway inhibitor BAY11-7082 partially impaired the expression of PD-L1 induced by the combination of IFN-γ and TNF-α (Figure 4A; Supplementary 3D). This suggests that the NF-κB pathway is involved in the regulation of PD-L1 expression induced by IFN-γ and TNF-α. Therefore, we examined the expression of IFNGR1 and the activation of the NF-κB pathway in hUC-MSCs induced by TNF-α. As predicted, TNF-α upregulated IFNGR1 expression by activating the NF-κB pathway, while BAY11-7082 decreased the phosphorylation levels of IKK-α/β, IKB-α, and p65, as well as the expression of IFNGR1 (Figure 5G; Supplementary Figure 4A). To explore NF-κB pathway activation by TNF-α in hUC-MSCs, we assessed nuclear and cytoplasmic p65 and IκB expression after TNF-α treatment. The expression of IκB in the cytoplasm was reduced at 60 min and then restored, while the expression of p65 in the nucleus was significantly increased at 60 min (Figure 5H; Supplementary Figure 4B). These findings indicate that TNF-α can promote NF-κB pathway activation in hUC-MSCs, in addition to enhancing p65 translocation to the nuclei. Moreover, when the expression of p65 was downregulated by siRNA, the effect of TNF-α on the expression of IFNGR1 and PD-L1 induced by IFN-γ was significantly reduced (Figure 5I-K). Importantly, we found that IFNGR1-overexpressing lentivirus restored PD-L1 expression that was reduced by p65 siRNA (Figure 5L). Furthermore, TNF-α upregulated IFNGR1 expression through the NF-κB pathway, and synergistically amplified the activation of JAK/STAT1/IRF1 induced by IFN-γ, finally resulting in an increase in PD-L1 expression in hUC-MSCs.

To confirm that p65 binds to the IFNGR1 promoter to activate IFNGR1 expression, we constructed a luciferase reporter system with NF-κB-driven activity. In 293T cells, higher luciferase activity was observed when p65 and IFNGR1 promoter plasmids were co-transfected into the cells than when these were transfected separately (Figure 5M). As the proximal part of the IFNGR1 gene contained only one p65 binding site, we constructed an IFNGR1 promoter plasmid with a point

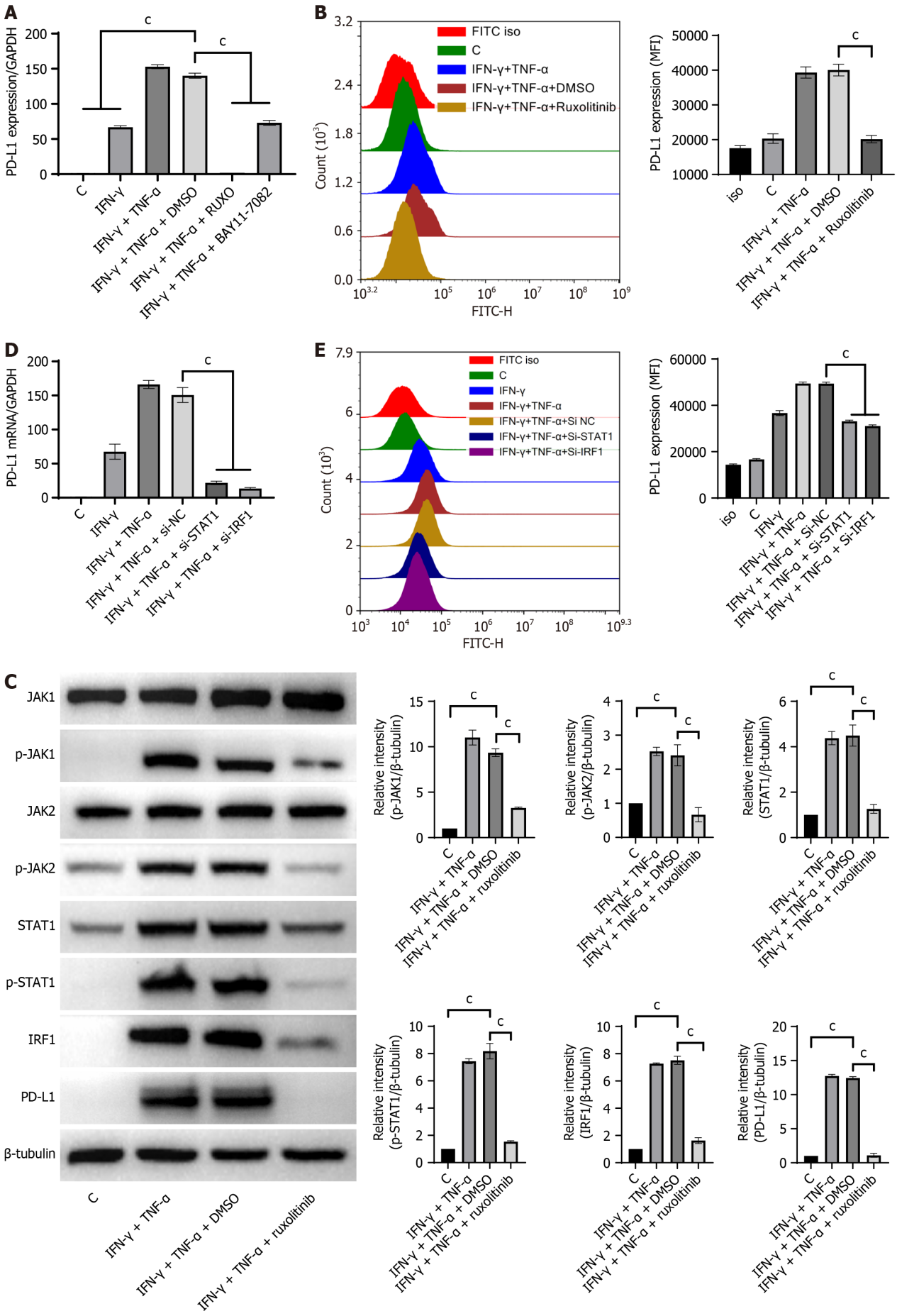
A
PD-L1 expression/GAPDH
C
IFN-γ
IFN-γ + TNF-α
IFN-γ + TNF-α + DMSO
IFN-γ + TNF-α + RUXO
IFN-γ + TNF-α + BAY11-7082
B
FITC iso
C
IFN-γ+TNF-α
IFN-γ+TNF-α+DMSO
IFN-γ+TNF-α+Ruxolitinib
Count (10³)
FITC-H
PD-L1 expression (MFI)
iso
IFN-γ + TNF-α + Ruxolitinib
D
PD-L1 mRNA/GAPDH
IFN-γ + TNF-α + si-NC
IFN-γ + TNF-α + si-STAT1
IFN-γ + TNF-α + si-IRF1
E
IFN-γ
IFN-γ+TNF-α+Si NC
IFN-γ+TNF-α+Si-STAT1
IFN-γ+TNF-α+Si-IRF1
C
JAK1
p-JAK1
JAK2
p-JAK2
STAT1
p-STAT1
IRF1
PD-L1
β-tubulin
IFN-γ + TNF-α + ruxolitinib
Relative intensity (p-JAK1/β-tubulin)
Relative intensity (p-JAK2/β-tubulin)
Relative intensity (STAT1/β-tubulin)
Relative intensity (p-STAT1/β-tubulin)
Relative intensity (IRF1/β-tubulin)
Relative intensity (PD-L1/β-tubulin)

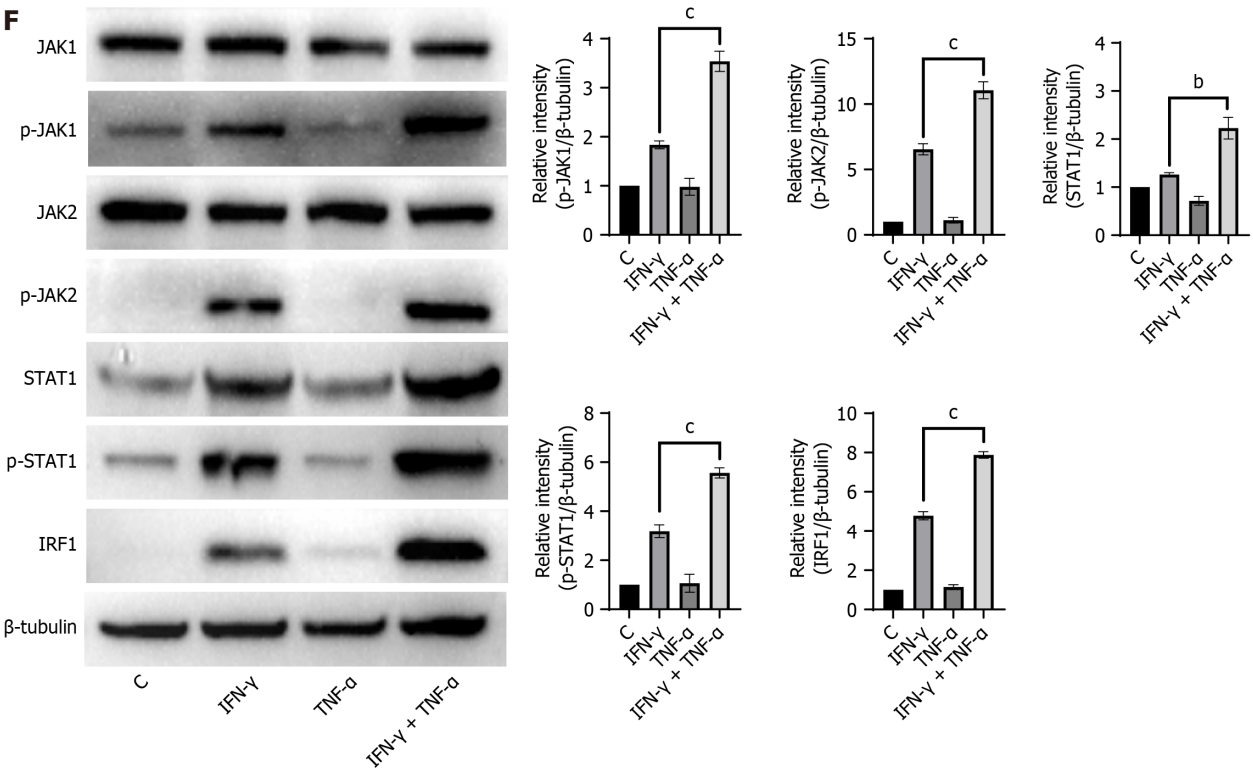

DOI: 10.4252/wjsc.v15.i8.787 **Copyright** ©The Author(s) 2023.

Figure 4 Tumor necrosis factor-alpha increased programmed cell death protein 1 ligand expression by promoting interferon-gamma-induced activation of the JAK/STAT1/interferon regulatory factor 1 pathway. A: Programmed cell death protein 1 ligand (PD-L1) expression was quantified by quantitative real-time PCR (qRT-PCR) in human umbilical-cord-mesenchymal stem cells (hUC-MSCs) after 4 h of incubation with IFN-γ and tumor necrosis factor-alpha (TNF-α) in the presence or absence of ruxolitinib (10 μM) or the NF-κB inhibitor BAY11-7082 (10 μM); B: PD-L1 expression in hUC-MSCs was quantified by flow cytometry after 24 h of incubation with IFN-γ and TNF-α in the presence or absence of ruxolitinib (10 μM); C: Activation of the JAK/STAT1/interferon regulatory factor 1 (IRF1) pathway and the expression of PD-L1 were analyzed by western blot in hUC-MSCs after 24 h of incubation with IFN-γ and TNF-α in the presence or absence of ruxolitinib (10 μM); D and E: PD-L1 expression was quantified by quantitative real-time PCR and flow cytometry in hUC-MSCs transfected with siRNA of NC, STAT1, or IRF1 and subsequently treated with IFN-γ and TNF-α for 4 h or 24 h; F: Activation of the JAK/STAT1/IRF1 pathway was analyzed by western blot in hUC-MSCs treated with IFN-γ (20 ng/mL), TNF-α (10 ng/mL), or a combination of IFN-γ (20 ng/mL) and TNF-α (10 ng/mL) for 24 h. Data were represented as mean ± SEM of n = 3. C: Control; Iso: Isotype; $^{c}P < 0.0001$. IFN-γ: Interferon-gamma; PD-L1: Programmed cell death protein 1 ligand 1; TNF-α: Tumor necrosis factor-alpha.

mutation at this binding site. We found that this p65 binding site mutant plasmid displayed weaker luciferase activity in response to TNF-α stimulation compared to the WT-type IFNGR1 promoter plasmid (Figure 5N). The results indicate that TNF-α induces NF-κB p65 activation of the IFNGR1 promoter.

Synergy of IFN-γ and TNF-α enhanced the immunosuppressive capacity of hUC-MSCs by inducing PD-L1 expression

To explore whether the high expression of PD-L1 in hUC-MSCs induced by a combination of IFN-γ and TNF-α could enhance their immunosuppressive function, we first conducted a T lymphocyte proliferation inhibition experiment *in vitro*. The results showed that PBMCs co-cultured with hUC-MSCs that were pre-treated with IFN-γ and TNF-α had higher CFSE fluorescence intensity than that in other groups, which indicated that IFN-γ- and TNF-α-pretreated hUC-MSCs showed a stronger inhibitory effect on PBMCs proliferation (Figure 6A). Meanwhile, the PD-L1 antibody eliminated the inhibitory effect of hUC-MSCs pre-treated with IFN-γ and TNF-α on PBMCs proliferation (Figure 6A). The results suggest that IFN-γ and TNF-α-pretreated hUC-MSCs, with high PD-L1 expression, exhibited a stronger inhibitory effect on T cell proliferation.

We further explored the therapeutic efficacy of hUC-MSCs pre-treated with a combination of IFN-γ and TNF-α in mice with DSS-induced colitis. Colitis was induced in mice by feeding them DSS added to drinking water, and hUC-MSCs were transplanted according to the schematic diagram shown in Figure 6B. Compared with the wild-type hUC-MSCs treatment group, hUC-MSCs pretreated with a combination of IFN-γ and TNF-α displayed a better therapeutic efficacy in DSS-induced mice, including mitigated bodyweight loss (Figure 6C); improved colonic morphology (Figure 6D); relieved colonic ulcer, mucosal edema, epithelial cell injury, and inflammatory cell infiltration (Figure 6E); lower histopathological scoring of colon tissue (Figure 6F); inhibited infiltration of immune cells including $CD4^+$ T cells, $CD11b^+$ macrophages, and neutrophils (lower MPO activity) in colon tissue (Figure 6G and 6H); more Treg ($Foxp3^+$) cells in colon tissue (Figure 6I), and significantly decreased levels of inflammatory factors such as TNF-α, IFN-γ, and IL-6 in colon tissue (Figure 6J). However, PD-L1 antibody treatment significantly inhibited such effects. In addition, no adverse reactions related to hUC-MSCs transplantation were observed. The results suggest that the combination of IFN-γ and TNF-α synergistically enhanced the immunosuppressive capacity of hUC-MSCs by upregulating the expression of PD-L1,

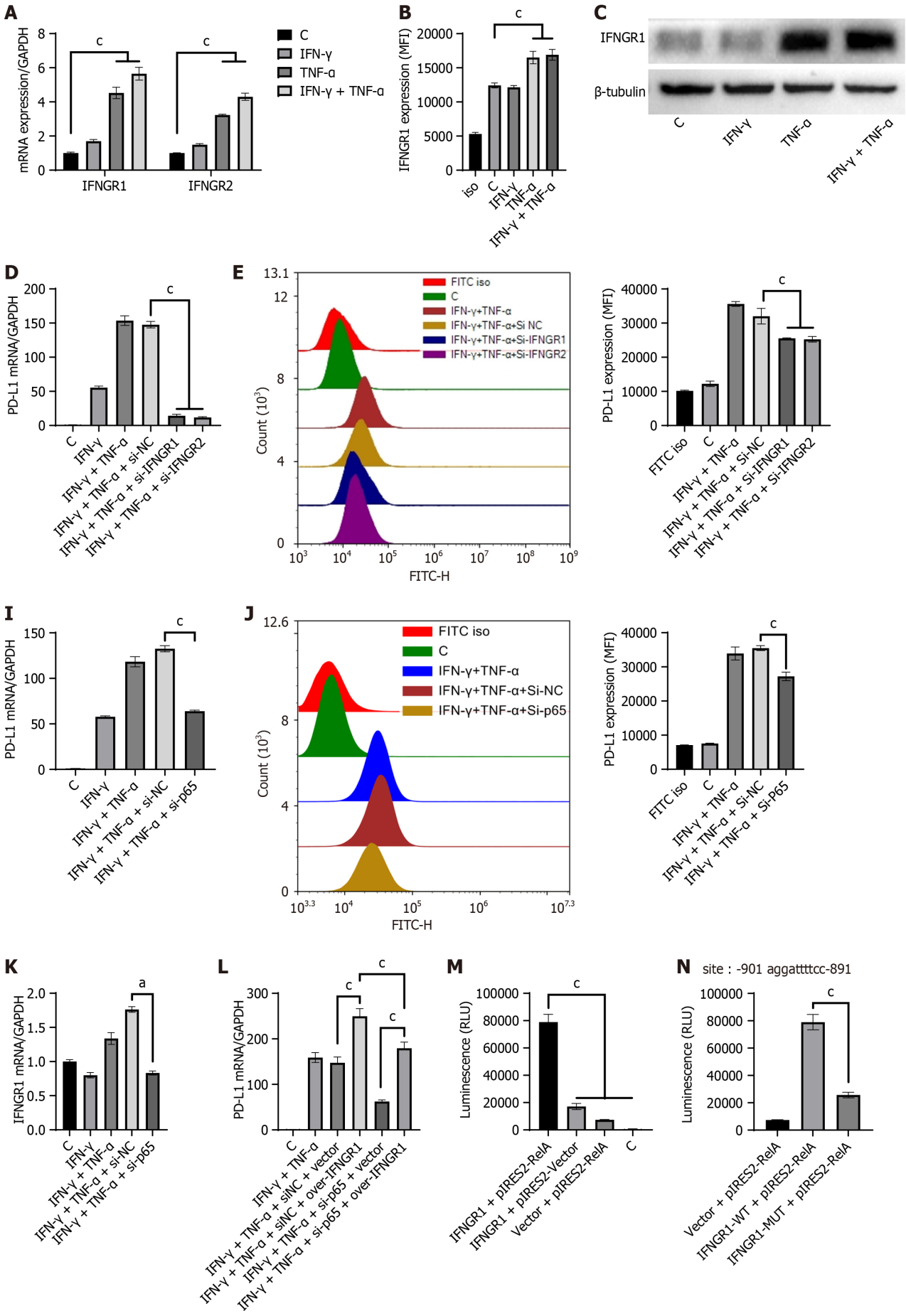
A
mRNA expression/GAPDH
C
IFN-γ
TNF-α
IFN-γ + TNF-α
IFNGR1
IFNGR2
B
IFNGR1 expression (MFI)
iso
C
IFN-γ
TNF-α
IFN-γ + TNF-α
C
IFNGR1
β-tubulin
C
IFN-γ
TNF-α
IFN-γ + TNF-α
D
PD-L1 mRNA/GAPDH
C
IFN-γ
IFN-γ + TNF-α
IFN-γ + TNF-α + si-NC
IFN-γ + TNF-α + si-IFNGR1
IFN-γ + TNF-α + si-IFNGR2
E
FITC iso
C
IFN-γ+TNF-α
IFN-γ+TNF-α+Si NC
IFN-γ+TNF-α+Si-IFNGR1
IFN-γ+TNF-α+Si-IFNGR2
Count (10³)
FITC-H
PD-L1 expression (MFI)
FITC iso
C
IFN-γ + TNF-α
IFN-γ + TNF-α + Si-NC
IFN-γ + TNF-α + Si-IFNGR1
IFN-γ + TNF-α + Si-IFNGR2
I
PD-L1 mRNA/GAPDH
C
IFN-γ
IFN-γ + TNF-α
IFN-γ + TNF-α + si-NC
IFN-γ + TNF-α + si-p65
J
FITC iso
C
IFN-γ+TNF-α
IFN-γ+TNF-α+Si-NC
IFN-γ+TNF-α+Si-p65
Count (10³)
FITC-H
PD-L1 expression (MFI)
FITC iso
C
IFN-γ + TNF-α
IFN-γ + TNF-α + Si-NC
IFN-γ + TNF-α + Si-P65
K
IFNGR1 mRNA/GAPDH
C
IFN-γ
IFN-γ + TNF-α
IFN-γ + TNF-α + si-NC
IFN-γ + TNF-α + si-p65
L
PD-L1 mRNA/GAPDH
C
IFN-γ + TNF-α
IFN-γ + TNF-α + siNC + vector
IFN-γ + TNF-α + siNC + over-IFNGR1
IFN-γ + TNF-α + si-p65 + vector
IFN-γ + TNF-α + si-p65 + over-IFNGR1
M
Luminescence (RLU)
IFNGR1 + pIRES2-RelA
IFNGR1 + pIRES2-Vector
Vector + pIRES2-RelA
C
N
site : -901 aggattttcc-891
Luminescence (RLU)
Vector + pIRES2-RelA
IFNGR1-WT + pIRES2-RelA
IFNGR1-MUT + pIRES2-RelA

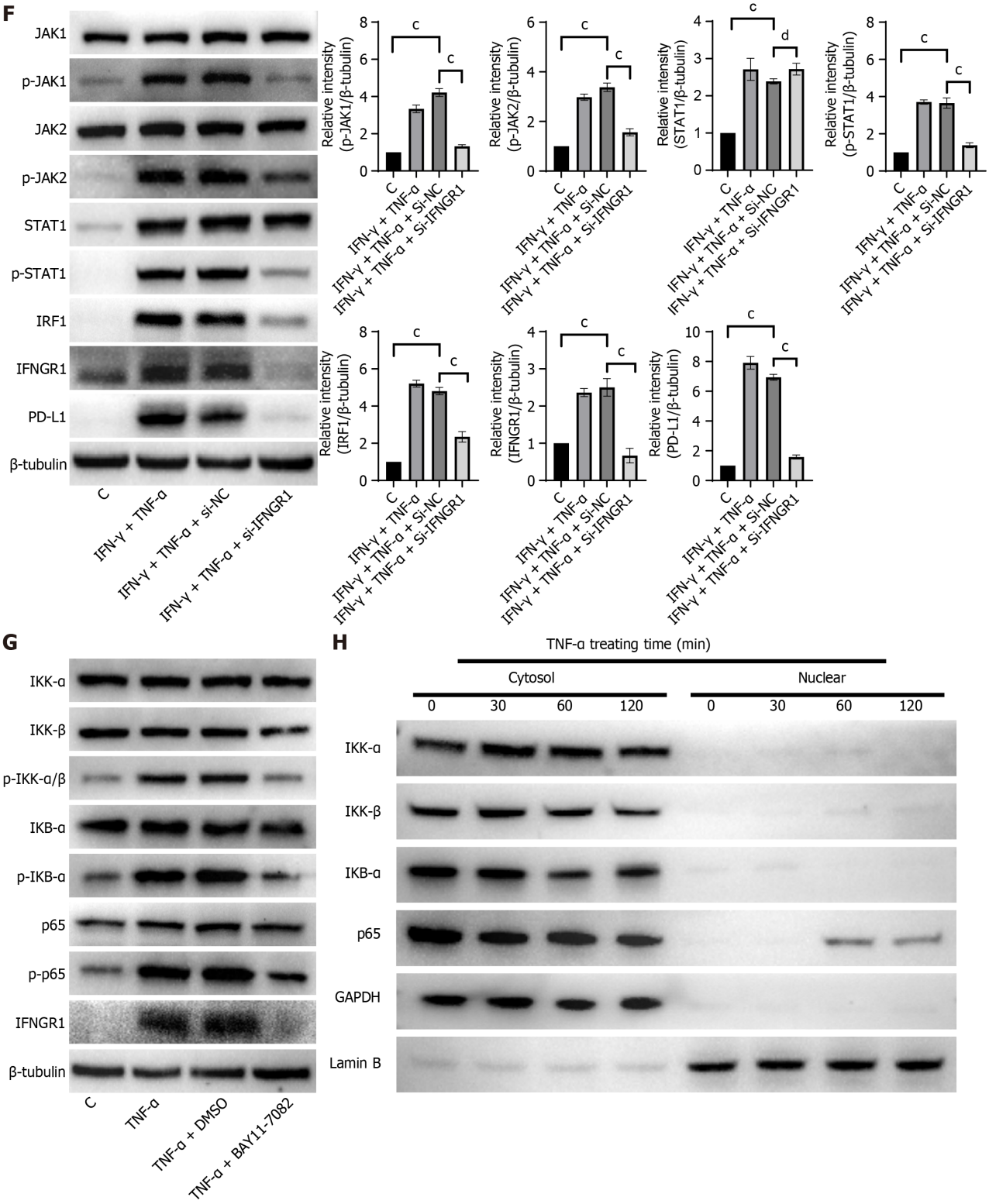

DOI: 10.4252/wjsc.v15.i8.787 **Copyright** ©The Author(s) 2023.

Figure 5 Tumor necrosis factor-alpha synergistically amplified interferon-gamma-induced JAK/STAT1/interferon regulatory factor 1 signaling activation by upregulating NF-κB-mediated interferon-gamma receptor 1/2 expression. A: The expression of NF-κB-mediated interferon-gamma receptor 1/2 (IFNGR1/2) were quantified by quantitative real-time PCR (qRT-PCR) in human umbilical-cord-mesenchymal stem cells (hUC-MSCs) treated with IFN-γ and tumor necrosis factor-alpha (TNF-α) alone or in combination for 4 h; B and C: IFNGR1 expression was quantified by flow cytometry or WB in hUC-MSCs treated with IFN-γ and TNF-α alone or in combination for 24 h; D and E: PD-L1 expression was quantified by qRT-PCR or flow cytometry in hUC-MSCs transfected with siRNA against NC, IFNGR1, or IFNGR2, and subsequently treated with IFN-γ and TNF-α for 4 h or 24 h; F: Activation of the JAK/STAT1/interferon regulatory factor 1 pathway and the expressions of PD-L1 and IFNGR1 were analyzed by western blot in hUC-MSCs after 24 h of incubation with IFN-γ and TNF-α in the presence or absence of IFNGR1 siRNA; G: Activation of the NF-κB pathway and expression of IFNGR1 were analyzed by western blot in hUC-MSCs after 24 h of incubation with TNF-α in the presence or absence of the NF-KB inhibitor BAY11-7082 (10 μM); H: IKKα, IKKβ, p65 and IκBα protein levels in the cytoplasm and nucleus of hUC-MSCs after TNF-α stimulation were measured through western blot; I: IFNGR1 expression was quantified by qRT-PCR in hUC-MSCs transfected

with p65 siRNA and subsequently treated with IFN-γ and TNF-α for 4 h; J and K: PD-L1 expression was quantified by qRT-PCR or flow cytometry in hUC-MSCs transfected with p65 siRNA and subsequently treated with IFN-γ and TNF-α for 4 h or 24 h; L: hUC-MSCs were infected with IFNGR1 overexpressed lentivirus and transfected with siRNA of p65, and induced with IFN-γ and TNF-α for 4 h, and then PD-L1 expression was quantified by qRT-PCR; M: PGL4.10-IFNGR1 promoter plasmid, pIRES2-p65 plasmid, and Renilla luciferase plasmid were transfected together or separately into 293T cells. Cells were lysed 24 h after transfection and luciferase activity was measured; N: pIRES2-p65 plasmid and Renilla luciferase plasmid were transfected into 293T cells with the PGL4.10-IFNGR1 promoter plasmid or the p65 binding site mutant PGL4.10-IFNGR1 promoter plasmid. Cells were lysed 24 h after transfection and luciferase activity was measured. The predicted binding sites of p65 to the IFNGR1 promoter are above the graph. Data were represented as mean ± SEM of $n = 3$. C: Control; Iso: Isotype; [b]$P < 0.001$; [c]$P < 0.0001$; [d]$P > 0.05$. IFN-γ: Interferon-gamma; PD-L1: Programmed cell death protein 1 ligand 1; TNF-α: Tumor necrosis factor-alpha.

yielding a better therapeutic efficacy in DSS-induced mice.

DISCUSSION

MSCs are usually derived from the umbilical cord, bone marrow, and adipose tissue. In the present study, hUC-MSCs were selected based on multiple considerations. First, as a type of medical waste, umbilical cord tissue is easier to obtain with less ethical controversy. A large number of MSCs are easily obtained from umbilical cord tissue by mature isolation methods. Second, hUC-MSCs have greater proliferative capacity and immunomodulatory ability than other types of MSCs[25,26]. Third, the major histocompatibility complex I (MHC-I) expression level and the immunogenicity of hUC-MSCs is lower. Hence, although the biosafety of MSCs has been a matter of great concern, hUC-MSCs have become the main source of cells for mesenchymal stem cell transplantation therapy[27]. Therefore, as hUC-MSCs have greater clinical application potential, they were selected for use in the study. In DSS-induced colitis mice, MSCs not only significantly improved the colonic lesions of mice but also ameliorated the tumorigenesis of colitis[28]. In a clinical trial, researchers followed up 34 patients with ulcerative colitis who received hUC-MSCs for up to two years, and no long-term complications such as malignant tumors and immune rejection were observed during follow-up[29]. Similarly, except for the therapeutic effect of hUC-MSCs on colitis mice, no MSC-related side effects or toxicities were observed in the present study. Overall, MSCs have a high safety profile in the treatment of ulcerative colitis.

PD-L1 plays an important role in the immunosuppressive capacity of hUC-MSCs. Although the mechanism of PD-L1 expression has been thoroughly elucidated in tumors[30], it remains to be explored in MSCs. The cytokines that induce MSCs to express PD-L1 include IFN-γ, IL25, and IL27, and the relevant pathways are STAT1, JNK/STAT3, and JAK/STAT1[31-33]. We performed this study to investigate the mechanism of PD-L1 expression in MSCs under IFN-γ and TNF-α stimulation and to find a way to enhance the immunosuppressive capacity of MSCs. In the present study, we confirmed that IFN-γ induces PD-L1 expression through the JAK/STAT1/IRF1 pathway in hUC-MSCs. TNF-α upregulates the expression of IFNGR1/2 *via* the NF-κB pathway, which promotes the activation of the JAK/STAT1/IRF1 pathway induced by IFN-γ, significantly increasing PD-L1 expression. Furthermore, synergistic IFN-γ and TNF-α induction of high PD-L1 expression in hUC-MSCs strongly inhibited T-cell proliferation[33]. In mice with DSS-induced colitis, tail vein infusion of pretreated hUC-MSCs reduced disease activity, colonic tissue damage, cytokine levels, and inflammatory cell infiltration. Thus, combined treatment with IFN-γ and TNF-α synergistically induces high PD-L1 expression in hUC-MSCs, which strengthens the immunosuppressive capacity of hUC-MSCs (Figure 7).

PD-L1 expression has been extensively studied in inflammatory diseases and tumors. In tumor cells, various pathways are involved in IFN-γ-induced PD-L1 expression[30]. For instance, IFN-γ induces PD-L1 expression *via* the JAK/STAT/IRF1 pathway in tumor cells[34,35]. Similarly, studies have shown that PD-L1 expression in MSCs can be induced by IFN-γ mediated by STAT1. Based on these studies, we speculated that these signals are similar, and that PD-L1 expression induced by IFN-γ in hUC-MSCs might have occurred through the JAK/STAT1/IRF1 pathway. To verify our hypothesis, we conducted signaling pathway inhibitor, RNA interference, and luciferase reporter gene experiments. Our results showed that IFN-γ activates the JAK/STAT1 pathway and promotes IRF1 binding to the PD-L1 promoter, increasing PD-L1 mRNA expression. The results reveal the molecular mechanism by which IFN-γ induces the expression of PD-L1 in hUC-MSCs in detail.

In tumor cells, TNF-α co-stimulation with IL4 or IFN-γ increased PD-L1 expression, and the effect was associated with the NF-κB pathway[20,36]. HCC cells induced by IFN-γ and TNF-α had higher PD-L1 expression than those induced by IFN-γ alone, and had stronger resistance to adaptive immunity[20]. Such findings suggest that TNF-α enhances PD-L1 expression induced by IFN-γ and NF-κB signaling might be involved. In our results, we found that TNF-α significantly increased IFN-γ-induced PD-L1 expression in hUC-MSCs. Importantly, we demonstrated that TNF-α upregulated IFNGR1 expression through the NF-κB pathway, which enhanced IFN-γ/IFNGR/JAK/STAT1/IRF1 signaling axis activation, significantly upregulating PD-L1 expression. In addition, we found that trends of PD-L1 expression in two others common MSCs pretreated with IFN-γ and TNF-α were similar to those of hUC-MSCs (Supplementary Figure 4C). The results suggest that IFN-γ and TNF-α synergistically induce high PD-L1 expression, which may be universally present in MSCs from different sources. Another issue to consider is that IFN-γ or TNF-α may affect cell survival. Therefore, the effect of such cytokines on the proliferation and apoptosis of hUC-MSCs was evaluated. Additionally, the results showed that IFN-γ and TNF-α stimulation alone or in combination had no effect on the proliferation and apoptosis of hUC-MSCs (Figure 3C and D; Supplementary Figure 3B and C).

Ulcerative colitis is an autoimmune disease with complex mechanisms[37]. PD-L1 is involved in the pathogenesis of colitis by targeting T cells[38]. The high PD-L1 expression in colitis regulates cytokine production in colonic dendritic

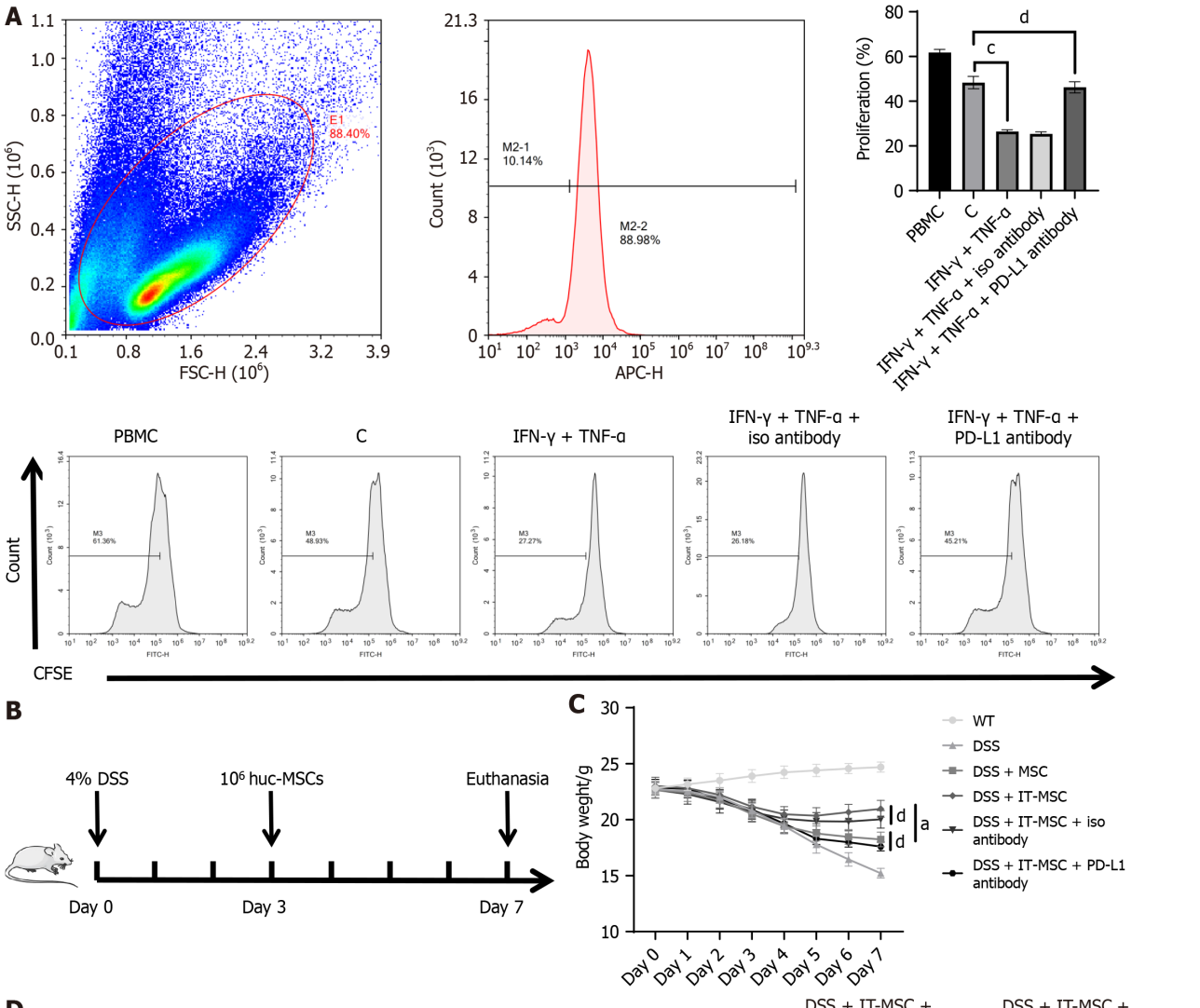
A
SSC-H (10^6)
FSC-H (10^6)
E1
88.40%
Count (10^3)
APC-H
M2-1
10.14%
M2-2
88.98%
Proliferation (%)
PBMC
C
IFN-γ + TNF-α
IFN-γ + TNF-α + iso antibody
IFN-γ + TNF-α + PD-L1 antibody
Count
CFSE
B
4% DSS
10^6 huc-MSCs
Euthanasia
Day 0
Day 3
Day 7
C
Body weight/g
WT
DSS
DSS + MSC
DSS + IT-MSC
DSS + IT-MSC + iso antibody
DSS + IT-MSC + PD-L1 antibody
D
WT
DSS
DSS + MSC
DSS + IT-MSC
DSS + IT-MSC + iso antibody
DSS + IT-MSC + PD-L1 antibody
1 cm
E
WT
DSS
MSC + DSS
IT-MSC + DSS
DSS + IT-MSC + iso antibody
DSS + IT-MSC + PD-L1 antibody
F
Pathological score

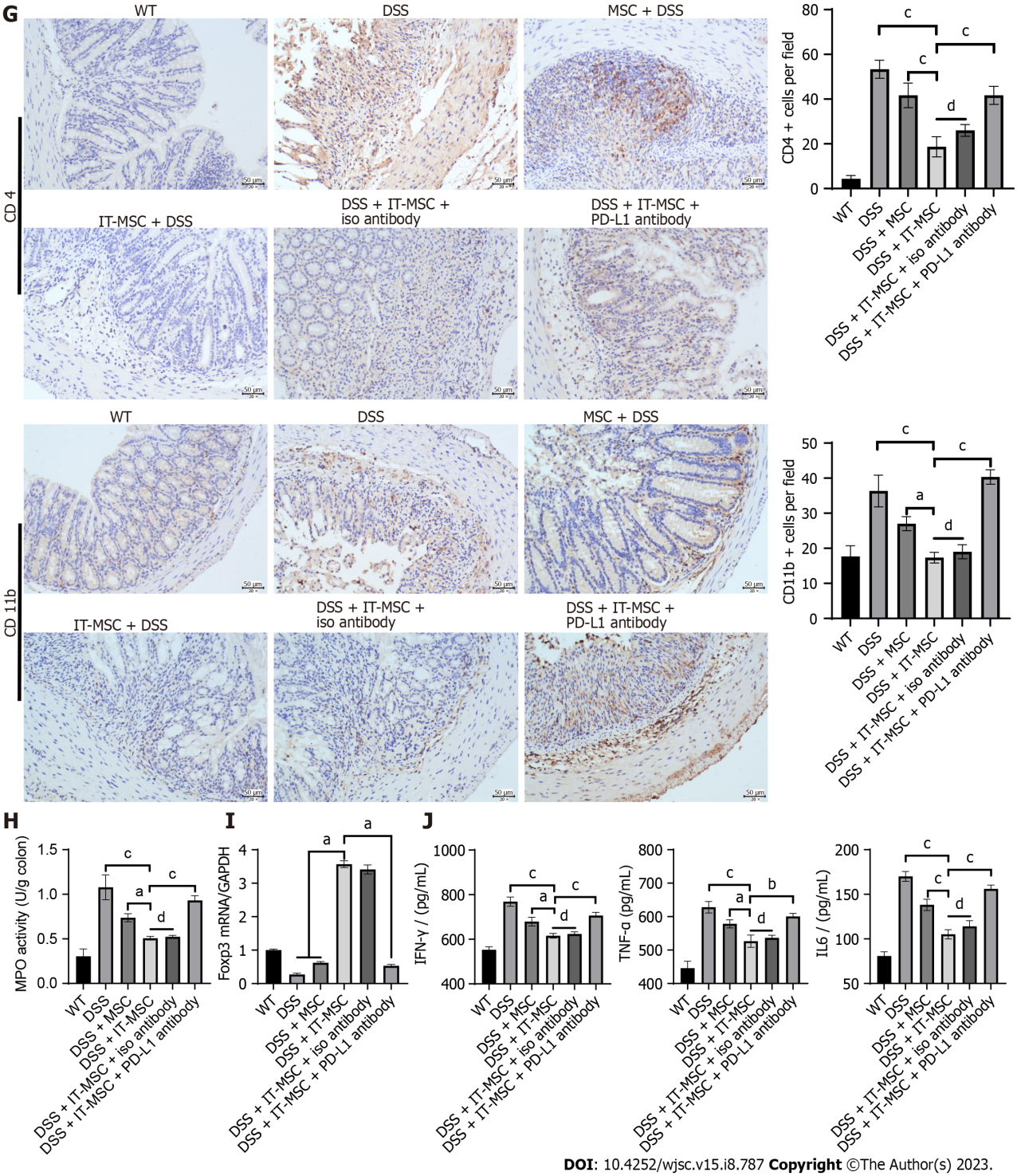

DOI: 10.4252/wjsc.v15.i8.787 **Copyright** ©The Author(s) 2023.

Figure 6 Synergy by IFN-γ and tumor necrosis factor-alpha enhanced the immunosuppressive capacity of human umbilical-cord-mesenchymal stem cells by inducing programmed cell death protein 1 ligand expression. A: The CFSE fluorescence intensity of CFSE-labeled peripheral blood mononuclear cells (PBMCs) was detected after co-culture with human umbilical-cord-mesenchymal stem cells (hUC-MSCs) with different treatments for 3 d. The CFSE fluorescence intensity of CD3-positive PBMCs on day 0 was used as the reference (1.29%). The histogram shows the quantification results pertaining to the mean fluorescent intensity of CFSE in each group; B: Schematic diagram of dextran sulfate sodium-induced colitis and MSCs transplantation therapy in mice; C: Bodyweight of mice in each group during the disease process (n = 6); D: Macroscopic appearance of the colon in each group; E: Colon sections embedded in paraffin were stained with hematoxylin and eosin for light microscopy assessment. Scale bar, 50 μm; F: Histopathological score of colons from each group was assessed for disease severity (n = 3); G: Infiltration cells expressing CD4 or CD11b in colon tissue sections from each group were analyzed by immunohistochemical staining (n = 3). Scale bar, 50 μm; H: Myeloperoxidase activity in the colon was determined (n = 3); I: The colonic mRNA expression of Treg (Foxp3) from each group were analyzed by quantitative real-time PCR (n = 3); J: Levels of inflammatory factors in colon tissue homogenates from each group were determined using ELISA (n = 3). IT-MSCs refer to hUC-MSCs pretreated with IFN-γ and tumor necrosis factor-alpha for 24 h. C: Control; $^{a}P < 0.01$; $^{b}P < 0.001$; $^{c}P < 0.0001$; $^{d}P > 0.05$.

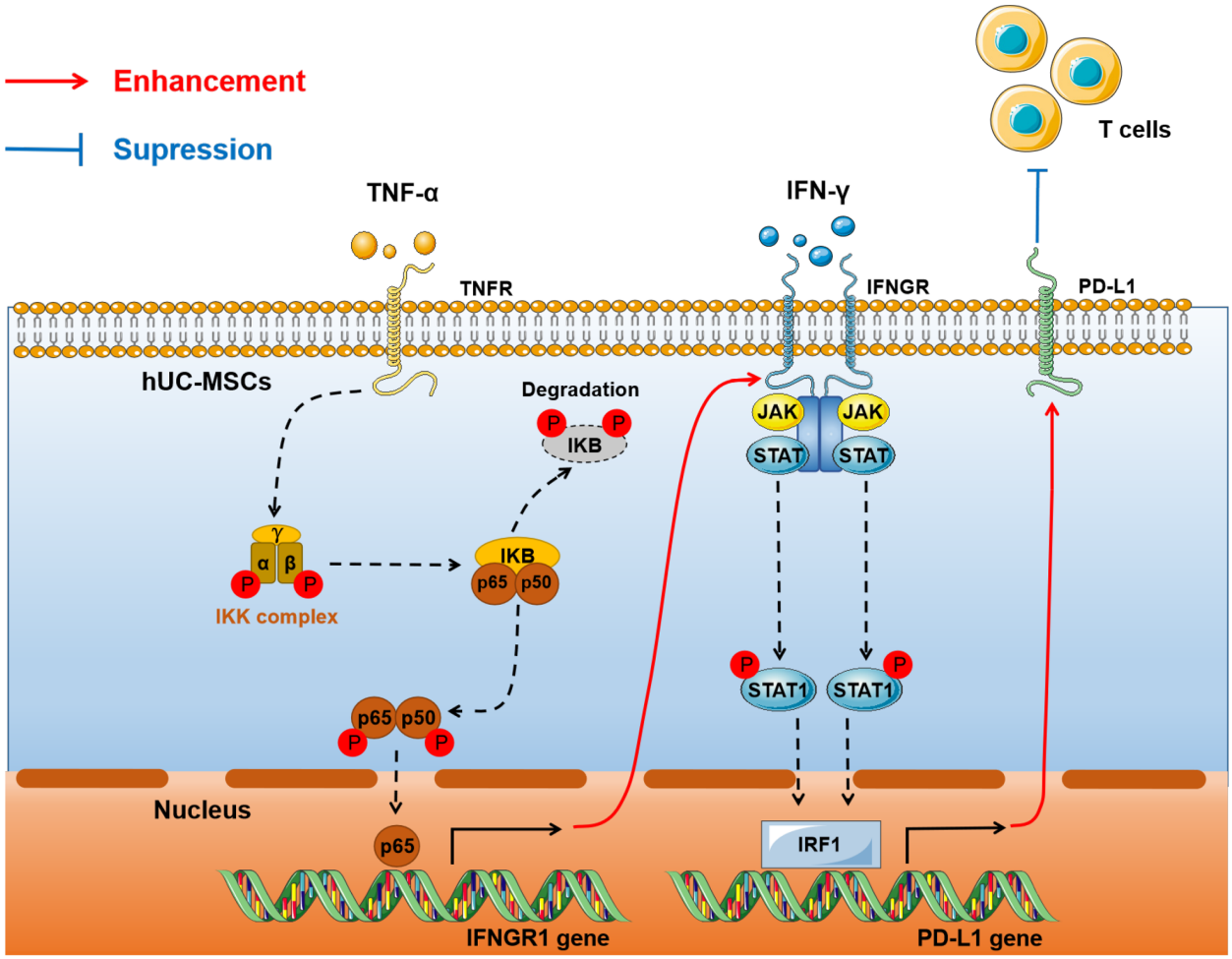

DOI: 10.4252/wjsc.v15.i8.787 **Copyright** ©The Author(s) 2023.

Figure 7 Molecular mechanism of interferon-gamma and tumor necrosis factor-alpha synergistically upregulated expression of programmed cell death protein 1 ligand in human umbilical-cord-mesenchymal stem cells to inhibit T cells. IFN-γ: Interferon-gamma; PD-L1: Programmed cell death protein 1 ligand 1; TNF-α: Tumor necrosis factor-alpha; hUC-MSCs: Human umbilical-cord-mesenchymal stem cells; IRF1: Interferon regulatory factor 1.

cells, inhibits Th1/Th17 cell activity, and promotes Treg cell proliferation[38-40]. Therefore, DSS-induced colitis models are often used to evaluate the efficacy of drugs and the immunomodulatory ability of MSCs[22,41,42]. We used T-cell proliferation inhibition experiments *in vitro* to confirm that hUC-MSCs treated with IFN-γ and TNF-α have a stronger immunosuppressive capacity than untreated hUC-MSCs. Furthermore, we evaluated the immunosuppressive capacity of hUC-MSCs treated with IFN-γ and TNF-α in a DSS-induced mouse colitis model and found that they exhibited fewer disease symptoms and less tissue damage, as well as lower inflammatory cell infiltration, lower inflammatory factors, and greater Treg cells recruitment than untreated hUC-MSCs. Moreover, we performed RNA-seq analysis on hUC-MSCs treated with IFN-γ and TNF-α. We found that with a combination of IFN-γ and TNF-α treatment, hUC-MSCs also expressed IDO, TSG-6, and other immunosuppressive molecules (data not shown). The results suggest that hUC-MSCs treated with IFN-γ and TNF-α have a stronger immunomodulatory capacity than untreated hUC-MSCs, perhaps because hUC-MSCs can express PD-L1 as well as other immunosuppressive molecules. This idea is worthy of further investigation.

In recent years, MSCT therapy has been rising in popularity for the treatment of various inflammatory diseases due to the immunosuppressive ability of MSCs. However, due to differences in both the sources of MSCs and the techniques of cell extraction and culture, the efficacy of MSCT in patients is not stable. Based on the present study, it is likely that the abundance of immunosuppressive molecules expressed by MSCs plays an important role. Therefore, this study provides two possible solutions to improve the efficacy of MSCT in diseases. On the one hand, MSCs can express more immunosuppressive molecules (PD-L1) after co-induction with lower concentrations of inflammatory factors (IFN-γ and TNF-α) without impairing cell viability. On the other hand, the efficacy of MSCT can be improved by detecting and screening for MSCs with high expression levels of immunosuppressive molecules before transplantation. In future studies, to compensate for some of the limitations of this study in a translational application, it is necessary to investigate the effect of more combinations of inflammatory factors on PD-L1 expression in MSCs, and also investigate the immunosuppressive molecules induced by other inflammatory factors. More research in this area will contribute to the translational application of MSCT in clinical practice.

CONCLUSION

In the present study, we found that IFN-γ and TNF-α synergistically induce a high level of PD-L1 expression in hUC-MSCs, and we elucidated the molecular mechanism involved. More importantly, both *in vitro* and *in vivo* experiments confirmed that INF-γ- and TNF-α-pretreated hUC-MSCs with these high PD-L1 expression levels have strong immunosuppressive capacity and, therefore, have great potential for clinical application in the treatment of autoimmune diseases.

ARTICLE HIGHLIGHTS

Research background

The immunosuppressive capacity of Mesenchymal stem cells (MSCs) is dependent on the "license" of several proinflammatory factors to express immunosuppressive factors such as programmed cell death 1 ligand 1 (PD-L1), which determines the clinical therapeutic efficacy of MSCs for inflammatory or immune diseases. In MSCs, interferon-gamma (IFN-γ) is a key inducer of PD-L1 expression, which is synergistically enhanced by tumor necrosis factor-alpha (TNF-α), but this; however, the mechanism is unclear.

Research motivation

The efficacy of MSCs transplantation (MSCT) is limited by the expression of immunosuppressive molecules of MSCs, including PD-L1. However, the mechanism of IFN-γ alone or in combination with TNF-α inducing MSCs high expression of PD-L1 remains unclear.

Research objectives

To reveal the mechanism of high PD-L1 expression in MSCs pretreated with IFN-γ and TNF-α and explore the application prospects of MSCs with high PD-L1 expression in ulcerative colitis.

Research methods

We assessed PD-L1 expression in human umbilical cord-MSCs (hUC-MSCs) induced by IFN-γ and TNF-α, alone or in combination. Additionally, we performed signaling inhibition and RNA interference experiments to elucidate the specific cross-talk signaling pathways between IFN-γ and TNF-α. Finally, we evaluated the immunosuppressive capacity of hUC-MSCs treated with IFN-γ and TNF-α in an *in vitro* mixed lymphocyte culture assay, and *in vivo* in mice with dextran sulfate sodium (DSS)-induced acute colitis.

Research results

Our results showed that IFN-γ upregulated PD-L1 expression in hUC-MSCs to enhance their immunosuppressive activities through the JAK/STAT1/interferon regulatory factor 1 (IRF1) pathway. TNF-α synergistically enhanced IFN-γ-induced PD-L1 expression in hUC-MSCs by upregulating nuclear factor kappa-B (NF-κB)-mediated expression of IFN-γ receptor 1 to activate JAK/STAT1/IRF1 signaling. Furthermore, high PD-L1 expression in hUC-MSCs induced by IFN-γ and TNF-α significantly attenuated DSS-induced acute colitis in mice.

Research conclusions

Our study revealed that IFN-γ and TNF-α synergistically induce the high PD-L1 expression of hUC-MSCs through the JAK/STAT1/IRF1 pathway and the NF-κB pathway, which effectively improves the immunosuppressive capacity of hUC-MSCs.

Research perspectives

The results of the present study could facilitate the optimization of clinical application strategies of MSCT.

FOOTNOTES

Author contributions: Chen Z and Yao MW contributed equally to this work; Chen Z and Yao MW designed all the project and the experiment; Chen Z, Ao X, Guo W, Xing W, Shen ZL, and Lian QZ developed the methodology; Chen Z, Yao MW, and Ao LQ performed the *in vivo* experiments; Chen Z, Yao MW, Li Z, Li SD, and Lu WY performed the *in vitro* experiments; Chen Z and Ao X wrote the manuscript; Xu X, Ao X, and Chen Z reviewed and edited the paper; and all authors read and approved the final manuscript.

Supported by the National Natural Science Foundation of China, No. 81871568 and No. 32100643; and COVID-19 Infection and Prevention Emergency Special Project of Chongqing Education Commission, No. KYYJ202009.

Institutional animal care and use committee statement: All procedures involving animals were reviewed and approved by the Institutional Animal Care and Use Committee of the Army Medical University (SYXK2022-0018).

Conflict-of-interest statement: The authors confirm that this article has no conflict of interest to report.

Data sharing statement: Data sets used or analyzed during the current study can be obtained reasonably request of the corresponding authors.

ARRIVE guidelines statement: The authors have read the ARRIVE Guidelines, and the manuscript was prepared and revised according to the ARRIVE Guidelines.

Open-Access: This article is an open-access article that was selected by an in-house editor and fully peer-reviewed by external reviewers. It is distributed in accordance with the Creative Commons Attribution NonCommercial (CC BY-NC 4.0) license, which permits others to distribute, remix, adapt, build upon this work non-commercially, and license their derivative works on different terms, provided the original work is properly cited and the use is non-commercial. See: https://creativecommons.org/Licenses/by-nc/4.0/

Country/Territory of origin: China

ORCID number: Zhuo Chen 0000-0001-7936-7857; Meng-Wei Yao 0000-0002-7484-8552; Zhi-Lin Shen 0009-0003-4923-8984; Shi-Dan Li 0000-0002-0428-2557; Wei Xing 0000-0002-8512-3821; Wei Guo 0000-0003-3422-5606; Zhan Li 0000-0001-5664-3863; Xiao-Feng Wu 0000-0002-6187-5981; Luo-Quan Ao 0000-0002-9760-5334; Wen-Yong Lu 0000-0001-9651-0424; Qi-Zhou Lian 0000-0001-8189-7160; Xiang Xu 0000-0002-1026-2210; Xiang Ao 0000-0002-8487-9483.

S-Editor: Chen YL
L-Editor: A
P-Editor: Zhao S

REFERENCES

1 **Lv FJ**, Tuan RS, Cheung KM, Leung VY. Concise review: the surface markers and identity of human mesenchymal stem cells. *Stem Cells* 2014; **32**: 1408-1419 [PMID: 24578244 DOI: 10.1002/stem.1681]
2 **Nauta AJ**, Fibbe WE. Immunomodulatory properties of mesenchymal stromal cells. *Blood* 2007; **110**: 3499-3506 [PMID: 17664353 DOI: 10.1182/blood-2007-02-069716]
3 **Ni K**, Liu M, Zheng J, Wen L, Chen Q, Xiang Z, Lam KT, Liu Y, Chan GC, Lau YL, Tu W. PD-1/PD-L1 Pathway Mediates the Alleviation of Pulmonary Fibrosis by Human Mesenchymal Stem Cells in Humanized Mice. *Am J Respir Cell Mol Biol* 2018; **58**: 684-695 [PMID: 29220578 DOI: 10.1165/rcmb.2017-0326OC]
4 **He X**, Yang Y, Yao M, Yang L, Ao L, Hu X, Li Z, Wu X, Tan Y, Xing W, Guo W, Bellanti JA, Zheng SG, Xu X. Combination of human umbilical cord mesenchymal stem (stromal) cell transplantation with IFN-γ treatment synergistically improves the clinical outcomes of patients with rheumatoid arthritis. *Ann Rheum Dis* 2020; **79**: 1298-1304 [PMID: 32561603 DOI: 10.1136/annrheumdis-2020-217798]
5 **Taki Z**, Gostjeva E, Thilly W, Yaseen B, Lopez H, Mirza M, Hassuji Z, Vigneswaran S, Ahmed Abdi B, Hart A, Arumalla N, Thomas G, Denton CP, Suleman Y, Liu H, Venturini C, O'Reilly S, Xu S, Stratton R. Pathogenic Activation of Mesenchymal Stem Cells Is Induced by the Disease Microenvironment in Systemic Sclerosis. *Arthritis Rheumatol* 2020; **72**: 1361-1374 [PMID: 32237059 DOI: 10.1002/art.41267]
6 **Regmi S**, Seo Y, Ahn JS, Pathak S, Acharya S, Nguyen TT, Yook S, Sung JH, Park JB, Kim JO, Young CS, Kim HS, Jeong JH. Heterospheroid formation improves therapeutic efficacy of mesenchymal stem cells in murine colitis through immunomodulation and epithelial regeneration. *Biomaterials* 2021; **271**: 120752 [PMID: 33730631 DOI: 10.1016/j.biomaterials.2021.120752]
7 **Yang Y**, He X, Zhao R, Guo W, Zhu M, Xing W, Jiang D, Liu C, Xu X. Serum IFN-γ levels predict the therapeutic effect of mesenchymal stem cell transplantation in active rheumatoid arthritis. *J Transl Med* 2018; **16**: 165 [PMID: 29903026 DOI: 10.1186/s12967-018-1541-4]
8 **Yao M**, Chen Z, He X, Long J, Xia X, Li Z, Yang Y, Ao L, Xing W, Lian Q, Liang H, Xu X. Cross talk between glucose metabolism and immunosuppression in IFN-γ-primed mesenchymal stem cells. *Life Sci Alliance* 2022; **5** [PMID: 36260750 DOI: 10.26508/lsa.202201493]
9 **Carvalho AÉS**, Sousa MRR, Alencar-Silva T, Carvalho JL, Saldanha-Araujo F. Mesenchymal stem cells immunomodulation: The road to IFN-γ licensing and the path ahead. *Cytokine Growth Factor Rev* 2019; **47**: 32-42 [PMID: 31129018 DOI: 10.1016/j.cytogfr.2019.05.006]
10 **Li M**, Soder R, Abhyankar S, Abdelhakim H, Braun MW, Trinidad CV, Pathak HB, Pessetto Z, Deighan C, Ganguly S, Dawn B, McGuirk J, Dunavin N, Godwin AK. WJMSC-derived small extracellular vesicle enhance T cell suppression through PD-L1. *J Extracell Vesicles* 2021; **10**: e12067 [PMID: 33598108 DOI: 10.1002/jev2.12067]
11 **Liu S**, Liu F, Zhou Y, Jin B, Sun Q, Guo S. Immunosuppressive Property of MSCs Mediated by Cell Surface Receptors. *Front Immunol* 2020; **11**: 1076 [PMID: 32849489 DOI: 10.3389/fimmu.2020.01076]
12 **Hudson K**, Cross N, Jordan-Mahy N, Leyland R. The Extrinsic and Intrinsic Roles of PD-L1 and Its Receptor PD-1: Implications for Immunotherapy Treatment. *Front Immunol* 2020; **11**: 568931 [PMID: 33193345 DOI: 10.3389/fimmu.2020.568931]
13 **Sun C**, Mezzadra R, Schumacher TN. Regulation and Function of the PD-L1 Checkpoint. *Immunity* 2018; **48**: 434-452 [PMID: 29562194 DOI: 10.1016/j.immuni.2018.03.014]
14 **Dai S**, Jia R, Zhang X, Fang Q, Huang L. The PD-1/PD-Ls pathway and autoimmune diseases. *Cell Immunol* 2014; **290**: 72-79 [PMID: 24908630 DOI: 10.1016/j.cellimm.2014.05.006]
15 **Nakamori Y**, Park EJ, Shimaoka M. Immune Deregulation in Sepsis and Septic Shock: Reversing Immune Paralysis by Targeting PD-1/PD-L1 Pathway. *Front Immunol* 2020; **11**: 624279 [PMID: 33679715 DOI: 10.3389/fimmu.2020.624279]
16 **Kim JY**, Park M, Kim YH, Ryu KH, Lee KH, Cho KA, Woo SY. Tonsil-derived mesenchymal stem cells (T-MSCs) prevent Th17-mediated autoimmune response *via* regulation of the programmed death-1/programmed death ligand-1 (PD-1/PD-L1) pathway. *J Tissue Eng Regen Med* 2018; **12**: e1022-e1033 [PMID: 28107610 DOI: 10.1002/term.2423]
17 **Mrahleh MA**, Matar S, Jafar H, Wehaibi S, Aslam N, Awidi A. Human Wharton's Jelly-Derived Mesenchymal Stromal Cells Primed by Tumor Necrosis Factor-α and Interferon-γ Modulate the Innate and Adaptive Immune Cells of Type 1 Diabetic Patients. *Front Immunol* 2021; **12**: 732549 [PMID: 34650558 DOI: 10.3389/fimmu.2021.732549]

18 **Guan Q**, Li Y, Shpiruk T, Bhagwat S, Wall DA. Inducible indoleamine 2,3-dioxygenase 1 and programmed death ligand 1 expression as the potency marker for mesenchymal stromal cells. *Cytotherapy* 2018; **20**: 639-649 [PMID: 29548707 DOI: 10.1016/j.jcyt.2018.02.003]

19 **Su W**, Wan Q, Huang J, Han L, Chen X, Chen G, Olsen N, Zheng SG, Liang D. Culture medium from TNF-α-stimulated mesenchymal stem cells attenuates allergic conjunctivitis through multiple antiallergic mechanisms. *J Allergy Clin Immunol* 2015; **136**: 423-32.e8 [PMID: 25652765 DOI: 10.1016/j.jaci.2014.12.1926]

20 **Li N**, Wang J, Zhang N, Zhuang M, Zong Z, Zou J, Li G, Wang X, Zhou H, Zhang L, Shi Y. Cross-talk between TNF-α and IFN-γ signaling in induction of B7-H1 expression in hepatocellular carcinoma cells. *Cancer Immunol Immunother* 2018; **67**: 271-283 [PMID: 29090321 DOI: 10.1007/s00262-017-2086-8]

21 **Ao X**, Yang Y, Li W, Tan Y, Guo W, Ao L, He X, Wu X, Xia J, Xu X, Guo J. Anti-αFR CAR-engineered NK-92 Cells Display Potent Cytotoxicity Against αFR-positive Ovarian Cancer. *J Immunother* 2019; **42**: 284-296 [PMID: 31261167 DOI: 10.1097/CJI.0000000000000286]

22 **Xu F**, Fei Z, Dai H, Xu J, Fan Q, Shen S, Zhang Y, Ma Q, Chu J, Peng F, Zhou F, Liu Z, Wang C. Mesenchymal Stem Cell-Derived Extracellular Vesicles with High PD-L1 Expression for Autoimmune Diseases Treatment. *Adv Mater* 2022; **34**: e2106265 [PMID: 34613627 DOI: 10.1002/adma.202106265]

23 **Garcia-Diaz A**, Shin DS, Moreno BH, Saco J, Escuin-Ordinas H, Rodriguez GA, Zaretsky JM, Sun L, Hugo W, Wang X, Parisi G, Saus CP, Torrejon DY, Graeber TG, Comin-Anduix B, Hu-Lieskovan S, Damoiseaux R, Lo RS, Ribas A. Interferon Receptor Signaling Pathways Regulating PD-L1 and PD-L2 Expression. *Cell Rep* 2017; **19**: 1189-1201 [PMID: 28494868 DOI: 10.1016/j.celrep.2017.04.031]

24 **Hayden MS**, Ghosh S. Regulation of NF-κB by TNF family cytokines. *Semin Immunol* 2014; **26**: 253-266 [PMID: 24958609 DOI: 10.1016/j.smim.2014.05.004]

25 **Shin S**, Lee J, Kwon Y, Park KS, Jeong JH, Choi SJ, Bang SI, Chang JW, Lee C. Comparative Proteomic Analysis of the Mesenchymal Stem Cells Secretome from Adipose, Bone Marrow, Placenta and Wharton's Jelly. *Int J Mol Sci* 2021; **22** [PMID: 33467726 DOI: 10.3390/ijms22020845]

26 **Abbaszadeh H**, Ghorbani F, Derakhshani M, Movassaghpour AA, Yousefi M, Talebi M, Shamsasenjan K. Regenerative potential of Wharton's jelly-derived mesenchymal stem cells: A new horizon of stem cell therapy. *J Cell Physiol* 2020; **235**: 9230-9240 [PMID: 32557631 DOI: 10.1002/jcp.29810]

27 **Liau LL**, Ruszymah BHI, Ng MH, Law JX. Characteristics and clinical applications of Wharton's jelly-derived mesenchymal stromal cells. *Curr Res Transl Med* 2020; **68**: 5-16 [PMID: 31543433 DOI: 10.1016/j.retram.2019.09.001]

28 **Kim HS**, Shin TH, Lee BC, Yu KR, Seo Y, Lee S, Seo MS, Hong IS, Choi SW, Seo KW, Núñez G, Park JH, Kang KS. Human umbilical cord blood mesenchymal stem cells reduce colitis in mice by activating NOD2 signaling to COX2. *Gastroenterology* 2013; **145**: 1392-403.e1 [PMID: 23973922 DOI: 10.1053/j.gastro.2013.08.033]

29 **Hu J**, Zhao G, Zhang L, Qiao C, Di A, Gao H, Xu H. Safety and therapeutic effect of mesenchymal stem cell infusion on moderate to severe ulcerative colitis. *Exp Ther Med* 2016; **12**: 2983-2989 [PMID: 27882104 DOI: 10.3892/etm.2016.3724]

30 **Cha JH**, Chan LC, Li CW, Hsu JL, Hung MC. Mechanisms Controlling PD-L1 Expression in Cancer. *Mol Cell* 2019; **76**: 359-370 [PMID: 31668929 DOI: 10.1016/j.molcel.2019.09.030]

31 **Wang WB**, Yen ML, Liu KJ, Hsu PJ, Lin MH, Chen PM, Sudhir PR, Chen CH, Sytwu HK, Yen BL. Interleukin-25 Mediates Transcriptional Control of PD-L1 *via* STAT3 in Multipotent Human Mesenchymal Stromal Cells (hMSCs) to Suppress Th17 Responses. *Stem Cell Reports* 2015; **5**: 392-404 [PMID: 26321145 DOI: 10.1016/j.stemcr.2015.07.013]

32 **Xu F**, Yi J, Wang Z, Hu Y, Han C, Xue Q, Zhang X, Luan X. IL-27 regulates the adherence, proliferation, and migration of MSCs and enhances their regulatory effects on Th1 and Th2 subset generations. *Immunol Res* 2017; **65**: 903-912 [PMID: 28612255 DOI: 10.1007/s12026-017-8929-8]

33 **Jang IK**, Jung HJ, Noh OK, Lee DH, Lee KC, Park JE. B7H1mediated immunosuppressive properties in human mesenchymal stem cells are mediated by STAT1 and not PI3K/Akt signaling. *Mol Med Rep* 2018; **18**: 1842-1848 [PMID: 29901104 DOI: 10.3892/mmr.2018.9102]

34 **Bellucci R**, Martin A, Bommarito D, Wang K, Hansen SH, Freeman GJ, Ritz J. Interferon-γ-induced activation of JAK1 and JAK2 suppresses tumor cell susceptibility to NK cells through upregulation of PD-L1 expression. *Oncoimmunology* 2015; **4**: e1008824 [PMID: 26155422 DOI: 10.1080/2162402X.2015.1008824]

35 **Mimura K**, Teh JL, Okayama H, Shiraishi K, Kua LF, Koh V, Smoot DT, Ashktorab H, Oike T, Suzuki Y, Fazreen Z, Asuncion BR, Shabbir A, Yong WP, So J, Soong R, Kono K. PD-L1 expression is mainly regulated by interferon gamma associated with JAK-STAT pathway in gastric cancer. *Cancer Sci* 2018; **109**: 43-53 [PMID: 29034543 DOI: 10.1111/cas.13424]

36 **Quandt D**, Jasinski-Bergner S, Müller U, Schulze B, Seliger B. Synergistic effects of IL-4 and TNFα on the induction of B7-H1 in renal cell carcinoma cells inhibiting allogeneic T cell proliferation. *J Transl Med* 2014; **12**: 151 [PMID: 24885059 DOI: 10.1186/1479-5876-12-151]

37 **Kobayashi T**, Siegmund B, Le Berre C, Wei SC, Ferrante M, Shen B, Bernstein CN, Danese S, Peyrin-Biroulet L, Hibi T. Ulcerative colitis. *Nat Rev Dis Primers* 2020; **6**: 74 [PMID: 32913180 DOI: 10.1038/s41572-020-0205-x]

38 **Song MY**, Hong CP, Park SJ, Kim JH, Yang BG, Park Y, Kim SW, Kim KS, Lee JY, Lee SW, Jang MH, Sung YC. Protective effects of Fc-fused PD-L1 on two different animal models of colitis. *Gut* 2015; **64**: 260-271 [PMID: 24902766 DOI: 10.1136/gutjnl-2014-307311]

39 **Beswick EJ**, Grim C, Singh A, Aguirre JE, Tafoya M, Qiu S, Rogler G, McKee R, Samedi V, Ma TY, Reyes VE, Powell DW, Pinchuk IV. Expression of Programmed Death-Ligand 1 by Human Colonic CD90(+) Stromal Cells Differs Between Ulcerative Colitis and Crohn's Disease and Determines Their Capacity to Suppress Th1 Cells. *Front Immunol* 2018; **9**: 1125 [PMID: 29910803 DOI: 10.3389/fimmu.2018.01125]

40 **Moreira TG**, Mangani D, Cox LM, Leibowitz J, Lobo ELC, Oliveira MA, Gauthier CD, Nakagaki BN, Willocq V, Song A, Guo L, Lima DCA, Murugaiyan G, Butovsky O, Gabriely G, Anderson AC, Rezende RM, Faria AMC, Weiner HL. PD-L1(+) and XCR1(+) dendritic cells are region-specific regulators of gut homeostasis. *Nat Commun* 2021; **12**: 4907 [PMID: 34389726 DOI: 10.1038/s41467-021-25115-3]

41 **DA Costa Gonçalves F**, Serafini MA, Mello HF, Pfaffenseller B, Araújo AB, Visioli F, Paz AH. Bioactive factors secreted from mesenchymal stromal cells protect the intestines from experimental colitis in a three-dimensional culture. *Cytotherapy* 2018; **20**: 1459-1471 [PMID: 30523788 DOI: 10.1016/j.jcyt.2018.06.007]

42 **Bilsborough J**, Fiorino MF, Henkle BW. Select animal models of colitis and their value in predicting clinical efficacy of biological therapies in ulcerative colitis. *Expert Opin Drug Discov* 2021; **16**: 567-577 [PMID: 33245673 DOI: 10.1080/17460441.2021.1851185]

World Journal of Stem Cells

Submit a Manuscript: https://www.f6publishing.com

World J Stem Cells 2023 August 26; 15(8): 807-820

DOI: 10.4252/wjsc.v15.i8.807

ISSN 1948-0210 (online)

ORIGINAL ARTICLE

Basic Study

Constitutive aryl hydrocarbon receptor facilitates the regenerative potential of mouse bone marrow mesenchymal stromal cells

Jing Huang, Yi-Ning Wang, Yi Zhou

Specialty type: Cell and tissue engineering

Provenance and peer review: Unsolicited article; Externally peer reviewed.

Peer-review model: Single blind

Peer-review report's scientific quality classification

Grade A (Excellent): 0
Grade B (Very good): B, B, B, B
Grade C (Good): 0
Grade D (Fair): 0
Grade E (Poor): 0

P-Reviewer: Jaing TH, Taiwan; Kode JA, India; Stogov MV, Russia; Tanabe S, Japan

Received: March 28, 2023
Peer-review started: March 28, 2023
First decision: June 25, 2023
Revised: June 29, 2023
Accepted: July 14, 2023
Article in press: July 14, 2023
Published online: August 26, 2023

Jing Huang, Yi-Ning Wang, Yi Zhou, State Key Laboratory of Oral & Maxillofacial Reconstruction and Regeneration, Key Laboratory of Oral Biomedicine Ministry of Education, Hubei Key Laboratory of Stomatology, School & Hospital of Stomatology, Wuhan University, Wuhan 430079, Hubei Province, China

Corresponding author: Yi Zhou, PhD, Associate Professor, Chief Doctor, State Key Laboratory of Oral & Maxillofacial Reconstruction and Regeneration, Key Laboratory of Oral Biomedicine Ministry of Education, Hubei Key Laboratory of Stomatology, School & Hospital of Stomatology, Wuhan University, No. 237 Luoyu Road, Hongshan District, Wuhan 430079, Hubei Province, China. dryizhou@whu.edu.cn

Abstract

BACKGROUND

Bone marrow mesenchymal stromal cells (BMSCs) are the commonly used seed cells in tissue engineering. Aryl hydrocarbon receptor (AhR) is a transcription factor involved in various cellular processes. However, the function of constitutive AhR in BMSCs remains unclear.

AIM

To investigate the role of AhR in the osteogenic and macrophage-modulating potential of mouse BMSCs (mBMSCs) and the underlying mechanism.

METHODS

Immunochemistry and immunofluorescent staining were used to observe the expression of AhR in mouse bone marrow tissue and mBMSCs. The overexpression or knockdown of AhR was achieved by lentivirus-mediated plasmid. The osteogenic potential was observed by alkaline phosphatase and alizarin red staining. The mRNA and protein levels of osteogenic markers were detected by quantitative polymerase chain reaction (qPCR) and western blot. After coculture with different mBMSCs, the cluster of differentiation (CD) 86 and CD206 expressions levels in RAW 264.7 cells were analyzed by flow cytometry. To explore the underlying molecular mechanism, the interaction of AhR with signal transducer and activator of transcription 3 (STAT3) was observed by co-immunoprecipitation and phosphorylation of STAT3 was detected by western blot.

RESULTS

AhR expressions in mouse bone marrow tissue and isolated mBMSCs were detected. AhR overexpression enhanced the osteogenic potential of mBMSCs

while AhR knockdown suppressed it. The ratio of CD86+ RAW 264.7 cells cocultured with AhR-overexpressed mBMSCs was reduced and that of CD206+ cells was increased. AhR directly interacted with STAT3. AhR overexpression increased the phosphorylation of STAT3. After inhibition of STAT3 *via* stattic, the promotive effects of AhR overexpression on the osteogenic differentiation and macrophage-modulating were partially counteracted.

CONCLUSION
AhR plays a beneficial role in the regenerative potential of mBMSCs partially by increasing phosphorylation of STAT3.

Key Words: Aryl hydrocarbon receptor; Bone marrow mesenchymal stromal cells; Osteogenesis; Macrophage; Signal transducer and activator of transcription 3; Interaction

©The Author(s) 2023. Published by Baishideng Publishing Group Inc. All rights reserved.

Core Tip: Aryl hydrocarbon receptor (AhR) was positively expressed in murine bone marrow tissue and bone marrow mesenchymal stromal cells (BMSCs). *In vitro*, overexpression of AhR enhanced the osteogenic potential of mouse BMSCs. Additionally, AhR-overexpressed BMSCs had an increased ability to polarize macrophages to an anti-inflammatory phenotype. While knockdown of AhR showed the opposite effects. Mechanistically, the beneficial effects of AhR were partially dependent on increased phosphorylation of signal transducer and activator of transcription 3. This study suggests that AhR might be a target for achieving optimal bone regeneration in mouse BMSCs-based tissue engineering.

Citation: Huang J, Wang YN, Zhou Y. Constitutive aryl hydrocarbon receptor facilitates the regenerative potential of mouse bone marrow mesenchymal stromal cells. *World J Stem Cells* 2023; 15(8): 807-820
URL: https://www.wjgnet.com/1948-0210/full/v15/i8/807.htm
DOI: https://dx.doi.org/10.4252/wjsc.v15.i8.807

INTRODUCTION

Cell-based tissue engineering is an important method for the treatment of bone defects. Bone marrow mesenchymal stromal cells (BMSCs) are one of the most commonly used seed cells. The osteogenic potential of BMSCs is the premise of their applications in bone regeneration[1]. Additionally, the crosstalk between BMSCs and immune cells like macrophages has been recognized as a critical element in achieving ideal bone tissue repair[2]. Plenty studies have demonstrated that BMSCs are able to trigger a functional switch in macrophages from pro-inflammatory classically activated macrophages (M1) to anti-inflammatory alternatively activated macrophages (M2)[3]. In turn, macrophage polarization is essential for the osteogenic potency of BMSCs. M2 macrophages promote the osteogenesis of BMSCs by secreting pro-regenerative cytokines[4], while M1 macrophages suppress the process[5]. Accordingly, approaches to enhance the osteogenic potential and macrophage-modulating capacity of BMSCs, such as genetic engineering to express specific genes, are continuously being explored.

Aryl hydrocarbon receptor (AhR) is a member of the helix-loop-helix transcription factor superfamily[6]. Historically, AhR has been recognized as a nuclear receptor that responds to environmental toxic stimuli. Recently, increasing number of studies have demonstrated that AhR is an essential modulator in bone turnover[7] and immune responses[8]. AhR can be activated by chemosynthetic agonists such 6-formyl (3,2-b) carbazole (FICZ)[9]. In our previous studies, AhR signaling was suppressed in periodontitis, and FICZ alleviated the inflammatory responses by activating AhR and promoting the phosphorylation of signal transducer and activator of transcription 3 (STAT3)[10]. In another study of our group, FICZ was found to play a beneficial role in the proliferation, osteogenic potential and macrophage-modulation of rat BMSCs and primed cartilage templates[11].

Except for ligand-activated AhR, the role of constitutive unligated AhR in the osteogenic and macrophage-modulating potential of BMSCs has not been investigated. Therefore, the aim of the present study was to: (1) Establish stable AhR-overexpressing or AhR-knockdown mouse BMSCs (mBMSCs); (2) explore the osteogenic differentiation of different mBMSCs; (3) observe the phenotype of macrophages cocultured with different mBMSCs; and (4) investigate the involved molecular mechanism.

MATERIALS AND METHODS

Animal

Six-week-old male C57BL/6 mice were obtained from the Hubei Research Centre of Laboratory Animals (Wuhan, China) and kept in specific pathogen free condition. All experimental protocols were approved by the Institutional Animal Care and Use Committee of School and Hospital of Stomatology, Wuhan University (No. 2020-A08).

Isolation of BMSCs

BMSCs was isolated from 6-week-old male C57BL/6 mice *via* whole femur bone marrow adherent culturing. The femora were excised aseptically, cleaned of soft tissues, and passed through 3 washes with phosphate buffered saline (PBS). The ends of the bones were removed, and the marrow flushed out. The released cells were collected in two 75 cm^2 flasks (Corning) containing 10 mL of 10% fetal bovine serum (Hyclone) in -minimum essential medium. Cultures were maintained in a humidified atmosphere of 95% air and 5% CO_2, at 37°C. After 72 h, all medium was aspirated and replaced to remove the non-adherent cells. The medium was replaced every 2–3 d.

Immunohistochemistry staining

The mice femurs were collected and fixed with 4% paraformaldehyde and then decalcified in 10% ethylene diamine tetraacetic acid for 6 wk. The tissue was subsequently processed for paraffin embedding and serial 4-mm-thick sections were prepared. Then the sections were dewaxed in xylene and rehydrated through graded ethanol to water. Antigen retrieval was conducted in stomach enzyme antigen repair solution for 30 min at 37 °C. Immunostaining was performed by incubating the sections with anti-AhR (NB300-515, 1:200, Novus) at 4 °C overnight. The slides were then washed with PBS and incubated with secondary antibody (Maxim Biotechnology) for 30 min at 37 °C. Staining was visualized with 3, 3-diaminobenzidine and counterstained with hematoxylin.

Immunofluorescent staining

BMSCs at third passage were seeded in cell dish (801002, NEST). After the cells reached 80% confluence, BMSCs were fixed with 4% paraformaldehyde for 15 min and permeabilized with 0.1% Triton X-100 for 20min. Then the cells were blocked with bovine serum albumin (BSA) for 1 h. Subsequently, the cells were incubated with primary antibody against AhR (NB300-515, 1:100, Novus) at 4 °C overnight. After washing, cells were incubated with dylight 594-conjugated secondary antibody (1:200, A23420, Abbkine) for 1 h at room temperature. Then, the cells were stained with 4',6-diamidino-2-phenylindole staining solution (C1005, Beyotime) for 5 min. Finally, the stained cells were observed and photographed under confocal microscope (Leica-LCS-SP8-STED).

Short hairpin RNA design and plasmid preparation

Based on the published sequence of mouse AhR (NM_013464), certain short hairpin RNA (shRNAs) specifically targeting AhR were designed to knockdown their expressions in mBMSCs. The shRNA sequences are as follows: 5′-CATCGA-CATAACGGACGAAAT-3′ (AhR sense) and 5′-ATTTCGTCCGTTATGTCGATG–3′ (antisense). These plasmid DNAs transcribed shRNAs with loop sequences of 5′-CTCGAG–3′. In parallel, a negative control (NC) sequences were projected (sense: 5′-TTCTCCGAACGTGTCACGT-3′, antisense: 5′-ACGTGACACGTTCGGAGAA-3′), which had no homology with human proteins. The generated oligo DNA was cloned into GV493 vector (hU6-MCS-CBh-gcGFP-IRES-puromycin) (GENECHEM, Shanghai).

AhR overexpression plasmid

The coding sequences of mouse AhR (NM_013464) was cloned into GV358 vector (Ubi-MCS-3FLAG-SV40-EGFP-IRES-puromycin) (GENECHEM, Shanghai). The empty Ubi-MCS-SV40-EGFP-IRES-puromycin vector was served as NC.

Lentiviral packaging and infection of mBMSCs

The 293T packaging cell line was co-transfected with plasmid and lentiviral helper vectors (GENECHEM, Shanghai). The medium was replaced with fresh dulbecco's modified eagle medium overnight. After another 48 h, the supernatants were collected and filtered. The viral supernatants were concentrated *via* ultracentrifuging at the speed of 25000 rpm for 2 h at 4°C. One day prior to infection, mBMSCs were seeded in 6-well plates at the density of 10^5 cells/well. Then the mBMSCs were infected with lentiviral particles containing plasmids of knockdown-NC (sh-NC), knockdown-AhR (sh-AhR), overexpression-NC (oe-NC) or overexpression-AhR (oe-AhR) *via* multiplicity of infection level of 20. After 12-16 h, the culture medium was refreshed. Then the cells were cultured in complete medium containing 2 mg/mL puromycin.

qPCR

Total RNA from different cell samples were isolated by Trizol reagent (Takara Bio). SYBR Green Reagent (Takara Bio) was used to perform qPCR in a 7500 Fast Real-Time PCR system (Applied Biosystem). The primer sequences used in the study was showed in Table 1. The relative expression levels were calculated using the 2-DDCt method. Three biological replicates were conducted.

Western blot

Total proteins were extracted from cells with radio immunoprecipitation assay buffer supplemented with 1:100 proteinase and phosphatase inhibitors. The proteins were separated by 10% sodium dodecyl sulphate (SDS)-polyvinylidene fluoride membranes (Roche). After blocked with 5% milk, the membranes were incubated with primary antibody at 4°C overnight. Then the membranes were then incubated with horseradish peroxidase-conjugated secondary antibody for 1 h at room temperature. Subsequently, the bands were visualized with electro-chemi-luminescence detection reagents (Thermo Scientific). Anti-AhR (NB300-515, 1:200, Novus), anti-biomineralization associated [tissue-nonspecific alkaline phosphatase (ALPL)] (11187-1-AP, 1:1000, Proteintech), anti-runt-related transcription factor 2 (RUNX2) (PB0171, 1:2000, Boster), anti-phosphorylated STAT3 (Tyr705) (9145, 1:1000, CST), anti-STAT3 (9139, 1:1000, CST) and anti-glyceraldehyde-3-phosphate dehydrogenase (GAPDH) (BM3876, 1:5000, Boster) primary antibodies were

Table 1 Primer sequences for quantitative polymerase chain reaction (5'-3')

Gene	Sequences
GAPDH	Forward: TGGAAAGCTGTGGCGTGAT
	Reverse: GTCATCATACTTGGCAGGTTTCT
AhR	Forward: GGCTTTCAGCAGTCTGATGTC
	Reverse: CATGAAAGAAGCGTTCTCTGG
ALPL	Forward: GGGCGTCTCCACAGTAACCG
	Reverse: ACTCCCACTGTGCCCTCGTT
RUNX2	Forward: GAGTCAGATTACAGATCCCA
	Reverse: TGGCTCTTCTTACTGAGAGA

GAPDH: Glyceraldehyde-3-phosphate dehydrogenase; AhR: Aryl hydrocarbon receptor; ALPL: Tissue-nonspecific alkaline phosphatase; RUNX2: Runt-related transcription factor 2.

used. Three biological replicates were conducted.

Osteogenic induction, alkaline phosphatase staining and alizarin red staining

For osteogenic induction, mBMSCs at passage 3 from different groups (sh-NC, sh-AhR, oe-NC or oe-AhR) were cultured in medium supplemented with 50 mg/mL ascorbic acid, 10 mmol/L b-glycerophosphate and 10^{-8} mol/L dexamethasone (Sigma). Then, cells were fixed in 4% paraformaldehyde for 10 min and stained using alkaline phosphatase (ALP) Color Development Kit (C3206, Beyotime) following the manufacturer's instructions. For alizarin red staining (ARS), cells were fixed and stained with alizarin red solution (Cyagen) for 10 min. Three biological replicates were conducted.

Co-culture of mBMSCs and RAW264.7 cells

For direct coculture, mBMSCs from all groups (sh-NC, sh-AhR, oe-NC or oe-AhR) were plated in monoculture at the density of 5 10^5 cells/well at 6-well plate. After the adherence of mBMSCs, the macrophage linage RAW264.7 cells (ScienceCell, Shanghai) (1 10^5 cells/well) were seeded into the wells. The cells were harvested after 24 h of coculture.

For indirect coculture, conditional medium from the culture of sh-NC, sh-AhR, oe-NC or oe-AhR mBMSCs were collected. The conditioned medium was harvested and centrifuged for 10 min at 1000 rpm and then frozen at -20 °C until used. The RAW 264.7 was treated with 1:2 fresh medium and conditioned medium for 24 h.

Flow cytometry

The macrophage surface markers of RAW264.7 cells in the coculture system was detected by flow cytometry. Three biological replicates were conducted.

For direct coculture, the mBMSCs and RAW264.7 cells were collected from 6-well plates after coculture for 24 h and washed three times with PBS. The cell suspensions were divided into 1.5 mL Eppendorf micro test tubes (EP tubes) and incubated with blocking 3% BSA. Then the cell suspensions were incubated with allophycocyanin anti-F4/80 (157305, BioLegend), combined with fluorescein isothiocyanate (FITC) anti-cluster of differentiation (CD) 86 (105005, BioLegend) or PerCP/Cy5.5 anti-CD206 (141715, BioLegend) at 4°C for 1 h.

For indirect coculture, the RAW264.7 cells were collected and washed three times with PBS. The cell suspensions were divided into 1.5 mL EP tubes and incubated with blocking 2% BSA. Then the cell suspensions were successively incubated with CD86 (13395-1-AP, Proteintech) or CD206 (18704-1-AP, Proteintech), and FITC conjugated immunoglobulin G (BA1105, Boster).

The above cells were washed three times after incubation and suspended in 500 mL containing 3% fetal bovine serum and then detected by Beckman Coulter CytoFLEX S and analyzed by CytoExpert.

Co-immunoprecipitation

The AhR and p65 protein-protein interaction was detected by co-immunoprecipitation (Co-IP) kit (P2179S, Beyotime) following manufacturer's instructions. The mBMSCs protein sample was extracted from cells with lysis buffer supplemented with protease inhibitor cocktail. The AhR antibody (NB300-515, 1:100, Novus) was incubated with protein A+G beads at room temperature for 2 h and then washed three times using Tris buffered saline. Then the beads-antibody complex was immunoprecipitated with mBMSCs protein sample at 4°C overnight. After washed three times using lysis buffer, the beads-antibody-antigen complex was eluted SDS-polyacrylamide gel electrophoresis sample loading buffer. After magnetic separation, the expression of STAT3 in the supernatant was detected using STAT3 primary antibody (9139, 1:1000, CST) *via* western blot. Three biological replicates were conducted.

STAT3 inhibitor stattic

To testify whether the effects of AhR in osteogenic differentiation and macrophage-modulating was partially STAT3-

dependent or not, a specific STAT3 inhibitor stattic (Selleck) was introduced. In osteogenic induction, oe-NC and oe-AhR mBMSCs were cultured in osteogenic medium supplemented with or without 2 mmol/L stattic. For indirect coculture system of mBMSCs and RAW 264.7 cells, the mixed fresh and conditioned medium from mBMSCs was supplemented with or without 2 mmol/L stattic. Three biological replicates were conducted for each treatment.

Statistical analysis

All data were expressed as the mean ± SD. For comparison between two groups, statistical differences were evaluated by a two-tailed Student's *t* test. For multiple comparisons, a one-way analysis of variance (ANOVA) followed by Tukey's test were conducted. *P*-value < 0.05 was considered statistically significant.

RESULTS

The expression of AhR in bone marrow of mouse femurs and isolated mBMSCs

The immunohistochemistry (IHC) staining showed that AhR was expressed in parts of mouse femur bone marrow (Figure 1A-C). In isolated mBMSCs derived from femurs, AhR expression was positively observed *via* immunofluorescence staining (Figure 1D-I), which was consistent with the IHC results.

AhR overexpression or knockdown in mBMSCs

At 48 h after infection with oe-AhR or sh-AhR and their NC lentivirus (oe-NC and sh-NC), the efficiencies of AhR overexpression or knockdown were confirmed by qPCR and western blot. The qPCR data (Figure 2A) showed that the relative AhR mRNA expression level of the oe-NC and oe-AhR groups were 0.85 ± 0.08 and 4.39 ± 0.23 respectively, and those of the sh-NC and sh-AhR groups were 1.13 ± 0.14 and 0.16 ± 0.01, respectively. The western blot results (Figure 2B and C) demonstrated that the relative AhR/GAPDH protein levels of the oe-NC and oe-AhR groups were (0.29 ± 0.05) and (0.45 ± 0.07), and those of the sh-NC and sh-AhR groups were 0.31 ± 0.11 and 0.04 ± 0.01 respectively. The data indicated that AhR was significantly overexpressed or knocked down in oe-AhR or sh-AhR mBMSCs.

The effect of oe-AhR or sh-AhR on the osteogenic differentiation of mBMSCs

At the 7th day of osteogenic induction, ALP staining showed that AhR overexpression resulted in more positive nodules than the NC (Figure 3A). Consistently, after 14 d of osteogenic induction, the visualization of calcium deposits and mineralized nodules by ARS also demonstrated that AhR overexpression promoted the osteogenic potential of mBMSCs (Figure 3A). In contrast, AhR knockdown suppressed the nodules formation and calcium deposition, as showed by ALP staining and ARS, compared to the NC (Figure 3A).

At the 7th day of osteogenic induction, the mRNA levels of the osteogenic markers ALP, ALPL and RUNX2 in oe-AhR mBMSCs were significantly higher than those in oe-NC mBMSCs (Figure 3B), while those in sh-AhR cells were lower than those in sh-NC cells (Figure 3C). Then, the protein samples were harvested after 7 d of osteogenic induction and were subjected to western blotting. The bands showed increased protein expressions of ALPL and RUNX2 in oe-AhR mBMSCs compared to oe-NC mBMSCs, while sh-AhR inhibited their expressions compared to sh-NC (Figure 3D), which was basically consistent with the mRNA results.

The effect of oe-AhR or sh-AhR on the macrophage-modulating capacity of mBMSCs

Brightfield images of direct coculture were captured prior to analysis (Figure 4A), and the morphologies of the RAW 264.7 cells and different groups of mBMSCs were similar. In flow cytometry analysis of direct coculture samples, the ratio of M1-like macrophages among RAW 264.7 cells was calculated as CD86 + (Q1-UR)/F4/80 + (Q1-UR + Q1-LR) (Figure 4B). Similarly, the ratio of M2-like macrophages among RAW 264.7 cells was calculated as CD206 + (Q2-UR)/F4/80 + (Q2-UR + Q2-LR) (Figure 4C). Quantitative analysis (Figure 4D) demonstrated that the ratio of CD86+ cells and CD206+ cells was not significantly different between RAW 264.7 cells cocultured with oe-AhR and those cocultured with oe-NC mBMSCs. While the ratio of CD86+ cells among RAW 264.7 cocultured with sh-AhR mBMSCs was significantly higher than that among RAW 264.7 cocultured with sh-NC mBMSCs.

In the indirect coculture system, RAW 264.7 cells were cultured with conditioned medium from different mBMSCs. The CD86 and CD206 expressions were demonstrated using histograms (Figure 5A and B). Quantitative analysis (Figure 5C) showed that the ratio of CD86+ cells was significantly lower and the ratio of CD206+ cells was significantly higher in the oe-AhR group than oe-NC. The ratio of CD86+ cells in the sh-AhR group was significantly higher than that in sh-NC.

The above data suggested that knockdown of AhR in mBMSCs tends to drive macrophages toward the M1-like phenotype and inhibit M2-like polarization. Overexpression of AhR in mBMSCs showed the opposite macrophage-modulating effect.

The molecular mechanism underlying the role of AhR in the osteogenic differentiation and macrophage modulation of mBMSCs

First, the AhR and STAT3 protein-protein interaction was detected *via* Co-IP (Figure 6A). Then, the effect of AhR overexpression or knockdown on the phosphorylation of STAT3 was explored by western blotting (Figure 6B). The results showed that oe-AhR promoted the phosphorylation of STAT3 while sh-AhR suppressed it. To test whether the effects of AhR on osteogenic differentiation and macrophage-modulating were partially STAT3-dependent or not, a specific STAT3

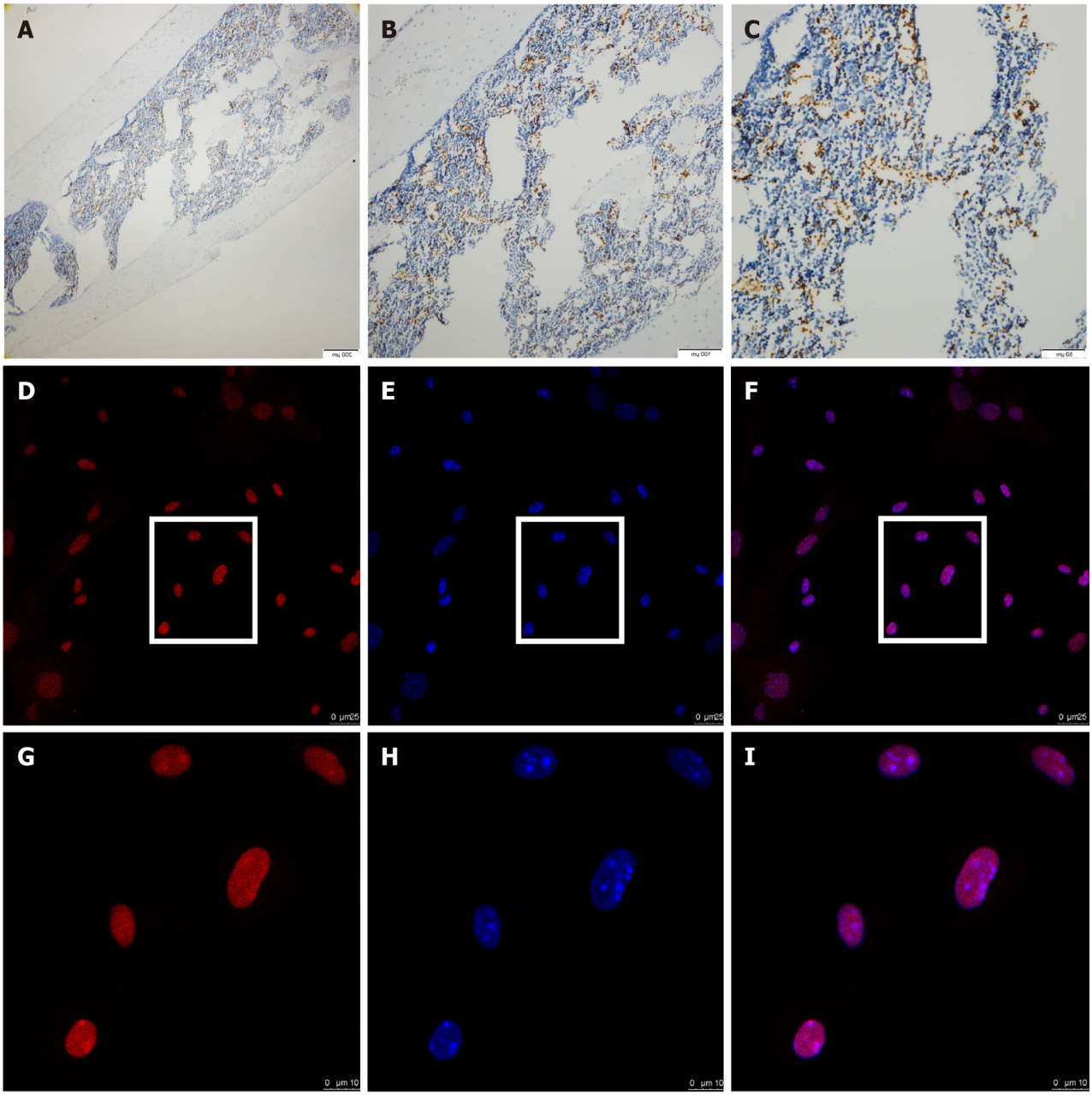

DOI: 10.4252/wjsc.v15.i8.807 **Copyright** ©The Author(s) 2023.

Figure 1 The expression of aryl hydrocarbon receptor in bone marrow tissue of mouse femur and isolated bone marrow mesenchymal stromal cells. A-C: Immunochemistry staining showed positive aryl hydrocarbon receptor (AhR) expression in bone marrow tissue [bar: 200 mm (left), 100 mm (middle) and 50 mm (right)]. D-I: Immunofluorescence staining of AhR in mouse bone marrow mesenchymal stromal cells *via* confocal microscopy (red: AhR; blue: 4',6-diamidino-2-phenylindole; pink: Merge) [bar: 25mm (D-F) and 10mm (G-I)].

inhibitor, stattic, was introduced. The western blotting lanes testified that 2 mmol/L stattic partially alleviated the AhR overexpression-mediated increase in STAT3 phosphorylation (Figure 6C). ALP staining at the 7th day of osteogenic induction and ARS at the 15th day indicated that 2 mmol/L stattic partially reversed the elevated osteogenic potential mediated by AhR overexpression (Figure 6D). Regarding macrophage modulation, the flow cytometry and quantitative analysis manifested that 2 mmol/L stattic partially reversed the inhibition of CD86 expression and promotion of CD206 in RAW 264.7 cells cultured with conditioned medium from oe-AhR mBMSCs (Figure 6E and F). The above data suggested that AhR promoted the osteogenic and macrophage-modulating potentials of mBMSCs partially by interacting with STAT3 and increasing the phosphorylation of STAT3.

DISCUSSION

Based on the results, and within the limitations of the present study, it could be concluded that: (1) Endogenous unligated AhR promoted osteogenic potential of mBMSCs; (2) endogenous unligated AhR played a positive role in polarizing

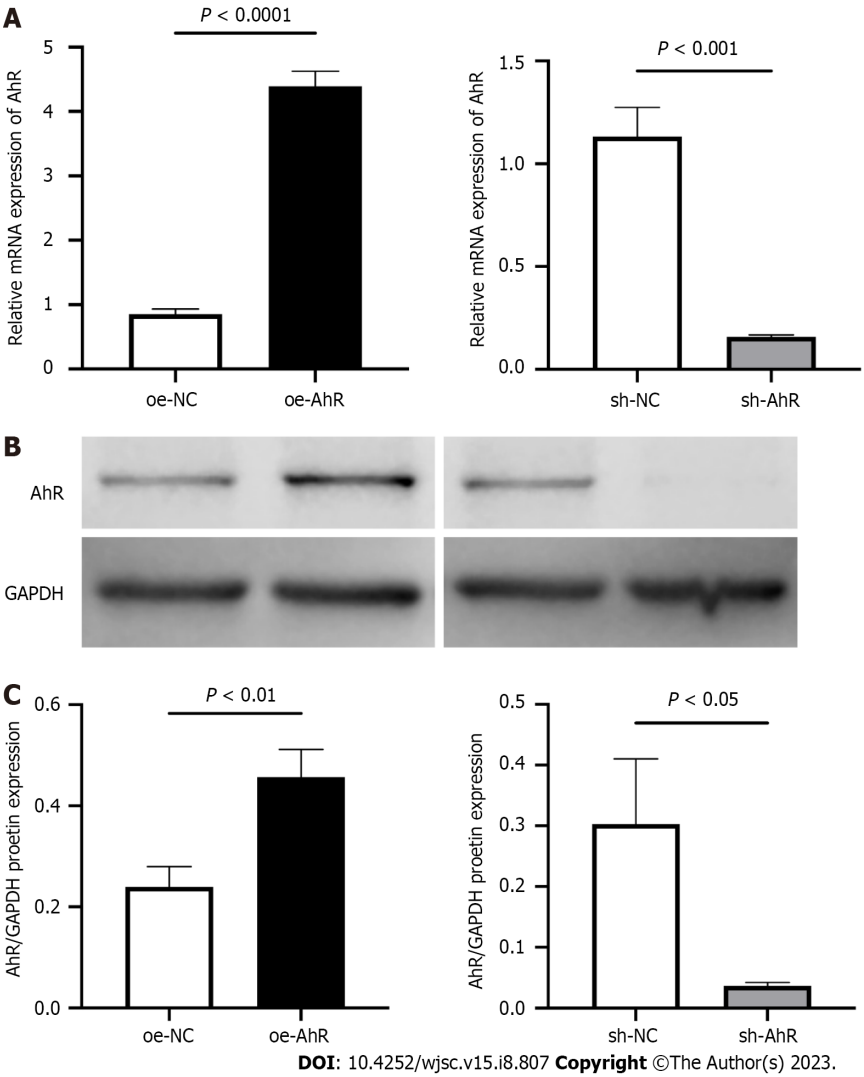

DOI: 10.4252/wjsc.v15.i8.807 **Copyright** ©The Author(s) 2023.

Figure 2 Overexpression or knockdown of aryl hydrocarbon receptor in mouse bone marrow mesenchymal stromal cells. A: Quantitative polymerase chain reaction data of aryl hydrocarbon receptor (AhR) mRNA level of overexpression-AhR (oe-AhR) or knockdown-AhR (sh-AhR) and their negative controls; B: Representative images of western blot of AhR in oe-AhR or sh-AhR; C: Semi-quantitation of lanes in western blot. AhR: Aryl hydrocarbon receptor; GAPDH: Glyceraldehyde-3-phosphate dehydrogenase; oe-NC: Overexpression-negative control; oe-AhR: Overexpression-AhR; sh-NC: Knockdown-negative control; sh-AhR: Knockdown-AhR.

macrophages towards the M2-like phenotype of mBMSCs; and (3) the function of AhR was partially dependent on interacting with STAT3 and increasing the phosphorylation of STAT3. The present study offered new insights into the role of AhR and the involved molecular mechanism in the regenerative potential of mBMSCs, which might be a target for achieving optimal bone regeneration in mBMSCs-based tissue engineering.

The nuclear receptor AhR is positively expressed in bone tissue, including osteoblasts and osteoclasts, and the AhR signaling pathway plays a vital role in bone homeostasis[12]. AhR was previously considered as an environment xenobiotic sensor and mediates oxidative stress[13]. In recent decades, the roles of AhR as a transcription factor in regulating various biological processes have been revealed. Plenty studies have focused on the functions of ligand-activated AhR in biological processes. However, the effects of AhR might vary due to interactions with different ligands. The first identified AhR ligand was a dioxin-like compound (DLC), 2,3,7,8-tetrachlorodibenzo-p-dioxin (TCDD), which mediates toxic effects after binding to AhR. Then, various kinds of non-dioxin-like endogenous ligands were identified, such as FICZ, 2-(1′-H–indole–3-carbonyl) thiazole–4-carboxylic acid methyl ester, and tryptophan metabolites such as kynurenine, which demonstrated functional diversity[9].

Regarding osteogenic potential, AhR activated by DLC ligands such as TCDD is basically harmful[14], but the effects of endogenous ligands such as FICZ are controversial. In a recent study, two different AhR ligands, benzo[a]pyrene (B[a]P) and FICZ, were analyzed in mice temporomandibular joint osteoarthritis[15]. The above study demonstrated that B[a]P induced mandibular subchondral bone resorption in an AhR-dependent manner. However, FICZ exerted a therapeutic effect and rescued the bone loss *in vivo* at both low (100mg/kg) and high (100mg/kg) concentrations. Moreover, 200ng/mL FICZ promoted the osteogenic differentiation on MC3T3 E1 cells *in vitro*, resulting in more obvious ALP staining and ARS, and increased mRNA expressions of osteogenic markers, including ALP, osteocalcin (OCN) and collagen type I alpha 1. Consistently, in a previous study by our group, 500 nM FICZ enhanced the ALP staining and ARS of rat BMSCs

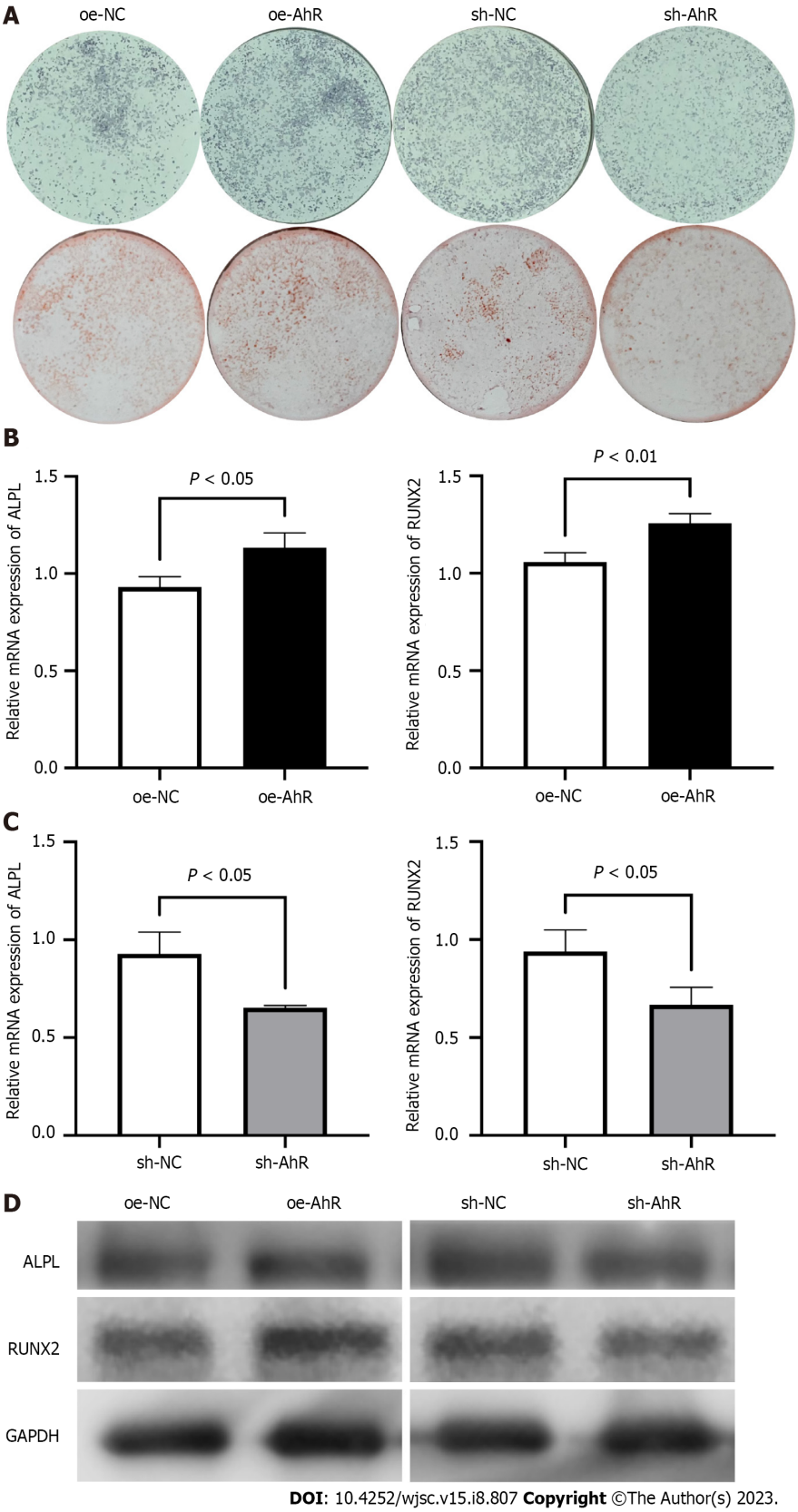

DOI: 10.4252/wjsc.v15.i8.807 **Copyright** ©The Author(s) 2023.

Figure 3 The effect of aryl hydrocarbon receptor overexpression or knockdown on the osteogenic differentiation in mouse bone marrow mesenchymal stromal cells. A: Alkaline phosphatase (ALP) staining (upper) at 7th day and Alizarin red staining staining (lower) at 14th day of osteogenic induction; B: Relative mRNA expression of ALP, biomineralization associated [tissue-nonspecific alkaline phosphatase (ALPL)] and runt-related transcription factor 2 (RUNX2) of overexpression-negative control and overexpression-aryl hydrocarbon receptor (AhR) mouse bone marrow mesenchymal stromal cells (mBMSCs); C: Relative ALPL and RUNX2 mRNA expression of knockdown-negative control and knockdown-AhR mBMSCs at 7th day of osteogenic induction; D: Representative images of western blot of ALPL and RUNX2 in mBMSCs of different groups at 7th day of osteogenic induction. oe-NC: Overexpression-negative control; oe-AhR: Overexpression-aryl hydrocarbon receptor; sh-NC: Knockdown-negative control; sh-AhR: Knockdown-aryl hydrocarbon receptor; ALPL: Tissue-nonspecific alkaline

phosphatase; RUNX2: Runt-related transcription factor 2; GAPDH: Glyceraldehyde-3-phosphate dehydrogenase.

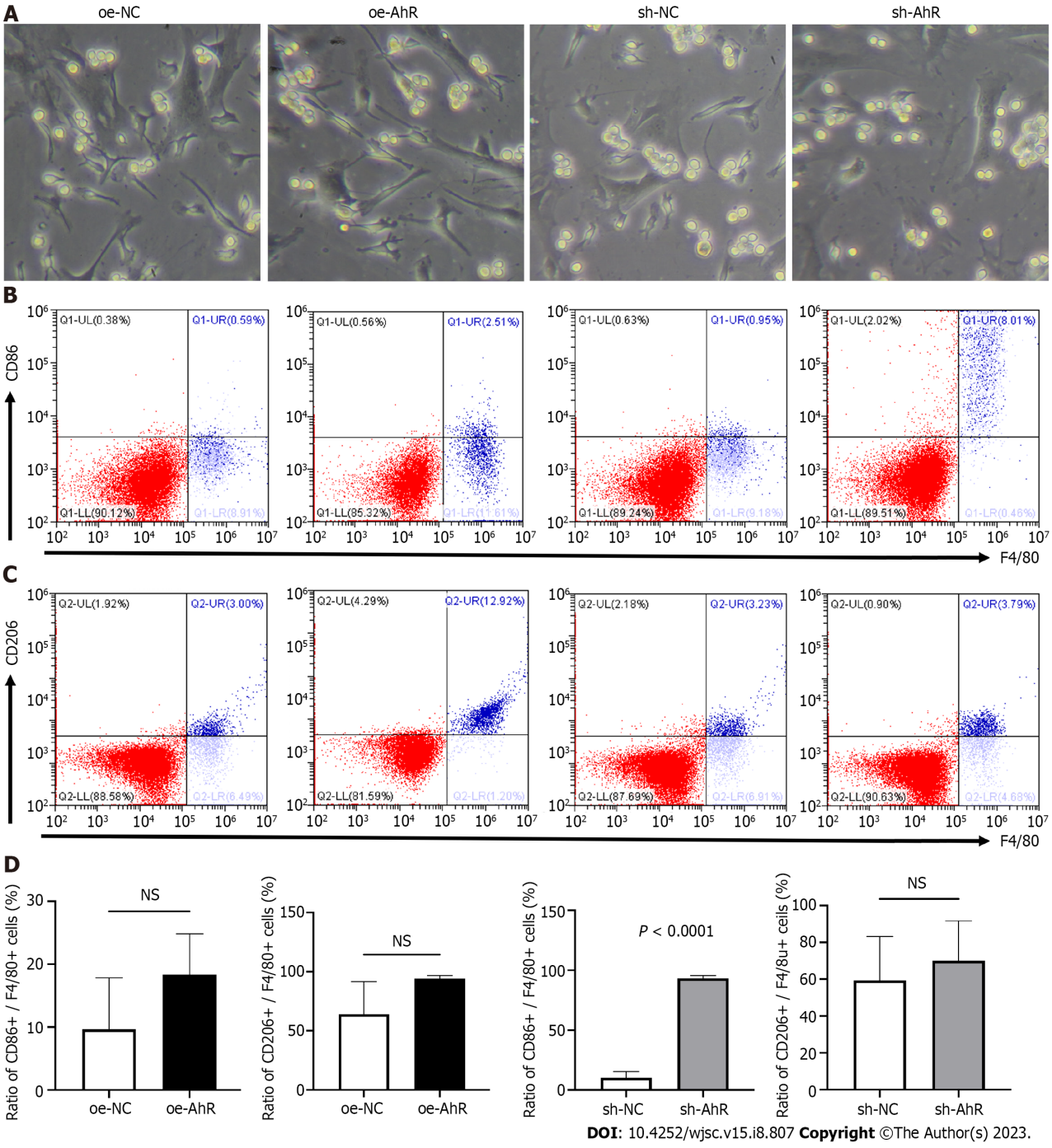

DOI: 10.4252/wjsc.v15.i8.807 Copyright ©The Author(s) 2023.

Figure 4 The cluster of differentiation (CD) 86 and CD206 expressions of RAW 264.7 cells that directly co-cultured with different mouse bone marrow mesenchymal stromal cells. A: The brightfield images of the coculture system (10 objective lens); B: The typical four-quadrant images of flow cytometry after direct coculture of RAW 264.7 cells and mBMSCs (X-axis: F4/80; Y-axis: CD86); C: The typical four-quadrant images of flow cytometry after direct coculture of RAW 264.7 cells and mBMSCs (X-axis: F4/80; Y-axis: CD206); D: Quantitative analysis of CD86 + (Q1-UR)/F4/80 + (Q1-UR + Q1-LR) and CD206 + (Q2-UR)/F4/80 + (Q2-UR + Q2-LR) ratios in direct coculture system. oe-NC: Overexpression-negative control; oe-AhR: Overexpression-aryl hydrocarbon receptor; sh-NC: Knockdown-negative control; sh-AhR: Knockdown-aryl hydrocarbon receptor; NS: Not significant.

after osteogenic induction[11]. In addition to ligand-activated AhR, its role in bone ossification was investigated in transgenic mice. In the semistable fracture healing model in mice, the expression of AhR in the healing callus tissue was more than 2-fold higher on the seventh day after fracture than in uninjured samples. On the 14th day after fracture, AhR expression had increased by 10-fold in callus tissue. To determine whether the loss of AhR affects bone healing, the researchers established a tibial fracture model in wild type (WT) mice and AhR knockout (KO) mice and performed micro-computed tomography (micro-CT) scan analysis two weeks later. Mineralized callus tissue in the fracture gap was

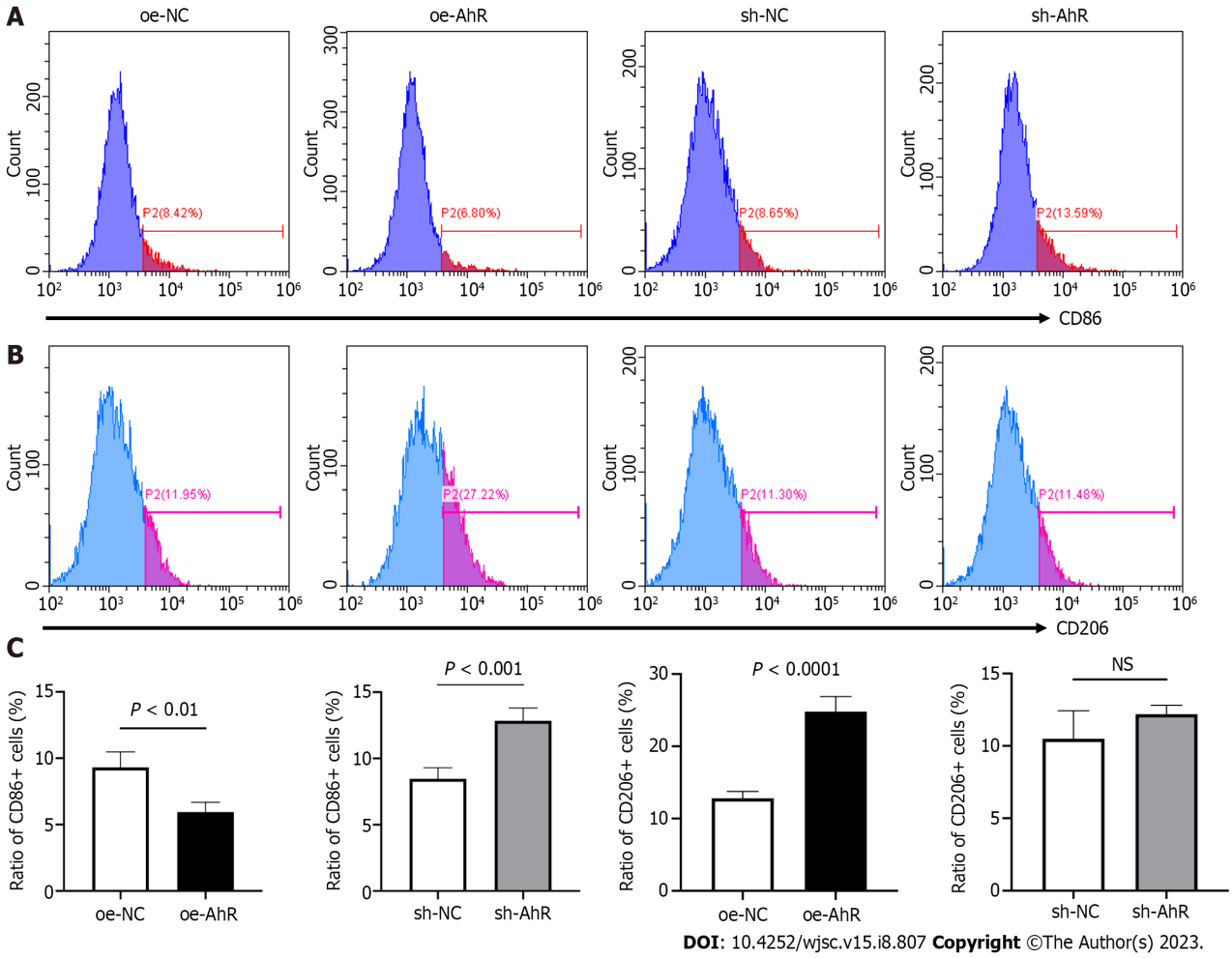

DOI: 10.4252/wjsc.v15.i8.807 **Copyright** ©The Author(s) 2023.

Figure 5 The cluster of differentiation (CD) 86 and CD206 expressions of RAW 264.7 cells that cocultured with conditioned medium from different mouse bone marrow mesenchymal stromal cells. A: The typical histograms of CD86 expressions of RAW 264.7 cells; B: The typical histograms of CD206 expressions of RAW 264.7 cells; C: Quantitative analysis of ratios of CD86+ and CD206+ cells. oe-NC: Overexpression-negative control; oe-AhR: Overexpression-aryl hydrocarbon receptor; sh-NC: Knockdown-negative control; sh-AhR: Knockdown-aryl hydrocarbon receptor; NS: Not significant.

observed in the former but not the latter mice. At the third week, micro-CT analysis also showed that AhR KO mice had less bone formation than WT mice[7]. In another study[16], the ALP and OCN mRNA expression levels of BMSCs obtained from AhR KO mice were lower than those of WT mice after 8-10 d of osteogenic induction. Interestingly, the ALP and OCN expression patterns in the BMSCs of AhR KO mice after osteogenic induction were rather parallel to the TCDD-suppressed responses in BMSCs from WT mice. The results of present study were consistent with above literatures.

Additionally, AhR has been proven to be involved in modulating immune/inflammatory disease by targeting specific gene expression and altering immune differentiation[8]. Similarly, complex ligand interactions that control AhR function might result in diverse immunologic effects including immunosuppressive or pro-inflammatory downstream functions [17]. In another study, peritoneal macrophages from WT and AhR-null mice were polarized toward the M1 or M2 phenotype by stimulation with lipopolysaccharide/interferon-g or interleukin (IL)-4[18]. The results indicated that AhR-null macrophages presented higher levels of M1 markers including IL-1b, IL-6, IL-12 and tumor necrosis factor-a, and lower levels of M2 markers, including chitinase-like 3 (or called Ym1) and IL-10. It was found that the binding of AhR to the promoters of IL-10 and arginase-1 was increased in macrophages after uptake of apoptotic cells to promote M2 polarization[19]. AhR not only affects the phenotype of macrophages themselves but also influences the results of other cells in regulating macrophage polarization. Treatment with the AhR ligand FICZ attenuated calcium oxalate nephrocalcinosis in a mouse model. Bone marrow-derived macrophages (BMDMs) and calcium oxalate monohydrate (100mg/mL)-treated renal tubular epithelial cells were cocultured in transwell system. FICZ supplement in the system promoted the expression of M2 markers and diminished the expression of M1 markers in BMDMs. The molecular mechanism was that AhR directly targeted downstream microRNA-142a-3p, which suppressed interferon regulatory factor 1 and hypoxia inducible factor 1 alpha by binding to their 3′ untranslated region[20]. In another study, another AhR ligand, TCDD, was added to a coculture system of mBMSCs and macrophages. Treatment of BMSCs with TCDD resulted in a significant increase in M2 markers and a decrease in M1 markers in macrophages. The AhR antagonist CH223191 alleviated the macrophage-modulating effect[21]. In the present study, AhR overexpression in mBMSCs promoted its ability of polarizing macrophages into M2-like phenotype.

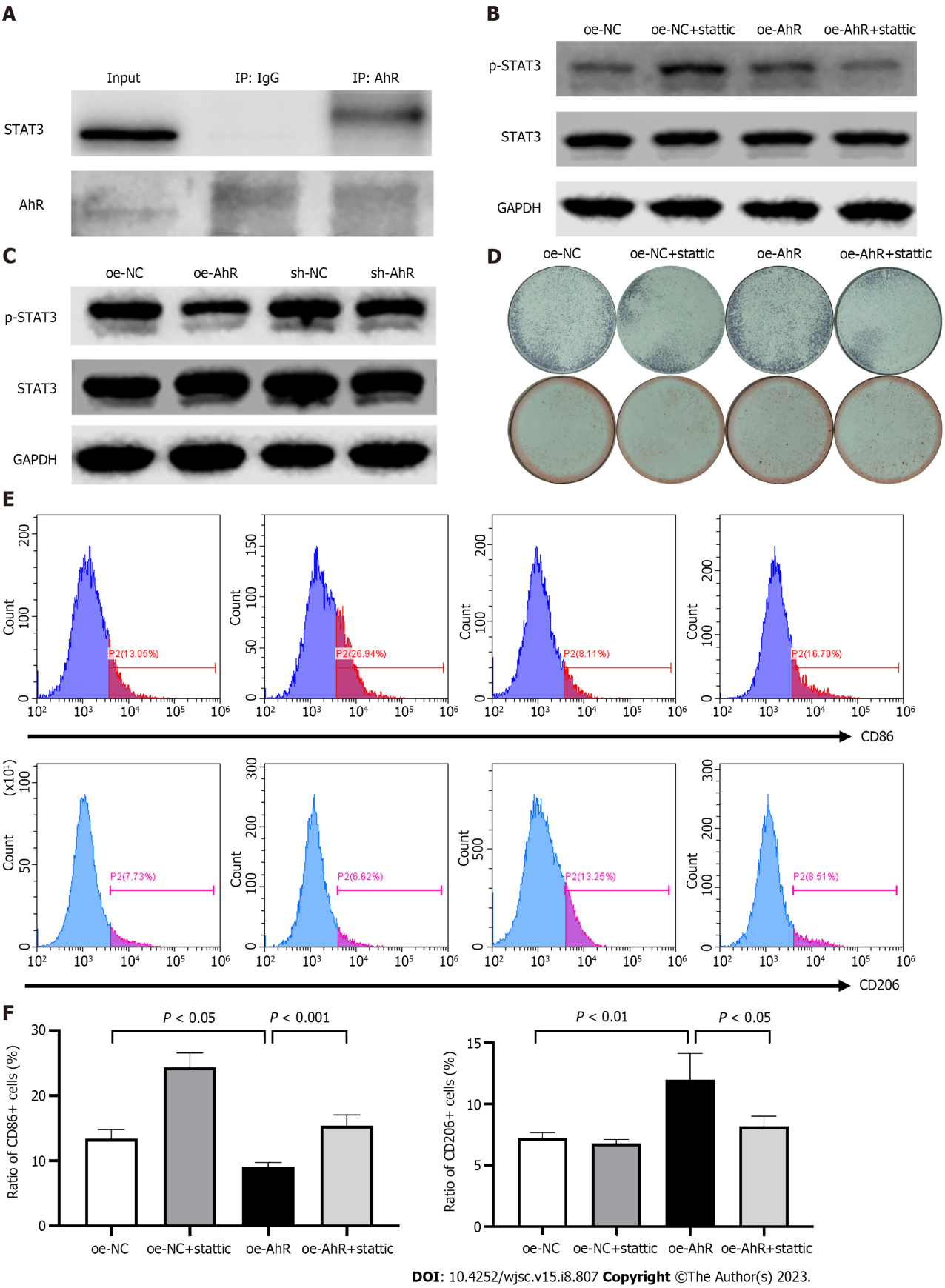

DOI: 10.4252/wjsc.v15.i8.807 **Copyright** ©The Author(s) 2023.

Figure 6 The molecular mechanism of the role of aryl hydrocarbon receptor in osteogenic differentiation and macrophage-modulating in mouse bone marrow mesenchymal stromal cells. A: Co-immunoprecipitation assay showed that aryl hydrocarbon receptor (AhR) and signal transducer and activator of transcription 3 (STAT3) directly interacted in mouse bone marrow mesenchymal stromal cells (mBMSCs); B: Western blot lanes demonstrated that AhR overexpression promoted phosphorylation of STAT3 compared to negative control, while AhR knockdown suppressed it; C: The specific STAT3 inhibitor stattic (2

mmol/L) partially alleviated the promoted STAT3 phosphorylation by AhR overexpression; D: Alkaline phosphatase (upper) and alizarin red staining (lower) staining indicated that 2 mmol/L stattic partially inhibited the elevated osteogenic potential by AhR overexpression; E and F: The histograms of flow cytometry and quantitative analysis manifested that 2 mmol/L stattic partially reversed the CD86 inhibition and CD206 promotion in RAW 264.7 by conditioned medium from overexpression-AhR mBMSCs. AhR: Aryl hydrocarbon receptor; oe-NC: Overexpression-negative control; oe-AhR: Overexpression-AhR; sh-NC: Knockdown-negative control; sh-AhR: Knockdown-AhR; STAT3: Signal transducer and activator of transcription 3; p-STAT3: Phosphorylated STAT3; GAPDH: Glyceraldehyde-3-phosphate dehydrogenase.

It was reported that AhR signaling exhibits considerable crosstalk with other transcription factors, such as those in the nuclear factor-kB family and signal transducer and activator of transcription family[17,22]. AhR can bind to other molecules to undergo a conformational change exposing a nuclear localization signal[17]. STAT3 is critical in regulating immune responses[23] and osteogenic differentiation processes[24]. Our previous study showed that FICZ-stimulated AhR alleviated the inflammatory response in periodontal ligament cells by increasing the phosphorylation of STAT3[10]. The interplay between AhR and STAT3 was explored in various cell types. In A549 cells the interaction of AhR and STAT3 was detected *via* Co-IP. Increased AhR by reduning upregulated the expression of STAT3 and the downstream IL-10, which alleviate severe pneumonia[25]. *Lactobacillus johnsonii* N6.2-derived nano-sized vesicles led to the nuclear translocation of AhR in pancreatic b cells and enhanced the phosphorylation of STAT3 and expression of IL-10, which reduced the apoptosis and improved the expression of genes related to glucose transport[26]. In the present study, the direct AhR and STAT3 interaction was also observed in mBMSCs. Moreover, AhR overexpression upregulated the phosphorylation of STAT3. However, the further research is needed to fully understand the precise molecular mechanisms underlying the AhR-STAT3 interaction.

CONCLUSION

In conclusion, AhR plays a promotive role in the regenerative potential of mBMSCs, including osteogenic differentiation and polarizing macrophages to an anti-inflammatory phenotype. Mechanistically, AhR can interact with STAT3, thereby increasing the phosphorylation level of STAT3. Inhibition of STAT3 partially counteracted the beneficial effect of AhR. Hence, AhR might be a target for achieving optimal bone regeneration in mBMSCs-based tissue engineering.

ARTICLE HIGHLIGHTS

Research background

Bone marrow mesenchymal stromal cells (BMSCs) are one of the most commonly used seed cells in bone tissue engineering. Aryl hydrocarbon receptor (AhR) has been recognized as a nuclear receptor that modulates bone turnover. However, the function of constitutive AhR in BMSCs remains unclear.

Research motivation

To explore whether AhR is involved in the regenerative potential of mouse BMSCs (mBMSCs).

Research objectives

To investigate the role of AhR in the osteogenic and macrophage-modulating potential of mBMSCs and the underlying mechanism.

Research methods

Immunochemistry and immunofluorescent staining were used to observe the expression of AhR in mouse bone marrow tissue and mBMSCs. The overexpression or knockdown of AhR was achieved by lentivirus-mediated plasmid. The osteogenic potential was observed by alkaline phosphatase and alizarin red staining. The mRNA and protein levels of osteogenic markers were detected by quantitative polymerase chain reaction and western blot. After coculture with different mBMSCs, the cluster of differentiation (CD) 86 and CD206 expressions levels in RAW 264.7 cells were analyzed by flow cytometry. To explore the underlying molecular mechanism, the interaction of AhR with signal transducer and activator of transcription 3 (STAT3) was observed by co-immunoprecipitation and phosphorylation of STAT3 was detected by western blot.

Research results

AhR expressions in mouse bone marrow tissue and isolated mBMSCs were detected. AhR overexpression enhanced the osteogenic potential of mBMSCs while AhR knockdown suppressed it. The ratio of CD86+ RAW 264.7 cells cocultured with AhR-overexpressed mBMSCs was reduced and that of CD206+ cells was increased. AhR directly interacted with STAT3. AhR overexpression increased the phosphorylation of STAT3. After inhibition of STAT3 *via* stattic, the promotive effects of AhR overexpression on the osteogenic differentiation and macrophage-modulating were partially counteracted.

Research conclusions

AhR plays a beneficial role in the regenerative potential of mBMSCs partially by increasing phosphorylation of STAT3.

Research perspectives

This study suggested that AhR and its interaction with STAT3 might be a potential candidate target for achieving optimal bone regeneration in mBMSCs-based tissue engineering.

FOOTNOTES

Author contributions: Huang J, Wang YN and Zhou Y designed the study and analyzed the data; Huang J performed the experiments, collected the data, and wrote the manuscript; All authors have read and approved the final manuscript.

Supported by National Natural Science Foundation of China, No. 82001014 and No. 82071090; Hubei Provincial Natural Science Foundation of China, No. 2022CFB115.

Institutional review board statement: The study was reviewed and approved by the Institutional Review Board of Hospital of Stomatology, Wuhan University (Approval No. 2020-A08).

Institutional animal care and use committee statement: All procedures involving animals were reviewed and approved by the Institutional Animal Care and Use Committee of the Hospital of Stomatology, Wuhan University [Protocol No. 2020-A08].

Conflict-of-interest statement: All the authors declare no conflicts of interest.

Data sharing statement: No additional data are available.

ARRIVE guidelines statement: The authors have read the ARRIVE Guidelines, and the manuscript was prepared and revised according to the ARRIVE Guidelines.

Open-Access: This article is an open-access article that was selected by an in-house editor and fully peer-reviewed by external reviewers. It is distributed in accordance with the Creative Commons Attribution NonCommercial (CC BY-NC 4.0) license, which permits others to distribute, remix, adapt, build upon this work non-commercially, and license their derivative works on different terms, provided the original work is properly cited and the use is non-commercial. See: https://creativecommons.org/Licenses/by-nc/4.0/

Country/Territory of origin: China

ORCID number: Jing Huang 0000-0001-7234-7749; Yi-Ning Wang 0000-0002-6749-4362; Yi Zhou 0000-0002-2912-7721.

S-Editor: Cong Lin
L-Editor: Lin C
P-Editor: Zhang XD

REFERENCES

1 **Yousefi AM**, James PF, Akbarzadeh R, Subramanian A, Flavin C, Oudadesse H. Prospect of Stem Cells in Bone Tissue Engineering: A Review. *Stem Cells Int* 2016; **2016**: 6180487 [PMID: 26880976 DOI: 10.1155/2016/6180487]
2 **Zhang Y**, Du Z, Li D, Wan Z, Zheng T, Zhang X, Yu Y, Yang X, Cai Q. Catalpol modulating the crosstalking between mesenchymal stromal cells and macrophages *via* paracrine to enhance angiogenesis and osteogenesis. *Exp Cell Res* 2022; **418**: 113269 [PMID: 35817196 DOI: 10.1016/j.yexcr.2022.113269]
3 **Tasso R**, Ulivi V, Reverberi D, Lo Sicco C, Descalzi F, Cancedda R. In vivo implanted bone marrow-derived mesenchymal stem cells trigger a cascade of cellular events leading to the formation of an ectopic bone regenerative niche. *Stem Cells Dev* 2013; **22**: 3178-3191 [PMID: 23924051 DOI: 10.1089/scd.2013.0313]
4 **Mahon OR**, Browe DC, Gonzalez-Fernandez T, Pitacco P, Whelan IT, Von Euw S, Hobbs C, Nicolosi V, Cunningham KT, Mills KHG, Kelly DJ, Dunne A. Nano-particle mediated M2 macrophage polarization enhances bone formation and MSC osteogenesis in an IL-10 dependent manner. *Biomaterials* 2020; **239**: 119833 [PMID: 32062479 DOI: 10.1016/j.biomaterials.2020.119833]
5 **Qi Y**, Zhu T, Zhang T, Wang X, Li W, Chen D, Meng H, An S. M1 macrophage-derived exosomes transfer miR-222 to induce bone marrow mesenchymal stem cell apoptosis. *Lab Invest* 2021; **101**: 1318-1326 [PMID: 34230646 DOI: 10.1038/s41374-021-00622-5]
6 **Mulero-Navarro S**, Fernandez-Salguero PM. New Trends in Aryl Hydrocarbon Receptor Biology. *Front Cell Dev Biol* 2016; **4**: 45 [PMID: 27243009 DOI: 10.3389/fcell.2016.00045]
7 **Izawa T**, Arakaki R, Mori H, Tsunematsu T, Kudo Y, Tanaka E, Ishimaru N. The Nuclear Receptor AhR Controls Bone Homeostasis by Regulating Osteoclast Differentiation *via* the RANK/c-Fos Signaling Axis. *J Immunol* 2016; **197**: 4639-4650 [PMID: 27849171 DOI: 10.4049/jimmunol.1600822]
8 **Neavin DR**, Liu D, Ray B, Weinshilboum RM. The Role of the Aryl Hydrocarbon Receptor (AHR) in Immune and Inflammatory Diseases. *Int J Mol Sci* 2018; **19** [PMID: 30513921 DOI: 10.3390/ijms19123851]
9 **Safe S**, Jin UH, Park H, Chapkin RS, Jayaraman A. Aryl Hydrocarbon Receptor (AHR) Ligands as Selective AHR Modulators (SAhRMs). *Int*

J Mol Sci 2020; **21** [PMID: 32932962 DOI: 10.3390/ijms21186654]

10 **Huang J**, Cai X, Ou Y, Fan L, Zhou Y, Wang Y. Protective roles of FICZ and aryl hydrocarbon receptor axis on alveolar bone loss and inflammation in experimental periodontitis. *J Clin Periodontol* 2019; **46**: 882-893 [PMID: 31286538 DOI: 10.1111/jcpe.13166]

11 **Huang J**, Wang Y, Zhou Y. Beneficial roles of the AhR ligand FICZ on the regenerative potentials of BMSCs and primed cartilage templates. *RSC Adv* 2022; **12**: 11505-11516 [PMID: 35425032 DOI: 10.1039/d2ra00622g]

12 **Miki Y**, Hata S, Saito R, Ono K, Sasano H, Kumamoto H. Expression of Aryl Hydrocarbon Receptor in Bone Tissues. In: Sasaki K, Suzuki O, Takahashi N, editors. Interface Oral Health Science. 2011. Tokyo: Springer, 2021:134–136

13 **Rothhammer V**, Quintana FJ. The aryl hydrocarbon receptor: an environmental sensor integrating immune responses in health and disease. *Nat Rev Immunol* 2019; **19**: 184-197 [PMID: 30718831 DOI: 10.1038/s41577-019-0125-8]

14 **Watson ATD**, Nordberg RC, Loboa EG, Kullman SW. Evidence for Aryl hydrocarbon Receptor-Mediated Inhibition of Osteoblast Differentiation in Human Mesenchymal Stem Cells. *Toxicol Sci* 2019; **167**: 145-156 [PMID: 30203000 DOI: 10.1093/toxsci/kfy225]

15 **Yoshikawa Y**, Izawa T, Hamada Y, Takenaga H, Wang Z, Ishimaru N, Kamioka H. Roles for B[a]P and FICZ in subchondral bone metabolism and experimental temporomandibular joint osteoarthritis *via* the AhR/Cyp1a1 signaling axis. *Sci Rep* 2021; **11**: 14927 [PMID: 34290363 DOI: 10.1038/s41598-021-94470-4]

16 **Korkalainen M**, Kallio E, Olkku A, Nelo K, Ilvesaro J, Tuukkanen J, Mahonen A, Viluksela M. Dioxins interfere with differentiation of osteoblasts and osteoclasts. *Bone* 2009; **44**: 1134-1142 [PMID: 19264158 DOI: 10.1016/j.bone.2009.02.019]

17 **Lamorte S**, Shinde R, McGaha TL. Nuclear receptors, the aryl hydrocarbon receptor, and macrophage function. *Mol Aspects Med* 2021; **78**: 100942 [PMID: 33451803 DOI: 10.1016/j.mam.2021.100942]

18 **Climaco-Arvizu S**, Domínguez-Acosta O, Cabañas-Cortés MA, Rodríguez-Sosa M, Gonzalez FJ, Vega L, Elizondo G. Aryl hydrocarbon receptor influences nitric oxide and arginine production and alters M1/M2 macrophage polarization. *Life Sci* 2016; **155**: 76-84 [PMID: 27153778 DOI: 10.1016/j.lfs.2016.05.001]

19 **Shinde R**, Hezaveh K, Halaby MJ, Kloetgen A, Chakravarthy A, da Silva Medina T, Deol R, Manion KP, Baglaenko Y, Eldh M, Lamorte S, Wallace D, Chodisetti SB, Ravishankar B, Liu H, Chaudhary K, Munn DH, Tsirigos A, Madaio M, Gabrielsson S, Touma Z, Wither J, De Carvalho DD, McGaha TL. Apoptotic cell-induced AhR activity is required for immunological tolerance and suppression of systemic lupus erythematosus in mice and humans. *Nat Immunol* 2018; **19**: 571-582 [PMID: 29760532 DOI: 10.1038/s41590-018-0107-1]

20 **Yang X**, Liu H, Ye T, Duan C, Lv P, Wu X, Liu J, Jiang K, Lu H, Yang H, Xia D, Peng E, Chen Z, Tang K, Ye Z. AhR activation attenuates calcium oxalate nephrocalcinosis by diminishing M1 macrophage polarization and promoting M2 macrophage polarization. *Theranostics* 2020; **10**: 12011-12025 [PMID: 33204326 DOI: 10.7150/thno.51144]

21 **Cui Z**, Feng Y, Li D, Li T, Gao P, Xu T. Activation of aryl hydrocarbon receptor (AhR) in mesenchymal stem cells modulates macrophage polarization in asthma. *J Immunotoxicol* 2020; **17**: 21-30 [PMID: 31922435 DOI: 10.1080/1547691x.2019.1706671]

22 **Øvrevik J**, Låg M, Lecureur V, Gilot D, Lagadic-Gossmann D, Refsnes M, Schwarze PE, Skuland T, Becher R, Holme JA. AhR and Arnt differentially regulate NF-κB signaling and chemokine responses in human bronchial epithelial cells. *Cell Commun Signal* 2014; **12**: 48 [PMID: 25201625 DOI: 10.1186/s12964-014-0048-8]

23 **Hillmer EJ**, Zhang H, Li HS, Watowich SS. STAT3 signaling in immunity. *Cytokine Growth Factor Rev* 2016; **31**: 1-15 [PMID: 27185365 DOI: 10.1016/j.cytogfr.2016.05.001]

24 **Zhou S**, Dai Q, Huang X, Jin A, Yang Y, Gong X, Xu H, Gao X, Jiang L. STAT3 is critical for skeletal development and bone homeostasis by regulating osteogenesis. *Nat Commun* 2021; **12**: 6891 [PMID: 34824272 DOI: 10.1038/s41467-021-27273-w]

25 **Luo S**, Gan L, Liu S, Zhong L, Chen M, Zhang H, Li J, Huang L, Lv C. The synergistic Reduning and cefmetazole sodium treatment of severe pneumonia is mediated by the AhR-Src-STAT3 pathway. *J Thorac Dis* 2022; **14**: 474-493 [PMID: 35280469 DOI: 10.21037/jtd-22-126]

26 **Teixeira LD**, Harrison NA, da Silva DR, Mathews CE, Gonzalez CF, Lorca GL. Nanovesicles From Lactobacillus johnsonii N6.2 Reduce Apoptosis in Human Beta Cells by Promoting AHR Translocation and IL10 Secretion. *Front Immunol* 2022; **13**: 899413 [PMID: 35757772 DOI: 10.3389/fimmu.2022.899413]

World Journal of Stem Cells

Submit a Manuscript: https://www.f6publishing.com

World J Stem Cells 2023 August 26; 15(8): 821-841

DOI: 10.4252/wjsc.v15.i8.821

ISSN 1948-0210 (online)

ORIGINAL ARTICLE

Basic Study

Wnt signaling pathway inhibitor promotes mesenchymal stem cells differentiation into cardiac progenitor cells *in vitro* and improves cardiomyopathy *in vivo*

Rabbia Muneer, Rida-e-Maria Qazi, Abiha Fatima, Waqas Ahmad, Asmat Salim, Luciana Dini, Irfan Khan

Specialty type: Cell and tissue engineering

Provenance and peer review: Invited article; Externally peer reviewed.

Peer-review model: Single blind

Peer-review report's scientific quality classification

Grade A (Excellent): 0
Grade B (Very good): B, B
Grade C (Good): C
Grade D (Fair): 0
Grade E (Poor): 0

P-Reviewer: Shamseldeen AM, Egypt; Wang MK, China

Received: March 26, 2023
Peer-review started: March 26, 2023
First decision: May 17, 2023
Revised: May 31, 2023
Accepted: July 3, 2023
Article in press: July 3, 2023
Published online: August 26, 2023

Rabbia Muneer, Rida-e-Maria Qazi, Abiha Fatima, Waqas Ahmad, Asmat Salim, Irfan Khan, Dr. Panjwani Center for Molecular Medicine and Drug Research, International Center for Chemical and Biological Sciences, University of Karachi, Karachi 75270, Sindh, Pakistan

Luciana Dini, Department of Biology and Biotechnologies Charles Darwin, Sapienza University of Rome, Rome 00185, Italy

Corresponding author: Irfan Khan, PhD, Assistant Professor, Dr. Panjwani Center for Molecular Medicine and Drug Research, International Center for Chemical and Biological Sciences, University of Karachi, University Road, Karachi 75270, Sindh, Pakistan. khan@iccs.edu

Abstract

BACKGROUND

Cardiovascular diseases particularly myocardial infarction (MI) are the leading cause of mortality and morbidity around the globe. As cardiac tissue possesses very limited regeneration potential, therefore use of a potent small molecule, inhibitor Wnt production-4 (IWP-4) for stem cell differentiation into cardiomyocytes could be a promising approach for cardiac regeneration. Wnt pathway inhibitors may help stem cells in their fate determination towards cardiomyogenic lineage and provide better homing and survival of cells *in vivo*. Mesenchymal stem cells (MSCs) derived from the human umbilical cord have the potential to regenerate cardiac tissue, as they are easy to isolate and possess multilineage differentiation capability. IWP-4 may promote the differentiation of MSCs into the cardiac lineage.

AIM

To evaluate the cardiac differentiation ability of IWP-4 and its subsequent *in vivo* effects.

METHODS

Umbilical cord tissue of human origin was utilized to isolate the MSCs which were characterized by their morphology, immunophenotyping of surface markers specific to MSCs, as well as by tri-lineage differentiation capability. Cytotoxicity analysis was performed to identify the optimal concentration of IWP-4. MSCs were treated with 5 μM IWP-4 at two different time intervals. Differentiation of MSCs into cardiomyocytes was evaluated at DNA and protein levels. The MI rat

model was developed. IWP-4 treated as well as untreated MSCs were implanted in the MI model, then the cardiac function was analyzed *via* echocardiography. MSCs were labeled with 1,1′-dioctadecyl-3,3,3′,3′-tetramethylindocarbocyanine perchlorate (DiI) dye for tracking, while the regeneration of infarcted myocardium was examined by histology and immunohistochemistry.

RESULTS

MSCs were isolated and characterized. Cytotoxicity analysis showed that IWP-4 was non-cytotoxic at 5 μM concentration. Cardiac specific gene and protein expression analyses exhibited more remarkable results in fourteen days treated group that was eventually selected for *in vivo* transplantation. Cardiac function was restored in the IWP-4 treated group in comparison to the MI group. Immunohistochemical analysis confirmed the homing of pre-differentiated MSCs that were labeled with DiI cell labeling dye. Histological analysis confirmed the significant reduction in fibrotic area, and improved left ventricular wall thickness in IWP-4 treated MSC group.

CONCLUSION

Treatment of MSCs with IWP-4 inhibits Wnt pathway and promotes cardiac differentiation. These pre-conditioned MSCs transplanted *in vivo* improved cardiac function by cell homing, survival, and differentiation at the infarcted region, increased left ventricular wall thickness, and reduced infarct size.

Key Words: Myocardial infarction; Inhibitor Wnt production-4; Differentiation; Mesenchymal stem cells; Wnt pathway; Cardiac function

©The Author(s) 2023. Published by Baishideng Publishing Group Inc. All rights reserved.

Core Tip: This study highlights the role of Wnt signaling pathway in the differentiation of mesenchymal stem cells (MSCs) into cardiac progenitor cells and the therapeutic potential of MSCs conditioned with inhibitor Wnt production-4 (IWP-4) for the treatment of heart disease. Further studies are required to comprehend the mode of action of IWP-4 on MSCs and to assess its potency and safety in human clinical trials. Nevertheless, this research is an exciting step forward for new treatments for heart diseases and is more focused on the importance of continued investment in the development of innovative therapies for this devastating condition.

Citation: Muneer R, Qazi REM, Fatima A, Ahmad W, Salim A, Dini L, Khan I. Wnt signaling pathway inhibitor promotes mesenchymal stem cells differentiation into cardiac progenitor cells *in vitro* and improves cardiomyopathy *in vivo*. *World J Stem Cells* 2023; 15(8): 821-841

URL: https://www.wjgnet.com/1948-0210/full/v15/i8/821.htm

DOI: https://dx.doi.org/10.4252/wjsc.v15.i8.821

INTRODUCTION

Cardiovascular diseases (CVDs) remain the major mortality cause around the globe[1]. The associated morbidity and mortality may rise to 23.6 million by 2030, which emphasizes the urgent need of addressing the issue of regenerating the damaged heart[2]. CVDs account for a wide range of pathological changes in the blood vessels and heart. Current treatment strategies include inhibitors of beta and aldosterone, angiotensin altering enzyme inhibitors, and biventricular striding. However, heart failure related morbidity and mortality cause temporary success due to these therapeutic interventions and highlight the need for novel therapy that can inhibit and reverse heart dysfunction. Cell therapy emerged in the 1990s and was perceived as a promising strategy to repair an injured heart after myocardial infarction (MI)[3].

Mesenchymal stem cells (MSCs) are the epitome of tissue regeneration due to their easy isolation and existence in almost all types of tissues. They can be differentiated into multiple lineages. Their immunological properties such as immunosuppressive, anti-inflammatory, and immunoregulatory potential make them potent immunotolerant cells[4]. MSCs isolated from the umbilical cord are relatively advantageous over other adult sources owing to their ability to high passaging, expansion on a larger scale, higher anti-inflammatory effects, and more significant senescence retardation[5].

The Wnt signaling pathway comprises a complex network of signaling molecules that play a crucial role in stem cell growth, survival, and differentiation. Wnt antagonists (IWPs) inhibit Wnt ligand release by inhibiting a membrane bound O-acyltransferase, Porcn, responsible for catalyzing Wnt palmitoylation[6]. Several studies reported that the inhibition of Wnt pathway promotes the differentiation of stem cells toward cardiomyocytes. Inhibitor Wnt production-4 (IWP-4) was also reported to produce functional cardiomyocytes from induced pluripotent stem cells and embryonic stem cells[7,8].

In this study, we investigated the role of IWP-4, a potent inhibitor of the Wnt signaling pathway on human umbilical cord derived MSCs. Our results showed that treatment with IWP-4 promotes MSCs differentiation into cardiac progenitor cells *in vitro*, which is a promising step towards the development of stem cell treatment for heart disease. To assess the

therapeutic potential of IWP-4 treated MSCs, cells were transplanted in rat MI model. Our results demonstrated that treatment with IWP-4 improves the efficacy of the MSCs to recover cardiac function of the MI rats, as evidenced by an increase in the ejection fraction. These findings suggest that preconditioning of MSCs with IWP-4 may be a promising approach for the treatment of heart diseases and that targeting Wnt signaling pathway may represent a promising approach for this debilitating condition.

MATERIALS AND METHODS

In vitro studies

Ethical approval: This study was conducted according to the institutional ethical standards outlined in the protocol #ICCBS/IEC-067-HT/UCB-2021/Protocol/1.0, which was approved by the ethical review committee. Healthy donors' umbilical cords were obtained from Zainab Panjwani Memorial Hospital with informed consent after C-section delivery. The cord samples were collected aseptically and transferred into a sterile glass bottle filled with 0.5% EDTA in phosphate buffer saline (PBS) and kept at 4 °C. The samples were processed immediately after collection.

Human umbilical cord tissue processing: The biosafety cabinet class II, type A2 (ESCO, Singapore) was used for sample processing. The cord sample was washed with sterile PBS and then cut into 1-3 mm pieces. These pieces were placed in T-75 flasks containing 10-12 mL complete DMEM (10% fetal bovine serum, 100 U of streptomycin/penicillin, and 1 mmol/L sodium pyruvate). The flasks were kept at 37 °C in a humidified CO_2 incubator. The flask was monitored regularly for cell growth, and the medium was changed after every 3 d. After 10-14 d of initial culture, MSCs from the explant were migrated and adhered to the surface of the flask. When the cells were adequately attached, explants were removed and cells were supplied with fresh medium for further propagation. The cells were labeled as passage zero (Po). When the cells became 80% confluent, they were trypsinized for the next passage using 1× trypsin-EDTA. The experiments were carried out using passages (P_2 to P_3) MSCs.

Characterization of MSCs: The isolated MSCs were characterized based on phase contrast microscopy, immunocytochemistry, immunophenotyping, and trilineage differentiation.

Phase contrast microscopy: Phase contrast microscopy was performed for the morphological analysis of MSCs at different passages. The images were captured with phase contrast microscope (Ti-2, Nikon, Tokyo, Japan).

Immunocytochemistry: Coverslips were placed in a 24-well tissue culture plate and 5000 cells were seeded with 200 µL of complete DMEM in each well, then the plate was incubated in a CO_2 incubator at 37 °C for 24-48 h to allow for monolayer formation. The next day, DMEM was discarded and cells were washed with 1× PBS, and fixed with 200 µL of 4% Paraformaldehyde (PFA) for 10 min. Cells were again washed with PBS and then permeabilized with 300 µL of 0.1% Triton X-100 for 10 min followed by 3 washes with PBS. The cells were then blocked for 1 h at 37 °C using a blocking solution containing 2% BSA, 0.1% Tween-20, and 1× PBS to prevent non-specific binding. After blocking, the monoclonal primary antibodies CD117 (32-9000, Zymed, United States), CD29 (MAB-1981, Chemicon International, United States), Lin28 (PA1- 096, Invitrogen, United States), CD105 (560839, BD Pharmingen, United States), Vimentin (V6389, Sigma-Aldrich, United States), and CD45 (CBL415, BD Pharmingen, United States) were added to each well, and the plate was incubated at 4 °C overnight. The next day, primary antibodies were removed, and cells were washed with 1× PBS. Cells were then incubated with Alexa Fluor 546 conjugated goat anti-mouse secondary antibody (A-11010, Molecular Probes, Invitrogen, United States) at 37 °C for 1 h, followed by washing with 1× PBS. The cells were stained with a 0.5 µg/mL solution of DAPI-PBS (4', 6-diamidino-2-phenylindole) for 15 min at room temperature followed by washing with 1× PBS. Finally, coverslips were placed on a glass slide, and then slides were mounted with 5 µL of aqueous mounting medium. The fluorescence microscope (Nikon Ti2; Nikon, Japan) was used to observe the slides.

Flow cytometry: Immunophenotypic characterization was performed by flow cytometry. MSCs were trypsinized and washed with PBS then resuspended in FACS buffer (1 mmol/L EDTA, 1% BSA, and 0.1% sodium azide). Cells were incubated with primary antibody CD73 (550256, BD Pharmingen, United States), CD105, Vimentin, and CD45 incubated at 37 °C for 2 h. The primary antibody was removed and cells were washed with PBS. Then Alexa Fluor 488 goat anti-mouse secondary antibody was added for 1 h at 37 °C. Cells were washed and analyzed *via* FACS Calibur (Becton Dickinson, United States). For control, unlabeled and isotype labeled cells were used.

Tri-lineage differentiation: For the characterization of MSCs through tri-lineage differentiation, cells were allowed to grow in complete DMEM in a 6-well plate. For the differentiation of MSCs into adipocytes, MSCs were allowed to grow in adipogenic induction medium containing complete DMEM, 1 µM dexamethasone, 10 µg/mL insulin, 200 µM indomethacin, and 0.5 µM isobutyl methylxanthine for 21 d. MSCs were differentiated into osteocytes in osteogenic induction medium containing complete DMEM with 0.1 µM dexamethasone, 0.2 mmol/L L-ascorbic acid-2-phosphate, and 10 mmol/L glycerol-2- phosphate for 28 d. For chondrogenic differentiation, MSCs were allowed to grow in chondrogenic induction medium containing complete DMEM, 1 µM dexamethasone, 20 ng/mL transforming growth factor-β, 100 mmol/L ascorbic acid, and 10 ng/mL insulin for 21 d. Differentiated cells were stained with Oil Red O for the detection of lipid droplets inside the cells for adipocytes. Alizarin Red staining was performed to detect calcium deposits in osteocytes. Alcian Blue staining confirmed the presence of proteoglycans and glycosaminoglycans (GAG).

Cytotoxicity analysis of IWP-4 by JC-1 assay: JC-1 cytotoxicity analysis was performed to determine the cytotoxic effect of IWP-4 on MSCs. MSCs were grown in complete DMEM in T-75 flasks and then treated with the different concentrations (5, 10, 20, 30, 50, and 100 µM) of IWP-4 for 24 h. Cells were trypsinized, washed, and then stained with 500 µL of 10µg/mL JC-1 dye working dilution and incubated for 15 min at 37 °C. Afterwards, MSCs were washed and resuspended in PBS. Data were analyzed with BD CellQuest pro software.

Treatment with IWP-4: The concentration of 5 µM was selected for cardiac differentiation based on JC-1 cytotoxicity assay. Working solutions were prepared from 2 mmol/L IWP-4 stock solution. Complete DMEM was used for the preparation of conditioned medium. 20 µL stock compound was added in 50 mL of media and stored at 4 °C. When cells became 60% confluent, normal media was discarded, and conditioned media was added to the flask and then kept in a CO_2 incubator for seven, and fourteen days. The conditioned medium was replaced every 3 d.

Gene expression of cardiac markers: For cardiac gene expression analysis, RNA was isolated from untreated, seven and fourteen days IWP-4 treated MSCs *via* Trizol method according to the manufacturer's instructions. The concentration and purity of RNA were checked by using Nanodrop2000 (Thermo Fisher Scientific, United States) at 260 nm absorbance. A 260/280 absorbance ratio was used to determine the purity of isolated RNA. cDNA was synthesized from 1 µg of RNA by using RevertAid First Strand cDNA Synthesis Kit (K1621, Thermo Fisher Scientific, United States), according to the manufacturer's protocol. Cardiac specific genes were amplified using primer sequences enlisted in Table 1, by quantitative real-time polymerase chain reaction (qPCR) using a CFX96 Touch Real-Time PCR Detection System (Bio-Rad Laboratories, United States). Bright Green 2× qPCR master mix (Applied Biological Materials, Canada) was used for the amplification. For gene amplification, initial denaturation was performed at 95 °C for 10 min, 40 cycles of denaturation at 95 °C for 15 s, and extension at 60 °C for 1 min. The *GAPDH* gene (a housekeeping gene) was used as endogenous control. To analyze the relative gene expression level, the cycle threshold (Ct) value was acquired after the completion of the reaction, and the fold change was calculated using $2^{-\Delta\Delta Ct}$ method.

Gene expression of Wnt pathway genes: For Wnt pathway gene expression analysis, total RNA was isolated and cDNA was prepared and amplified as described above. For gene amplification, initial denaturation was performed at 95 °C for 10 min, and 40 cycles of denaturation at 95 °C for 15 s, and extension at 60 °C for 1 min. Wnt specific genes were amplified using primer sequences enlisted in Table 2. The *GAPDH* gene (a housekeeping gene) was used as endogenous control. To analyze relative gene expression level, the Ct value was acquired after completion of the reaction, and the fold change was calculated using $2^{-\Delta\Delta Ct}$ method.

Immunocytochemistry of cardiac protein: To examine protein expression, immunofluorescence staining was performed on both untreated and fourteen days IWP-4 treated MSCs by the same protocol as explained earlier for the characterization of MSCs. Untreated and IWP-4 treated MSCs were washed with PBS and fixed with 4% PFA, and then incubated in cardiac specific antibodies such as α-actinin (sc-17829, Santa Cruz Biotech, United States), Connexin-43 (C-43) (13-8300, Thermo scientific, United States), cardiac troponin I (cTnI) (Ab209809, Abcam, United Kingdom), Desmin (MAB3430 Chemicon International, United States), GATA-4 (sc-25310, Santa Cruz Biotech, United States), Nkx 2.5 (sc-376565, Santa Cruz Biotech, United States). Next, Alexa Fluor 488 conjugated goat anti-mouse secondary antibody (A-11001, Invitrogen, United States) was added followed by washing with 1× PBS. The cell nuclei were counterstained with DAPI in 1× PBS for 15 min at room temperature and washed again with 1× PBS. Protein expression was observed using a fluorescence microscope. Fluorescent images were processed and quantified by ImageJ software.

In vivo studies

Animal care and ethical approval: MI model was developed using Wistar rats weighing between 220-230 g. The study was conducted in compliance with the international guidelines for laboratory animal care and use under protocol number 2021-006, with ethical approval obtained from the Institutional Animal Care and Use Committee at the Dr. Panjwani Center for Molecular Medicine and Drug Research, International Center for Chemical and Biological Sciences, University of Karachi. The animals were housed in separate cages, in a room maintained at a temperature of 22 °C ± 2 °C, 55 ± 5% relative humidity, and a 12 h light: 12 h dark cycle, with unrestricted access to water and food.

Cardiac model development: To develop the MI model, a metal rod was cooled in liquid nitrogen for 15 min. Rats were anesthetized with xylazine and ketamine (7 mg/kg and 60 mg/kg, respectively), according to their body weights. To initiate artificial ventilation, a rodent ventilator was used and endotracheal intubation was performed. Left thoracotomy was performed through the anterolateral 4th and 5th intercostal space, and a retractor was used to expose the heart. Then the rod was removed from liquid nitrogen and placed on the left ventricle of the heart for 10 s. Successful MI model development was confirmed with the change in color of the infarcted region from red to pale color. The chest cavity was closed with 5-0 suture (Ethicon, United States), and the skin was closed with a 4-0 suture. Trachea was closed with the help of 6-0 suture. Animals were administered diclofenac sodium (25 mg/mL) and antibiotics (penicillin and streptomycin 10000 U/mL) subcutaneously. Animals were observed until they regained consciousness. In the sham control group, the chest cavity was opened and then closed without the exposure of an ultracold rod.

Transplantation of cells in MI model: After model development, one million cells resuspended in 1× PBS were transplanted in the left ventricular wall immediately after infarction. For *in vivo* cell tracking, untreated and IWP-4 treated MSCs were labeled with the red fluorescent dye, 1,1′-dioctadecyl-3,3,3′,3′-tetramethylindocarbocyanine perchlorate (DiI) according to the manufacturer's instructions and transplanted into the rats.

Table 1 Details of cardiac specific primers

Gene	Primer sequences (5'-3')	Annealing temperatures (°C)	Product size (bp)
α-actinin (F)	5′-CTCTTGCTTCTACCACGCTTT-3′	58.0	297
α-actinin (R)	5′-AGCGTGTTGAAGTTGATCTCC-3′		
cMHC (F)	5′-GAGGAGCAAGCCAACACCA-3′	58.0	106
cMHC (R)	5′-GCAGCTTGTTGACCTGGGA-3′		
Mef2D (F)	5′-GGGGGCTGGAGGAGTTACC-3′	58.0	292
Mef2D (R)	5′-TGGGGGAACGGTGTTGTCA-3′		
MLC-2v (F)	5′-CCTGAGGAAACCATTCTCAACG-3′	58.0	98
MLC-2v (R)	5′-GATGTGCACCAGGTTCTTGTAG-3′		
cTnC (F)	5′-CTCAACCCCAAATCCCCCGA-3′	58.0	148
cTnC (R)	5′-AGGAAGCGGCCATTGGGTAA-3′		
cTnI (F)	5′-GAACATCACGGAGATTGCAGA-3′	58.0	236
cTnI (R)	5′-TCAGTGCATCGATGTTCTTCC-3′		
cTnT (F)	5′-TCCAGAAGGCCCAGACAGAG-3′	58.0	89
cTnT (R)	5′-CACCTTCCTCCTCTCAGCCA-3′		
Ca- channel (F)	5′-GAGAGCACCCCGGCTTC-3′	58.0	164
Ca-channel (R)	5′-GAAGTCCTGCCCCGCTC-3′		
Na-channel (F)	5′-ACTAGGCAATTTGTCGGCTC-3′	58.0	325
Na-channel (R)	5′-GCCGTTCTTGAGCAGGTAAT-3′		
GATA4 (F)	5′-CTGCCCTCCGTCTTCTGC-3′	58.0	286
GATA4 (R)	5′-CTCGCAGGTCAAGGAGCC-3′		
Nkx-2.5 (F)	5′-CAAGTGTGCGTCTGCCTTTC-3′	58.0	106
Nkx-2.5 (R)	5′-CGCGCACAGCTCTTTCTTT-3′		
GAPDH (F)	5′-CAC CAT GGG GAA GGT GAA GG-3′	58.0	274
GAPDH (R)	5′-AGC ATC GCC CCA CTT GAT TT-3′		

Echocardiography: Cardiac functional analysis was performed by echocardiography after 2 and 4 wk of MI with the help of an Echo machine (Aloka, Japan) provided with 7-MHz transducer. Motion-mode (M-mode) and 2D-bright mode (B-mode) were used to scan the parasternal long-axis view of papillary muscles. Left ventricular internal systolic and diastolic dimensions (LVIDs and LVIDd) were calculated using M-mode scans, and averaged three consecutive cardiac cycles were taken for measurements. Percent ejection fraction (%EF) and fractional shortening (%FS), and end diastolic and systolic volumes (EDV and ESV) were calculated by using the formula as given below:

$$FS\ (\%) = (LVIDd - LVIDs)/LVIDd \times 100$$

$$EF\ (\%) = SV/EDV \times 100$$

$$EDV = [7/(2.4) + LVIDd] \times LVIDd^3$$

$$ESV = [7/(2.4) + LVIDs] \times LVIDs^3$$

Heart harvesting and tissue processing for histology: After 4 wk from surgery and cell transplantation, rats were anesthetized, perfused with 1× PBS, and then fixed with 4% PFA. The hearts were removed and placed in 4% PFA overnight, then dehydrated in graded alcohol, and afterward immersed in xylene then xylene-paraffin mixture followed by embedding in paraffin. Microtome sectioning was performed to cut 5 μm thick sections of paraffin blocks. Sections were taken on gelatin coated slides. Hematoxylin-Eosin (H&E) and Masson's trichrome staining were performed according to the manufacturer's instructions. For histological analysis, the stained section images were observed under a bright-field microscope (NiE, Nikon, Japan).

Tracking of DiI labeled cells in MI model: For DiI labeled cell tracking in animals, hearts were perfused with 1× PBS, fixed with 4% PFA for 4 h, and then mold was prepared in optimal cutting temperature medium. Mold was cryosectioned and cells were tracked by observing them under a fluorescent microscope. To assess the long-term survival, distribution, and differentiation of the transplanted cells in the MI model, tissue was permeabilized with triton-X 100, and blocked with blocking solution. The sections were stained with cardiac specific primary antibodies against GATA-4, cTnI, and

Table 2 Details of Wnt pathway primers

Genes	Primer sequences (5'-3')	Annealing temperatures (°C)	Product size (bp)
GAPDH (F)	5'-CAC CAT GGG GAA GGT GAA GG-3'	58.0	274
GAPDH (R)	5'-AGC ATC GCC CCA CTT GAT TT-3'		
Wnt-2 (F)	5'-GTCGGGAATCTGCCTTTGTT-3'	58.0	376
Wnt-2 (R)	5'-GTTTTCCTGAAGTCGGCCAT-3'		
DVL (F)	5'CTATGGATCAGGATTTCGGGGT-3'	58.0	121
DVL (R)	5'-ATCTCGGGTTGGGGATTATCTG-3'		
GSK 3β (F)	5'-TGTGTTGGCTGAGCTGTTACTA-3'	58.0	200
GSK 3β (R)	5'-TGAAATGTCCTGTTCCTGACGA-3'		
β-catenin (F)	5'-TGATATTGGTGCCCAGGGAG-3'	58.0	102
β-catenin (R)	5'-TCCATACCCAAGGCATCCTG-3'		
c-myc (F)	5'-CACTAACATCCCACGCTCTGA-3'	58.0	217
c-myc (R)	5'-CGCATCCTTGTCCTGTGAGTA-3'		
cyc-D (F)	5'-CAGAGGCGGAGGAGAACAAA-3'	58.0	219
cyc-D (R)	5'-CCGGGTCACACTTGATCACT-3'		
c-jun (F)	5'-TGAGCCTACAGATGAACTCTTTCT-3'	58.0	191
c-jun (R)	5'-ACTCAGAGTGCTCCAAATCTCTTA-3'		
TCF (F)	5'-CGAGAAGAGCAGGCCAAGTA-3'	58.0	219
TCF (R)	5'-GAGCACTGTCATCGGAAGGA-3'		
Axin (F)	5'-GCATGGAGGAGGAAGGTGAG-3'	58.0	165
Axin (R)	5'-CCAGGATGCTCTCAGGGTTC-3'		

alpha actinin. Alexa fluor 488 secondary antibody was used to detect primary antibodies. Fluorescent microscope images were captured and quantified using Image J software and plotted using GraphPad Prism software.

Statistical analysis

The statistical analysis was conducted using IBM SPSS Statistics software version 23. For comparison between the two groups, independent sample *t*-test analysis was performed. However, for the comparison between multiple groups, One-way analysis of variance with post-hoc Bonferroni corrections was used. The results were expressed as mean ± SEM, and statistical significance was determined at $^{a}P < 0.05$, $^{b}P < 0.01$, and $^{c}P < 0.001$.

RESULTS

In vitro studies

Morphology of human umbilical cord-derived MSCs: MSCs culture exhibited spindle shape morphology. Explant of cord tissue culture showed outgrowth of MSCs after 7-10 d of processing after adhering to the tissue culture flask which then showed gradual expansion and propagation. After 15 d, P_o cells were grown in colonies and possessed elongated, fibroblast like morphology. P_o cells were trypsinized and sub-cultured to get the homogeneous population of MSCs at P_1. Human umbilical cord processing and morphology of MSCs sub-culture at different passages are shown in Figure 1A.

Immunocytochemistry of MSCs: MSCs showed positive expression of specific cell surface markers CD117, CD29, Lin28, CD105, Vimentin, and negative expression of CD45 which is a hematopoietic marker, as shown in Figure 1B.

Flow cytometric analysis

Immunophenotyping was performed with flow cytometry that showed greater than 90% of the cell population expressed CD105, Vimentin, and CD73, while CD45 exhibited negative expression that confirms the presence of MSCs in culture, as shown in Figure 1C.

Tri-lineage differentiation: MSCs possess tri-lineage differentiation potential that was confirmed by differentiating them into adipogenic, osteogenic, and chondrogenic lineages. Mineral deposition confirmed the differentiation of MSCs into

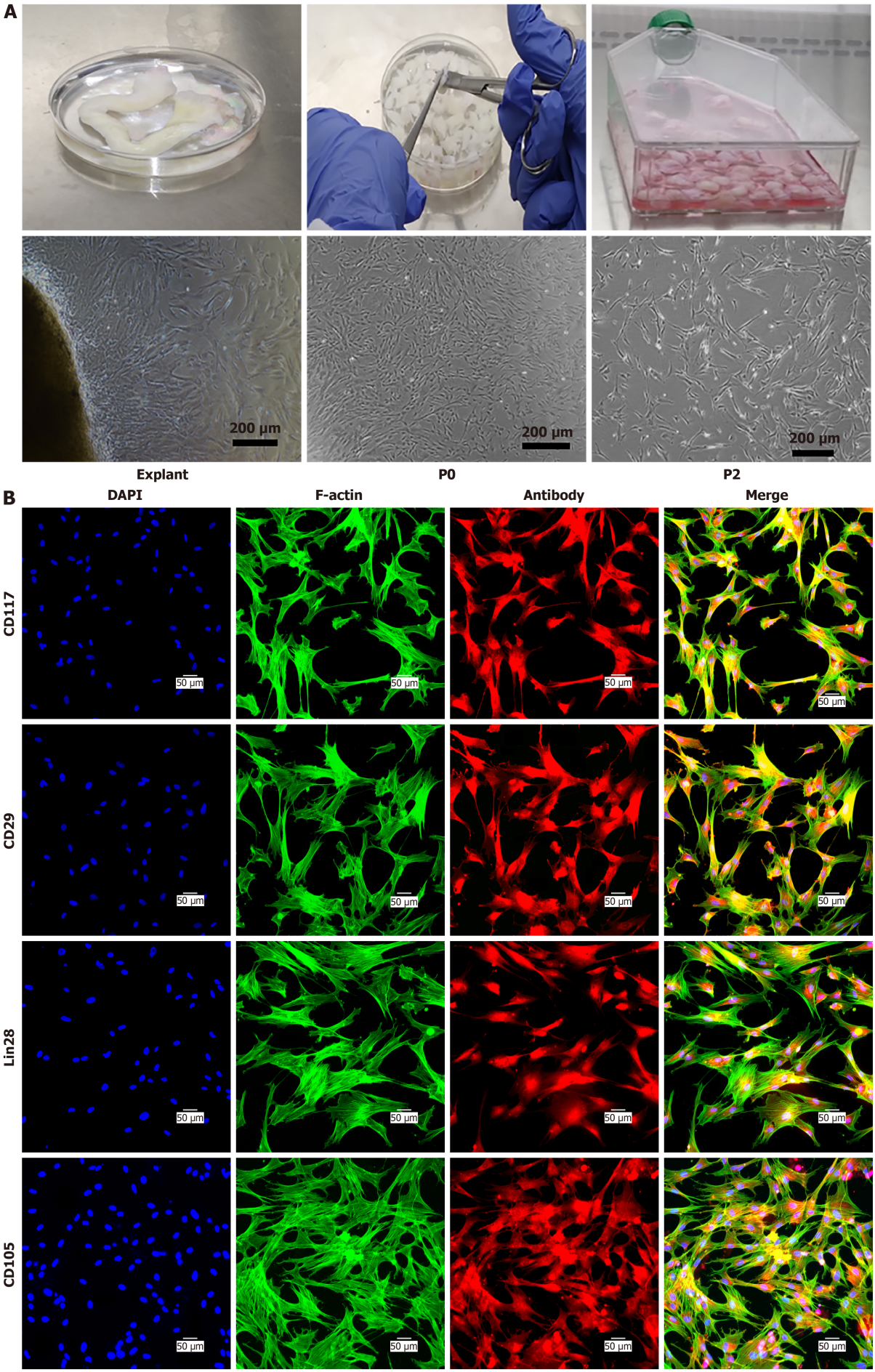
A
200 μm
200 μm
200 μm
Explant
P0
P2
B
DAPI
F-actin
Antibody
Merge
CD117
CD29
Lin28
CD105
50 μm

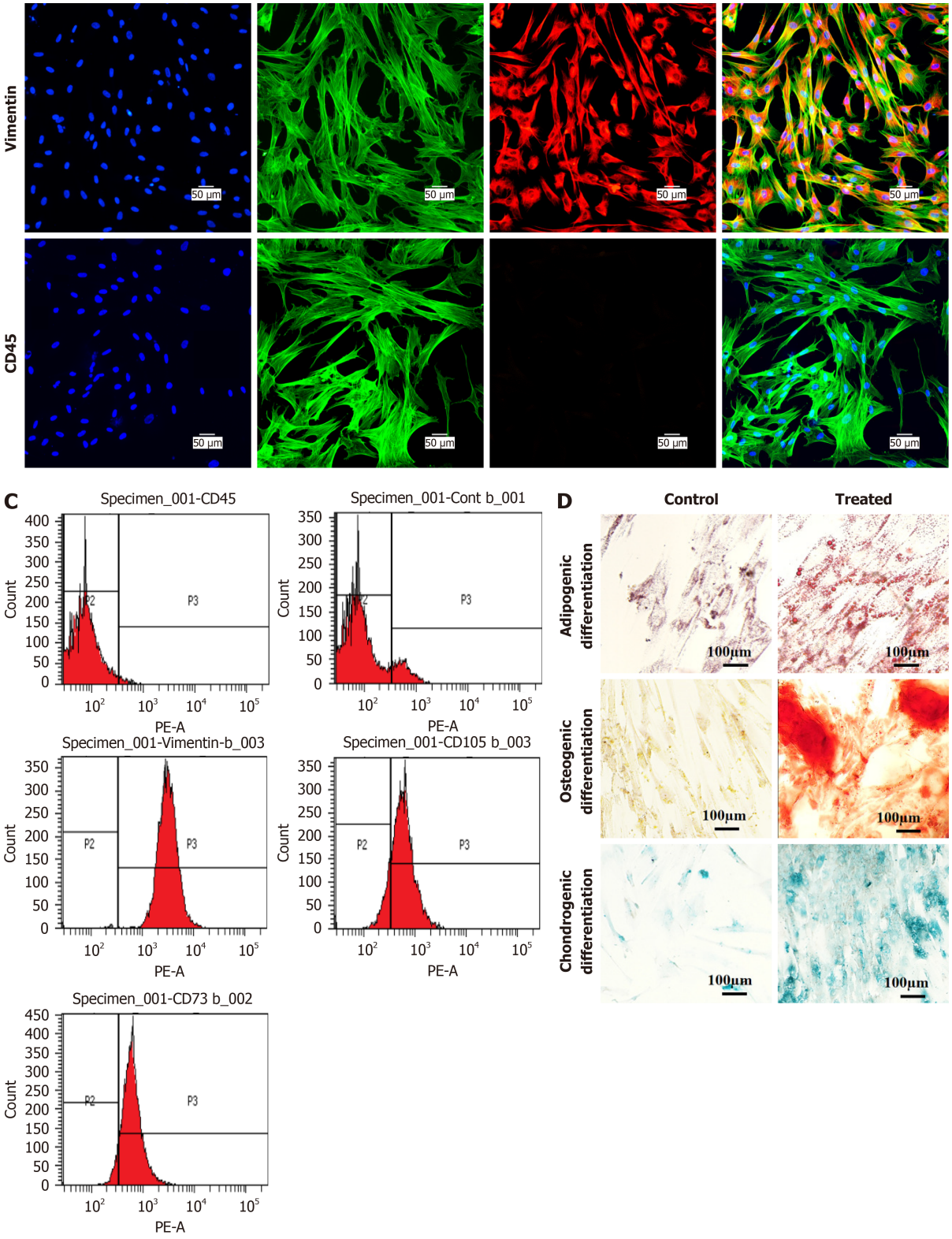

DOI: 10.4252/wjsc.v15.i8.821 **Copyright** ©The Author(s) 2023.

Figure 1 Isolation, propagation, and characterization of human umbilical cord-derived mesenchymal stem cells. A: Explant processing and isolation of human umbilical cord-derived mesenchymal stem cells (MSCs). Phase contrast images showing homogenous fibroblast like morphology and growth; B: Characterization of MSCs by immunocytochemistry representing the positive expression of CD117, CD29, Lin28, CD105, Vimentin, and negative expression of CD45; C: Immunophenotyping of MSCs by flow cytometry showing positive expression of CD105, Vimentin, and CD73, and negative expression of CD45; D: Tri-lineages differentiation of MSCs into osteogenic, adipogenic, and chondrogenic lineages.

the osteogenic lineage. Adipogenic differentiation was confirmed by the accumulation of intracellular lipid droplets in treated MSCs, which turn out to be bright red with an Oil Red O stain. Alizarin Red stained differentiated MSCs into orange red color, while large mineral deposits appeared dark red. Chondrogenic differentiation was observed by the

accumulation of GAG that stained blue after Alcian Blue staining. The results are shown in Figure 1D.

Cytotoxicity analysis by JC-1 assay: MSCs treated with different concentrations of IWP-4 were stained with JC-1 dye. Percent cell cytotoxicity was calculated by the shift of cells in the lower right quadrant of density plot in flow cytometer software. JC-1 assay showed that IWP-4 at 5 μmol/L concentration was non cytotoxic for MSCs. The results are shown in Figure 2.

Cardiac gene expression analysis: After fourteen days of treatment of MSCs with IWP-4, cardiac gene expression analysis showed significant upregulation of early and late cardiac genes. After seven days of treatment with IWP-4, myosin light chain-2 (MLC-2v) ($P < 0.01$), and Ca-channel ($P < 0.05$) genes were significantly upregulated, while MHC-β and cardiac troponin C (cTnC) showed non-significant change. However, Na-channel ($P < 0.05$), cardiac troponin T (cTnT), GATA4 ($P < 0.01$), alpha-actinin, cTnI, Mef2D, and Nkx2.5 ($P < 0.001$) showed significant downregulation as shown in Figure 3A. After fourteen days treatment of MSCs with IWP-4, when compared to control, alpha-actinin ($P < 0.05$), MHC-β, MLC-2v, Mef2D, cTnT, cTnC, cTnI, Ca-channel, Na-channel, Nkx2.5, and GATA4 ($P < 0.001$) were significantly upregulated as shown in Figure 3B.

Gene expression analysis of Wnt pathway genes: Wnt pathway gene expression profile was analyzed after seven and fourteen days treatment of MSCs with IWP-4. Gene expression profile showed that seven days treatment of MSCs with IWP-4 inhibit Wnt pathway. When compared to control, Wnt pathway genes, *GSK, DVL, Wnt, TCF, β-catenin,* and downstream transcription factors *C-jun, C-myc, Cyc-D* ($P < 0.001$) were significantly downregulated, while *Axin* showed upregulation ($P < 0.01$) (Figure 4A). After fourteen days treatment of MSCs with IWP-4, Wnt pathway was further downregulated. When compared to control, Wnt pathway genes *DVL, Wnt, and β-catenin* ($P < 0.001$) showed significant downregulation, while negative regulators of pathway *GSK* ($P < 0.01$), and *Axin* ($P < 0.05$) were upregulated. However, downstream transcription factors *C-jun, Cyc-D, TCF* showed non-significant change, while *C-myc* ($P < 0.05$) was upregulated as shown in Figure 4B.

Analysis of differentiated cells: Differentiated MSCs showed cardiac like cell morphology as shown in Figure 5A. Seven days IWP-4 treated MSCs showed positive expression of C-43, cTnI, ($P < 0.001$), desmin, GATA-4, and Nkx2.5 ($P < 0.05$), while alpha-actinin protein expression showed non-significant change. As compared to untreated MSC control, fourteen days IWP-4 treated MSCs showed positive expression of alpha-actinin, C-43, cTnI, desmin, GATA-4, and Nkx2.5 ($P < 0.001$). As compared to seven days IWP-4 treated MSCs, fourteen days IWP-4 treated MSCs showed positive expression of alpha-actinin, C-43, cTnI, desmin, GATA-4, and Nkx2.5 ($P < 0.001$) as shown in Figure 5B and C.

In vivo studies

Cardiac function analysis by echocardiography: Echocardiographic analysis of cardiac function showed decreased left ventricular wall contraction in rats with an infarcted heart (MI group) as compared to the sham control. A significant difference ($P < 0.001$) in the left ventricular systolic and diastolic dimensions, %EF, %FS, and end-systolic and -diastolic volumes were measured after two and four weeks of MI as compared to sham control. The infarcted hearts that received untreated MSCs and IWP-4 treated MSCs showed significant improvement in heart function. As compared to the MI group, left ventricular systolic and diastolic dimensions were significantly decreased ($P < 0.001$) after two and four weeks of transplantation. The %EF and %FS showed significant improvement ($P < 0.001$) in untreated and IWP-4 treated MSCs. End-systolic and -diastolic volumes were also significantly improved ($P < 0.001$) in both the cell transplantation groups as compared to the MI group as shown in Figure 6.

Analysis of isolated rat hearts: Treated and untreated MSCs were transplanted immediately after the MI model development. Hearts were isolated after 4 wk of surgery for histological (Figure 7A and B) and macroscopic analysis (Figure 7C). Macroscopic analysis revealed a major difference in the appearance of hearts in all groups. Hearts from the sham control group appeared normal, containing healthy myocardium, while in the case of MI group, the left ventricular wall of the heart showed a white fibrous scar. In the untreated MSCs transplanted group, the area of white fibrous scar was lower as compared to that of MI group, while in IWP-4 treated MSCs transplanted group, the white fibrous scar was greatly reduced as shown in Figure 7C.

Histological analysis: Cross-sections of heart tissue were differentially stained with Masson's trichrome staining which showed the fibrotic green regions of the collagen deposition in the left ventricle of the MI heart as compared to sham control, while red stained regions showed the normal tissue and myocytes with blue/black stained nuclei. At high magnification, the infarcted region of the MI heart showed fibrous tissue and tightly packed collagen fibrils. The sham control heart section showed healthy myocytes with interconnected cytoplasmic junctions in the left ventricle. The untreated MSCs transplanted group showed reduced fibrosis, while the IWP-4 treated MSCs transplanted group showed complete restoration of the left ventricle and regeneration of the myocytes as shown in Figure 7A and B. Quantification of the total fibrotic area showed that the IWP-4 treated MSCs transplanted group has significantly reduced ($P < 0.001$) fibrosis as compared to the MI model and untreated MSCs transplanted group (Figure 7D). Measurements of left ventricular wall thickness revealed that in the untreated MSCs transplanted group, the restoration of left ventricular wall thickness was non-significant, while in the case of IWP-4 treated MSCs, the left ventricular wall thickness was significantly improved ($P < 0.001$) as compared to the MI group as shown in Figure 7E. H&E staining showed the accumulation of inflammatory cells in the left ventricular region of the infarcted heart in the MI group as compared to the sham control. However, it was improved in untreated MSCs and IWP-4 treated MSCs transplanted group as shown in Figure 8.

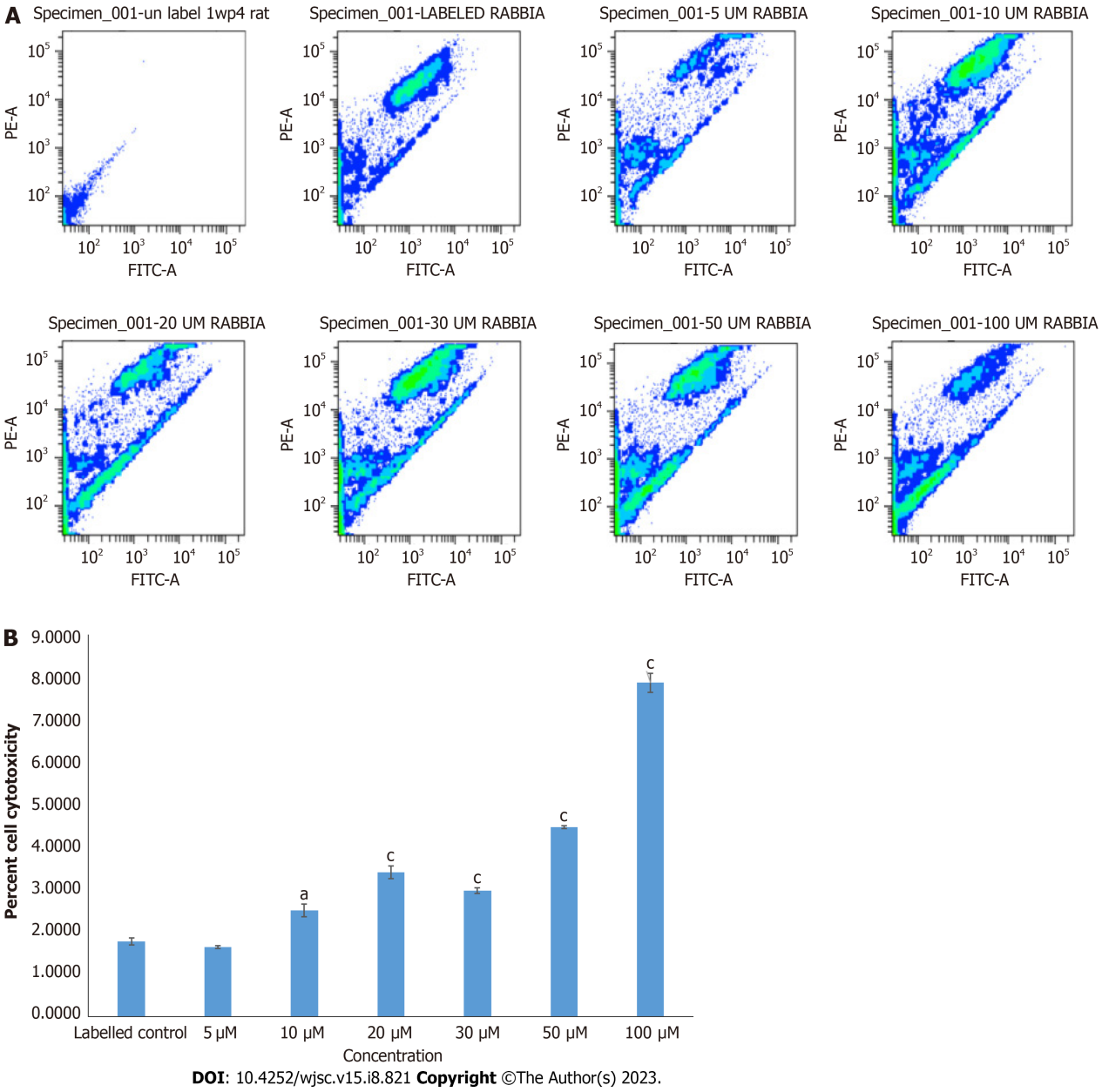

DOI: 10.4252/wjsc.v15.i8.821 **Copyright** ©The Author(s) 2023.

Figure 2 Cytotoxicity analysis of mesenchymal stem cells treated with different concentrations of inhibitor Wnt production-4 by JC-1 assay. A: Mesenchymal stem cells (MSCs) treated with 5 μM concentration of inhibitor Wnt production-4 showed non-significant number of apoptotic cells, while 10 μM concentration or above showed significant cytotoxic effect on MSCs; B: Quantification of apoptotic and non-apoptotic cells presented in bar graphs. For statistical analysis, One-way ANOVA was used followed by the Bonferroni post-hoc test. Values are expressed as means ± SEM; level of significance is $P < 0.05$ ($^{a}P < 0.05$, $^{c}P < 0.001$).

Tracking of DiI labeled cell: Fluorescence images of DiI labeled untreated MSCs, as well as IWP-4 treated MSCs showed cell distribution and homing in the infarcted myocardium, in both transplanted heart sections. The DiI labeled cells in the cardiac tissue were immunohistochemically stained for cardiac proteins including GATA-4, cTnI, and alpha actinin which showed that the transplanted cells differentiated into cardiac lineage. However, more pronounced cardiac differentiation and cell density were observed in the IWP-4 treated MSCs transplanted group, with GATA-4, cTnI ($P < 0.001$), and alpha actinin ($P < 0.01$) as compared to untreated MSCs group as shown in Figure 9.

DISCUSSION

In this study, we explored the role of IWP-4 on MSCs in cardiac differentiation *in vitro* and cardiac function restoration *in vivo*. Human umbilical cord derived MSCs are a potential candidate for cell therapy as they are easy to isolate and have a high proliferation rate, low immunogenicity, and immunomodulatory effects. MSCs have various therapeutic advantages that have been explained in several MI models[9]. Unfortunately, transplanted MSCs show poor survival and homing in

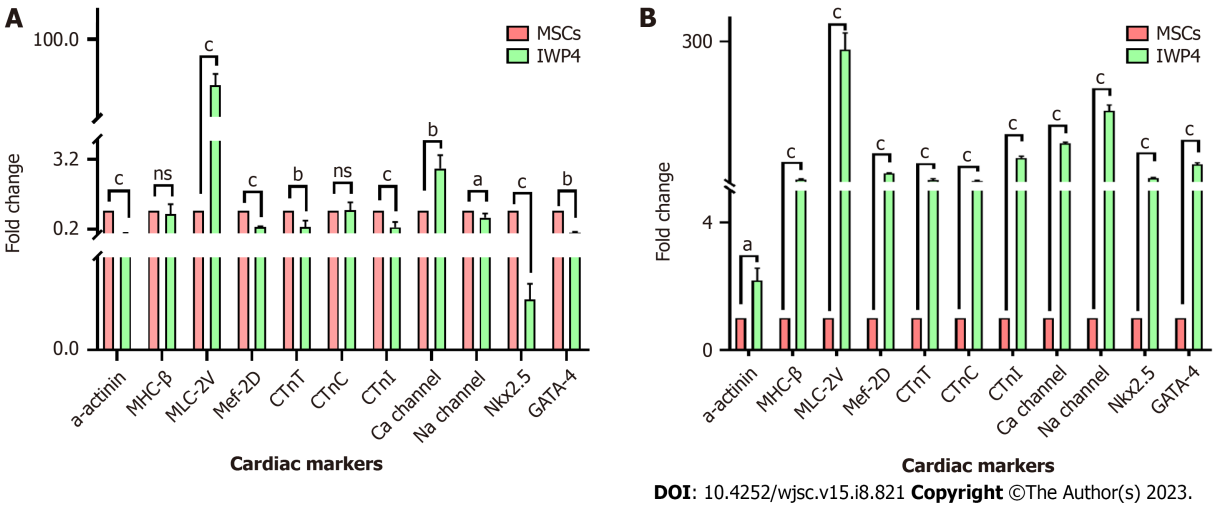

DOI: 10.4252/wjsc.v15.i8.821 **Copyright** ©The Author(s) 2023.

Figure 3 Cardiac markers gene expression analysis by quantitative real-time polymerase chain reaction. A: Seven days treatment of mesenchymal stem cells (MSCs) with inhibitor Wnt production-4 (IWP-4); B: Fourteen days treatment of MSCs with IWP-4 in comparison with untreated control showing significant increase in the expression of early cardiac markers, *GATA-4, Nkx2.5,* and late cardiac markers, *MHC-β, MLC-2v*, *Mef-2D*, *cTnT*, *cTnC*, *cTnI*, *α-actinin*, *Ca-channel* and *Na-channel*. Quantitative two fold ($2^{-\Delta\Delta CT}$) difference of mean is represented by ΔΔCt method. Statistical analysis was performed using an Independent sample t-test. Values are presented as mean ± SEM from three independent biological triplicates; level of significance is $P < 0.05$ ($^{a}P < 0.05$, $^{b}P < 0.01$, and $^{c}P < 0.001$). IWP-4: Inhibitor Wnt production-4; MSC: Mesenchymal stem cell; NS: No significant.

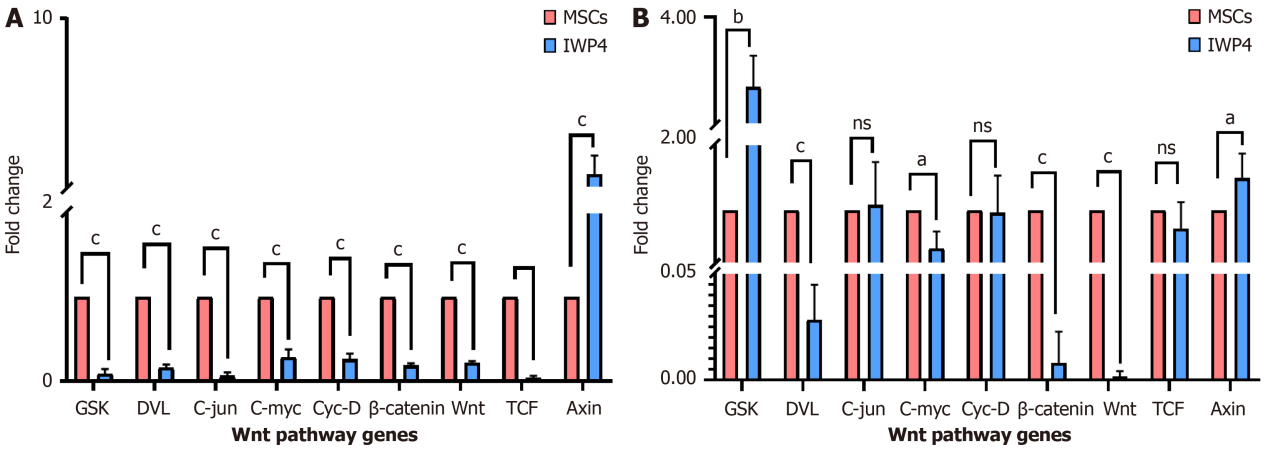

DOI: 10.4252/wjsc.v15.i8.821 **Copyright** ©The Author(s) 2023.

Figure 4 Wnt pathway gene expression analysis: Wnt pathway gene expression analysis by quantitative real-time polymerase chain reaction. Seven days, and fourteen days treatment of mesenchymal stem cells with inhibitor Wnt production-4, in comparison with untreated control showing significant decrease in the expression of Wnt pathway genes, *DVL*, *Wnt*, *TCF*, *Axin*, and *β-catenin*, and downstream transcription factors *C-jun*, *C-myc*, and *Cyc-D*. A: Seven days; B: Fourteen days. *GSK* increased in the fourteen days treatment. Quantitative two fold ($2^{-\Delta\Delta CT}$) difference of mean is represented by ΔΔCt method. Statistical analysis was performed using an Independent sample t-test. Values are presented as mean ± SEM from three independent biological triplicates; level of significance is $P < 0.05$ ($^{a}P < 0.05$, $^{b}P < 0.01$, and $^{c}P < 0.001$). IWP-4: Inhibitor Wnt production-4; MSC: Mesenchymal stem cell; NS: No significant.

the infarcted myocardium[10], while pre-differentiated MSCs have several advantages over MSCs[11].

Wnt and Smad signaling pathways play an important role in the fate determination of stem cell and their potential for cardiovascular differentiation. Several studies reported that Wnt and Smad signaling pathways play an important role in the fate determination of stem cells and their potential for cardiovascular differentiation. Several studies reported that early application of Wnt/β-catenin signaling pathway inhibitor, IWR1 promotes cardiomyocyte differentiation[12]. Similarly, IWP-4 is a potent small molecule that has been reported to differentiate embryonic stem cells into cardiomyocyte like cells[7]. IWP-4 was also reported to differentiate human umbilical cord derived induced pluripotent stem cells into cardiomyocyte like cells[13].

In this study, IWP-4 was used to differentiate human umbilical cord derived MSCs into cardiomyocyte like cells. First, MSCs were isolated, propagated, and expanded from cord tissue according to the minimum criteria established by the International Society for Cellular Therapy.

To identify the optimal non-toxic concentration of IWP-4, MSCs were treated with different concentrations of IWP-4. 5 μM concentration was found to be non-cytotoxic after 24 h of treatment and analyzed *via* JC-1 assay.

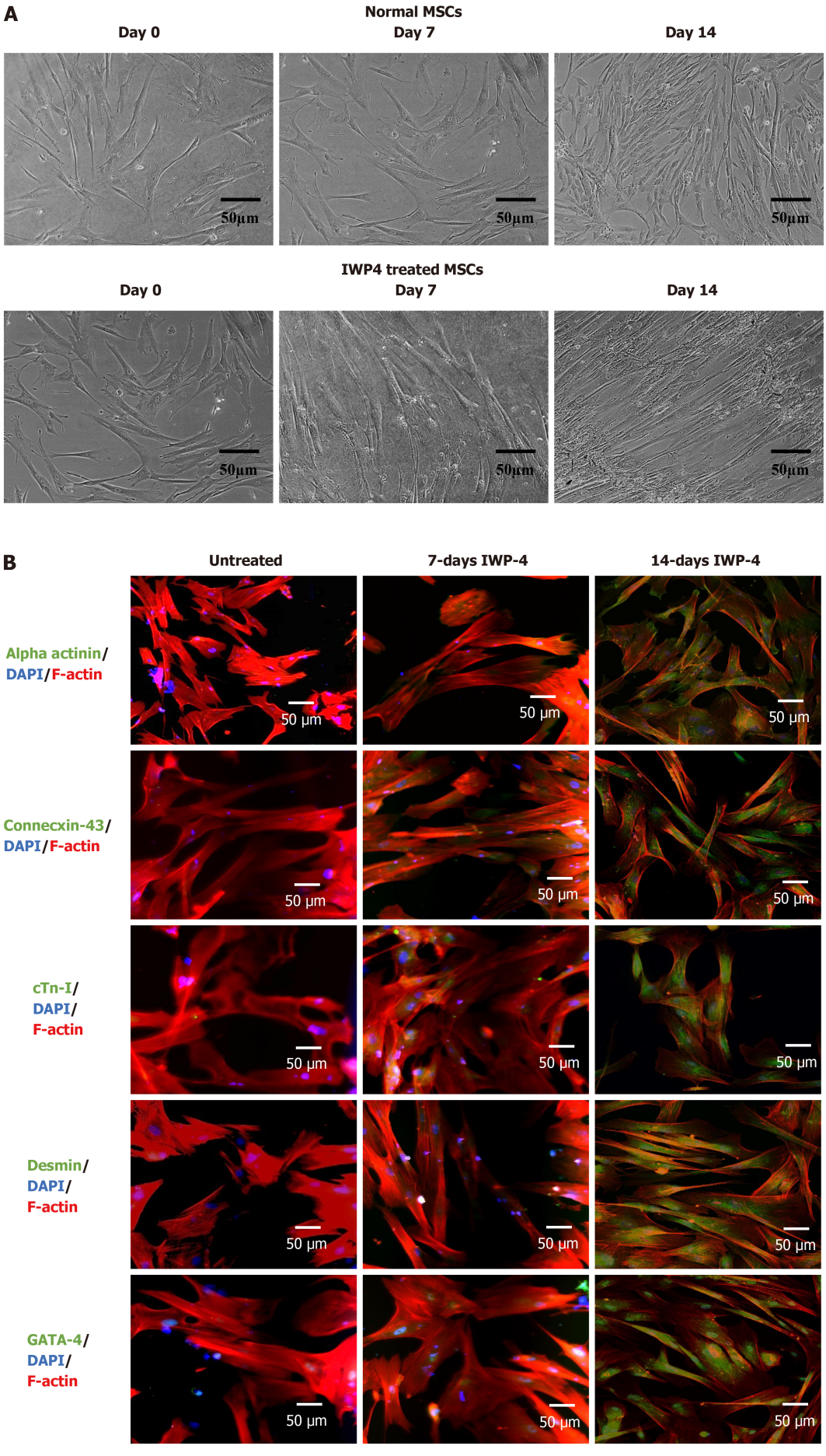
A
Normal MSCs
Day 0
Day 7
Day 14
50μm
IWP4 treated MSCs
Day 0
Day 7
Day 14
50μm
B
Untreated
7-days IWP-4
14-days IWP-4
Alpha actinin/
DAPI/F-actin
Connecxin-43/
DAPI/F-actin
cTn-I/
DAPI/
F-actin
Desmin/
DAPI/
F-actin
GATA-4/
DAPI/
F-actin
50 μm

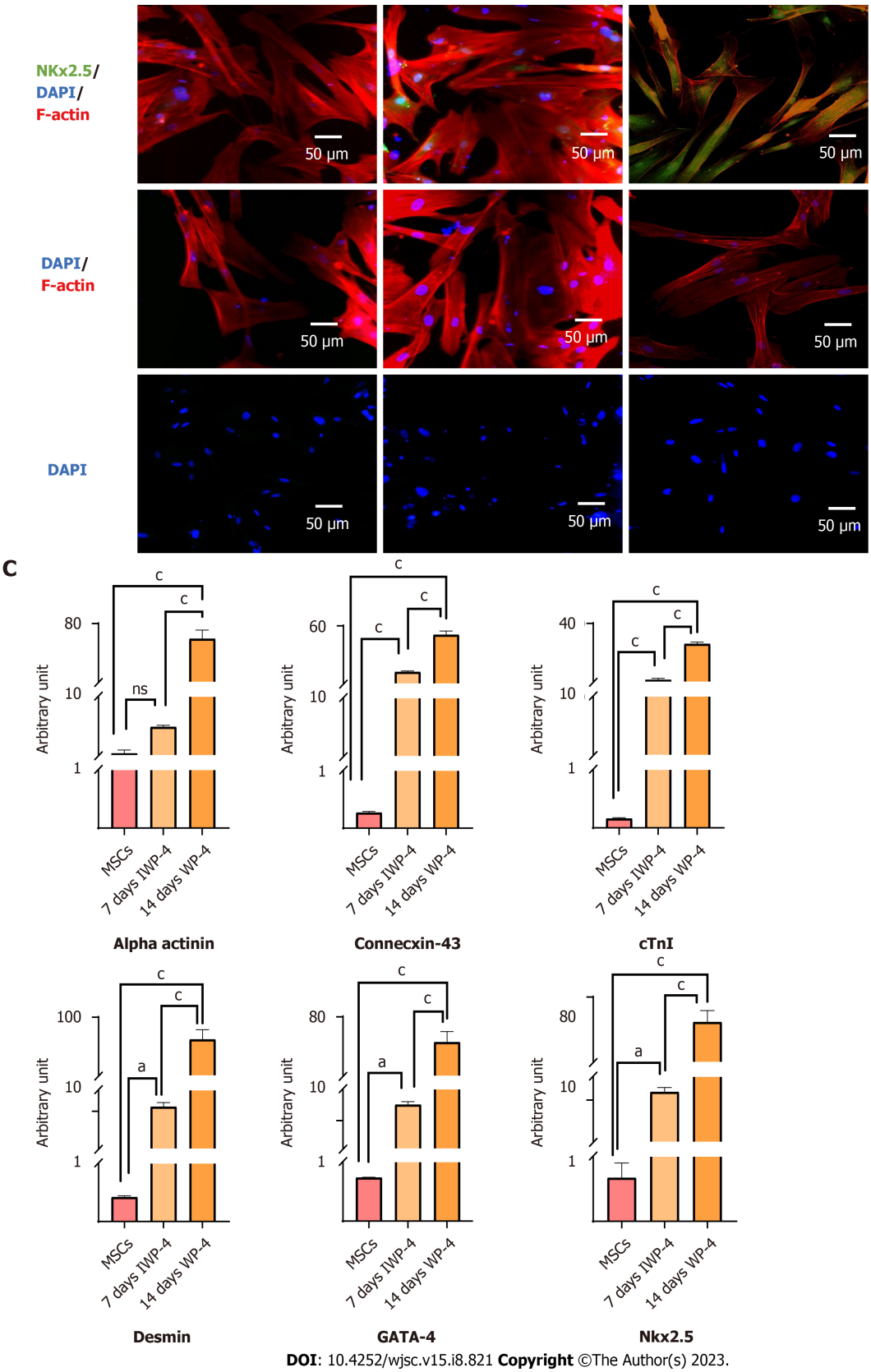

DOI: 10.4252/wjsc.v15.i8.821 **Copyright** ©The Author(s) 2023.

Figure 5 Analysis of fourteen days inhibitor Wnt production-4 treated mesenchymal stem cells. A: Morphology of untreated mesenchymal stem cells (MSCs), seven days inhibitor Wnt production-4 (IWP-4) treated MSCs and fourteen days IWP-4 treated MSCs; B: Immunocytochemical analysis of untreated MSCs, seven days and fourteen days IWP-4 treated MSCs showing positive expression of cardiac-specific proteins *α-actinin*, *connexin-43*, *cTnI*, *Desmin*, *GATA-4*, *Nkx2.5*, secondary control, and DAPI control. Alexa fluor 488 secondary antibody was used for detection, then counterstained with DAPI to stain the nuclei; C: Quantification of fluorescence intensities in untreated MSCs, seven days, and fourteen days IWP-4 treated MSCs. For statistical analysis, One-way ANOVA was used followed by the Bonferroni post-hoc test. Data are presented as mean ± SEM with significance level $P < 0.05$ (where $^{a}P < 0.05$, $^{c}P < 0.001$). IWP-4: Inhibitor Wnt production-4; MSC: Mesenchymal stem cell; NS: No significant.

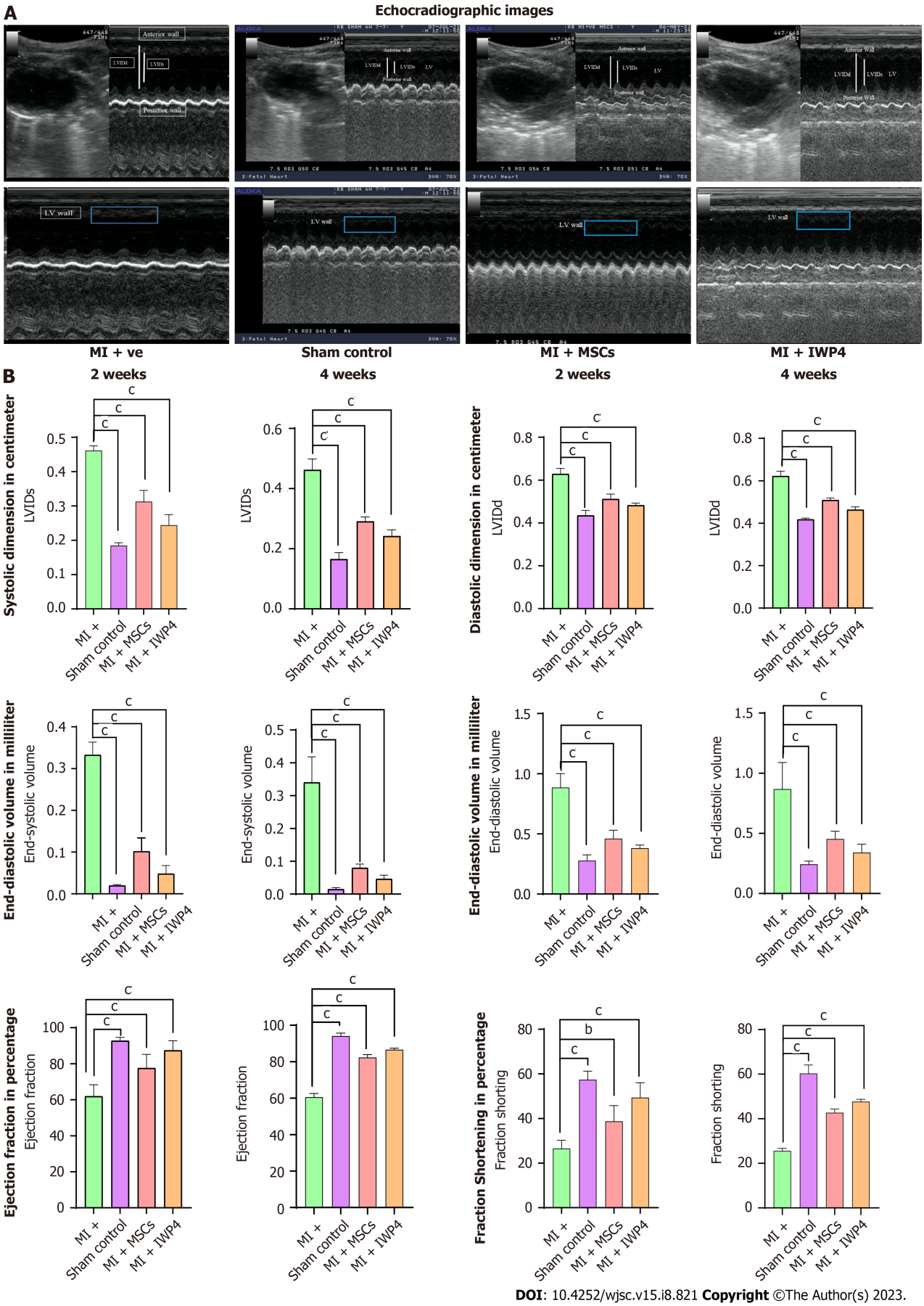

DOI: 10.4252/wjsc.v15.i8.821 **Copyright** ©The Author(s) 2023.

Figure 6 Cardiac functional analysis by echocardiography. A: Ultrasound images taken at parasternal long axis showing B and M mode scans of left ventricle in sham control, myocardial infarction (MI+) group, mesenchymal stem cells (MI+MSC) treated group, and inhibitor Wnt production-4 (IWP-4) (MI+IWP-4)

treated groups; B: Bar graphs representing cardiac functional analysis in terms of left ventricular systolic internal dimensions, left ventricular diastolic internal dimensions, end-systolic volume and end-diastolic volume, ejection fraction and fractional shortening, after 2 and 4 wk of MI model development. Both untreated and IWP-4 treated MSC groups showed cardiac functional improvement. However, IWP-4 treated group exhibited more significant results. Statistical analysis was performed using One-way ANOVA followed by Bonferroni post-hoc test. Data are presented as mean ± SEM with significance level $P < 0.05$ (where $^{b}P < 0.01$; $^{c}P < 0.001$). IWP-4: Inhibitor Wnt production-4; MSC: Mesenchymal stem cell; MI: Myocardial infarction; LVIDs: Left ventricular systolic internal dimensions; LVIDd: Left ventricular diastolic internal dimensions.

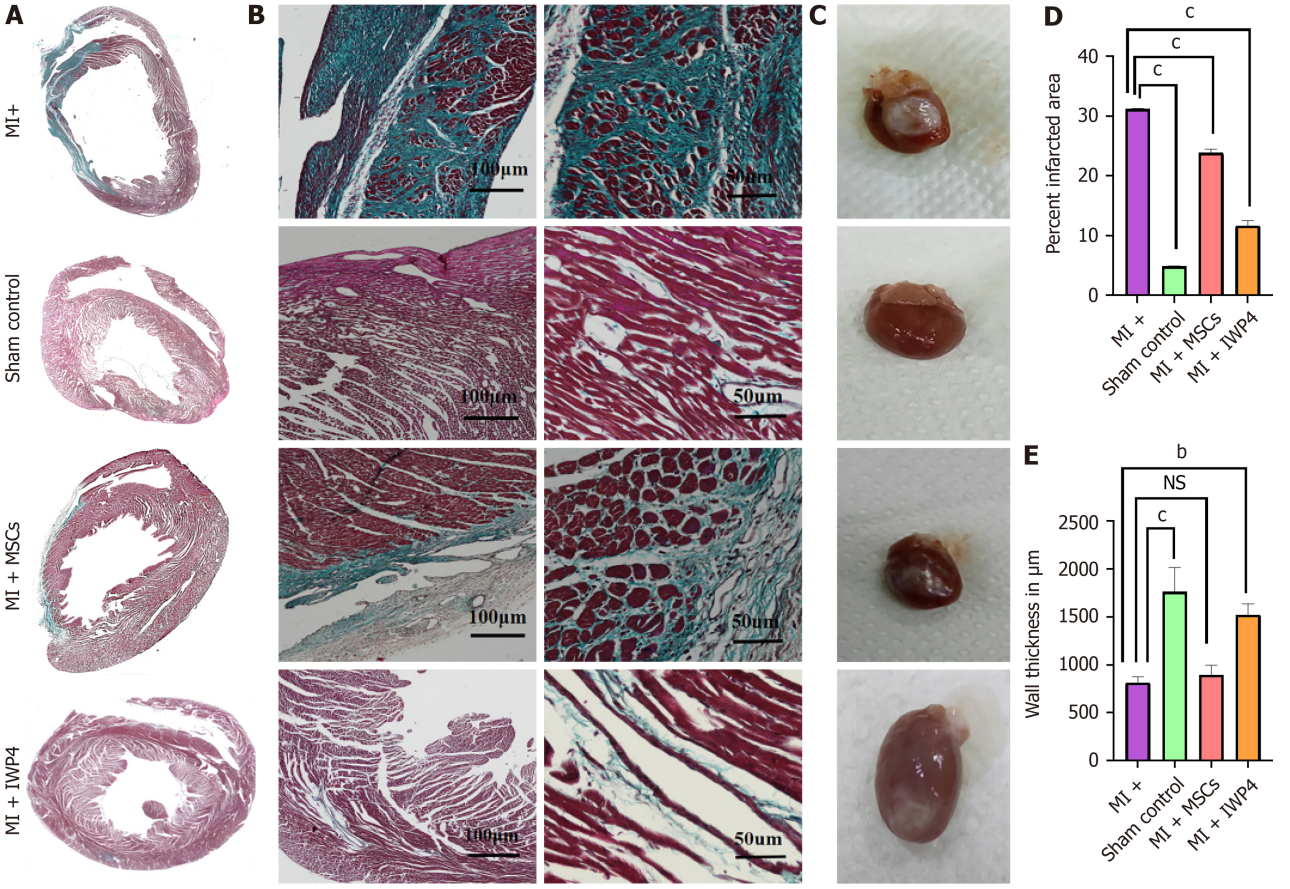

DOI: 10.4252/wjsc.v15.i8.821 **Copyright** ©The Author(s) 2023.

Figure 7 Histological analysis of heart sections. A: Large scan images showing Masson's trichrome stained transverse section of the whole heart; B: Magnified images showing Masson's trichrome stained sections in sham control, myocardial infarction (MI+), mesenchymal stem cells (MSCs) (MI+MSCs), and inhibitor Wnt production-4 (IWP-4) treated MSCs (MI+IWP-4) groups after 4 wk of MI; C: Images showing isolated rat hearts of sham control, MI+ group, MI+MSC group, and MI+IWP-4 groups; D: Bar graph showing percent infarcted area as compared to MI+ group. Percent infarcted area was significantly decreased in MI+MSC and MI+IWP-4 groups after 4 wk of MI; E: Bar graph showing left ventricular wall thickness as compared to MI+ group; left ventricular wall thickness was non-significant in MI+MSC group and significantly increased in the MI+IWP-4 group after 4 wk of MI. For statistical analysis, One-way ANOVA was used followed by the Bonferroni post-hoc test. Data is presented as mean ± SEM with significance level $P < 0.05$ where ($^{b}P < 0.01$, $^{c}P < 0.001$). IWP-4: Inhibitor Wnt production-4; MSC: Mesenchymal stem cell; MI: Myocardial infarction; NS: No significant.

To confirm the Wnt pathway inhibition, Wnt pathway gene expression profile was analyzed after seven and fourteen days treatment of MSCs with IWP-4. Gene expression profile revealed that seven days treatment of MSCs with IWP-4 inhibits Wnt pathway as compared to untreated MSCs; Wnt pathway genes, *GSK*, *DVL*, *Wnt*, *TCF*, *β-catenin*, and downstream transcription factors *C-jun*, *C-myc*, *Cyc-D* ($P < 0.001$) were significantly downregulated, while *Axin* showed upregulation ($P < 0.01$). However, fourteen days treatment of MSCs with IWP-4, further downregulated the Wnt pathway as compared to untreated control; Wnt pathway genes *DVL*, *Wnt*, *β-catenin* ($P < 0.001$) showed significant downregulation, while negative regulators of the pathway *GSK* ($P < 0.01$), and *Axin* ($P < 0.05$) were upregulated. Downstream transcription factors *C-jun*, *Cyc-D*, *TCF* were non-significant, while *C-myc* ($P < 0.05$) was upregulated.

The Wnt (β-catenin dependent) comprises several proteins that are crucial for embryonic development as well as adult tissue homeostasis. In the absence of Wnt ligands, cytoplasmic β-catenin is captured by the destruction complex including glycogen synthase kinase-3β (GSK3β), axin, adenomatous polyposis coli, and casein kinase 1 (CK1). This destruction complex induces the β-catenin phosphorylation at the amino terminus by CK1 and GSK3β, that results in the ubiquitination and degradation of β-catenin[14]. In the presence of ligands, Wnt binds to its receptor and activates the signaling pathway. This ligand receptor binding recruits the axin and DVL protein towards the cell membrane, thus resulting in the inactivation of the destruction complex. As a result, β-catenin translocate to the nucleus where it binds to the transcription

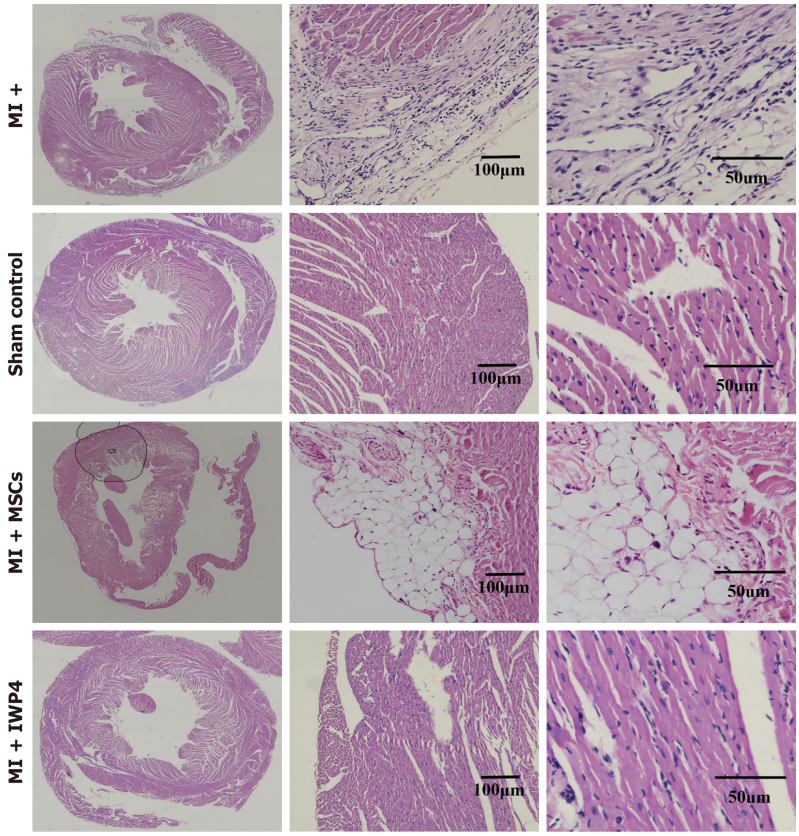

DOI: 10.4252/wjsc.v15.i8.821 **Copyright** ©The Author(s) 2023.

Figure 8 Hematoxylin-Eosin staining of heart section. Large scan images showing Hematoxylin-Eosin (H&E) stained transverse section of the whole heart. Magnified images showing H&E stained sections in sham control, myocardial infarction (MI) group, mesenchymal stem cells (MSCs) (MI+MSC) group, and inhibitor Wnt production-4 (IWP-4) treated MSCs (MI+IWP-4) group after 4 wk of MI. IWP-4: Inhibitor Wnt production-4; MSC: Mesenchymal stem cell; MI: Myocardial infarction.

factor TCF and increases the expression of Wnt target genes[13,15].

In our study, IWP-4 treatment was given for seven and fourteen days. Morphological features of fourteen days treated MSCs showed cardiomyogenic differentiation; the cells were flattened and appeared larger with myotube like structures. To confirm the differentiation of cells toward cardiac lineage, cardiac specific gene expression profile was analyzed through qPCR. In the seven days treated MSCs, only two cardiac genes *MLC-2v* ($P < 0.01$) and *Ca-channel* ($P < 0.05$) showed upregulation, while *Na-channel* ($P < 0.05$), *cTnT*, *GATA4* ($P < 0.01$), *alpha-actinin*, *cTnI*, *Mef2D* and *Nkx2.5* ($P < 0.001$) genes showed significant downregulation; *MHC-β* and *cTnC* were non-significant. However, fourteen days treated MSCs showed significant upregulation of all cardiac genes including *alpha-actinin* ($P < 0.05$), *MHC-β*, *MLC-2v*, *Mef2D*, *cTnT*, *cTnC*, *cTnI*, *Ca-channel*, *Na-channel*, *Nkx2.5* and *GATA4* ($P < 0.001$) as compared to untreated MSCs.

The cardiac markers GATA-4 and Nkx2.5 play important role in the cardiac development[16]. GATA-4 is an important early cardiac transcription factor that regulates several cardiac genes[17]. Nkx2.5 is another important transcription factor that showed high expression in the cardiac progenitor cells and promotes cardiomyocyte maturation[18]. Cardiac troponin exists in three different subunits, cTnT, cTnI, and cTnC. Troponin proteins are linked with tropomyosin which is present in all skeletal and cardiac muscle cells and plays an essential role in cardiac contractile movement. cTnT directly binds with the thin filaments, while cTnI and cTnC bind with cTnT. It is also reported to be circulated into the blood after cardiomyocyte injury[19]. cTnI and cTnT are the essential components of the cardiac troponin complex particularly involved in the formation of cardiomyocyte contractile network and regulate cardiac contraction and relaxation[20,21].

In the human heart, cardiac myosin heavy chain is expressed in two isoforms *i.e.* α-MHC and β-MHC. β-MHC is an important cardiac marker, predominant ventricular isoform, and principal mediator of cardiac contractile function[22]. Any change regarding the expression of MHC isoforms disturbs the cardiac contractile functions[23]. Ventricular MLC-2v is the ventricular cardiac muscle form of myosin light chain 2. MLC-2v is regarded as a ventricular-specific marker of the myocardium. MLC-2v is expressed during early cardiac development in humans[24]. Mef2 is a transcription factor that is important for right ventricle development[25]. Cardiac α-actinin-2, also known as alpha actinin, is a homodimer, Z-disk component of sarcomere responsible for three important functions: Anchoring of thin filaments actin, sarcomere formation, and interaction with titin[26]. The upregulation of cardiac ion channels (sodium and calcium) decides the cell fate to become mature functional cardiomyocytes[27]. Calcium acts as a second messenger in signal transduction pathways as well as necessary for muscular contraction. Calcium is controlled by calcium transport proteins, calcium channels, carriers and pumps[28]. Voltage-gated sodium channels are transmembrane proteins that generate action potentials in neurons and cardiac cells[29].

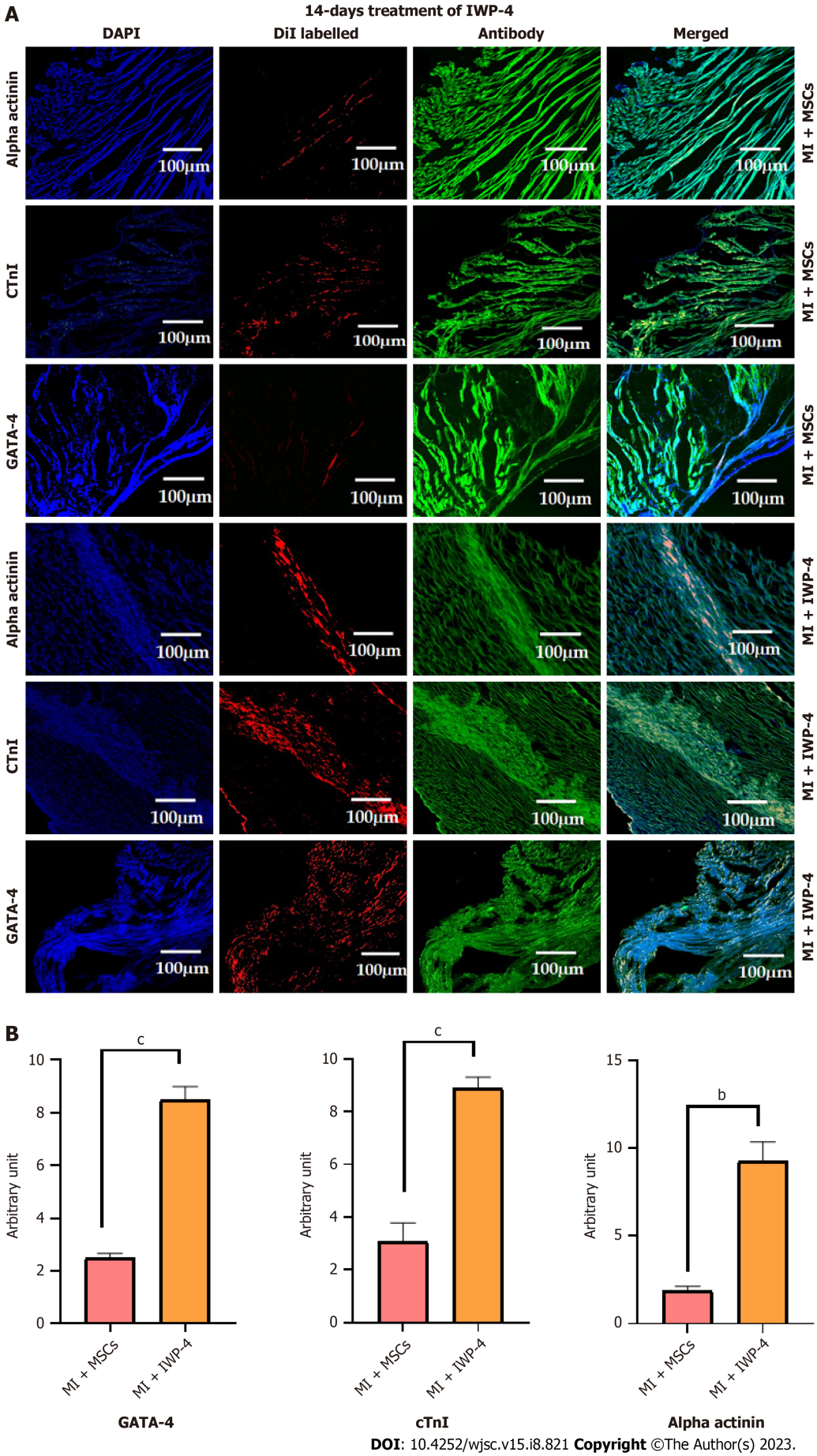

DOI: 10.4252/wjsc.v15.i8.821 **Copyright** ©The Author(s) 2023.

Figure 9 Immunohistochemistry of heart tissue section. A: Immunohistochemical images of heart sections showing the transplanted untreated

mesenchymal stem cells (MSCs) and fourteen days inhibitor Wnt production-4 (IWP-4) treated MSCs labeled with red fluorescent DiI dye. Cardiac specific proteins α-actinin, cTnI, and GATA-4 were immunostained for the expression of cardiac proteins. Alexa fluor 488 secondary antibody was used for detection; B: Quantification of the fluorescence intensities of the DiI labeled cells presented in bar graphs. As compared to normal MSCs, fluorescence intensity was significantly increased in case of alpha actinin, GATA-4, and cTnI in the fourteen days IWP-4 treated MSCs group in the infarcted myocardium. For statistical analysis, One-way ANOVA was used followed by the Bonferroni post-hoc test. Data are presented as mean ± SEM with significance level $P < 0.05$ where ($^{b}P < 0.01$, $^{c}P < 0.001$). IWP-4: Inhibitor Wnt production-4; MSC: Mesenchymal stem cell; MI: Myocardial infarction.

Cardiac specific protein expression analysis was also performed to further confirm myogenic differentiation. Cardiac protein expression was analyzed in untreated, and seven and fourteen days treated MSCs. Seven days treated MSCs showed less protein expression of C-43, cTnI, ($P < 0.001$), desmin, GATA-4, and Nkx2.5 ($P < 0.05$), while alpha-actinin protein expression was non-significant. Fourteen days treated MSCs showed significant positive expression of cardiac proteins including alpha-actinin, C-43, cTnI, desmin, GATA-4, and Nkx2.5 ($P < 0.001$). C-43 is a gap junction protein that connects the neighboring cardiac cells. C-43 is abundant and expressed in atrial as well as ventricular cardiomyocytes [30]. Desmin is an important intermediate filament that maintains the cytoskeletal structure and cellular integrity in skeletal, smooth, and cardiac muscles[31]. The presence of cardiac specific proteins further confirmed the differentiation of MSCs into cardiomyocytes, as these proteins are necessary for several developmental processes and functioning of the heart. Hence, a pronounced effect was observed in fourteen days treated MSCs, so it was selected for *in vivo* studies.

To examine the ability of pre-differentiated MSCs to regenerate the infarcted myocardium *in vivo*, a rat MI model was established and fourteen days treated pre-differentiated MSCs were transplanted. In previous studies, it was reported that the pre-differentiated MSCs homed and survived better than the untreated MSCs in the injured myocardium[11,32]. To confirm, untreated MSCs, as well as IWP-4 treated MSCs, were transplanted in the left ventricular wall of the infarcted hearts immediately after MI induction.

For cardiac functional analysis, echocardiography was performed after 2 and 4 wk of MI. Functional studies revealed a significant increase in LVIDd, LVIDs, EDV, and ESV in the MI model; however, FS and EF were significantly decreased as compared to the sham control. These results confirmed the successful MI model development. When compared with the MI group, LVIDd, LVIDs, EDV, and ESV were significantly reduced, while EF and FS were significantly improved after 2 and 4 wk in both untreated and IWP-4 treated MSCs transplanted groups. However, the IWP-4 treated group showed more pronounced results.

For histological analysis, heart tissue was harvested after 4 wk of infarction. The MI heart exhibited a whitish scar with no blood vessels in the infarcted area, while in the IWP-4 transplanted heart, the area of scar was reduced with blood vessels in the repaired myocardium. To observe the histology, and to calculate the fibrotic area and wall thickness, H&E and Masson's trichrome staining were performed. Histological analysis revealed that the fibrotic area was reduced and wall thickness was increased in the untreated MSCs transplanted heart sections, while the IWP-4 treated group showed significantly reduced fibrosis, and improved wall thickness as compared to the MI group. Untreated as well as IWP-4 treated MSCs were labeled with DiI dye to track the localization and homing of cells in the infarcted myocardium, and analyzed through immunohistochemistry. Cardiac functional proteins GATA-4, alpha actinin and cTnI were used for immunohistochemical analysis of the cryosectioned heart that showed cardiac proteins as well as DiI dye expression in the myocardium. Fluorescence intensity calculation revealed the transplanted cell density and significantly higher cardiac protein expression in the IWP-4 treated MSCs group as compared to the untreated group. This data further supports the histological results that revealed a markedly decreased fibrotic area and increased regeneration of the infarcted myocardium. Altogether, the results showed that IWP-4 treated MSCs regenerated myocardium, ventricular remodeling, and improved heart function.

CONCLUSION

This study focused on the treatment of hUC-MSCs with IWP-4 for differentiation of MSCs into cardiomyogenic lineage *via* inhibiting Wnt pathway and their consequent role in the cardiac function restoration in the rat MI model. Fourteen days IWP-4 treatment increases the expression of cardiac markers in MSCs, both at the gene and protein levels, as compared to the untreated control. Transplanted pre-differentiated cells in the rat MI model not only distributed, survived, and homed, but also differentiated into mature cardiomyocytes better than untreated MSCs. The results obtained from the current preclinical study suggests that treatment with the small molecule IWP-4 could be a good option for the differentiation of MSCs into functional cardiomyocytes in clinical trials of MI patients in future.

ARTICLE HIGHLIGHTS

Research background

Cardiovascular diseases particularly myocardial infarction (MI) is a global health complication with high mortality and morbidity rate. As cardiac tissue lacks regeneration potential, so cardiac tissue regeneration using a potent small molecule inhibitor Wnt production-4 (IWP-4) for stem cell fate transition towards cardiomyocytes could be an effective approach.

Research motivation
Inhibition of Wnt pathway is important in stem cell fate determination towards cardiomyocytes. Wnt pathway inhibitor, such as IWP-4, may promote the differentiation of mesenchymal stem cells (MSCs) into cardiac lineage. These pre-conditioned cells may provide better survival, homing and migration capability at the site of injury.

Research objectives
This study was designed to evaluate the IWP-4 cardiac differentiation capability and its subsequent *in vivo* effects.

Research methods
Human umbilical cord-derived MSCs were characterized on the basis of morphology, immunophenotyping of surface markers associated with MSCs and tri-lineage differentiation capability. Isolated MSCs were treated with 5 μM IWP-4 at two different time intervals. Cardiomyogenic differentiation of treated MSCs was evaluated at DNA and protein levels. MI rat model was developed. IWP-4 treated as well as untreated MSCs were implanted in the MI model, and cardiac function was analyzed *via* echocardiography. MSCs were labeled with 1,1′-dioctadecyl-3,3,3′,3′-tetramethylindocarbocyanine perchlorate (DiI) dye for tracking, and regeneration of the infarcted myocardium was examined by histology and immunohistochemistry.

Research results
Isolated MSCs were characterized and then pre-conditioned with 5 μM concentration of IWP-4. The cardiac specific gene and protein expression analysis exhibited more remarkable results in fourteen days treated group that was eventually selected for *in vivo* transplantation. Cardiac function was restored in the IWP-4 treated group in comparison to the MI group. Immunohistochemical analysis confirmed the homing of pre-differentiated MSCs that were labeled with DiI cell labeling dye. Histological analysis confirmed the significant reduction in the fibrotic area, and improved the left ventricular wall thickness in the IWP-4 treated MSC group.

Research conclusions
Our data suggest that treatment of MSCs with IWP-4 inhibits Wnt pathway and promotes cardiac differentiation. These pre-conditioned MSCs transplanted *in vivo* improved cardiac function by cell homing, survival, and differentiation at the infarcted region, increased left ventricular wall thickness, and reduced infarct size.

Research perspectives
The study demonstrated that treatment with IWP-4 improves the efficacy of the MSCs to ameliorate the cardiac function of the MI rats, as evidenced by an increase in the ejection fraction. Pre-conditioning of MSCs with IWP-4 may serve as a promising strategy to treat heart disease. Targeting the Wnt signaling pathway may represent a promising therapeutic approach for this debilitating condition.

FOOTNOTES

Author contributions: Muneer R performed experiments and wrote the original manuscript; Qazi R, Fatima A, and Ahmad W helped in experimentation and writing; Salim A evaluated and analyzed the data, and reviewed the manuscript; Dini L evaluated and analyzed the data; Khan I conceived and designed the studies, evaluated and analyzed the data, and finalized the manuscript.

Institutional review board statement: The independent ethical committee of PCMD, ICCBS, University of Karachi, for human subjects has approved the protocol, No. ICCBS/IEC-067-HT/UCB-2021/Protocol/1.0.

Institutional animal care and use committee statement: Ethical approval for the use of animals was obtained from the Institutional Animal Care and Use Committee at the PCMD, ICCBS, University of Karachi with protocol number 2021-006.

Informed consent statement: Informed consent was obtained from the donor.

Conflict-of-interest statement: Authors declare no conflict of interest.

Data sharing statement: No additional data to share.

ARRIVE guidelines statement: The authors have read the ARRIVE guidelines, and the manuscript was prepared and revised according to the ARRIVE guidelines.

Open-Access: This article is an open-access article that was selected by an in-house editor and fully peer-reviewed by external reviewers. It is distributed in accordance with the Creative Commons Attribution NonCommercial (CC BY-NC 4.0) license, which permits others to distribute, remix, adapt, build upon this work non-commercially, and license their derivative works on different terms, provided the original work is properly cited and the use is non-commercial. See: https://creativecommons.org/Licenses/by-nc/4.0/

Country/Territory of origin: Pakistan

ORCID number: Rabbia Muneer 0000-0001-8223-8212; Rida-e-Maria Qazi 0000-0002-0458-0263; Abiha Fatima 0000-0002-9991-1669; Waqas Ahmad 0000-0002-3291-0629; Asmat Salim 0000-0001-5181-0458; Luciana Dini 0000-0002-2633-9040; Irfan Khan 0000-0003-1878-7836.

S-Editor: Fan JR
L-Editor: A
P-Editor: Xu ZH

REFERENCES

1 **Dritsas E**, Alexiou S, Moustakas K. Cardiovascular Disease Risk Prediction with Supervised Machine Learning Techniques. *In ICT4AWE* 2022; **1**: 315-321 [DOI: 10.5220/0011088300003188]
2 **Gupta S**, Sharma A, S A, Verma RS. Mesenchymal Stem Cells for Cardiac Regeneration: from Differentiation to Cell Delivery. *Stem Cell Rev Rep* 2021; **17**: 1666-1694 [PMID: 33954876 DOI: 10.1007/s12015-021-10168-0]
3 **Poomani MS**, Mariappan I, Perumal R, Regurajan R, Muthan K, Subramanian V. Mesenchymal Stem Cell (MSCs) Therapy for Ischemic Heart Disease: A Promising Frontier. *Glob Heart* 2022; **17**: 19 [PMID: 35342702 DOI: 10.5334/gh.1098]
4 **Han Y**, Li X, Zhang Y, Han Y, Chang F, Ding J. Mesenchymal Stem Cells for Regenerative Medicine. *Cells* 2019; **8** [PMID: 31412678 DOI: 10.3390/cells8080886]
5 **Jin HJ**, Bae YK, Kim M, Kwon SJ, Jeon HB, Choi SJ, Kim SW, Yang YS, Oh W, Chang JW. Comparative analysis of human mesenchymal stem cells from bone marrow, adipose tissue, and umbilical cord blood as sources of cell therapy. *Int J Mol Sci* 2013; **14**: 17986-18001 [PMID: 24005862 DOI: 10.3390/ijms140917986]
6 **García-Reyes B**, Witt L, Jansen B, Karasu E, Gehring T, Leban J, Henne-Bruns D, Pichlo C, Brunstein E, Baumann U, Wesseler F, Rathmer B, Schade D, Peifer C, Knippschild U. Discovery of Inhibitor of Wnt Production 2 (IWP-2) and Related Compounds As Selective ATP-Competitive Inhibitors of Casein Kinase 1 (CK1) δ/ε. *J Med Chem* 2018; **61**: 4087-4102 [PMID: 29630366 DOI: 10.1021/acs.jmedchem.8b00095]
7 **Hudson J**, Titmarsh D, Hidalgo A, Wolvetang E, Cooper-White J. Primitive cardiac cells from human embryonic stem cells. *Stem Cells Dev* 2012; **21**: 1513-1523 [PMID: 21933026 DOI: 10.1089/scd.2011.0254]
8 **Wu KH**, Wang SY, Xiao QR, Yang Y, Huang NP, Mo XM, Sun J. Small-molecule-based generation of functional cardiomyocytes from human umbilical cord-derived induced pluripotent stem cells. *J Cell Biochem* 2019; **120**: 1318-1327 [PMID: 30317643 DOI: 10.1002/jcb.27094]
9 **Guo Y**, Yu Y, Hu S, Chen Y, Shen Z. The therapeutic potential of mesenchymal stem cells for cardiovascular diseases. *Cell Death Dis* 2020; **11**: 349 [PMID: 32393744 DOI: 10.1038/s41419-020-2542-9]
10 **Razeghian-Jahromi I**, Matta AG, Canitrot R, Zibaeenezhad MJ, Razmkhah M, Safari A, Nader V, Roncalli J. Surfing the clinical trials of mesenchymal stem cell therapy in ischemic cardiomyopathy. *Stem Cell Res Ther* 2021; **12**: 361 [PMID: 34162424 DOI: 10.1186/s13287-021-02443-1]
11 **Ali SR**, Ahmad W, Naeem N, Salim A, Khan I. Small molecule 2'-deoxycytidine differentiates human umbilical cord-derived MSCs into cardiac progenitors *in vitro* and their *in vivo* xeno-transplantation improves cardiac function. *Mol Cell Biochem* 2020; **470**: 99-113 [PMID: 32415417 DOI: 10.1007/s11010-020-03750-6]
12 **Le MNT**, Takahi M, Ohnuma K. Auto/paracrine factors and early Wnt inhibition promote cardiomyocyte differentiation from human induced pluripotent stem cells at initial low cell density. *Sci Rep* 2021; **11**: 21426 [PMID: 34728657 DOI: 10.1038/s41598-021-00763-z]
13 **Bilir B**, Kucuk O, Moreno CS. Wnt signaling blockage inhibits cell proliferation and migration, and induces apoptosis in triple-negative breast cancer cells. *J Transl Med* 2013; **11**: 280 [PMID: 24188694 DOI: 10.1186/1479-5876-11-280]
14 **Liu J**, Xiao Q, Xiao J, Niu C, Li Y, Zhang X, Zhou Z, Shu G, Yin G. Wnt/β-catenin signalling: function, biological mechanisms, and therapeutic opportunities. *Signal Transduct Target Ther* 2022; **7**: 3 [PMID: 34980884 DOI: 10.1038/s41392-021-00762-6]
15 **Zhang Y**, Wang X. Targeting the Wnt/β-catenin signaling pathway in cancer. *J Hematol Oncol* 2020; **13**: 165 [PMID: 33276800 DOI: 10.1186/s13045-020-00990-3]
16 **Yin J**, Qian J, Dai G, Wang C, Qin Y, Xu T, Li Z, Zhang H, Yang S. Search of Somatic Mutations of NKX2-5 and GATA4 Genes in Chinese Patients with Sporadic Congenital Heart Disease. *Pediatr Cardiol* 2019; **40**: 17-22 [PMID: 30121862 DOI: 10.1007/s00246-018-1955-z]
17 **Välimäki MJ**, Tölli MA, Kinnunen SM, Aro J, Serpi R, Pohjolainen L, Talman V, Poso A, Ruskoaho HJ. Discovery of Small Molecules Targeting the Synergy of Cardiac Transcription Factors GATA4 and NKX2-5. *J Med Chem* 2017; **60**: 7781-7798 [PMID: 28858485 DOI: 10.1021/acs.jmedchem.7b00816]
18 **Yuan F**, Qiu XB, Li RG, Qu XK, Wang J, Xu YJ, Liu X, Fang WY, Yang YQ, Liao DN. A novel NKX2-5 Loss-of-function mutation predisposes to familial dilated cardiomyopathy and arrhythmias. *Int J Mol Med* 2015; **35**: 478-486 [PMID: 25503402 DOI: 10.3892/ijmm.2014.2029]
19 **Aakre KM**, Omland T. Physical activity, exercise and cardiac troponins: Clinical implications. *Prog Cardiovasc Dis* 2019; **62**: 108-115 [PMID: 30797799 DOI: 10.1016/j.pcad.2019.02.005]
20 **Hammarsten O**, Mair J, Möckel M, Lindahl B, Jaffe AS. Possible mechanisms behind cardiac troponin elevations. *Biomarkers* 2018; **23**: 725-734 [PMID: 29976112 DOI: 10.1080/1354750X.2018.1490969]
21 **Guo S**, Schlecht W, Li L, Dong WJ. Paper-based cascade cationic isotachophoresis: Multiplex detection of cardiac markers. *Talanta* 2019; **205**: 120112 [PMID: 31450472 DOI: 10.1016/j.talanta.2019.07.007]
22 **Kim MS**, Fleres B, Lovett J, Anfinson M, Samudrala SSK, Kelly LJ, Teigen LE, Cavanaugh M, Marquez M, Geurts AM, Lough JW, Mitchell ME, Fitts RH, Tomita-Mitchell A. Contractility of Induced Pluripotent Stem Cell-Cardiomyocytes With an MYH6 Head Domain Variant Associated With Hypoplastic Left Heart Syndrome. *Front Cell Dev Biol* 2020; **8**: 440 [PMID: 32656206 DOI: 10.3389/fcell.2020.00440]
23 **Mohammad MA**, Alqudah MA, Alhorani R, Khatib S, Gharaibeh NS. Ca^{2+} sensitivity of skinned ventricular cardiac muscle and expression of cardiac myosin heavy chain isoforms in hibernating *vs* active frogs. *Comp Clin Path* 2017; **26**: 799-804
24 **Luo XL**, Zhang P, Liu X, Huang S, Rao SL, Ding Q, Yang HT. Myosin light chain 2 marks differentiating ventricular cardiomyocytes derived from human embryonic stem cells. *Pflugers Arch* 2021; **473**: 991-1007 [PMID: 34031754 DOI: 10.1007/s00424-021-02578-3]

25 **Clapham KR**, Singh I, Capuano IS, Rajagopal S, Chun HJ. MEF2 and the Right Ventricle: From Development to Disease. *Front Cardiovasc Med* 2019; **6**: 29 [PMID: 30984767 DOI: 10.3389/fcvm.2019.00029]

26 **Chopra A**, Kutys ML, Zhang K, Polacheck WJ, Sheng CC, Luu RJ, Eyckmans J, Hinson JT, Seidman JG, Seidman CE, Chen CS. Force Generation *via* β-Cardiac Myosin, Titin, and α-Actinin Drives Cardiac Sarcomere Assembly from Cell-Matrix Adhesions. *Dev Cell* 2018; **44**: 87-96.e5 [PMID: 29316444 DOI: 10.1016/j.devcel.2017.12.012]

27 **Gasiūnienė M**, Zubova A, Utkus A, Navakauskienė R. Epigenetic and metabolic alterations in human amniotic fluid stem cells induced to cardiomyogenic differentiation by DNA methyltransferases and p53 inhibitors. *J Cell Biochem* 2019; **120**: 8129-8143 [PMID: 30485506 DOI: 10.1002/jcb.28092]

28 **Lee JH**, Yoo YM, Jung EM, Ahn CH, Jeung EB. Inhibitory effect of octyl-phenol and bisphenol A on calcium signaling in cardiomyocyte differentiation of mouse embryonic stem cells. *J Physiol Pharmacol* 2019; **70** [PMID: 31566189 DOI: 10.26402/jpp.2019.3.10]

29 **DeMarco KR**, Clancy CE. Cardiac Na Channels: Structure to Function. *Curr Top Membr* 2016; **78**: 287-311 [PMID: 27586288 DOI: 10.1016/bs.ctm.2016.05.001]

30 **Michela P**, Velia V, Aldo P, Ada P. Role of connexin 43 in cardiovascular diseases. *Eur J Pharmacol* 2015; **768**: 71-76 [PMID: 26499977 DOI: 10.1016/j.ejphar.2015.10.030]

31 **Agnetti G**, Herrmann H, Cohen S. New roles for desmin in the maintenance of muscle homeostasis. *FEBS J* 2022; **289**: 2755-2770 [PMID: 33825342 DOI: 10.1111/febs.15864]

32 **Mirza A**, Khan I, Qazi RE, Salim A, Husain M, Herzig JW. Role of Wnt/β-catenin pathway in cardiac lineage commitment of human umbilical cord mesenchymal stem cells by zebularine and 2'-deoxycytidine. *Tissue Cell* 2022; **77**: 101850 [PMID: 35679684 DOI: 10.1016/j.tice.2022.101850]

World Journal of Stem Cells

Submit a Manuscript: https://www.f6publishing.com

World J Stem Cells 2023 August 26; 15(8): 842-865

DOI: 10.4252/wjsc.v15.i8.842

ISSN 1948-0210 (online)

ORIGINAL ARTICLE

Basic Study

Quercetin ameliorates oxidative stress-induced senescence in rat nucleus pulposus-derived mesenchymal stem cells *via* the miR-34a-5p/SIRT1 axis

Wen-Jie Zhao, Xin Liu, Man Hu, Yu Zhang, Peng-Zhi Shi, Jun-Wu Wang, Xu-Hua Lu, Xiao-Fei Cheng, Yu-Ping Tao, Xin-Min Feng, Yong-Xiang Wang, Liang Zhang

Specialty type: Cell and tissue engineering

Provenance and peer review: Unsolicited article; Externally peer reviewed.

Peer-review model: Single blind

Peer-review report's scientific quality classification

Grade A (Excellent): A
Grade B (Very good): B, B
Grade C (Good): 0
Grade D (Fair): 0
Grade E (Poor): 0

P-Reviewer: Li SC, United States; Rezus E, Romania; Shamseldeen AM, Egypt

Received: April 18, 2023
Peer-review started: April 18, 2023
First decision: May 17, 2023
Revised: May 25, 2023
Accepted: June 27, 2023
Article in press: June 27, 2023
Published online: August 26, 2023

Wen-Jie Zhao, Man Hu, Peng-Zhi Shi, Graduate School, Dalian Medical University, Dalian 116044, Liaoning Province, China

Xin Liu, Yu Zhang, Jun-Wu Wang, Yu-Ping Tao, Xin-Min Feng, Yong-Xiang Wang, Liang Zhang, Department of Orthopedics, Clinical Medical College, Yangzhou University, Yangzhou 225001, Jiangsu Province, China

Xu-Hua Lu, Department of Orthopedics, Changzheng Hospital of The Second Military Medical University, Shanghai 200003, China

Xiao-Fei Cheng, Department of Orthopedic Surgery, Shanghai Key Laboratory of Orthopedics Implants, Shanghai Ninth People's Hospital, Shanghai Jiaotong University School of Medicine, Shanghai 200011, China

Corresponding author: Liang Zhang, PhD, Professor, Department of Orthopedics, Clinical Medical College, Yangzhou University, No. 98 Nantong West Road, Yangzhou, 225001, Jiangsu Province, China. zhangliang6320@sina.com

Abstract

BACKGROUND

Intervertebral disc degeneration (IDD) is a main contributor to low back pain. Oxidative stress, which is highly associated with the progression of IDD, increases senescence of nucleus pulposus-derived mesenchymal stem cells (NPMSCs) and weakens the differentiation ability of NPMSCs in degenerated intervertebral discs (IVDs). Quercetin (Que) has been demonstrated to reduce oxidative stress in diverse degenerative diseases.

AIM

To investigate the role of Que in oxidative stress-induced NPMSC damage and to elucidate the underlying mechanism.

METHODS

In vitro, NPMSCs were isolated from rat tails. Senescence-associated β-galactosidase (SA-β-Gal) staining, cell cycle, reactive oxygen species (ROS), real-time quantitative polymerase chain reaction (RT-qPCR), immunofluorescence,

and western blot analyses were used to evaluated the protective effects of Que. Meanwhile the relationship between miR-34a-5p and Sirtuins 1 (SIRT1) was evaluated by dual-luciferase reporter assay. To explore whether Que modulates tert-butyl hydroperoxide (TBHP)-induced senescence of NPMSCs *via* the miR-34a-5p/SIRT1 pathway, we used adenovirus vectors to overexpress and downregulate the expression of miR-34a-5p and used SIRT1 siRNA to knockdown SIRT1 expression. *In vivo,* a puncture-induced rat IDD model was constructed, and X rays and histological analysis were used to assess whether Que could alleviate IDD *in vivo*.

RESULTS

We found that TBHP can cause NPMSCs senescence changes, such as reduced cell proliferation ability, increased SA-β-Gal activity, cell cycle arrest, the accumulation of ROS, and increased expression of senescence-related proteins. While abovementioned senescence indicators were significantly alleviated by Que treatment. Que decreased the expression levels of senescence-related proteins (p16, p21, and p53) and senescence-associated secreted phenotype (SASP), including IL-1β, IL-6, and MMP-13, and it increased the expression of SIRT1. In addition, the protective effects of Que on cell senescence were partially reversed by miR-34a-5p overexpression and SIRT1 knockdown. *In vivo*, X-ray, and histological analyses indicated that Que alleviated IDD in a puncture-induced rat model.

CONCLUSION

In summary, the present study provides evidence that Que reduces oxidative stress-induced senescence of NPMSCs *via* the miR-34a/SIRT1 signaling pathway, suggesting that Que may be a potential agent for the treatment of IDD.

Key Words: Quercetin; Nucleus pulposus-derived mesenchymal stem cells; Oxidative stress; Senescence; Intervertebral disc degeneration; miR-34a-5p/SIRT1 pathway

©The Author(s) 2023. Published by Baishideng Publishing Group Inc. All rights reserved.

Core Tip: In our article, we provide the evidence that quercetin (Que) can prevent oxidative stress induced senescence of nucleus pulposus-derived mesenchymal stem cells *via* miR-34a/SIRT1 signaling pathway. Moreover, Que could ameliorate the progression of intervertebral disc degeneration (IDD) in rat model. Thus, Que can be considered as a potential agent for the treatment of IDD.

Citation: Zhao WJ, Liu X, Hu M, Zhang Y, Shi PZ, Wang JW, Lu XH, Cheng XF, Tao YP, Feng XM, Wang YX, Zhang L. Quercetin ameliorates oxidative stress-induced senescence in rat nucleus pulposus-derived mesenchymal stem cells *via* the miR-34a-5p/SIRT1 axis. *World J Stem Cells* 2023; 15(8): 842-865
URL: https://www.wjgnet.com/1948-0210/full/v15/i8/842.htm
DOI: https://dx.doi.org/10.4252/wjsc.v15.i8.842

INTRODUCTION

As a widely known musculoskeletal disorder, low back pain (LBP) is the leading cause of disability and results in a huge economic burden on the family and society[1,2]. Intervertebral disc degeneration (IDD) is a main contributor to LBP, but the etiology of IDD is multifactorial[3]. Therefore, elucidating the underlying molecular mechanisms of IDD will help develop solutions for the prevention and treatment of IDD.

Several previous studies have indicated that oxidative stress and reactive oxygen species (ROS) are highly associated with the progression of IDD[4-7]. While ROS production is inevitable during the metabolic processes of disc cells, the progression of IDD is considered to be the result of disc cell senescence caused by ROS accumulation[7,8]. Recently, stem cell-based endogenous repair has been shown to play a significant role in the repair and regeneration of degenerative intervertebral discs (IVDs)[9,10]. Nucleus pulposus-derived mesenchymal stem cells (NPMSCs) were first reported by Risbud *et al*[11] in 2007, which rendered a basis for the endogenous repair of IDD[11]. We also previously found NPMSCs in normal and degenerated IVDs[12-15]. Wu *et al*[16] indicated that the regenerative potential of NPMSCs decreases with aging and degeneration of IVDs[16]. In addition, Ma *et al*[17] proposed that the decrease in endogenous NPMSCs caused by adverse microenvironments, such as oxidative stress, low nutrition, and inflammation, is one of the main reasons for the failure of endogenous repair of IDD[17]. Therefore, inhibition of oxidative stress-induced senescence of NPMSCs may be of great significance in alleviating IDD.

Quercetin (Que), a natural flavonoid widely present in various plants, has antioxidative stress, anti-inflammatory, and antiaging properties. Que has been used as a senolytic to prevent diverse degenerative diseases[18-20]. Zhu *et al*[21] found that Que reduces senescent cells by selectively killing senescent human epithelial cells and mouse bone marrow mesenchymal stem cells[21]. Feng *et al*[22] reported that Que attenuates oxidative stress-induced apoptosis in rat

chondrocytes and prevents the progression of osteoarthritis in a rat model[22]. Previous clinical studies have also demonstrated that Que reduces the expression levels of senescence-related markers[23].

MicroRNAs (miRNAs) are small double-stranded noncoding RNAs that are approximately 20 nucleotides in length and interfere with RNA translation by binding to the 3'UTR sequence of the target gene RNA. Abnormal expression of miRNAs has been observed in degenerative IVD, indicating that miRNAs play an important role in the pathophysiological process of IDD[24,25]. A previous study has also demonstrated that the expression of miR-34a-5p is significantly upregulated in degenerated IVDs and that miR-34a-5p increases extracellular matrix degradation and cell apoptosis. Sirtuins 1 (SIRT1), the target of miR-34a, is a member of the sirtuin family and plays a significant role in cancer, age-related diseases, and degenerative diseases[26-28]. Several studies have reported that SIRT1 delays the senescence of IVD cells by decreasing oxidative stress and inflammation as well as by improving mitochondrial function[29,30]. However, the protective effect of Que on NPMSCs is still unknown.

In the present study, tert-butyl hydroperoxide (TBHP) was used to trigger oxidative stress in NPMSCs, which is widely accepted as an apoptosis and senescence *in vitro* model. The effects of Que on senescence in NPMSCs under oxidative stress and the role of the miR-34a-5p/SIRT1 pathway were investigated. Finally, the therapeutic effects were also evaluated in a puncture-induced rat IDD model.

MATERIALS AND METHODS

Isolation and culture of NPMSCs

All the procedures performed in this study were approved by the Ethical Committee of the Clinical Medical College of Yangzhou University. Sprague-Dawley (SD) rats (2-4 mo old and weighing 200-300 g) were obtained from Yangzhou University, No. SYXK (Su) 2017-0044. The separation of nucleus pulposus (NP) tissues and the isolation of NPMSCs were performed as previously described[14]. Briefly, the NP tissues obtained from SD rats were carefully separated by a microscope under sterile conditions, and the NP tissue was mechanically fragmented into 1 mm^3 pieces and digested with 0.2% collagenase type II (Gibco, United States) at 37 °C in 5% CO_2 for 12 h. Cells were filtered through a 75-μm cellular filter, centrifuged at 1000 rpm for 3 min, washed with phosphate-buffered saline (PBS), resuspended in Mesenchymal Stem Cell Complete Medium (Cyagen, United States) with 10% fetal bovine serum (FBS; HyClone, United States) and 1% antibiotics (Gibco, United States), and cultured in an incubator at 37 °C with 5% CO_2. NPMSCs were subcultured at a ratio of 1:3 when they reached 80% confluence. The third passages of NPMSCs were used for the subsequent experiments.

Surface marker identification of NPMSCs

NPMSCs were cultured in a 12-well plate with a 25 mm diameter cell slide in complete medium. Cells were fixed in 4% paraformaldehyde for 15 min and permeabilized with 0.5% Triton X-100 for 15 min. Subsequently, cells were blocked with 10% bovine serum albumin for 1 h at room temperature and incubated with the following primary antibodies (1:100) overnight at 4 °C according to the International Society for Cellular Therapy (ISCT): CD34 (ABclonal, China), CD45 (ABclonal, China), CD73 (ABclonal, China), CD90 (ABclonal, China), CD105 (Proteintech, China), and tyrosine kinase with Ig and EGF homology domains 2 (Tie2, a disc NP progenitor marker) (Biodragon, China). Cells were then incubated with FITC- or Cy3-conjugated secondary antibodies (1:200) at room temperature for 1 h in the dark. After treatment with 4',6-diamidino-2-phenylindole (DAPI) for 5 min, the cell slides were observed under a fluorescence microscope (Leica, Wetzlar, Germany).

Cell treatment and cell viability assay

To establish an oxidative stress-induced model of NPMSCs, NPMSCs were cultured in complete medium with different concentrations (0, 25, 50, 100, 200, and 400 μM) of TBHP (Sigma-Aldrich, United States) for 12 h. Cells were pretreated with different concentrations (0, 10, 20, 40, 80, and 160 μM) of Que (MedChem Express, China) for 24 h before the addition of a suitable concentration of TBHP to investigate the suitable dose of Que. A cell counting kit-8 (CCK-8, Beyotime, China) was used to evaluate cell viability according to the manufacturer's instructions. Briefly, 2 × 10^3 cells/well were seeded in 96-well plates and cultured overnight at 37 °C in 5% CO_2. After the cells were treated as described above, a mixture of 10 μL of CCK-8 reagent and 100 μL of fresh medium was added to each well for 1 h at 37 °C. The optical density (OD) value of each well was measured at 450 nm by a microplate reader (Bio-Rad, United States). Cells were divided into the following groups: Control group (untreated), TBHP group (treated with 100 μM TBHP) and Que + TBHP group (treated with 20 μM Que and 100 μM TBHP).

Cell proliferation assay

Cell proliferation was evaluated by an 5-ethynyl-2'-deoxyuridine (EdU) assay (Beyotime, China). Cells (5 × 10^5 cells/well) were seeded in 12-well plates and cultured at 37 °C in 5% CO_2. According to the manufacturer's instructions, NPMSCs were incubated with EdU for 2 h, fixed with 4% paraformaldehyde for 10 min, permeabilized with 0.5% Triton X-100 for 15 min, and incubated with Click Reaction Mixture for 30 min. After washing with PBS, cells were counterstained with Hoechst 33342 in the dark for 10 min. Finally, cells were observed under a fluorescence microscope and analyzed by ImageJ software (NIH, United States).

Senescence-associated β-galactosidase (SA-β-Gal) staining

NPMSCs were seeded in a 6-well plate at a density of 4 × 10^5 cells/well at 37 °C in 5% CO_2. Cells were stained with SA-β-

Gal using a SA-β-Gal staining kit (Beyotime, China) according to the manufacturer's instructions. Cells were fixed with SA-β-gal fixing solution for 15 min at room temperature and then incubated overnight with an SA-β-Gal working solution at 37 °C without CO_2. Cells were observed under a microscope and analyzed by ImageJ software.

ROS assay

According to the manufacturer's instructions provided by a ROS detection fluorescent probe-DHE kit (Keygen, China), NPMSCs were incubated with 20 μM DHE for 30 min at 37 °C. Cells were then observed under a fluorescence microscope and analyzed by ImageJ software.

JC-1 assay for mitochondrial membrane potential

A JC-1 Detection Kit (Keygen, China) was used to measure mitochondrial membrane potential (MMP). Briefly, NPMSCs were cultured in medium containing 2 μM JC-1 dye, a cationic dye, for 20 min. After being washed twice with incubation buffer, cells were cultured in complete medium, observed by fluorescence microscopy, and analyzed by ImageJ software.

Cell cycle assay

The cell cycle phases of TBHP-induced senescent NPMSCs were determined by flow cytometric analyses using a Cell Cycle Detection Kit (Keygen, China). Briefly, NPMSCs were harvested from 6-well plates, washed twice with ice-cold PBS, fixed with 75% ethanol at 4 °C for 2 h, and incubated with a mixed solution of propidium iodide (PI) and RNase A for 30 min in the dark. Flow cytometry (BD Company, USA) was used to analyze the cell cycle phases.

Cell transfection

Adenovirus vectors containing miR-34a-5p mimic, miR-34a-5p inhibitor, and their corresponding negative controls were obtained from GeneChem (Shanghai, China). SIRT1 siRNA and scrambled siRNA were obtained from Gene Pharma (Shanghai, China). NPMSCs (5×10^5/well) were seeded in 6-well plates and then transfected with miR-34a-5p mimic or miR-34a-5p inhibitor using Lipofectamine 2000 (Thermo Fisher, UT, USA) for 12 h at 37 °C according to the manufacturer's protocol. After replacing the medium with fresh complete medium, NPMSCs were cultured for an additional 24 h. Cells were then harvested for subsequent experiments.

Dual-luciferase reporter assay

The TargetScan Human database (https://www.targetscan.org/vert_80/) was used to predict the complementary binding site of miR-34a-5p in the 3'-UTR of SIRT1 mRNA. According to the Lipofectamine 2000 transfection protocol, SIRT1 3'-UTR wild-type plasmids or mutant plasmids were cotransfected with miR-34a-5p mimic and mimic control into cells. After 48 h, a dual-luciferase reporter assay kit was used to detect luciferase activity.

qRT-PCR

TRIzol reagent (Invitrogen, United States) was used to extract total RNA from NPMSCs. To measure the expression levels of mRNA, RNA was reverse-transcribed into complementary DNA (cDNA) by a Prime Script-RT reagent kit (Vazyme Biotech, China) according to the manufacturer's protocol. cDNA was amplified by SYBR Premix Ex Taq (Vazyme Biotech, China). To measure the expression levels of miR-34a, reverse transcription of RNA and amplification of cDNA were performed using the miRNA 1st Strand cDNA Synthesis Kit (by stem-loop) (Vazyme Biotech, China) and miRNA Universal SYBR qPCR Master Mix (Vazyme Biotech, China). The $2^{-\Delta\Delta CT}$ method was used to calculate the expression level of target genes. The expression levels of mRNA or miRNA were normalized to Gapdh or U6. The primers for the target genes used in this study are listed in Table 1.

Western blot analysis

The total protein of NPMSCs was extracted by a Whole Cell Lysis assay (Keygen Biotech, China), and the protein concentration was determined by a BCA protein assay kit (Beyotime, China). Each sample containing 30 μg of protein was separated by 10%-12% sodium dodecyl sulfate-polyacrylamide gel electrophoresis (SDS-PAGE) and transferred to a polyvinylidene difluoride membrane (Millipore, United States). After being blocked in 5% skim milk for 2 h at room temperature, the membranes were incubated overnight with the following primary antibodies at 4 °C: P16 (1:1000; Proteintech, China), p21 (1:1000; Proteintech, China), p53 (1:5000; Proteintech, China), SIRT1 (1:1000; ABclonal, China), IL-1β (1:1000; ABclonal, China), IL-6 (1:1000; ABclonal, China), matrix metalloproteinase-13 (MMP-13, 1:1000; ABclonal, China) and Gapdh (1:1000; Servicebio, China). The membranes were then incubated with horseradish peroxidase (HRP)-labeled secondary antibodies (1:5000; Abcam). The protein bands were observed with an enhanced chemiluminescence system, and the expression of protein was analyzed by ImageJ software.

Puncture-induced rat IDD model

In total, 15 male SD rats (2-4 mo old and weighing 200-300 g) were randomly divided into the following three groups: Control group (n = 5), IDD group (n = 5), and Que group (n = 5). The IDD model of SD rats was established as previously described[13]. Briefly, the rats were anesthetized with pentobarbital, and the tail skin was sterilized by povidone iodine. A 21 G needle was used to puncture the coccygeal IVD (Co 6-7), and the needle was rotated 180° and kept in the disc for 5 s at a depth of 5 mm. After surgery, the Que group was treated with Que (100 mg/kg, 5 mg/mL of Que suspended in 0.5% sodium carboxymethyl cellulose solution) every other day by intragastric administration for 4 wk. The control group and IDD group were treated with 0.5% sodium carboxymethyl cellulose solution for 4 wk.

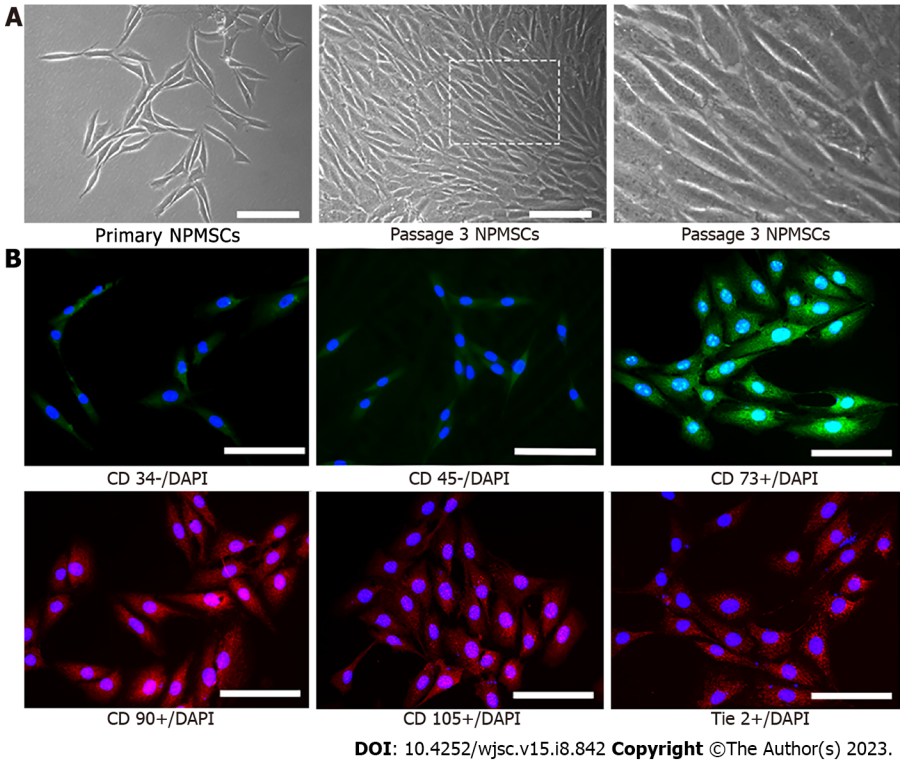

DOI: 10.4252/wjsc.v15.i8.842 **Copyright** ©The Author(s) 2023.

Figure 1 Identification of nucleus pulposus derived mesenchymal stem cells. A: Primary nucleus pulposus-derived mesenchymal stem cells (NPMSCs) presented with elongated spindle shape and grew in flower formation; B: NPMSCs exhibited low fluorescent expression of CD34 and CD45, but a high fluorescent expression of CD73, CD90, and CD105. Scar bar = 100 μm.

Radiographic evaluation and histological analysis

At 4 wk postinjury, all rats were placed in a prone position after anesthetization with pentobarbital, and X-ray images were acquired. ImageJ software was used to calculate the disc height index (DHI) as previously described[31]. The tails were harvested after the rats were euthanized with an overdose of sodium pentobarbital. The specimens were fixed in 4% paraformaldehyde for 48 h, decalcified in EDTA for 1 mo, dehydrated in gradient alcohol, and embedded in paraffin. The specimens were cut into 5 μm sections, and the sections were stained with hematoxylin-eosin (HE), Alcian blue, and Safranin O-fast Green. Histological scores were evaluated as previously described[31,32] based on the following scale: 5, normal discs; 6-11, moderately degenerated discs; and 12-14, severely degenerated discs.

Immunofluorescent staining

After the IVD specimens were prepared, a freezing microtome (Leica, Wetzlar, Germany) was used to cut the specimens into 5-μm sections. The sections were fixed in 4% paraformaldehyde for 15 min and permeabilized with 0.5% Triton X-100 for 15 min. Subsequently, the sections were blocked with 10% bovine serum albumin for 1 h at room temperature and incubated with the following primary antibodies (1:100) at 4 °C overnight: Collagen type II (ABclonal, China) and aggrecan (ABclonal, China). The sections were then incubated with FITC- or Cy3-conjugated secondary antibodies (1:200) at room temperature for 1 h in the dark. Fluorescence microscopy and ImageJ software were used to observe and analyze the sections.

Statistical analysis

All data were analyzed by GraphPad Prism 8 (GraphPad, La Jolla). Data are expressed as the mean ± SD. Student's t test and one-way analysis of variance (ANOVA) was used to analyze the data of two groups and multiple independent groups, respectively. The Kruskal-Wallis H test was used to analyze the histological score. A P value < 0.05 was considered significant.

RESULTS

Characterization of NPMSCs

Elongated spindle-shaped NPMSCs were successfully isolated and cultured from rat IVDs (Figure 1A). Based on the immunofluorescence staining analysis, the MSC-associated markers, namely, CD73, CD90, and CD105 were highly expressed, whereas the expression of CD34 and CD45 was low (Figure 1B). Moreover, the expression of Tie2, a disc NP progenitor marker, was also high in NPMSCs (Figure 1B). These results indicated that NPMSCs isolated from IVD

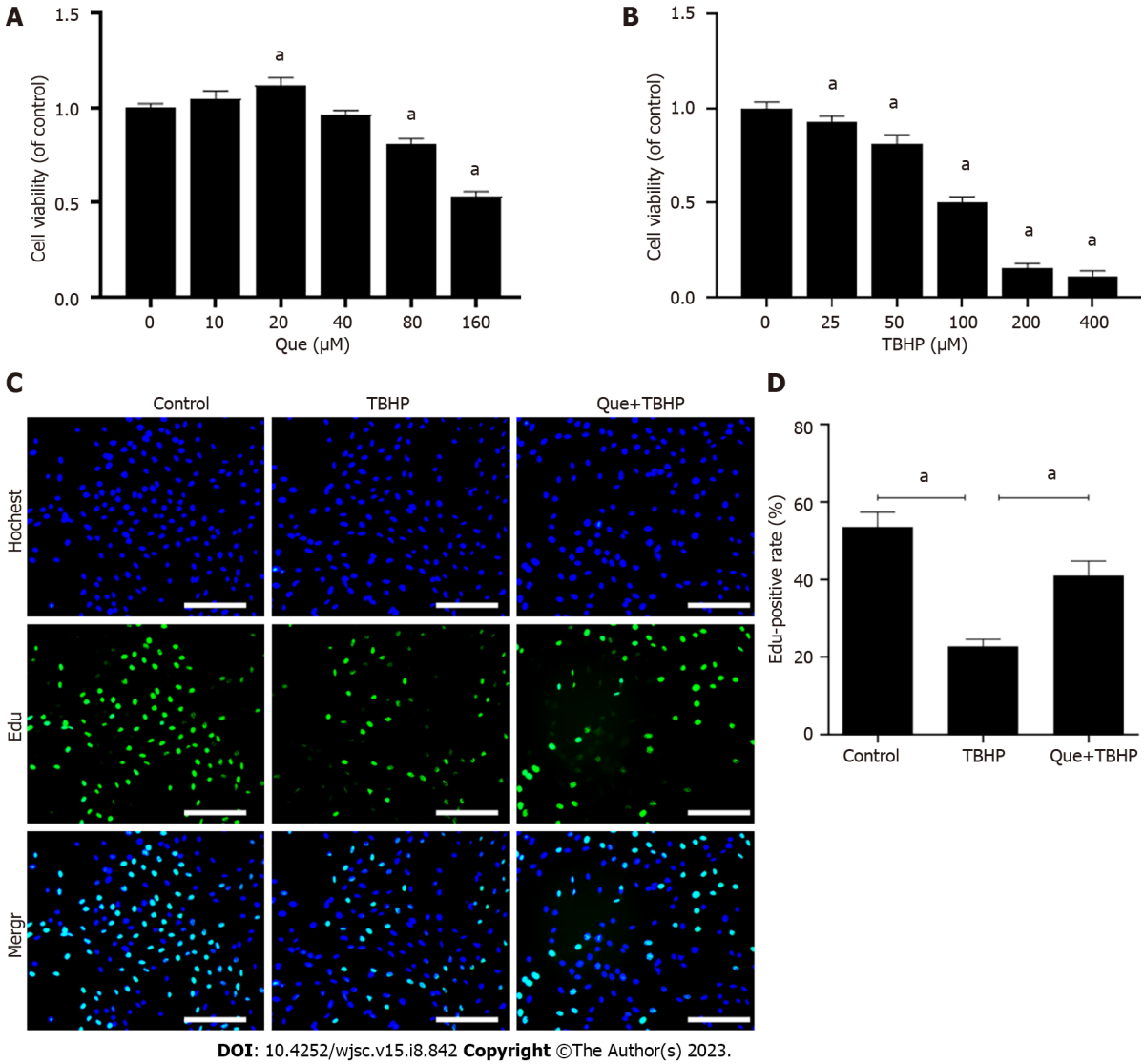

DOI: 10.4252/wjsc.v15.i8.842 **Copyright** ©The Author(s) 2023.

Figure 2 Cell viability assay and cell proliferation assay. A: Cell counting kit-8 (CCK-8) results of nucleus pulposus-derived mesenchymal stem cells (NPMSCs) treated with different concentrations of quercetin for 24 h; B: CCK-8 results of NPMSCs treated with different concentrations of tert-butyl hydroperoxide (TBHP) for 24 h; C: EdU assay results of NPMSCs in different groups. Green fluorescence represents cells in a proliferating state, and blue fluorescence represents cell nucleus (scale bar = 200 μm); D: Quantitative analysis of EdU results. Data are represented as mean ± SD. $^{a}P < 0.05$ compared with control group, $n = 3$. TBHP: Tert-butyl hydroperoxide; Que: Quercetin.

correspond to the standards of stem cells described by ISCT.

Effects of Que and TBHP on the viability and proliferation of NPMSCs

A CCK-8 assay was used to evaluate the effect of Que and TBHP on NPMSC viability. As shown in Figure 2A, Que showed no significant cytotoxic effect at concentrations up to 20 μM for 24 h. Therefore, a concentration of 20 μM Que was selected for the subsequent experiments. NPMSC viability was decreased after treatment with TBHP in a dose-dependent manner (Figure 2B), and 100 μM TBHP was selected for use in subsequent experiments. The effect of Que on NPMSC proliferation was detected by EdU staining. Compared to the control group, the positive rate of EdU in the TBHP group was significantly lower ($P < 0.05$), and the positive rate of EdU was partially increased in the Que + TBHP group ($P < 0.05$) (Figure 2C and D).

Effects of Que on SA-β-Gal staining and the cell cycle in NPMSCs

SA-β-Gal accumulation is an indicator of cellular senescence. Compared to the control group, the number of SA-β-Gal-positive senescent NPMSCs in the TBHP group was significantly higher ($P < 0.05$), while the number of SA-β-Gal-positive cells was decreased in Que + TBHP group (Figure 3A). Compared to the control group, the percentage of NPMSC in the G2/M phase in TBHP group was higher, which indicated cell cycle arrest, but treatment with Que decreased the percentage of NPMSCs arrested in G2/M phase (Figure 3B).

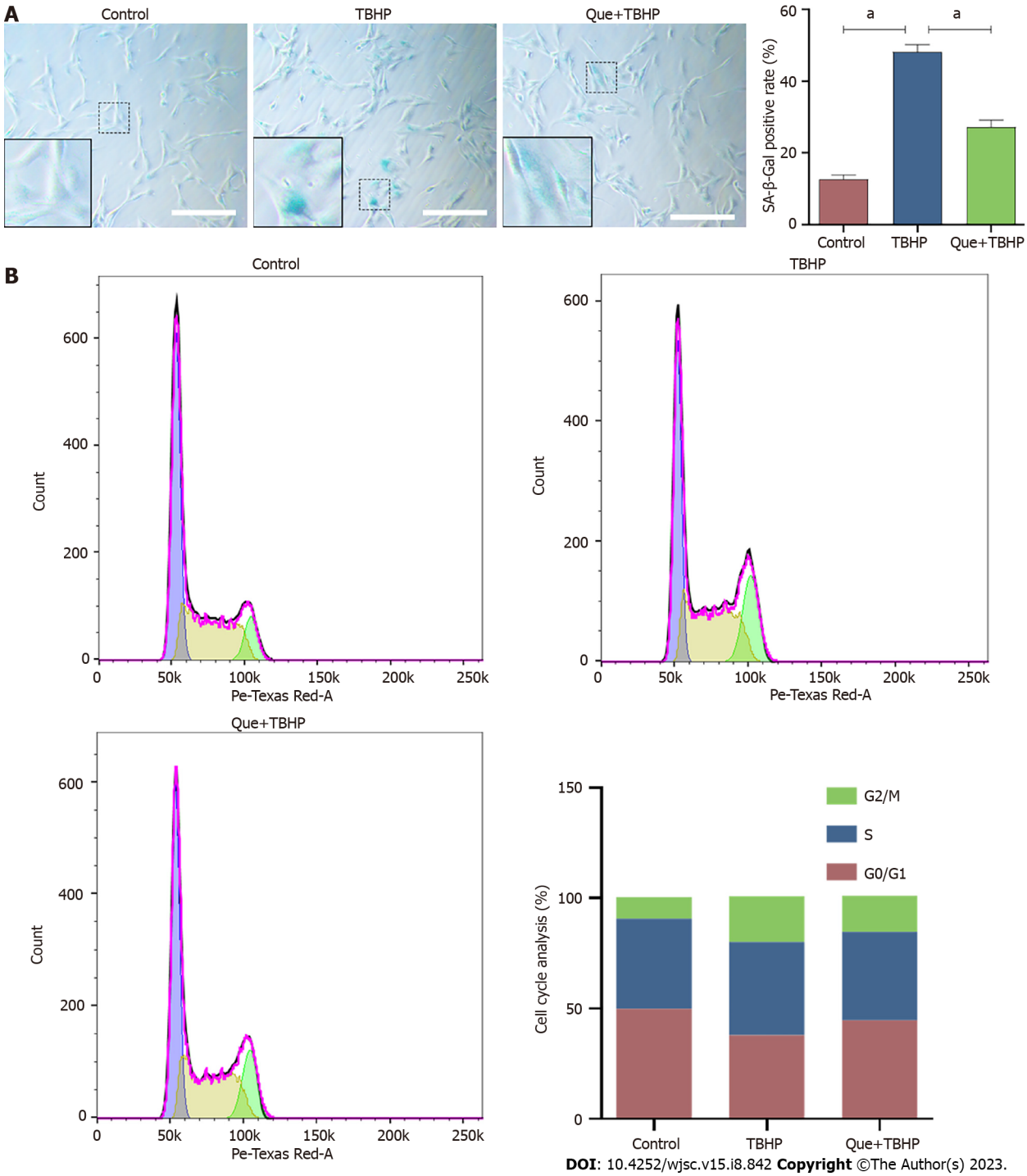

DOI: 10.4252/wjsc.v15.i8.842 **Copyright** ©The Author(s) 2023.

Figure 3 Senescence-associated β-Galactosidase staining assay and cell cycle assay. A: Senescence-associated β-Galactosidase (SA-β-gal) staining results of nucleus pulposus-derived mesenchymal stem cells (NPMSCs) in different groups. Senescent cells exhibit high expression of SA-β-gal in blue staining; B: Cell cycle results of NPMSCs in different groups. Scar bar = 200 μm. Data are represented as mean ± SD. Significant differences between groups are indicated as $^{a}P < 0.05$, $n = 3$. TBHP: Tert-butyl hydroperoxide; Que: Quercetin.

Effects of Que on MMP and ROS generated in TBHP-treated NPMSCs

When the MMP is high, JC-1 exists in the mitochondria as J-aggregates of polymers, which produce red fluorescence. When the MMP is low, JC-1 is released from the mitochondria matrix and exists in the cytoplasm in the form of monomers, which produce green fluorescence. As shown in Figure 4A and B, the MMP was decreased after TBHP treatment, and this effect was partially reversed by pretreatment with Que. Figure 4C and D show that NPMSCs in the TBHP group had higher ROS levels compared to the control group, and pretreatment with Que partially reversed the effect of TBHP on ROS generation.

Que inhibits oxidative stress-induced senescence of NPMSCs

Cell senescence is broadly characterized by cell cycle arrest and the production of SASP. To explore the effect of Que in

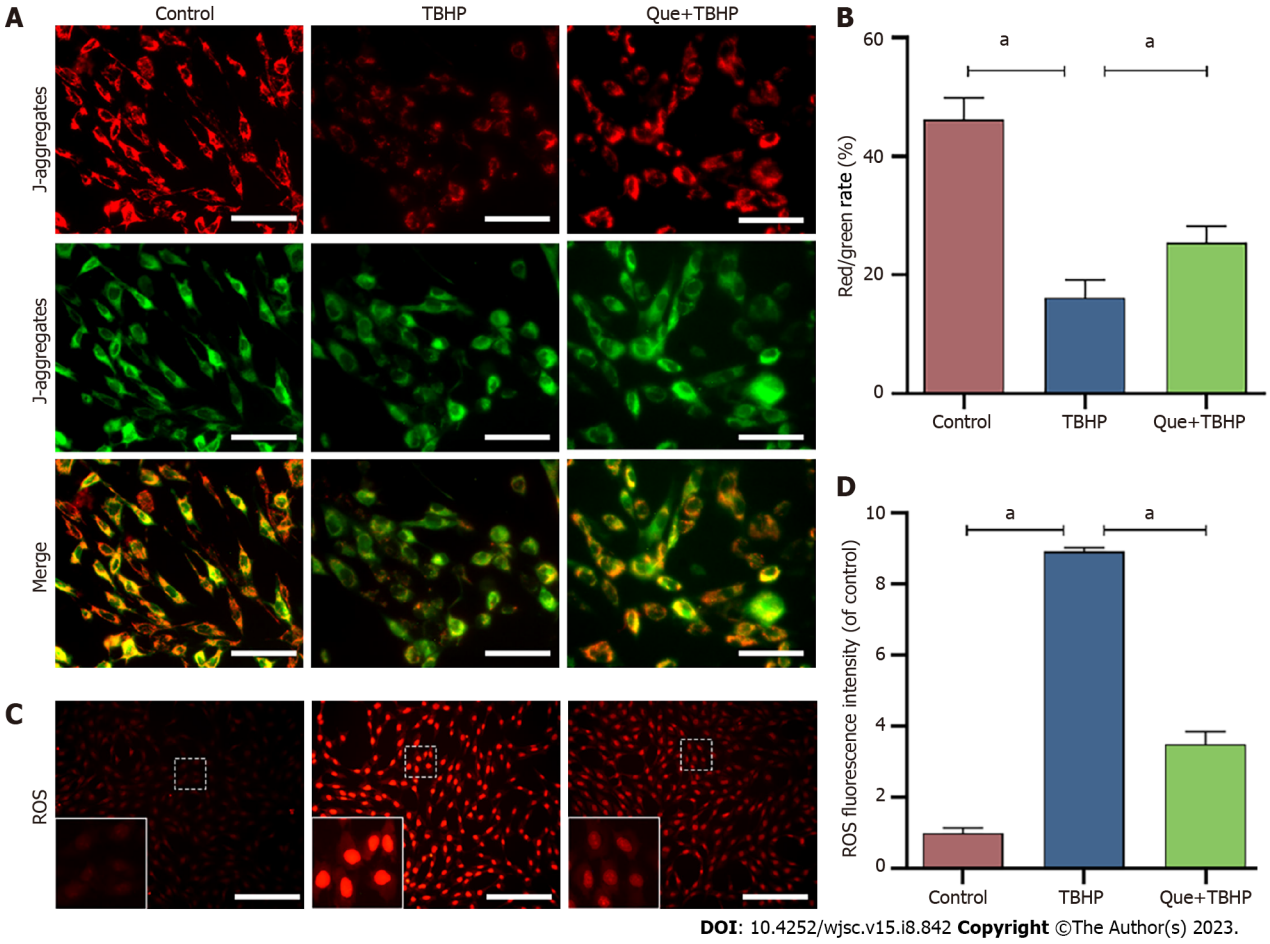

DOI: 10.4252/wjsc.v15.i8.842 **Copyright** ©The Author(s) 2023.

Figure 4 Mitochondrial membrane potential assay and reactive oxygen species assay. A: Results of Mitochondrial membrane potential (MMP) in different groups detected by fluorescence. Red fluorescence represents the mitochondrial aggregate JC-1 and green fluorescence indicates the monomeric JC-1. Scale bar = 100 μm; B: Quantitative analysis of MMP results; C: Results of ROS in different groups detected by fluorescence. Red fluorescence represents high level of reactive oxygen species assay (ROS). Scale bar = 200 μm; D: Quantitative analysis of ROS results. Data are represented as mean ± SD. Significant differences between groups are indicated as $^{a}P < 0.05$, $n = 3$. TBHP: Tert-butyl hydroperoxide; Que: Quercetin; ROS: Reactive oxygen species assay.

TBHP-induced NPMSCs, western blot analysis and immunofluorescence staining were used to evaluate the expression of SIRT1, cell senescence-related proteins (p16, p21, and p53), and SASP (IL-1β, IL-6, and MMP-13). The expression of SIRT1 was downregulated after TBHP treatment, and this effect was partially reversed by Que pretreatment ($P < 0.05$; Figure 5). Moreover, Que treatment significantly decreased the upregulation of p16, p21, p53, IL-1β, IL-6, and MMP-13 expression induced by TBHP ($P < 0.05$; Figures 5 and 6). Taken together, these results indicated that Que may have a protective role in TBHP-induced oxidative stress injury of NPMSCs.

MiR-34a-5p represses SIRT1 expression by targeting the 3'-UTR of SIRT1

According to the TargetScan online prediction database, SIRT1 is a potential target of miR-34a-5p (Figure 7A). A dual-luciferase reporter assay revealed that the miR-34a-5p mimic significantly inhibited the relative luciferase activity in the wild-type SIRT1 reporter vector (WT-SIRT1), whereas there was no significant change in the luciferase activity in the mutant SIRT1 reporter vector (MUT-SIRT1) (Figure 7B). These data indicated that miR-34a-5p inhibits SIRT1 expression by directly binding to the 3UTR of SIRT1. In addition, the mRNA and protein expression levels of SIRT1 were significantly inhibited by overexpression of miR-34a-5p (Figure 7C-E). Conversely, downregulation of miR-34a-5p increased the expression level of SIRT1 (Figure 7F-H). Moreover, the expression of SIRT1 was successfully downregulated by siRNA (Figure 7I-K).

MiR-34a-5p enhances oxidative stress-induced senescence of NPMSCs

According to the qRT-PCR analysis, the expression of miR-34a-5p was increased by TBHP treatment, and it was suppressed and promoted by the miR-34a-5p inhibitor and miR-34a-5p mimic, respectively (Figures 8A and 9A). In contrast, the expression of SIRT1 was suppressed after TBHP treatment, and it was promoted and suppressed and by miR-34a-5p inhibitor and miR-34a-5p mimic, respectively (Figures 8 and 9). The TBHP-enhanced senescence-related proteins (p16, p21, and p53) and SASP (IL-1β, IL-6, and MMP-13) were significantly suppressed after miR-34a-5p knockdown (Figure 8). In contrast, the expression levels of senescence-related proteins and SASP were increased when cells were treated with the miR-34a-5p mimic (Figure 9).

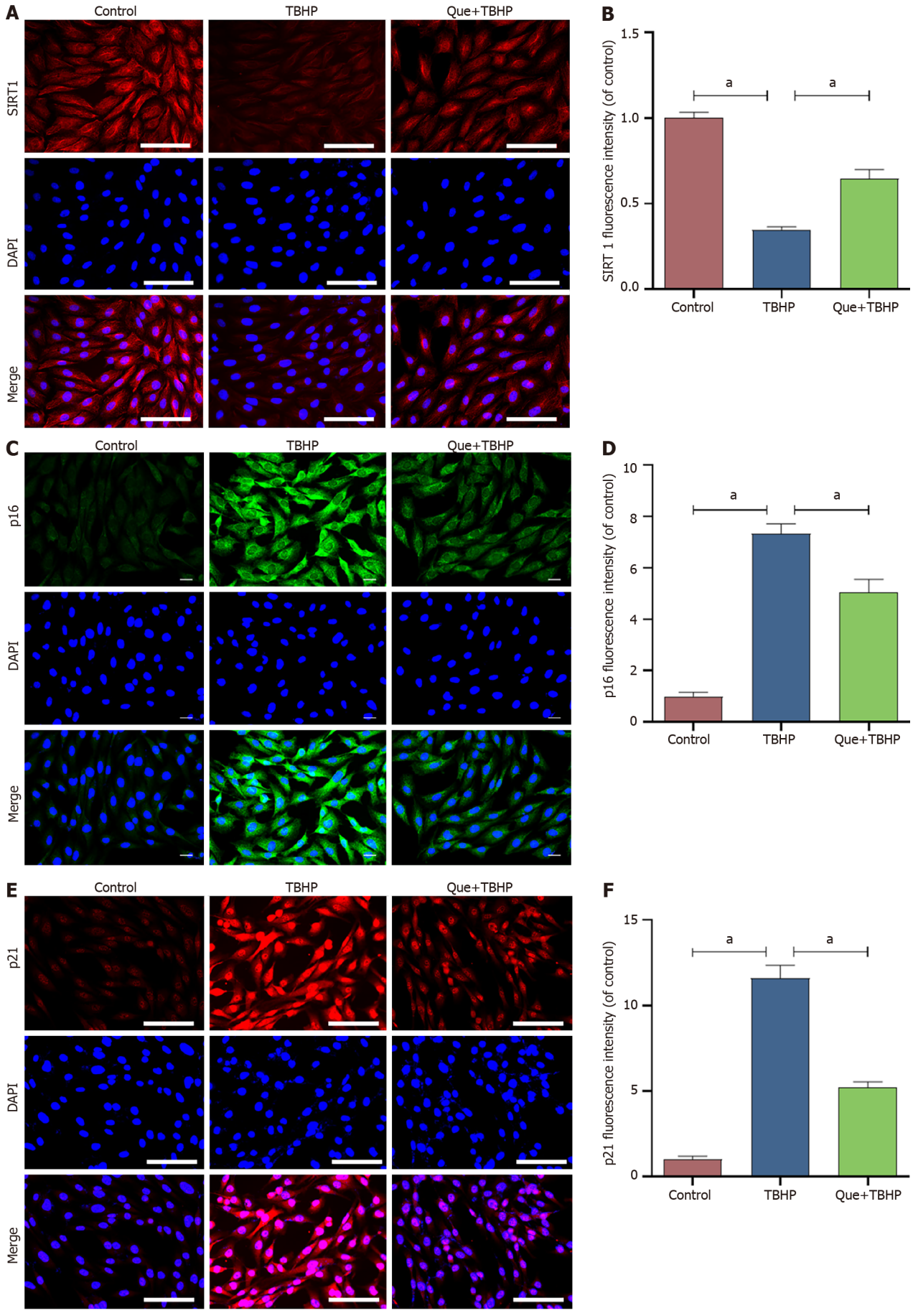
A
Control
TBHP
Que+TBHP
SIRT1
DAPI
Merge
B
SIRT 1 fluorescence intensity (of control)
1.5
1.0
0.5
0.0
a
a
Control
TBHP
Que+TBHP
C
Control
TBHP
Que+TBHP
p16
DAPI
Merge
D
p16 fluorescence intensity (of control)
10
8
6
4
2
0
a
a
Control
TBHP
Que+TBHP
E
Control
TBHP
Que+TBHP
p21
DAPI
Merge
F
p21 fluorescence intensity (of control)
15
10
5
0
a
a
Control
TBHP
Que+TBHP

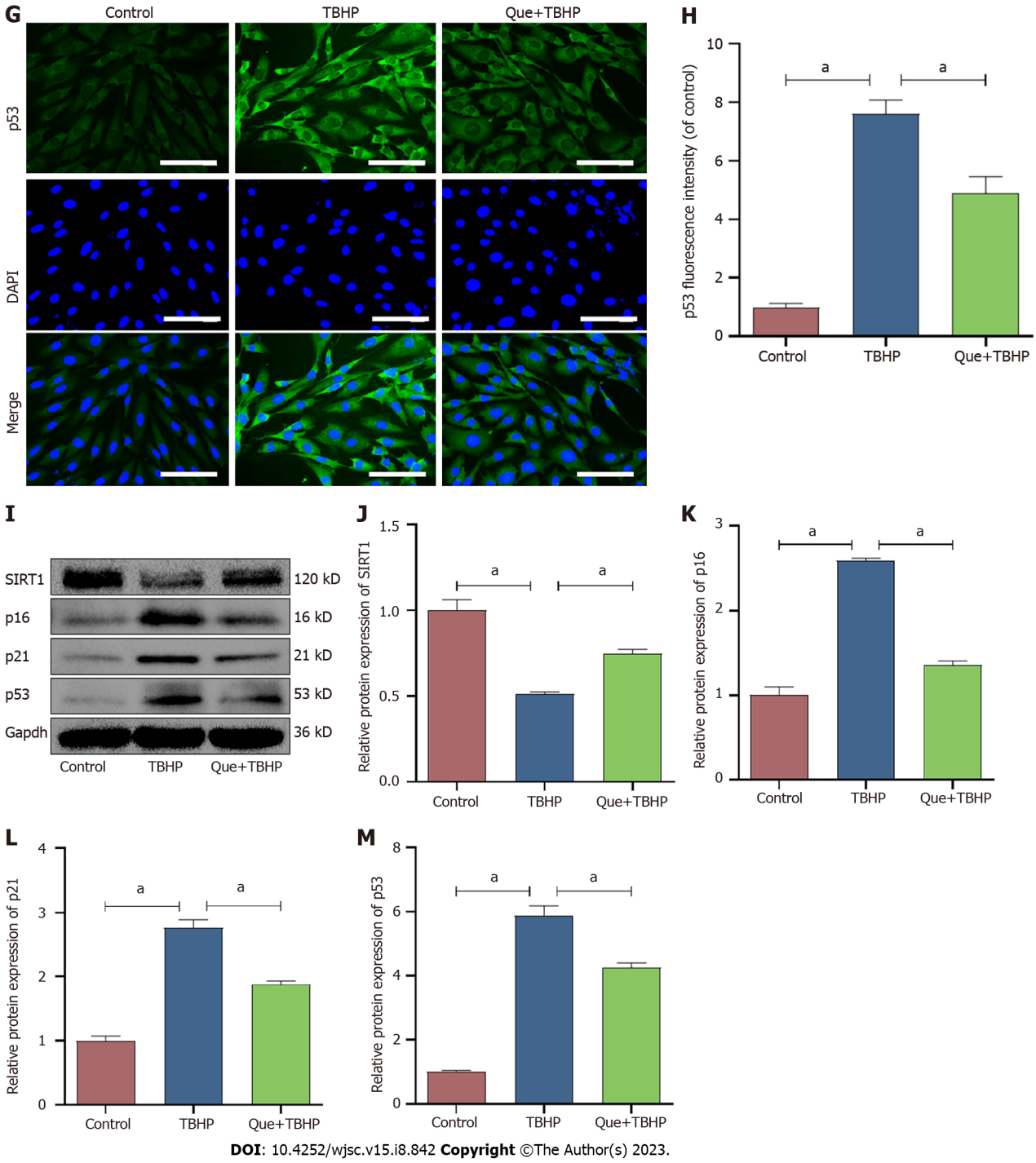

DOI: 10.4252/wjsc.v15.i8.842 **Copyright** ©The Author(s) 2023.

Figure 5 Quercetin upregulates the expression of SIRT1 and downregulates the expression of p16 and p21 and p53. A and B: Immunofluorescence staining and quantitative analysis of SIRT1; C and D: Immunofluorescence staining and quantitative analysis of p16; E and F: Immunofluorescence staining and quantitative analysis of p21; G and H; Immunofluorescence staining and quantitative analysis of p53; I-M: The protein expressions and quantitative analysis of SIRT1, p16, p21 and p53 in the different groups. Scale bar = 100 μm. Data are represented as mean ± SD. Significant differences between groups are indicated as $^{a}P < 0.05$, $n = 3$. TBHP: Tert-butyl hydroperoxide; Que: Quercetin.

Que modulates TBHP-induced senescence of NPMSCs via the miR-34a-5p/SIRT1 pathway

To explore the relationship between miR-34a-5p/SIRT1 and oxidative stress-induced senescence in Que-treated NPMSCs, the miR-34a-5p mimic and siSIRT1 were used to investigate whether overexpression of miR-34a-5p and knockdown of SIRT1, respectively, counteracts the effects of Que on the expression of senescence-related proteins (p16, p21, and p53), SASP (IL-1β, IL-6, and MMP-13), and SIRT1. As shown in Figures 10 and 11, Que suppressed the expression of senescence-related proteins and SASP but promoted the expression of SIRT1, whereas overexpression of miR-34a-5p and knockdown of SIRT1 impaired this protective effect in TBHP-treated NPMSCs. These results suggested that Que may protect NPMSCs from TBHP-induced senescence *via* the miR-34a-5p/SIRT1 pathway.

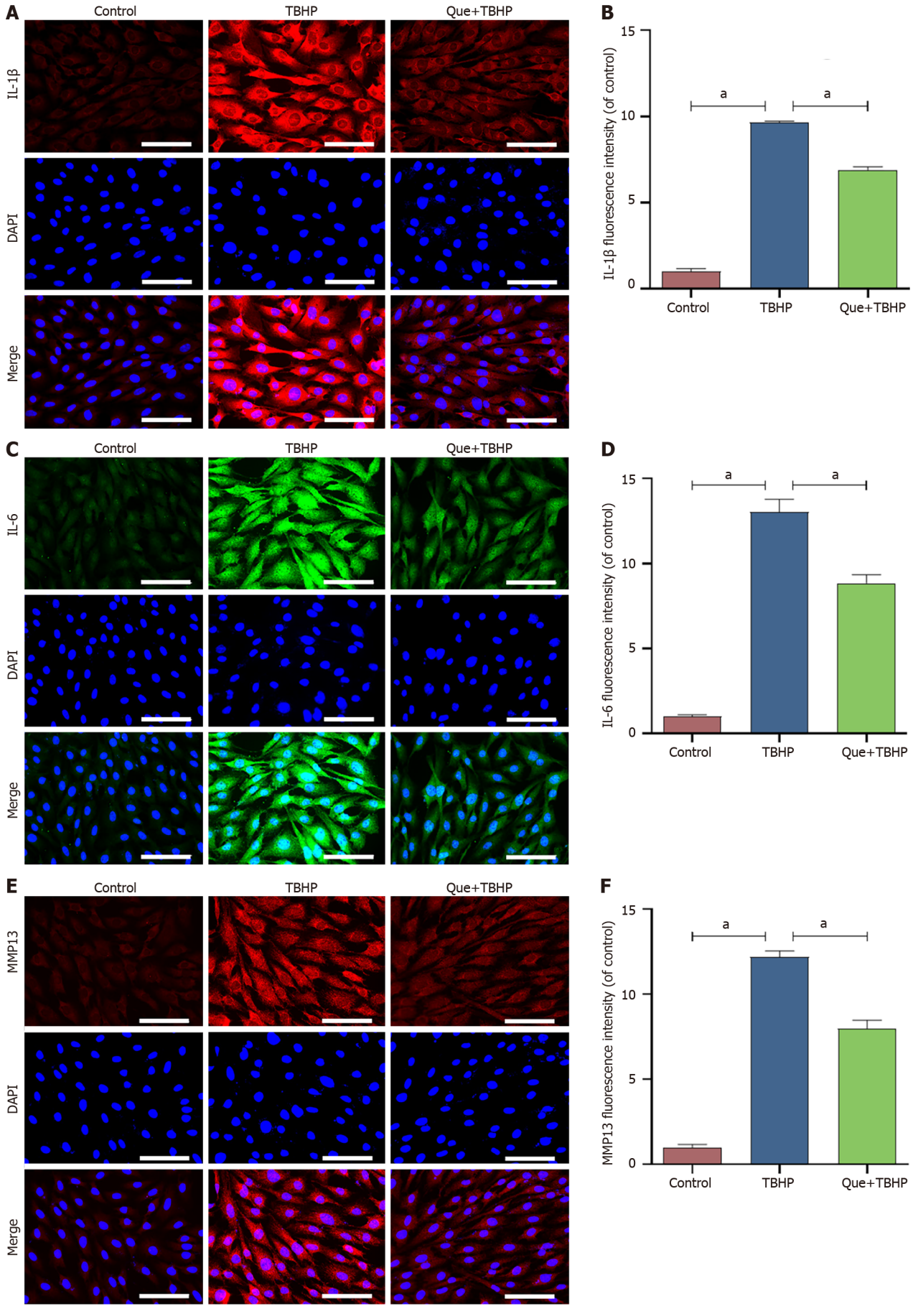
A
Control
TBHP
Que+TBHP
IL-1β
DAPI
Merge
B
IL-1β fluorescence intensity (of control)
15
10
5
0
a
a
Control
TBHP
Que+TBHP
C
Control
TBHP
Que+TBHP
IL-6
DAPI
Merge
D
IL-6 fluorescence intensity (of control)
15
10
5
0
a
a
Control
TBHP
Que+TBHP
E
Control
TBHP
Que+TBHP
MMP13
DAPI
Merge
F
MMP13 fluorescence intensity (of control)
15
10
5
0
a
a
Control
TBHP
Que+TBHP

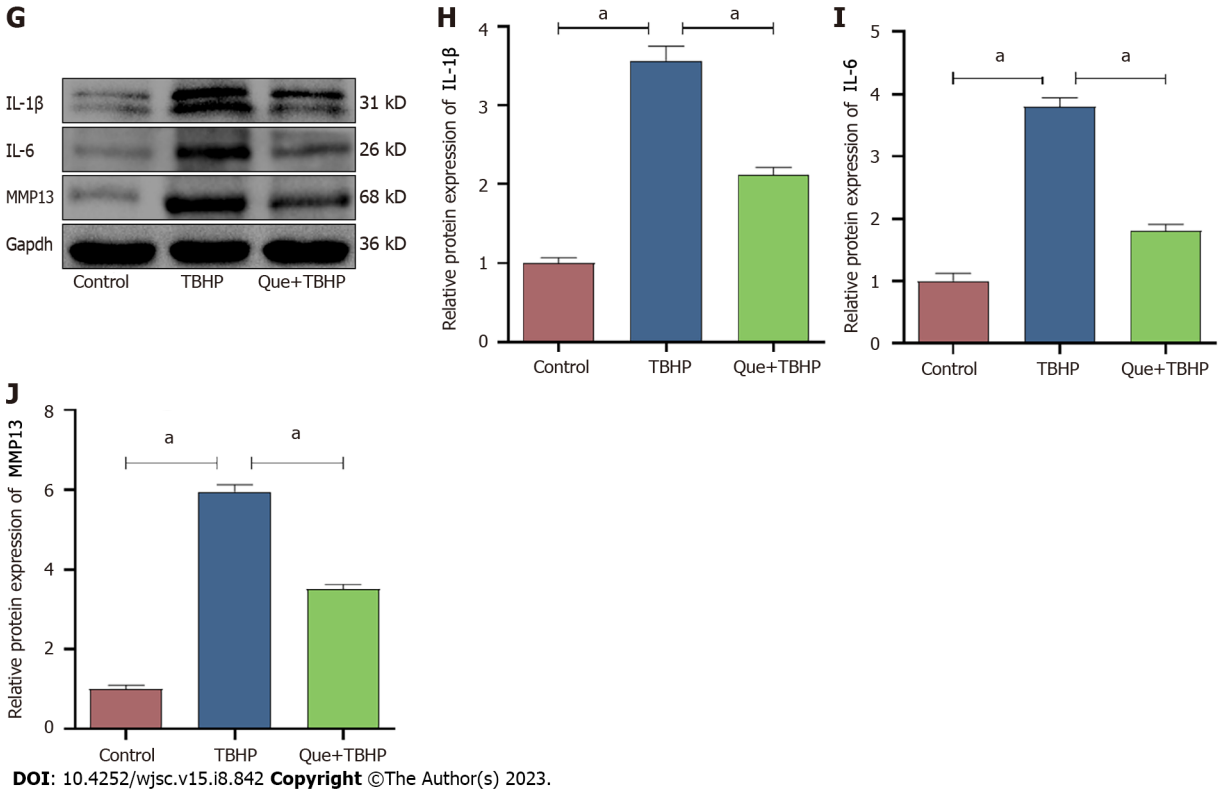

DOI: 10.4252/wjsc.v15.i8.842 **Copyright** ©The Author(s) 2023.

Figure 6 Quercetin downregulates the expression of senescence associated secreted phenotype: IL-1β, IL-6 and MMP13. A and B: Immunofluorescence staining and quantitative analysis of IL-1β; C and D: Immunofluorescence staining and quantitative analysis of IL-6; E and F: Immunofluorescence staining and quantitative analysis of MMP-13; G-J: The protein expressions and quantitative analysis of IL-1β, IL-6 and MMP-13 in different groups. Scale bar = 100 μm. Data are represented as mean ± SD. Significant differences between groups are indicated as $^{a}P < 0.05$, $n = 3$. TBHP: Tert-butyl hydroperoxide; Que: Quercetin.

Que ameliorates disc degeneration in a rat model

A puncture-induced rat model was established to investigate the effect of Que in IDD *in vivo*, and disc height was measured by X-ray images at Week 0 and Week 4 after puncture (Figure 12A). Compared to the control group, the DHI of the IDD group was significantly decreased (Figure 12B-E). Interestingly, the DHI of the Que group was significantly higher than that of the IDD group ($P < 0.05$) (Figure 12B-E). According to the Hematoxylin & eosin staining, NP tissues occupied most of the area in the discs, and NP cells were well dispersed in the matrix. The annulus fibrosus (AF) was well organized in the remaining area. In the IDD group, the NP tissues almost disappeared, and the border between NP and AF was severely disrupted (Figure 12F). However, Que treatment alleviated the degeneration and morphological changes in the NP and AF (Figure 12F). The histological score was higher in the IDD group compared to the control group ($P < 0.05$) (Figure 12G). Both Safranin-O Fast Green and Alcian blue staining showed that the proteoglycan matrix area was lower in the IDD group compared to the control group (Figure 12F). However, Que treatment alleviated the proteoglycan decrease compared to the IDD group (Figure 12H). Immunofluorescence was also used to assess the expression of collagen II and aggrecan in the disc tissue. Compared to the control group, the expression of collagen type II and aggrecan was significantly lower in the IDD group, and Que treatment significantly attenuated the decrease in collagen type II and aggrecan compared to the IDD group (Figure 12I and J). Taken together, these results suggested that Que alleviates the IDD process in a puncture-induced rat model.

DISCUSSION

In the present study, the results demonstrated that Que ameliorates oxidative stress-induced senescence in NPMSCs *via* the miR-34a-5p/SIRT1 axis. The *in vivo* results also demonstrated that Que inhibits the expression of senescence-related proteins (p16, p21, and p53) and SASP (IL-1β, IL-6, and MMP-13) as well as promotes the expression of SIRT1, suggesting that it has a therapeutic effect in the IDD rat model.

Several previous studies have found that oxidative stress is highly associated with the progression of IDD[4,7]. Oxidative stress is triggered in the microenvironment of degenerative IVD when the balance between generation and elimination of ROS is broken[33]. ROS not only trigger oxidative damage of the extracellular matrix of IVD but also induce oxidative damage to DNA, proteins, and mitochondria[33]. Moreover, ROS promote the production of ROS in IVD cells, forming a positive feedback loop[5-7,34]. The discovery of NPMSCs provides a theoretical basis for the endogenous repair of IDD[9,11]. The endogenous repair ability of NPMSCs in degenerative IVD is achieved by differentiation into NP

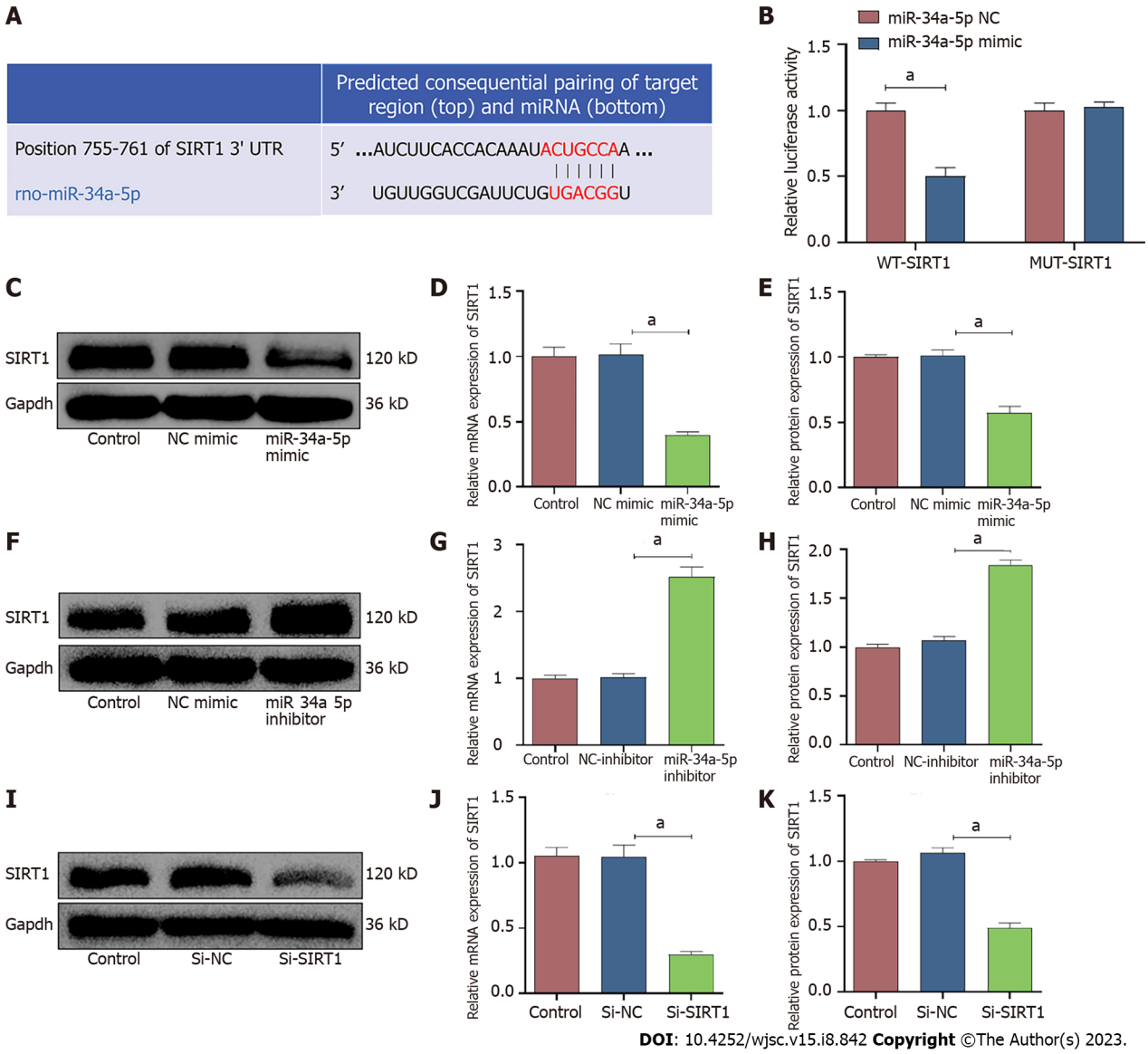

DOI: 10.4252/wjsc.v15.i8.842 **Copyright** ©The Author(s) 2023.

Figure 7 miR-34a-5p represses SIRT1 expression by targeting the 3'-UTR of SIRT1. A: Schematic of the predicted miR-34a-5p binding sites in the 3'-UTR of SIRT1 mRNA from TargetScan online database; B: Luciferase reporter activity of SIRT1 co-transfected with miR-34a-5p nc or miR-34a-5p mimic; C-E: The protein and mRNA expression level of SIRT1 in nucleus pulposus-derived mesenchymal stem cells (NPMSCs) transfected with miR-34a-5p mimic; F-H: The protein and mRNA expression level of SIRT1 in NPMSCs transfected with miR-34a-5p inhibitor; I-K: The protein and mRNA expression level of SIRT1 in NPMSCs transfected with Si-SIRT1. Data are represented as mean ± SD. Significant differences between groups are indicated as $^{a}P < 0.05$, $n = 3$. TBHP: Tert-butyl hydroperoxide.

cells and inhibiting cell apoptosis and/or senescence[10,35]. Oxidative stress in the microenvironment of IVD induces NPMSC senescence, and senescent NPMSCs decrease multipotency and self-renew ability, thus decreasing the regenerative potential and endogenous repair ability of NPMSCs[17,36-38]. In the present study, we found increased expression of senescence-related proteins (p16, p21, and p53), increased SASP (IL-1β, IL-6, and MMP-13), increased SA-β-Gal-positive senescent cells, decreased expression of SIRT1, decreased proliferation, and decreased viability after TBHP treatment in NPMSCs. Therefore, it is important to understand how to maintain the quantity and quality of NPMSCs under adverse microenvironments in degenerative IVD, such as oxidative stress, hypoxia, nutrient deficiency, and compression.

As a potent antioxidant, Que scavenges ROS, scavenges free radicals, inhibits lipid peroxidation, and inhibits xanthine oxidase activity[18-20,39]. Previous studies have reported that Que is an effective activator of SIRT1[40-42]. Feng *et al*[22] reported that Que attenuates oxidative stress-induced apoptosis of rat chondrocytes *via* the SIRT1/mitogen-activated protein kinase (AMPK) pathway and prevents the progression of osteoarthritis in a rat model[22]. Lou *et al*[43] confirmed that Que inhibits HepG2 cell apoptosis through the p53/miRNA-34a/SIRT1 pathway[43]. To evaluate the effect of Que in TBHP-induced NPMSCs, we pretreated cells with Que (20 μM) for 24 h before the addition of TBHP (100 μM) in the present study. Pretreatment with Que decreased ROS generation, decreased SA-β-Gal activity, and partially restored cell proliferation in oxidative stress induced-NPMSCs. Further, Que significantly reduced the expression of senescence-related proteins (p16, p21, and p53), reduced SASP (IL-1β, IL-6, and MMP-13), and increased the expression of SIRT1. Therefore, these results indicated that Que may have a protective effect against TBHP-induced oxidative stress in

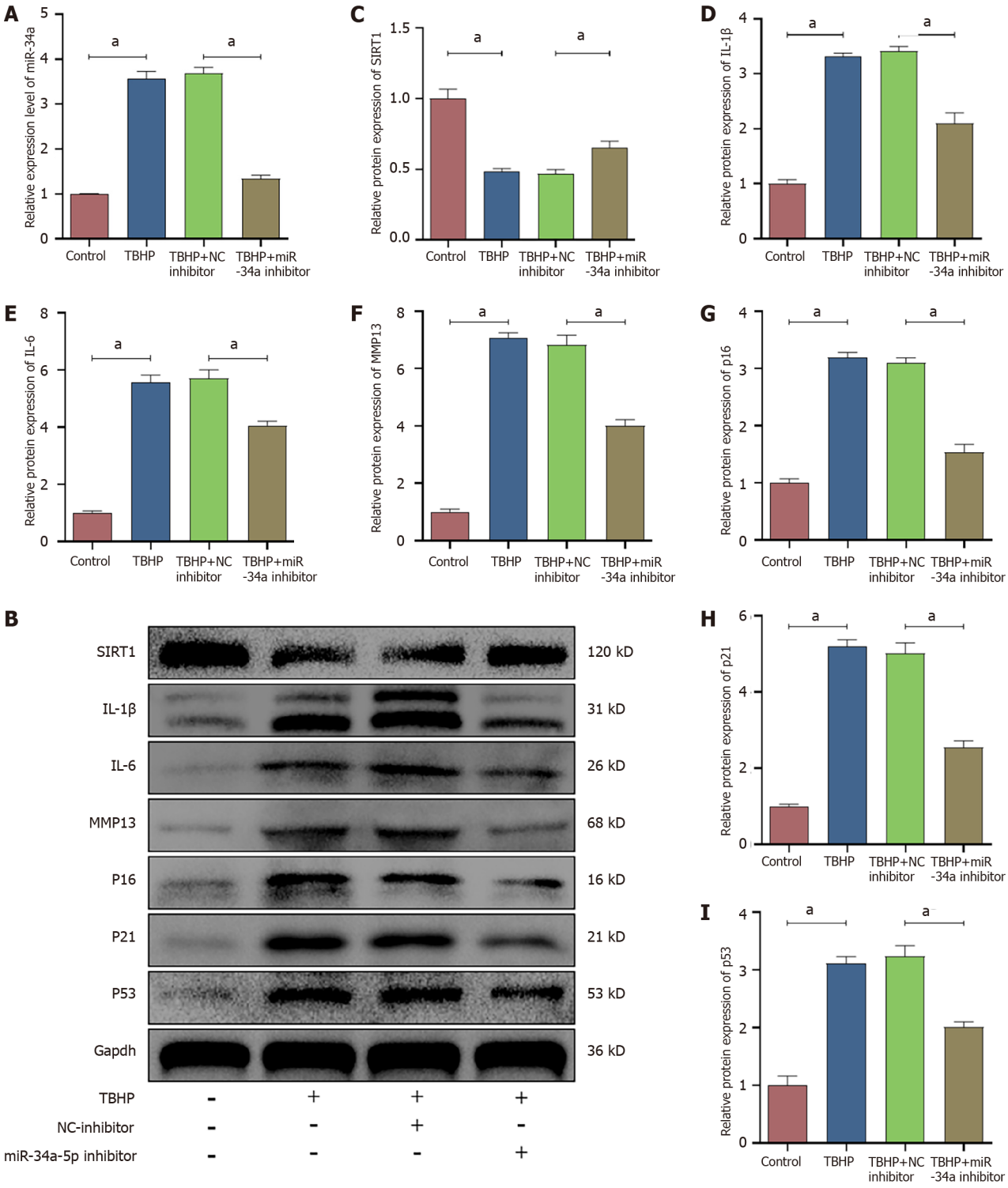

DOI: 10.4252/wjsc.v15.i8.842 **Copyright** ©The Author(s) 2023.

Figure 8 Downregulation of miR-34a-5p alleviated oxidative stress-induced nucleus pulposus-derived mesenchymal stem cells senescence. A: The RNA levels of miR-34a-5p in nucleus pulposus-derived mesenchymal stem cells (NPMSCs) were transfected with miR-34a-5p inhibitor and treated with tert-butyl hydroperoxide; B: The protein levels of SIRT1, p16, p21, p53, IL-1β, IL-6 and MMP-13 in NPMSCs transfected with miR-34a-5p inhibitor; C-I: Quantitative analysis of protein expression in the different groups. Data are represented as mean ± SD. Significant differences between groups are indicated as $^{a}P < 0.05$, $n = 3$. TBHP: Tert-butyl hydroperoxide.

NPMSCs.

A previous study has also demonstrated that the expression of miR-34a-5p is significantly upregulated in degenerative IVD and that miR-34a-5p increases extracellular matrix degradation and cell apoptosis. Chen *et al*[44] reported that miR-34a increases apoptosis in degenerated cartilage endplate (CEP) chondrocytes. In addition, inhibition of miR-34a reduces cell apoptosis, while upregulation of miR-34a has an opposite effect in CEP cells[44]. In the present study, TBHP significantly upregulated miR-34a-5p expression. Overexpression miR-34a aggravated the oxidative stress damage

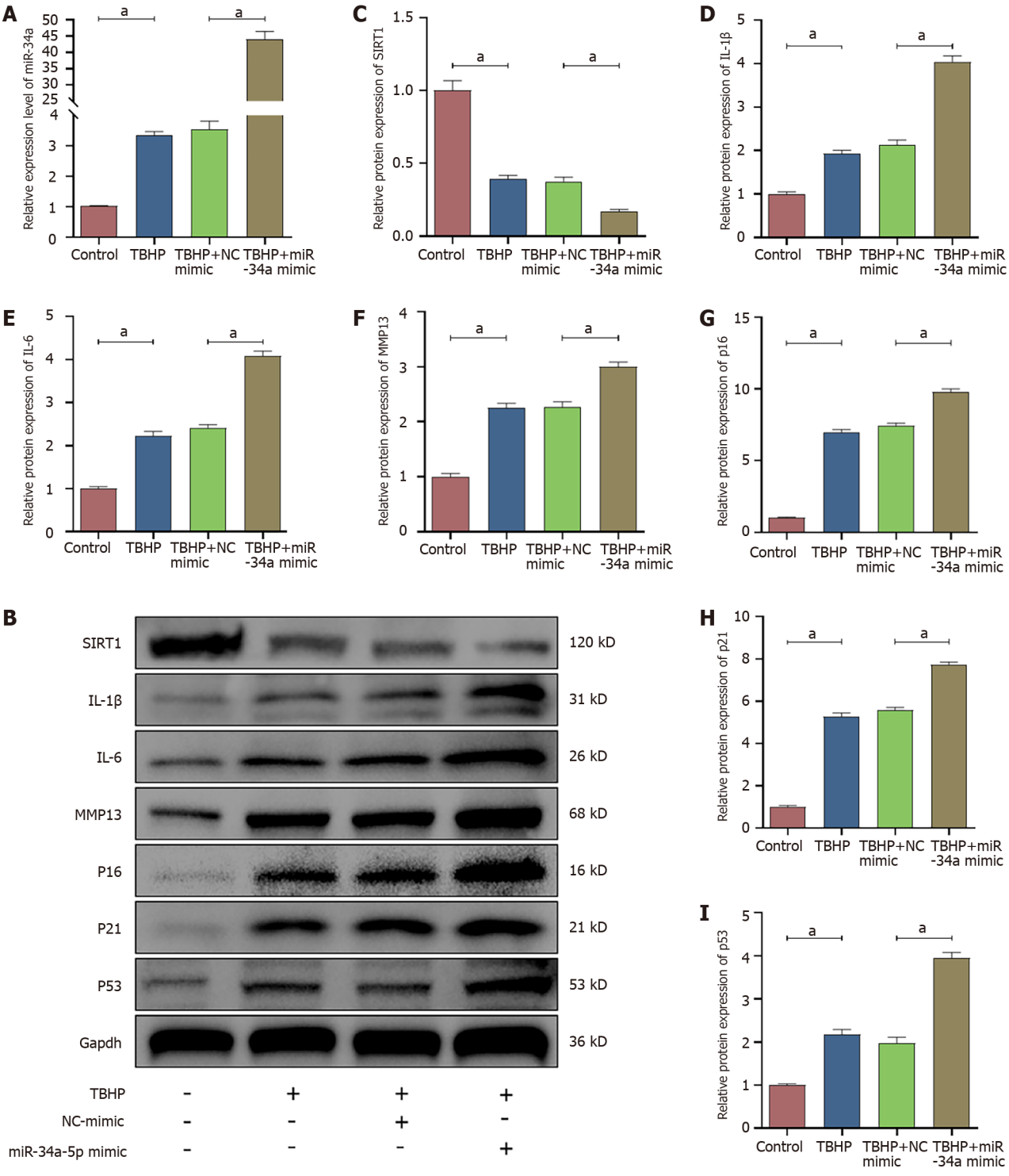

DOI: 10.4252/wjsc.v15.i8.842 **Copyright** ©The Author(s) 2023.

Figure 9 Overexpression of miR-34a-5p enhanced oxidative stress-induced nucleus pulposus-derived mesenchymal stem cells senescence. A: The RNA levels of miR-34a-5p in nucleus pulposus-derived mesenchymal stem cells (NPMSCs) were transfected with miR-34a-5p mimic and treated with TBHP; B: The protein levels of SIRT1, p16, p21, p53, IL-1β, IL-6 and MMP-13 in NPMSCs transfected with miR-34a-5p mimic; C-I: Quantitative analysis of protein expression in different groups. Data are represented as mean ± SD. Significant differences between groups are indicated as $^{a}P < 0.05$, $n = 3$. TBHP: Tert-butyl hydroperoxide.

induced by TBHP in NPMSCs, including increased the expression of senescence-related proteins and SASP as well as and decreased the expression of SIRT1, whereas knockdown of miR-34a had an opposite effect in NPMSCs. Accumulating studies have demonstrated that SIRT1 exerts important function in the progression of IDD. The expression level of SIRT1 in IVD cells decreases with the progression of IDD[45], and SIRT1 expression is negatively correlated with Pfirrmann grade in IDD[46]. It has been reported that SIRT1 decreases the oxidative stress-induced senescence in CEP cells through the p53/p21 pathway[47]. H_2O_2-induced oxidative stress reduces the expression of SIRT1 as the expression of SIRT1 is downregulated with the increasing concentration of H_2O_2, and SIRT1 activation alleviates oxidative stress-induced

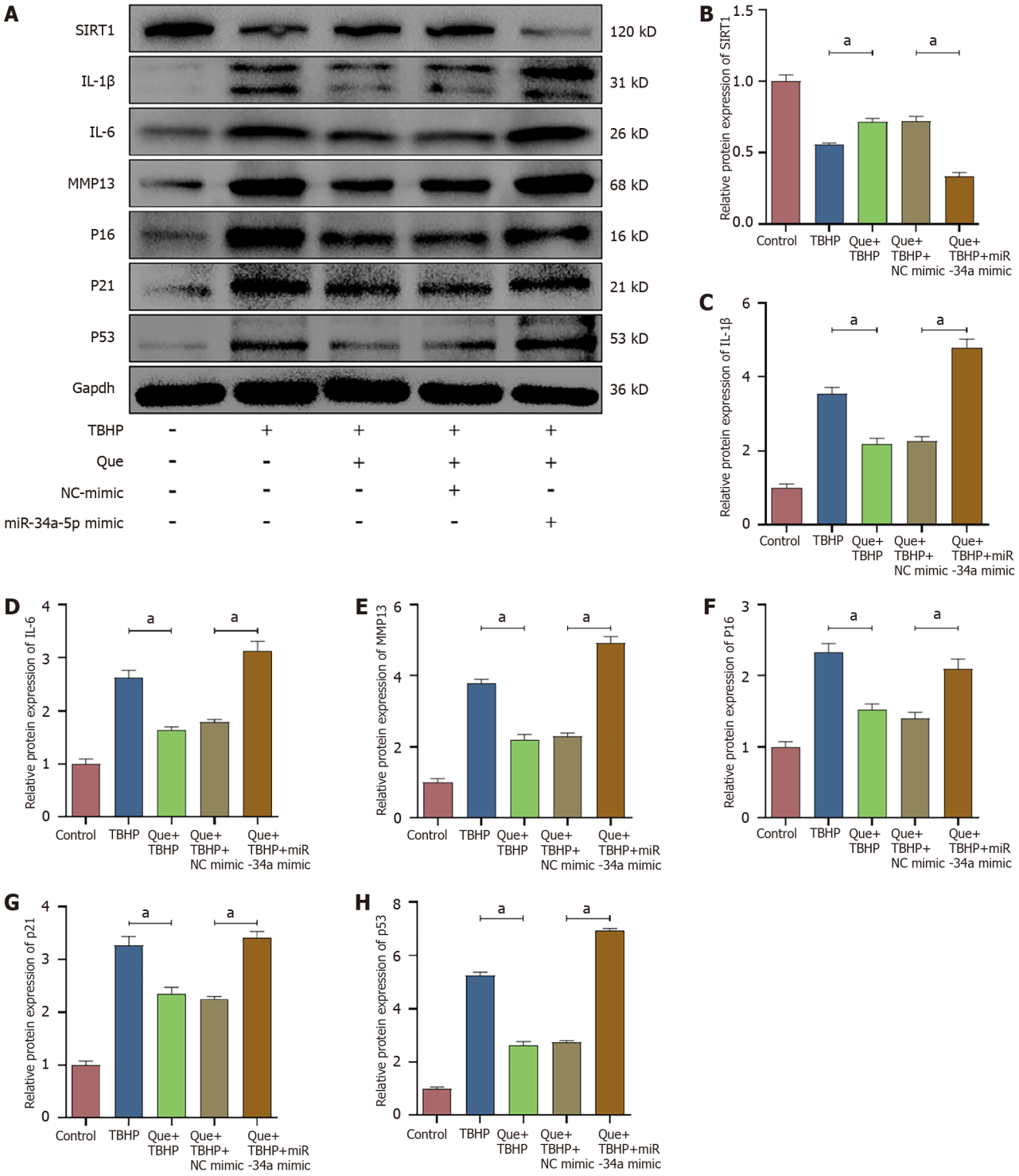

DOI: 10.4252/wjsc.v15.i8.842 **Copyright** ©The Author(s) 2023.

Figure 10 Quercetin alleviates TBHP-induced senescence *via* miR-34a-5p/SIRT1 axis. A: The protein levels of SIRT1, p16, p21, p53, IL-1β, IL-6 and MMP-13 in different groups; B-H: Quantitative analysis of protein expression in different groups. Data are represented as mean ± SD. Significant differences between groups are indicated as $^aP < 0.05$, $n = 3$. TBHP: Tert-butyl hydroperoxide; Que: Quercetin.

senescence in NP cells[29,48]. Xia *et al*[49] found that the expression of p16 is downregulated by activating SIRT1 in rat IDD model[49]. The present study found that SIRT1 expression was downregulated in TBHP induced-NPMSCs, which was rescued by Que and inhibiting miR-34a-5p. These results suggested that SIRT1 plays a protective role in TBHP induced-NPMSCs. miR-34a-5p overexpression and SIRT1 downregulation in NPMSCs were utilized to investigate whether Que reduces oxidative stress damage *via* the miR-34a/SIRT1 pathway to delay NPMSC senescence. The results demonstrated that the protective effect of Que is reversed by miR-34a-5p overexpression and SIRT1 knockdown.

In the present study, Que was also administered to IDD animal models to evaluate the protective effect of Que *in vivo*. X-ray analysis indicated the loss of DHI in the IDD model, but Que treatment ameliorated the decreased DHI. Moreover, histological analysis using HE, Alcian blue, and S-O staining as well as immunofluorescence analysis of collagen type II

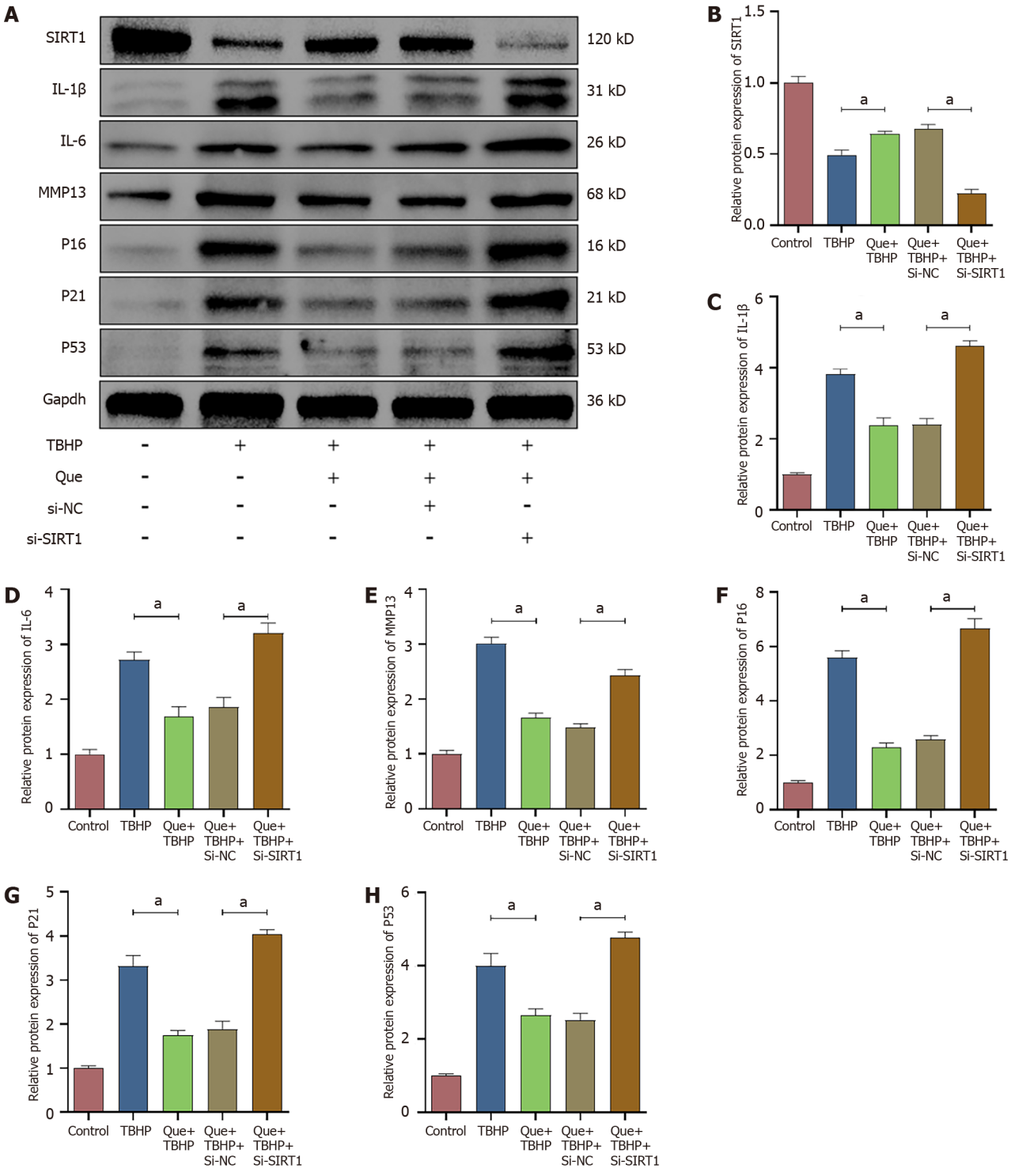

DOI: 10.4252/wjsc.v15.i8.842 **Copyright** ©The Author(s) 2023.

Figure 11 Quercetin alleviates TBHP-induced senescence *via* miR-34a-5p/SIRT1 axis. A: The protein levels of SIRT1, p16, p21, p53, IL-1β, IL-6 and MMP-13 in different groups; B-H: Quantitative analysis of protein expression in different groups. Data are represented as mean ± SD. Significant differences between groups are indicated as $^{a}P < 0.05$, $n = 3$. TBHP: Tert-butyl hydroperoxide; Que: Quercetin.

and aggrecan confirmed that Que had a positive effect on delaying the degree of IDD.

The present study had several limitations. Previous studies have shown Que has pleiotropic properties. In addition to the activation of SIRT1, Que has anti-inflammatory and antioxidative effects *via* activating nuclear factor erythroid 2-related factor 2 (NRF2)[39], mitogen-activated protein kinase (MAPK)[39], and phosphatidylinositol 3-kinases/protein kinase B (PI3K/AKT)[50]. Hence, it remains unknown whether Que plays a role in NPMSC senescence induced by oxidative stress *via* other signaling pathways, suggesting that further study is needed to explore the other mechanisms underlying the protective effect of Que on NPMSCs. Moreover, future clinical studies are needed to evaluate the effect of Que on IDD progress.

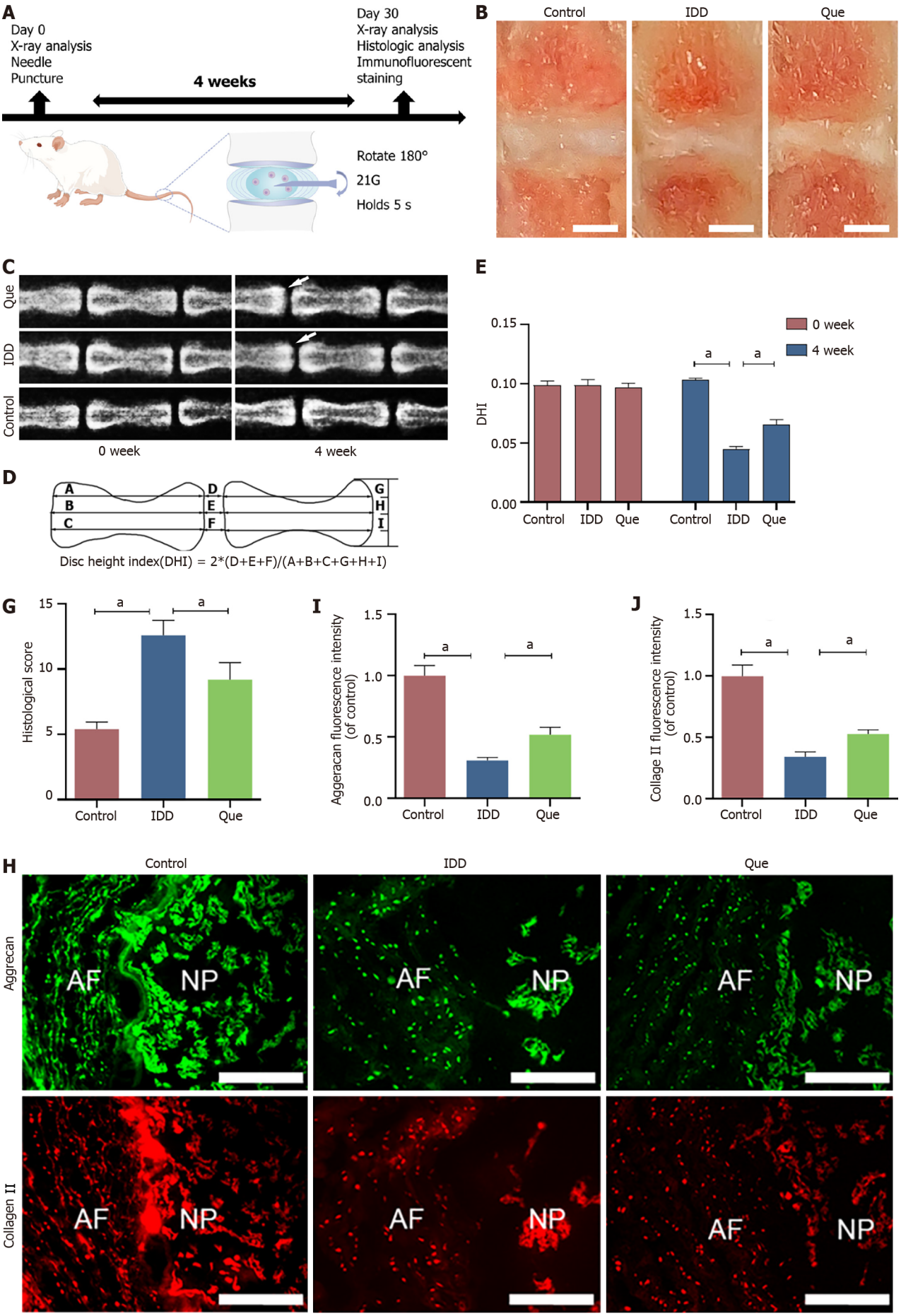
A
Day 0
X-ray analysis
Needle
Puncture
4 weeks
Day 30
X-ray analysis
Histologic analysis
Immunofluorescent staining
Rotate 180°
21G
Holds 5 s
B
Control
IDD
Que
C
Que
IDD
Control
0 week
4 week
D
A
B
C
D
E
F
G
H
I
Disc height index(DHI) = 2*(D+E+F)/(A+B+C+G+H+I)
E
DHI
0.15
0.10
0.05
0.00
0 week
4 week
a
a
Control
IDD
Que
Control
IDD
Que
G
Histological score
15
10
5
0
a
a
Control
IDD
Que
I
Aggrecan fluorescence intensity (of control)
1.5
1.0
0.5
0.0
a
a
Control
IDD
Que
J
Collage II fluorescence intensity (of control)
1.5
1.0
0.5
0.0
a
a
Control
IDD
Que
H
Control
IDD
Que
Aggrecan
Collagen II
AF
NP

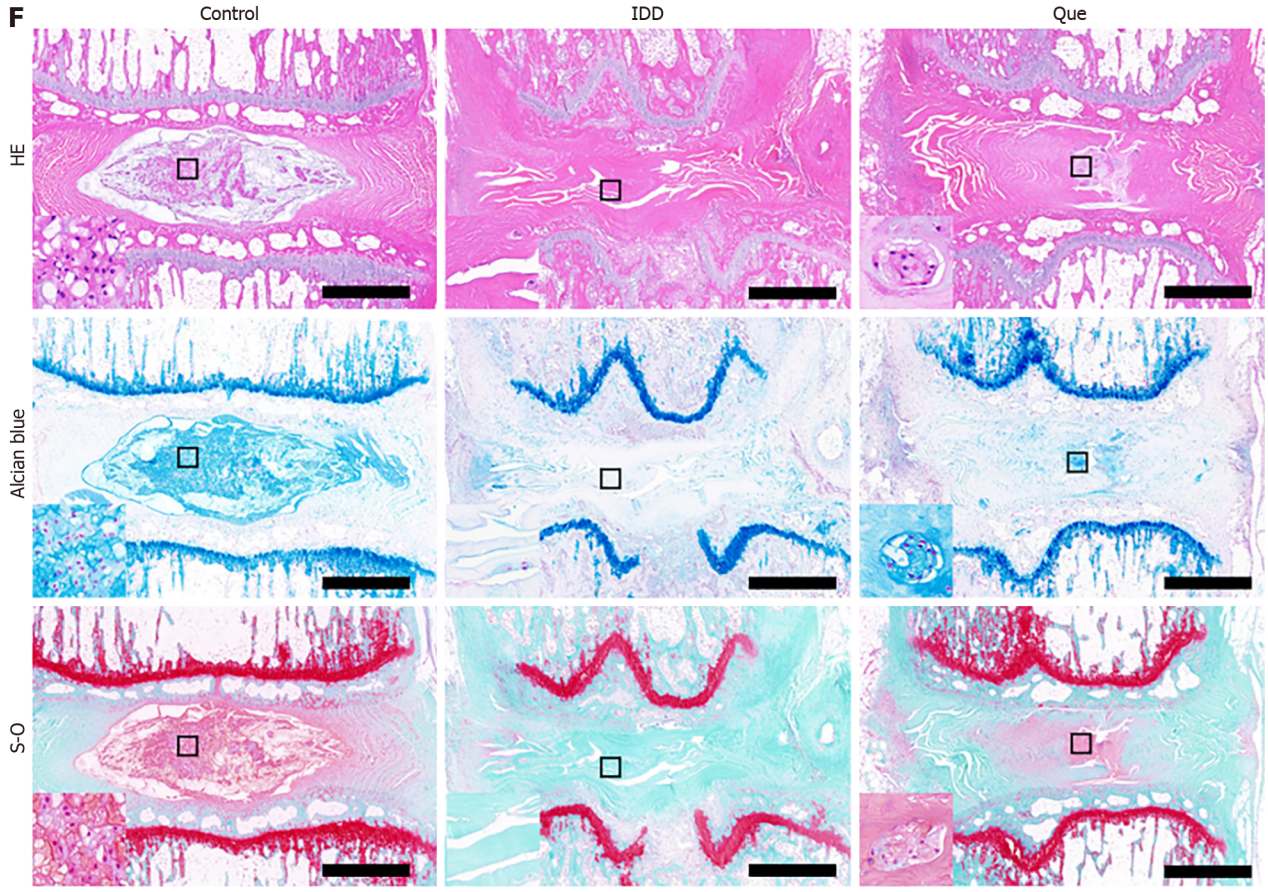

DOI: 10.4252/wjsc.v15.i8.842 **Copyright** ©The Author(s) 2023.

Figure 12 Quercetin ameliorates IVDD *in vivo*. A: Schematic of the basic process of *in vivo* experiment (By Figdraw); B: Macroscopic appearances of rat tail intact disc mid-sagittal sections in control group, intervertebral disc degeneration group and quercetin group (Scar bar = 2 mm); C: The X-ray in different groups at 0 wk and 4 wk after puncturing; D: Measurements of intervertebral disc height index (DHI); E: Quantitative analysis of DHI; F-G: Hematoxylin-eosin staining and quantitative analysis of histological score at 4 wk after puncture in different groups (scale bar = 1mm); H: The expression of aggrecan and collagen type II in different groups (scale bar = 400 μm); I-J: Quantitative analysis of aggrecan and collagen type II in different groups. Data are represented as mean ± SD. Significant differences between groups are indicated as $^{a}P < 0.05$, $n = 3$. HE: Hematoxylin-eosin; NP: Nucleus pulposus; AF: Annulus fibrosus; IDD: Intervertebral disc degeneration; TBHP: Tert-butyl hydroperoxide; Que: Quercetin.

CONCLUSION

In summary, the present study demonstrated that Que prevents oxidative stress-induced senescence of NPMSCs *via* the miR-34a/SIRT1 signaling pathway (Figure 13). Moreover, Que ameliorates the progression of IDD in a rat model. These findings suggested that Que may be a potential agent for the treatment of IDD.

Table 1 Sequences of primers used for real-time polymerase chain reaction

Gapdh	F: CTGGAGAAACCTGCCAAGTATG
	R: GGTGGAAGAATGGGAGTTGCT
SIRT1	F: TGACCTCCTCATTGTTATTGGG
	R: GGCATACTCGCCACCTAACCT
U6	F: CTCGCTTCGGCAGCACA
	R: AACGCTTCACGAATTTGCGT
miR-34a-5p	F: ACACTCCAGCTGGGTGGCAGTGTCTTAGCT
	R: TGGTGTCGTGGAGTCG

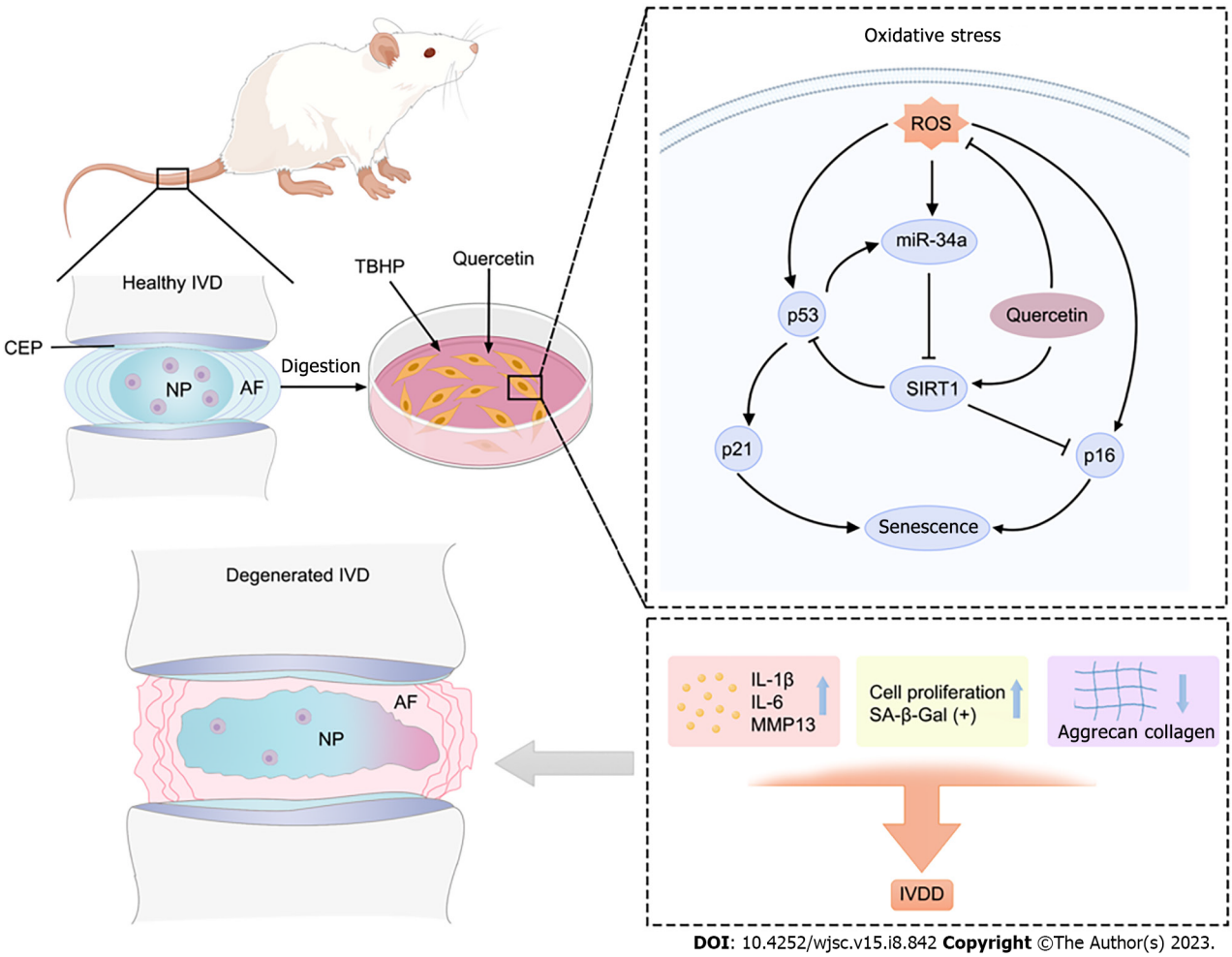

DOI: 10.4252/wjsc.v15.i8.842 **Copyright** ©The Author(s) 2023.

Figure 13 Schematic representation of the mode of action of quercetin. Quercetin ameliorates oxidative stress-induced senescence in nucleus pulposus-derived mesenchymal stem cells *via* miR-34a-5p/SIRT1 axis. HE: Hematoxylin-eosin; NP: Nucleus pulposus; AF: Annulus fibrosus; IVD: Intervertebral disc; TBHP: Tert-butyl hydroperoxide; ROS: Reactive oxygen species assay. By Figdraw.

ARTICLE HIGHLIGHTS

Research background

Intervertebral disc degeneration (IDD) is a main contributor to low back pain. Oxidative stress, which is highly associated with the progression of IDD, increases senescence of nucleus pulposus-derived mesenchymal stem cells (NPMSCs) and weakens the differentiation ability of NPMSCs in degenerated intervertebral discs (IVDs). Quercetin (Que) has been demonstrated to reduce oxidative stress in diverse degenerative diseases.

Research motivation

An adverse microenvironments of degenerative intervertebral disc such as oxidative stress, low nutrition, and inflammation leads to increased senescence NPMSCs, which severely affects endogenous repair. Therefore, inhibition senescence of NPMSCs may be of great significance in alleviating IDD.

Research objectives

The present study aimed to investigate the role of Que in oxidative stress-induced NPMSC damage and to elucidate the underlying mechanism.

Research methods

In vitro, NPMSCs were isolated from rat tails. Senescence-associated β-galactosidase (SA-β-Gal) staining, cell cycle, reactive oxygen species (ROS), real-time quantitative polymerase chain reaction (RT-qPCR), immunofluorescence, and western blot analyses were used to evaluate the protective effects of Que. Meanwhile the relationship between miR-34a-5p and Sirtuins 1(SIRT1) was evaluated by dual-luciferase reporter assay. To explore whether Que modulates tert-butyl hydroperoxide (TBHP)-induced senescence of NPMSCs *via* the miR-34a-5p/SIRT1 pathway, we used adenovirus vectors to overexpress and downregulate the expression of miR-34a-5p, and used SIRT1 siRNA to knockdown SIRT1 expression. *In vivo*, a puncture-induced rat IDD model was constructed, and X rays and histological analysis were used to assess

whether Que could alleviate IDD *in vivo*.

Research results

We found that TBHP can cause NPMSCs senescence changes, such as reduced cell proliferation ability, increased SA-β-Gal activity, cell cycle arrest, the accumulation of ROS, and increased expression of senescence-related proteins. While abovementioned senescence indicators were significantly alleviated by Que treatment. Que decreased the expression levels of senescence-related proteins (p16, p21, and p53) and senescence-associated secreted phenotype (SASP), including IL-1β, IL-6, and MMP-13, and it increased the expression of SIRT1. In addition, the protective effects of Que on cell senescence were partially reversed by miR-34a-5p overexpression and SIRT1 knockdown. *In vivo*, X-ray, and histological analyses indicated that Que alleviated IDD in a puncture-induced rat model.

Research conclusions

In summary, the present study provides evidence that Que reduces oxidative stress-induced senescence of NPMSCs *via* the miR-34a/SIRT1 signaling pathway, suggesting that Que may be a potential agent for the treatment of IDD.

Research perspectives

We demonstrated Que ameliorates oxidative stress-induced senescence of NPMSCs and delays the progression of IDD. Que may be a potential agent for the treatment of IDD.

ACKNOWLEDGEMENTS

We also thank Figdraw for the assistance in drawing graphical abstract.

FOOTNOTES

Author contributions: Zhao WJ and Liu X contributed to data curation, Writing-Original draft preparation, contributed equally to this work; Hu M and Zhang Y contributed to Visualization, Validation; Shi PZ and Wang JW performed Investigation; Lu XH, Cheng XF and Tao YP performed conceptualization, methodology; Feng XM, Wang YX and Zhang L performed supervision, writing- reviewing, editing and share corresponding author.

Supported by the National Natural Science Foundation of China, No. 82172462 and No. 81972136; the Traditional Chinese Medicine Science and Technology Development Plan Project of Jiangsu Province, No. YB2020085; and Cross Cooperation Project of Northern Jiangsu People's Hospital, No. SBJC21014.

Institutional animal care and use committee statement: All animal experiments conformed to the internationally accepted principles for the care and use of laboratory animals, Yangzhou University, No. SYXK (Su) 2017-0044.

Conflict-of-interest statement: All the authors report no relevant conflicts of interest for this article. Figures 12A and 13 were created using Figdraw (www.figdraw.com).

Data sharing statement: All data during the study are available from the corresponding author by request at zhangliang6320@sina.com.

ARRIVE guidelines statement: The authors have read the ARRIVE Guidelines, and the manuscript was prepared and revised according to the ARRIVE Guidelines.

Open-Access: This article is an open-access article that was selected by an in-house editor and fully peer-reviewed by external reviewers. It is distributed in accordance with the Creative Commons Attribution NonCommercial (CC BY-NC 4.0) license, which permits others to distribute, remix, adapt, build upon this work non-commercially, and license their derivative works on different terms, provided the original work is properly cited and the use is non-commercial. See: https://creativecommons.org/Licenses/by-nc/4.0/

Country/Territory of origin: China

ORCID number: Wen-Jie Zhao 0000-0001-7384-8326; Xin Liu 0000-0003-2689-1414; Man Hu 0000-0003-4908-6864; Yu Zhang 0000-0002-2672-9786; Peng-Zhi Shi 0000-0002-8576-6819; Jun-Wu Wang 0000-0002-3553-4390; Xu-Hua Lu 0000-0002-8400-8960; Xiao-Fei Cheng 0000-0003-2470-2034; Yu-Ping Tao 0000-0001-7461-9269; Xin-Min Feng 0000-0001-9287-858X; Yong-Xiang Wang 0000-0003-3763-7411; Liang Zhang 0000-0001-7561-1488.

S-Editor: Li L
L-Editor: A
P-Editor: Yu HG

REFERENCES

1 **GBD 2017 Disease and Injury Incidence and Prevalence Collaborators**. Global, regional, and national incidence, prevalence, and years lived with disability for 354 diseases and injuries for 195 countries and territories, 1990-2017: a systematic analysis for the Global Burden of Disease Study 2017. *Lancet* 2018; **392**: 1789-1858 [PMID: 30496104 DOI: 10.1016/S0140-6736(18)32279-7]

2 **Fitzmaurice C**, Akinyemiju TF, Al Lami FH, Alam T, Alizadeh-Navaei R, Allen C, Alsharif U, Alvis-Guzman N, Amini E, Anderson BO, Aremu O, Artaman A, Asgedom SW, Assadi R, Atey TM, Avila-Burgos L, Awasthi A, Ba Saleem HO, Barac A, Bennett JR, Bensenor IM, Bhakta N, Brenner H, Cahuana-Hurtado L, Castañeda-Orjuela CA, Catalá-López F, Choi JJ, Christopher DJ, Chung SC, Curado MP, Dandona L, Dandona R, das Neves J, Dey S, Dharmaratne SD, Doku DT, Driscoll TR, Dubey M, Ebrahimi H, Edessa D, El-Khatib Z, Endries AY, Fischer F, Force LM, Foreman KJ, Gebrehiwot SW, Gopalani SV, Grosso G, Gupta R, Gyawali B, Hamadeh RR, Hamidi S, Harvey J, Hassen HY, Hay RJ, Hay SI, Heibati B, Hiluf MK, Horita N, Hosgood HD, Ilesanmi OS, Innos K, Islami F, Jakovljevic MB, Johnson SC, Jonas JB, Kasaeian A, Kassa TD, Khader YS, Khan EA, Khan G, Khang YH, Khosravi MH, Khubchandani J, Kopec JA, Kumar GA, Kutz M, Lad DP, Lafranconi A, Lan Q, Legesse Y, Leigh J, Linn S, Lunevicius R, Majeed A, Malekzadeh R, Malta DC, Mantovani LG, McMahon BJ, Meier T, Melaku YA, Melku M, Memiah P, Mendoza W, Meretoja TJ, Mezgebe HB, Miller TR, Mohammed S, Mokdad AH, Moosazadeh M, Moraga P, Mousavi SM, Nangia V, Nguyen CT, Nong VM, Ogbo FA, Olagunju AT, Pa M, Park EK, Patel T, Pereira DM, Pishgar F, Postma MJ, Pourmalek F, Qorbani M, Rafay A, Rawaf S, Rawaf DL, Roshandel G, Safiri S, Salimzadeh H, Sanabria JR, Santric Milicevic MM, Sartorius B, Satpathy M, Sepanlou SG, Shackelford KA, Shaikh MA, Sharif-Alhoseini M, She J, Shin MJ, Shiue I, Shrime MG, Sinke AH, Sisay M, Sligar A, Sufiyan MB, Sykes BL, Tabarés-Seisdedos R, Tessema GA, Topor-Madry R, Tran TT, Tran BX, Ukwaja KN, Vlassov VV, Vollset SE, Weiderpass E, Williams HC, Yimer NB, Yonemoto N, Younis MZ, Murray CJL, Naghavi M, Global Burden of Disease Cancer Collaboration. Global, Regional, and National Cancer Incidence, Mortality, Years of Life Lost, Years Lived With Disability, and Disability-Adjusted Life-Years for 29 Cancer Groups, 1990 to 2016: A Systematic Analysis for the Global Burden of Disease Study. *JAMA Oncol* 2018; **4**: 1553-1568 [PMID: 29860482 DOI: 10.1001/jamaoncol.2018.2706]

3 **Chou D**, Samartzis D, Bellabarba C, Patel A, Luk KD, Kisser JM, Skelly AC. Degenerative magnetic resonance imaging changes in patients with chronic low back pain: a systematic review. *Spine (Phila Pa 1976)* 2011; **36**: S43-S53 [PMID: 21952189 DOI: 10.1097/BRS.0b013e31822ef700]

4 **Suzuki S**, Fujita N, Hosogane N, Watanabe K, Ishii K, Toyama Y, Takubo K, Horiuchi K, Miyamoto T, Nakamura M, Matsumoto M. Excessive reactive oxygen species are therapeutic targets for intervertebral disc degeneration. *Arthritis Res Ther* 2015; **17**: 316 [PMID: 26542776 DOI: 10.1186/s13075-015-0834-8]

5 **Dimozi A**, Mavrogonatou E, Sklirou A, Kletsas D. Oxidative stress inhibits the proliferation, induces premature senescence and promotes a catabolic phenotype in human nucleus pulposus intervertebral disc cells. *Eur Cell Mater* 2015; **30**: 89-102; discussion 103 [PMID: 26337541 DOI: 10.22203/eCM.v030a07]

6 **Hou G**, Lu H, Chen M, Yao H, Zhao H. Oxidative stress participates in age-related changes in rat lumbar intervertebral discs. *Arch Gerontol Geriatr* 2014; **59**: 665-669 [PMID: 25081833 DOI: 10.1016/j.archger.2014.07.002]

7 **Feng C**, Yang M, Lan M, Liu C, Zhang Y, Huang B, Liu H, Zhou Y. ROS: Crucial Intermediators in the Pathogenesis of Intervertebral Disc Degeneration. *Oxid Med Cell Longev* 2017; **2017**: 5601593 [PMID: 28392887 DOI: 10.1155/2017/5601593]

8 **Lee DC**, Adams CS, Albert TJ, Shapiro IM, Evans SM, Koch CJ. In situ oxygen utilization in the rat intervertebral disc. *J Anat* 2007; **210**: 294-303 [PMID: 17331178 DOI: 10.1111/j.1469-7580.2007.00692.x]

9 **Sakai D**, Andersson GB. Stem cell therapy for intervertebral disc regeneration: obstacles and solutions. *Nat Rev Rheumatol* 2015; **11**: 243-256 [PMID: 25708497 DOI: 10.1038/nrrheum.2015.13]

10 **Lyu FJ**, Cheung KM, Zheng Z, Wang H, Sakai D, Leung VY. IVD progenitor cells: a new horizon for understanding disc homeostasis and repair. *Nat Rev Rheumatol* 2019; **15**: 102-112 [PMID: 30643232 DOI: 10.1038/s41584-018-0154-x]

11 **Risbud MV**, Guttapalli A, Tsai TT, Lee JY, Danielson KG, Vaccaro AR, Albert TJ, Gazit Z, Gazit D, Shapiro IM. Evidence for skeletal progenitor cells in the degenerate human intervertebral disc. *Spine (Phila Pa 1976)* 2007; **32**: 2537-2544 [PMID: 17978651 DOI: 10.1097/BRS.0b013e318158dea6]

12 **Liu Y**, Li Y, Huang ZN, Wang ZY, Nan LP, Wang F, Zhou SF, Wang JC, Feng XM, Zhang L. The effect of intervertebral disc degenerative change on biological characteristics of nucleus pulposus mesenchymal stem cell: an in vitro study in rats. *Connect Tissue Res* 2019; **60**: 376-388 [PMID: 31119993 DOI: 10.1080/03008207.2019.1570168]

13 **Wang F**, Nan LP, Zhou SF, Liu Y, Wang ZY, Wang JC, Feng XM, Zhang L. Injectable Hydrogel Combined with Nucleus Pulposus-Derived Mesenchymal Stem Cells for the Treatment of Degenerative Intervertebral Disc in Rats. *Stem Cells Int* 2019; **2019**: 8496025 [PMID: 31737077 DOI: 10.1155/2019/8496025]

14 **Wang JW**, Zhu L, Shi PZ, Wang PC, Dai Y, Wang YX, Lu XH, Cheng XF, Feng XM, Zhang L. 1,25(OH)(2)D(3) Mitigates Oxidative Stress-Induced Damage to Nucleus Pulposus-Derived Mesenchymal Stem Cells through PI3K/Akt Pathway. *Oxid Med Cell Longev* 2022; **2022**: 1427110 [PMID: 35340208 DOI: 10.1155/2022/1427110]

15 **Shi PZ**, Wang JW, Wang PC, Han B, Lu XH, Ren YX, Feng XM, Cheng XF, Zhang L. Urolithin a alleviates oxidative stress-induced senescence in nucleus pulposus-derived mesenchymal stem cells through SIRT1/PGC-1α pathway. *World J Stem Cells* 2021; **13**: 1928-1946 [PMID: 35069991 DOI: 10.4252/wjsc.v13.i12.1928]

16 **Wu H**, Shang Y, Yu J, Zeng X, Lin J, Tu M, Cheang LH, Zhang J. Regenerative potential of human nucleus pulposus resident stem/progenitor cells declines with ageing and intervertebral disc degeneration. *Int J Mol Med* 2018; **42**: 2193-2202 [PMID: 30015833 DOI: 10.3892/ijmm.2018.3766]

17 **Ma K**, Chen S, Li Z, Deng X, Huang D, Xiong L, Shao Z. Mechanisms of endogenous repair failure during intervertebral disc degeneration. *Osteoarthritis Cartilage* 2019; **27**: 41-48 [PMID: 30243946 DOI: 10.1016/j.joca.2018.08.021]

18 **de Oliveira MR**, Nabavi SM, Braidy N, Setzer WN, Ahmed T, Nabavi SF. Quercetin and the mitochondria: A mechanistic view. *Biotechnol Adv* 2016; **34**: 532-549 [PMID: 26740171 DOI: 10.1016/j.biotechadv.2015.12.014]

19 **Liao YR**, Lin JY. Quercetin intraperitoneal administration ameliorates lipopolysaccharide-induced systemic inflammation in mice. *Life Sci* 2015; **137**: 89-97 [PMID: 26209141 DOI: 10.1016/j.lfs.2015.07.015]

20 **Sun Y**, Coppé JP, Lam EW. Cellular Senescence: The Sought or the Unwanted? *Trends Mol Med* 2018; **24**: 871-885 [PMID: 30153969 DOI: 10.1016/j.molmed.2018.08.002]

21 **Zhu Y**, Tchkonia T, Pirtskhalava T, Gower AC, Ding H, Giorgadze N, Palmer AK, Ikeno Y, Hubbard GB, Lenburg M, O'Hara SP, LaRusso NF, Miller JD, Roos CM, Verzosa GC, LeBrasseur NK, Wren JD, Farr JN, Khosla S, Stout MB, McGowan SJ, Fuhrmann-Stroissnigg H,

Gurkar AU, Zhao J, Colangelo D, Dorronsoro A, Ling YY, Barghouthy AS, Navarro DC, Sano T, Robbins PD, Niedernhofer LJ, Kirkland JL. The Achilles' heel of senescent cells: from transcriptome to senolytic drugs. *Aging Cell* 2015; **14**: 644-658 [PMID: 25754370 DOI: 10.1111/acel.12344]

22 **Feng K**, Chen Z, Pengcheng L, Zhang S, Wang X. Quercetin attenuates oxidative stress-induced apoptosis *via* SIRT1/AMPK-mediated inhibition of ER stress in rat chondrocytes and prevents the progression of osteoarthritis in a rat model. *J Cell Physiol* 2019; **234**: 18192-18205 [PMID: 30854676 DOI: 10.1002/jcp.28452]

23 **Kim SR**, Jiang K, Ogrodnik M, Chen X, Zhu XY, Lohmeier H, Ahmed L, Tang H, Tchkonia T, Hickson LJ, Kirkland JL, Lerman LO. Increased renal cellular senescence in murine high-fat diet: effect of the senolytic drug quercetin. *Transl Res* 2019; **213**: 112-123 [PMID: 31356770 DOI: 10.1016/j.trsl.2019.07.005]

24 **Li Z**, Yu X, Shen J, Chan MT, Wu WK. MicroRNA in intervertebral disc degeneration. *Cell Prolif* 2015; **48**: 278-283 [PMID: 25736871 DOI: 10.1111/cpr.12180]

25 **Ohrt-Nissen S**, Døssing KB, Rossing M, Lajer C, Vikeså J, Nielsen FC, Friis-Hansen L, Dahl B. Characterization of miRNA expression in human degenerative lumbar disks. *Connect Tissue Res* 2013; **54**: 197-203 [PMID: 23586579 DOI: 10.3109/03008207.2013.781594]

26 **Sosnowska B**, Mazidi M, Penson P, Gluba-Brzózka A, Rysz J, Banach M. The sirtuin family members SIRT1, SIRT3 and SIRT6: Their role in vascular biology and atherogenesis. *Atherosclerosis* 2017; **265**: 275-282 [PMID: 28870631 DOI: 10.1016/j.atherosclerosis.2017.08.027]

27 **Mendelsohn AR**, Larrick JW. The NAD+/PARP1/SIRT1 Axis in Aging. *Rejuvenation Res* 2017; **20**: 244-247 [PMID: 28537485 DOI: 10.1089/rej.2017.1980]

28 **Maiese K**. Moving to the Rhythm with Clock (Circadian) Genes, Autophagy, mTOR, and SIRT1 in Degenerative Disease and Cancer. *Curr Neurovasc Res* 2017; **14**: 299-304 [PMID: 28721811 DOI: 10.2174/1567202614666170718092010]

29 **He J**, Zhang A, Song Z, Guo S, Chen Y, Liu Z, Zhang J, Xu X, Liu J, Chu L. The resistant effect of SIRT1 in oxidative stress-induced senescence of rat nucleus pulposus cell is regulated by Akt-FoxO1 pathway. *Biosci Rep* 2019; **39** [PMID: 30967498 DOI: 10.1042/BSR20190112]

30 **Ji ML**, Jiang H, Zhang XJ, Shi PL, Li C, Wu H, Wu XT, Wang YT, Wang C, Lu J. Preclinical development of a microRNA-based therapy for intervertebral disc degeneration. *Nat Commun* 2018; **9**: 5051 [PMID: 30487517 DOI: 10.1038/s41467-018-07360-1]

31 **Han B**, Zhu K, Li FC, Xiao YX, Feng J, Shi ZL, Lin M, Wang J, Chen QX. A simple disc degeneration model induced by percutaneous needle puncture in the rat tail. *Spine (Phila Pa 1976)* 2008; **33**: 1925-1934 [PMID: 18708924 DOI: 10.1097/BRS.0b013e31817c64a9]

32 **Mao HJ**, Chen QX, Han B, Li FC, Feng J, Shi ZL, Lin M, Wang J. The effect of injection volume on disc degeneration in a rat tail model. *Spine (Phila Pa 1976)* 2011; **36**: E1062-E1069 [PMID: 21358491 DOI: 10.1097/BRS.0b013e3182027d42]

33 **Cao G**, Yang S, Cao J, Tan Z, Wu L, Dong F, Ding W, Zhang F. The Role of Oxidative Stress in Intervertebral Disc Degeneration. *Oxid Med Cell Longev* 2022; **2022**: 2166817 [PMID: 35069969 DOI: 10.1155/2022/2166817]

34 **Chen JW**, Ni BB, Zheng XF, Li B, Jiang SD, Jiang LS. Hypoxia facilitates the survival of nucleus pulposus cells in serum deprivation by down-regulating excessive autophagy through restricting ROS generation. *Int J Biochem Cell Biol* 2015; **59**: 1-10 [PMID: 25456445 DOI: 10.1016/j.biocel.2014.11.009]

35 **Clouet J**, Fusellier M, Camus A, Le Visage C, Guicheux J. Intervertebral disc regeneration: From cell therapy to the development of novel bioinspired endogenous repair strategies. *Adv Drug Deliv Rev* 2019; **146**: 306-324 [PMID: 29705378 DOI: 10.1016/j.addr.2018.04.017]

36 **Vono R**, Jover Garcia E, Spinetti G, Madeddu P. Oxidative Stress in Mesenchymal Stem Cell Senescence: Regulation by Coding and Noncoding RNAs. *Antioxid Redox Signal* 2018; **29**: 864-879 [PMID: 28762752 DOI: 10.1089/ars.2017.7294]

37 **Chen Y**, Tang L. Stem Cell Senescence: the Obstacle of the Treatment of Degenerative Disk Disease. *Curr Stem Cell Res Ther* 2019; **14**: 654-668 [PMID: 31490764 DOI: 10.2174/1574888X14666190906163253]

38 **Wang F**, Shi R, Cai F, Wang YT, Wu XT. Stem Cell Approaches to Intervertebral Disc Regeneration: Obstacles from the Disc Microenvironment. *Stem Cells Dev* 2015; **24**: 2479-2495 [PMID: 26228642 DOI: 10.1089/scd.2015.0158]

39 **Xu D**, Hu MJ, Wang YQ, Cui YL. Antioxidant Activities of Quercetin and Its Complexes for Medicinal Application. *Molecules* 2019; **24** [PMID: 30901869 DOI: 10.3390/molecules24061123]

40 **Sarubbo F**, Ramis MR, Kienzer C, Aparicio S, Esteban S, Miralles A, Moranta D. Chronic Silymarin, Quercetin and Naringenin Treatments Increase Monoamines Synthesis and Hippocampal Sirt1 Levels Improving Cognition in Aged Rats. *J Neuroimmune Pharmacol* 2018; **13**: 24-38 [PMID: 28808887 DOI: 10.1007/s11481-017-9759-0]

41 **Peredo-Escárcega AE**, Guarner-Lans V, Pérez-Torres I, Ortega-Ocampo S, Carreón-Torres E, Castrejón-Tellez V, Díaz-Díaz E, Rubio-Ruiz ME. The Combination of Resveratrol and Quercetin Attenuates Metabolic Syndrome in Rats by Modifying the Serum Fatty Acid Composition and by Upregulating SIRT 1 and SIRT 2 Expression in White Adipose Tissue. *Evid Based Complement Alternat Med* 2015; **2015**: 474032 [PMID: 26609312 DOI: 10.1155/2015/474032]

42 **Iskender H**, Dokumacioglu E, Sen TM, Ince I, Kanbay Y, Saral S. The effect of hesperidin and quercetin on oxidative stress, NF-κB and SIRT1 levels in a STZ-induced experimental diabetes model. *Biomed Pharmacother* 2017; **90**: 500-508 [PMID: 28395272 DOI: 10.1016/j.biopha.2017.03.102]

43 **Lou G**, Liu Y, Wu S, Xue J, Yang F, Fu H, Zheng M, Chen Z. The p53/miR-34a/SIRT1 Positive Feedback Loop in Quercetin-Induced Apoptosis. *Cell Physiol Biochem* 2015; **35**: 2192-2202 [PMID: 25896587 DOI: 10.1159/000374024]

44 **Chen H**, Wang J, Hu B, Wu X, Chen Y, Li R, Yuan W. MiR-34a promotes Fas-mediated cartilage endplate chondrocyte apoptosis by targeting Bcl-2. *Mol Cell Biochem* 2015; **406**: 21-30 [PMID: 25910896 DOI: 10.1007/s11010-015-2420-4]

45 **Wang D**, Hu Z, Hao J, He B, Gan Q, Zhong X, Zhang X, Shen J, Fang J, Jiang W. SIRT1 inhibits apoptosis of degenerative human disc nucleus pulposus cells through activation of Akt pathway. *Age (Dordr)* 2013; **35**: 1741-1753 [PMID: 22990594 DOI: 10.1007/s11357-012-9474-y]

46 **Guo J**, Shao M, Lu F, Jiang J, Xia X. Role of Sirt1 Plays in Nucleus Pulposus Cells and Intervertebral Disc Degeneration. *Spine (Phila Pa 1976)* 2017; **42**: E757-E766 [PMID: 27792110 DOI: 10.1097/BRS.0000000000001954]

47 **Zhou N**, Lin X, Dong W, Huang W, Jiang W, Lin L, Qiu Q, Zhang X, Shen J, Song Z, Liang X, Hao J, Wang D, Hu Z. SIRT1 alleviates senescence of degenerative human intervertebral disc cartilage endo-plate cells *via* the p53/p21 pathway. *Sci Rep* 2016; **6**: 22628 [PMID: 26940203 DOI: 10.1038/srep22628]

48 **Zhang GZ**, Deng YJ, Xie QQ, Ren EH, Ma ZJ, He XG, Gao YC, Kang XW. Sirtuins and intervertebral disc degeneration: Roles in inflammation, oxidative stress, and mitochondrial function. *Clin Chim Acta* 2020; **508**: 33-42 [PMID: 32348785 DOI: 10.1016/j.cca.2020.04.016]

49 **Xia X**, Guo J, Lu F, Jiang J. SIRT1 Plays a Protective Role in Intervertebral Disc Degeneration in a Puncture-induced Rodent Model. *Spine*

(Phila Pa 1976) 2015; **40**: E515-E524 [PMID: 25646749 DOI: 10.1097/BRS.0000000000000817]

50 **Lu XL**, Zhao CH, Yao XL, Zhang H. Quercetin attenuates high fructose feeding-induced atherosclerosis by suppressing inflammation and apoptosis *via* ROS-regulated PI3K/AKT signaling pathway. *Biomed Pharmacother* 2017; **85**: 658-671 [PMID: 27919735 DOI: 10.1016/j.biopha.2016.11.077]

World Journal of Stem Cells

Submit a Manuscript: https://www.f6publishing.com

World J Stem Cells 2023 August 26; 15(8): 866-875

DOI: 10.4252/wjsc.v15.i8.866

ISSN 1948-0210 (online)

META-ANALYSIS

Up-to-date meta-analysis of long-term evaluations of mesenchymal stem cell therapy for complex perianal fistula

Fang Cheng, Huang Zhong, Zhong Huang, Zhi Li

Specialty type: Cell biology

Provenance and peer review: Unsolicited article; Externally peer reviewed.

Peer-review model: Single blind

Peer-review report's scientific quality classification

Grade A (Excellent): A
Grade B (Very good): 0
Grade C (Good): C, C
Grade D (Fair): 0
Grade E (Poor): 0

P-Reviewer: Salaga M, Poland; Trebol J, Spain; Li SC, United States

Received: May 7, 2023
Peer-review started: May 7, 2023
First decision: June 9, 2023
Revised: June 21, 2023
Accepted: July 19, 2023
Article in press: July 19, 2023
Published online: August 26, 2023

Fang Cheng, Division of Gastroenterology, Zigong First People's Hospital, Zigong 643000, Sichuan Province, China

Fang Cheng, Huang Zhong, Zhong Huang, Zhi Li, Department of Gastroenterology, Zigong First People's Hospital, Zigong 643000, Sichuan Province, China

Corresponding author: Fang Cheng, Doctor, Division of Gastroenterology, Zigong First People's Hospital, No. 42 Shangyihao Road, Zigong 643000, Sichuan Province, China. 1072893878@qq.com

Abstract

BACKGROUND

Local mesenchymal stem cell (MSC) therapy for complex perianal fistulas (PFs) has shown considerable promise. But, the long-term safety and efficacy of MSC therapy in complex PFs remain unknown.

AIM

To explore the long-term effectiveness and safety of local MSC therapy for complex PFs.

METHODS

Sources included the PubMed, EMBASE, and Cochrane Library databases. A standard meta-analysis was performed using RevMan 5.3.

RESULTS

After screening, 6 studies met the inclusion criteria. MSC therapy was associated with an improved long-term healing rate (HR) compared with the control condition [odds ratio (OR) = 2.13; 95% confidence interval (95%CI): 1.34 to 3.38; P = 0.001]. Compared with fibrin glue (FG) therapy alone, MSC plus FG therapy was associated with an improved long-term HR (OR = 2.30; 95%CI: 1.21 to 4.36; P = 0.01). When magnetic resonance imaging was used to evaluate fistula healing, MSC therapy was found to achieve a higher long-term HR than the control treatment (OR = 2.79; 95%CI: 1.37 to 5.67; P = 0.005). There were no significant differences in long-term safety (OR = 0.77; 95%CI: 0.27 to 2.24; P = 0.64).

CONCLUSION

Our study indicated that local MSC therapy promotes long-term and sustained healing of complex PFs and that this method is safe.

Key Words: Complex perianal fistula; Mesenchymal stem cells; Long-term evaluation; Meta-analysis

©The Author(s) 2023. Published by Baishideng Publishing Group Inc. All rights reserved.

Core Tip: The long-term safety and efficacy of mesenchymal stem cell (MSC) therapy for complex perianal fistulas (PFs) remain unknown. So, we explored the long-term effectiveness and safety of local MSC therapy for complex PFs. We found that MSC treatment is a safe and effective method that can significantly improve the long-term healing of complex PFs, and this method confers no risk of MSC-related adverse events.

Citation: Cheng F, Zhong H, Huang Z, Li Z. Up-to-date meta-analysis of long-term evaluations of mesenchymal stem cell therapy for complex perianal fistula. *World J Stem Cells* 2023; 15(8): 866-875
URL: https://www.wjgnet.com/1948-0210/full/v15/i8/866.htm
DOI: https://dx.doi.org/10.4252/wjsc.v15.i8.866

INTRODUCTION

A perianal fistula (PF) is an epithelialized tract that connects the luminal surface of the anal canal or rectum with the perianal or perineal skin. It affects approximately 2 in 10000 people and represents a difficult therapeutic challenge and a source of physical and psychological morbidity with a long-term risk of proctectomy[1]. The most severe form is complex PF, which is difficult to manage, as it has a high rate of recurrence and may cause sphincter damage and fecal incontinence. Complex PF is defined as cases with more muscle involvement or anterior fistulas in female patients, as well as recurrent fistulas, suprasphincteric fistulas, extrasphincteric fistulas, horseshoe fistulas, fistulas associated with irritable bowel disease, transsphincteric fistulas that involve greater than 30% of the external sphincter and fistulas associated with preexisting fecal incontinence, inflammatory bowel disease, radiation, malignancy, or chronic diarrhea. PFs are also a probable consequence of Crohn's disease (CD) since as many as 26% of CD patients eventually develop a PF within 20 years after diagnosis[2,3]. Complex PFs in patients with CD have a high recurrence rate and cause a vast range of complications that significantly reduce quality of life (QoL)[4]. In addition, there is a risk of developing a neoplasm in the PF area related to the complexity and perianal disease duration[5]. The results of one study showed that complex PFs may lead to anal cancer in approximately 28% of patients within 20 years after diagnosis[6]. Complex PF is a chronic, recurrent immune-mediated disease with a variety of treatment options. Its exact pathogenesis is unknown. The key long-term therapeutic goals for the treatment of complex PF are to: (1) Resolve fistula discharge; (2) achieve fistula healing; (3) prevent fistula recurrence; (4) maintain fecal continence; (5) avoid long-term diversion (protectomy with stoma), and hence; and (6) improve and maintain QoL for patients. Although current treatments for PFs include a range of medical and surgical options, managing this condition is difficult. Patients with complex PFs tend to have poor treatment outcomes or experience frequent relapses, and most interventions are ineffective in providing long-term healing[7-10]. Immunomodulators can have serious side effects. Additionally, there is a risk of opportunistic infection associated with the use of biological treatments. In more severe cases of complex PF, fecal incontinence can occur, furthering morbidity. Complex PF is often not permanently cured by surgery, leading to multiple procedures and complications such as fecal incontinence. Therefore, there is a need for an effective therapy that provides long-term healing of complex PFs without the risk of fecal incontinence.

In recent years, local injection of mesenchymal stem cells (MSCs) has shown notable promising results in the treatment of PFs[11]. MSCs are a heterogeneous subset of stromal stem cells. They can be isolated from a wide variety of tissues and expanded *in vitro* to obtain large quantities. MSCs are characterized by multilineage differentiation and powerful immunomodulatory effects and are able to mitigate inflammatory states. Complex PF is thought to arise from an epithelial defect, which may be caused by ongoing inflammation. Current treatments cannot maintain long-term healing of the disease. Possible alternative treatments include cell therapy, especially MSC therapy. Local administration is the most performed approach to deliver MSCs. After being delivered directly to fistula tracts, MSCs induce peripheral tolerance and migrate to injured tissues, where they can inhibit the release of proinflammatory cytokines and promote the survival of damaged cells. Consequently, MSCs are capable of repairing damaged tissues and promoting tissue healing, which can lead to long-term fistula healing, significantly improving patients' quality of life. An increasing number of studies have indicated that local MSC therapy is safe and efficacious for complex PFs. In 2020, to evaluate whether local MSC therapy for complex PFs is effective and safe, we conducted a meta-analysis. That study, with a follow-up of 8 wk to 2 years, showed that local MSC therapy for complex PFs was safe and feasible. However, the efficacy and safety evaluation period of the study was short and middle term[12]. Therefore, the long-term efficacy of MSC therapy is unclear. To date, an increasing number of studies have aimed to perform long-term evaluations of MSC therapy for PFs. Thus, based on a previous study[12], this study aimed to explore the long-term effectiveness and safety of MSC therapy for complex PFs (48 wk to 4 years of follow-up after MSC therapy).

MATERIALS AND METHODS

Data source and search strategies

This meta-analysis followed the Preferred Reporting Items for Systematic Reviews and Meta-Analyses (PRISMA) guidelines[13]. In August 2022, a search was performed in the PubMed, EMBASE and Cochrane Library databases for clinical studies written in English regarding local MSC treatment in patients with complex PFs. The following search terms were used: "Mesenchymal stem cell'', "mesenchymal stromal cell", "complex perianal fistula", "perianal fistula", "complex perianal Crohn's disease", "Crohn's perianal fistula", "perianal Crohn's disease", "Crohn's disease", "perianal fistulizing Crohn's disease", "cryptoglandular perianal fistula", and "long-term". We also checked the reference lists of the screened full-text studies to identify other potentially eligible trials.

Study selection

Two authors independently assessed studies for inclusion by screening titles and abstracts. The inclusion criteria were: (1) Studies of human subjects; (2) randomized clinical trials (RCTs) and retrospective studies or cohort studies of patients with complex PFs treated with local injection(s) of autologous or allogeneic MSCs from any source; (3) local injection of MSCs or MSCs combined with fibrin glue (FG) for complex PFs; and (4) assessment of the efficacy and/or safety of MSC therapy at least 48 wk after treatment.

Data extraction and quality assessment

A customized data extraction form was used by two authors to extract data. These authors extracted study data features including: (1) Study characteristics (first author, publication year); (2) MSC origin; (3) definition of fistula healing [clinical and/or magnetic resonance imaging (MRI)]; (4) study outcomes; (5) dosage and modalities of intervention administration; (6) adverse events (AEs); and (7) concomitant treatment (anti-TNF). Table 1 lists the basic characteristics of the 6 identified studies. Quality assessment was performed using Review Manager (version 5.3) according to the recommendations from the Cochrane Collaboration. The bias risk assessment tool recommended by Cochrane was used to assess the quality of all enrolled studies. Each item of studies was judged as having a high, low or unclear risk of bias.

Statistical analysis

Based on the included studies, odds ratios (ORs) and corresponding 95% confidence intervals (95%CIs) were calculated to compare the MSC groups and control groups. Heterogeneity was quantified using the I^2 statistic. If the I^2 value was ≤ 50%, heterogeneity was considered low, and we employed a fixed-effect model. If the I^2 value was > 50%, heterogeneity was considered high, and we employed a random-effect model. All statistical analyses were performed using Review Manager (version 5.3). A value of $P < 0.05$ was considered statistically significant.

RESULTS

Literature search and quality assessment

The literature search process is illustrated in Figure 1. Using this search strategy, we identified 462 references related to local MSC treatment for complex PF, of which 358 duplicate articles were removed. After reading the titles and abstracts, we identified 20 articles for full-text review. Ultimately, after all criteria were applied, 6 articles were included in the meta-analysis[14-19]. A summary of the risk of bias in the included articles is presented in Figure 2.

Long-term efficacy of MSCs in complex PF (48 wk to 4 years of follow-up after MSC therapy)

Our meta-analysis included 6 studies that assessed the long-term efficacy of post-MSC treatment. The pooled analysis showed that MSC therapy was associated with an improved long-term healing rate (HR) compared with the control condition (OR = 2.13; 95%CI: 1.34 to 3.38; $P = 0.001$) (Figure 3). The benefit was sustained for at least 48 wk of follow-up after MSC therapy.

Long-term efficacy of MSCs for complex PF (MSCs + FG vs FG alone)

Cell therapy strategies using MSCs carried in FG have shown promising results in regenerative medicine. FG is a natural polymer involved in the coagulation process. In regenerative medicine, FG can be used as a delivery system for drugs, biomolecules, growth factors and cells. FG also provides a temporary structure that favors angiogenesis, extracellular matrix deposition and cell-matrix interactions and it also FG maintains the local and paracrine functions of MSCs, providing tissue regeneration through less invasive clinical procedures. The biological properties of FG as a growth environment for MSCs have been reported in several studies[20]. Now, local FG combined with MSCs therapy is still a relatively new treatment and has not yet gained popularity. So, the need for the local FG combined with MSCs therapy remains unknown. In our meta-analysis, three studies were included that reported local FG combined with MSCs therapy for PF[14,15,17], with low heterogeneity between the studies ($I^2 = 0\%$). In a fixed-effects model, MSCs plus FG had more long-term efficacy for fistula healing than FG alone (OR = 2.30; 95%CI: 1.21 to 4.36; $P = 0.01$) (Figure 4). So, we think local FG combined with MSCs therapy have synergistic effect on PF.

Table 1 Studies of local mesenchymal stem cells in complex perianal fistulas

Ref.	Cell type and source	Outcome assessment	Study outcomes	Intervention (mean)	AEs	Concurrent use of anti-TNF
Guadalajara *et al* [14], 2012	Autologous, ASCs	Re-epithelialization + MRI	10/18 for MSCs + FG; 3/12 for FG at 1 yr	First: 2 × 10^7 MSCs; second: 4 × 10^7 MSCs	/	Yes
Herreros *et al* [15], 2012	Autologous, ASCs	Re-epithelialization +MRI	24/42 for MSCs; 22/42 for MSCs + FG; 19/51 for FG at 48 wk	First: 2 × 10^7 MSCs; second: 4 × 10^7 MSCs	/	Yes
Garcia-Arranz *et al*[16], 2020	Autologous, ASCs	Re-epithelialization	10/20 for MSCs + FG; 5/19 for FG at 2 yr	First: 10 × 10^7 MSCs; second: 10 × 10^7 MSCs	7/23 for MSCs + FG *vs* 9/21 for FG	Yes
Barnhoorn *et al* [17], 2020	Allogeneic, BMSCs	MRI	8/13 for MSCs; 0/3 for placebo group at 4 yr	A: 1 × 10^7 MSCs; B: 3 × 10^7 MSCs; C: 9 × 10^7 MSCs	/	/
Panés *et al*[18], 2022	Allogeneic, ASCs	Re-epithelialization	23/43 for MSC; 21/46 for saline solution at 156 wk	12 × 10^7 MSCs	/	Yes
Garcia-Olmo *et al* [19], 2022	Allogeneic, ASCs	Re-epithelialization	14/25 for MSCs; 6/15 for saline solution at 104 wk	12 × 10^7 MSCs	3/25 for MSCs *vs* 1/15 for placebo	Yes

AEs: Adverse events; MSCs: Mesenchymal stem cells; ASCs: Adipose-derived mesenchymal stromal cells; BMSCs: Bone marrow-derived mesenchymal stromal cells; FG: Fibrin glue; MRI: Magnetic resonance imaging.

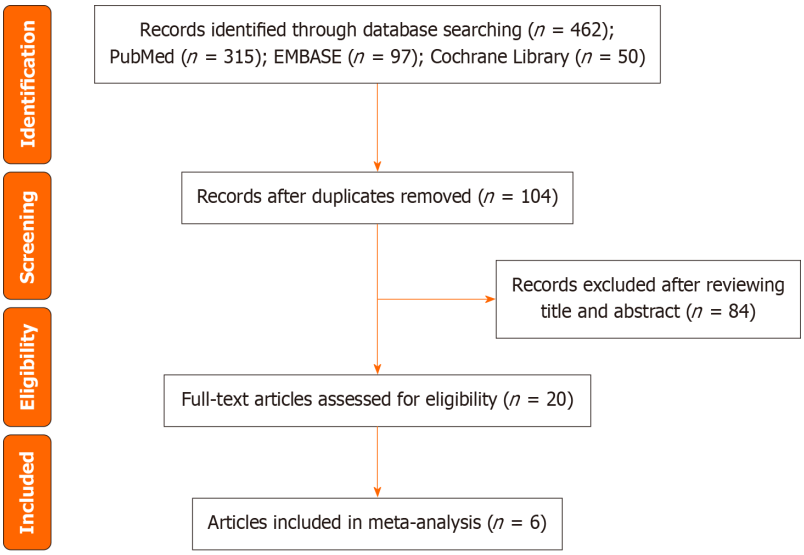

DOI: 10.4252/wjsc.v15.i8.866 **Copyright** ©The Author(s) 2023.

Figure 1 Study selection process.

MRI as the standard for evaluating fistula healing

In our meta-analysis, MRI was used to evaluate fistula healing in 3 studies. The pooled analysis showed that MSC therapy was associated with improved long-term HR (OR = 2.79; 95%CI: 1.37 to 5.67; P = 0.005) (Figure 5).

Long-term safety

Only two studies[16,19] in this review assessed the long-term safety of MSC treatment for complex PF. The pooled results demonstrated that MSC treatment did not increase the risk of any long-term adverse or serious AEs (OR = 0.77; 95%CI: 0.27 to 2.24; P = 0.64) (Figure 6). No serious AEs related to MSC therapy were found.

DISCUSSION

During the past decade, cell therapy-based treatments have been developed to manage several digestive tract diseases, including PF[21,22]. Previous research has shown that MSCs have a variety of mechanisms that promote wound healing. These cells also lack substantial immunogenicity and are thus suitable for use across human leukocyte antigen (HLA)

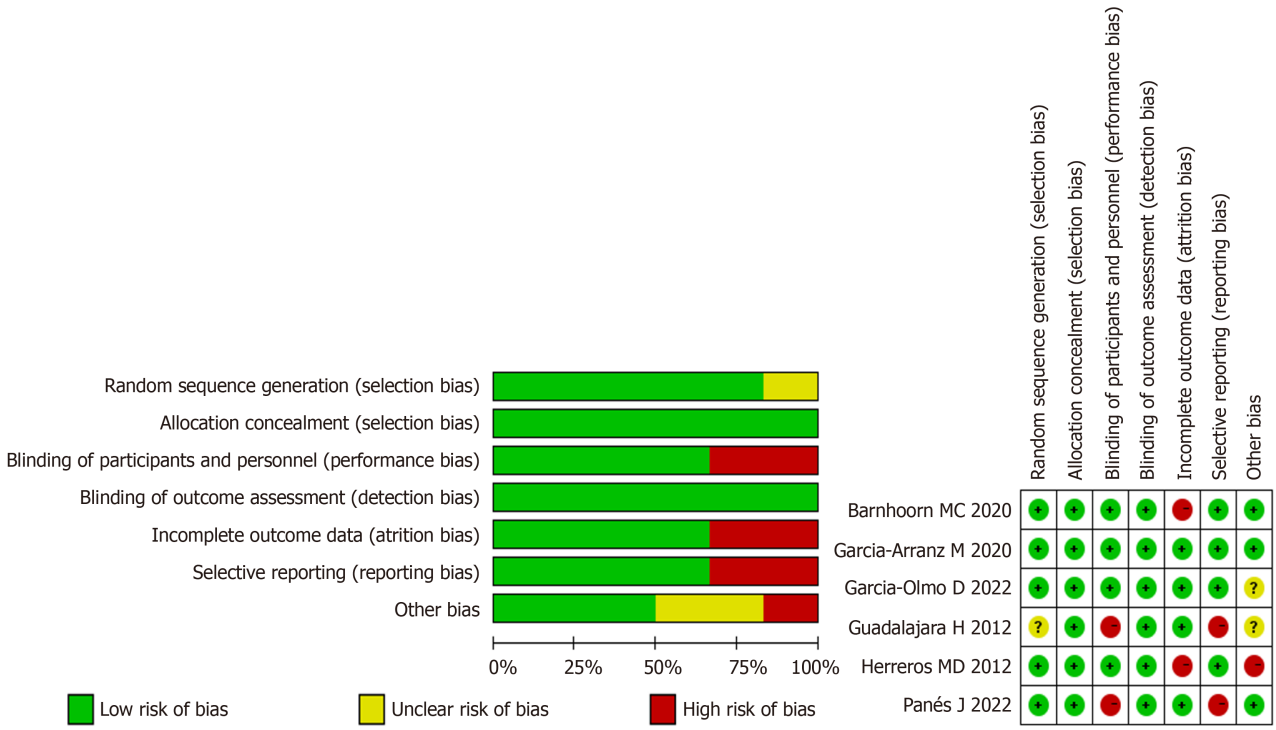

DOI: 10.4252/wjsc.v15.i8.866 **Copyright** ©The Author(s) 2023.

Figure 2 Risk of bias of the articles included in the meta-analysis.

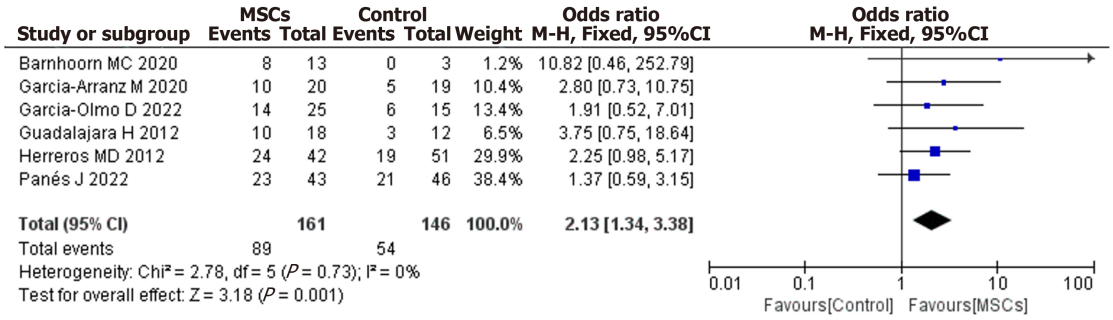

DOI: 10.4252/wjsc.v15.i8.866 **Copyright** ©The Author(s) 2023.

Figure 3 Forest plot showing the long-term effectiveness of mesenchymal stem cells for treating complex perianal fistula. MSCs: Mesenchymal stem cells; CI: Confidence interval.

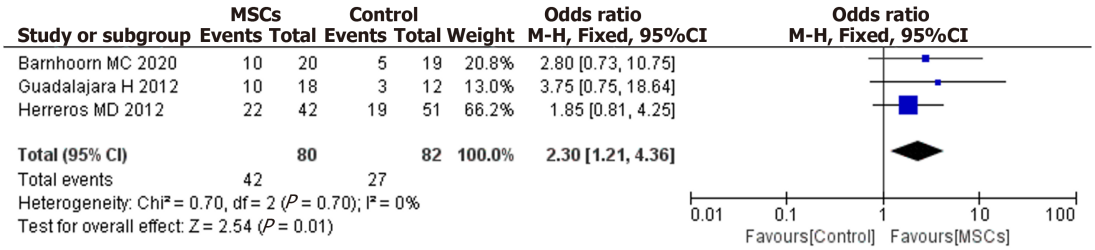

DOI: 10.4252/wjsc.v15.i8.866 **Copyright** ©The Author(s) 2023.

Figure 4 Differences in long-term effectiveness between mesenchymal stem cells plus fibrin glue and fibrin glue groups from meta-analysis. MSCs: Mesenchymal stem cells; CI: Confidence interval.

barriers[23,24]. An increasing number of studies have shown that MSC therapy is a safe and efficacious option for the short-term closure of PFs. However, maintaining continuous long-term fistula closure is also very important. A recurrent fistula is considered more difficult to treat surgically than the original fistula. Recently, an increasing number of studies have aimed to perform long-term follow-up of patients undergoing MSC administration to treat complex PFs. However,

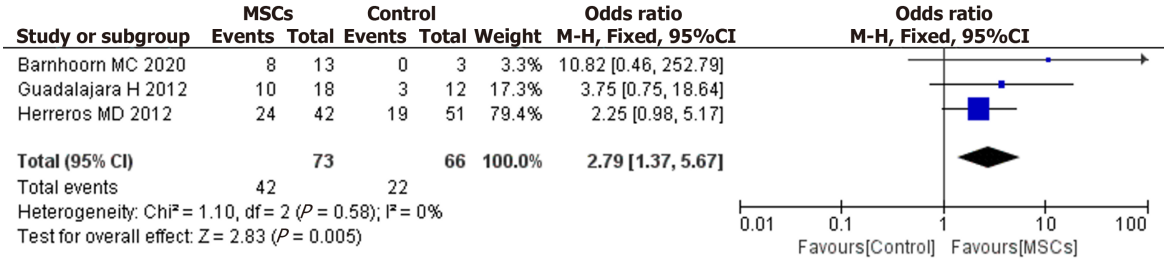

DOI: 10.4252/wjsc.v15.i8.866 **Copyright** ©The Author(s) 2023.

Figure 5 Forest plot showing the long-term effectiveness of mesenchymal stem cells for treating complex perianal fistula when magnetic resonance imaging is considered the standard for evaluating fistula healing. MSCs: Mesenchymal stem cells; CI: Confidence interval.

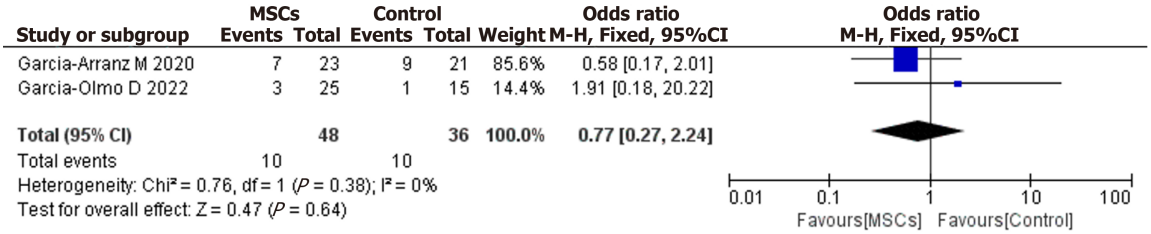

DOI: 10.4252/wjsc.v15.i8.866 **Copyright** ©The Author(s) 2023.

Figure 6 Pooled odds ratio of long-term safety. MSCs: Mesenchymal stem cells; CI: Confidence interval.

there has been no meta-analysis to comprehensively evaluate the long-term effectiveness and safety of MSC treatment. Therefore, this study aimed to find a treatment to maintain long-term PF healing and to provide a basis for clinical application.

To our knowledge, this is the first meta-analysis to evaluate the long-term safety and efficacy of local MSC therapy for complex PFs. Findings from our study show that MSC therapy promotes sustained healing of complex PFs and that this therapy alone or combined with FG treatment can promote the long-term healing of complex PFs (OR = 2.13; 95%CI: 1.34 to 3.38; P = 0.001). The benefit over the control was sustained for at least 48 wk after local injection of MSCs. In our study, the timepoint for the assessment of fistula healing fluctuated greatly (48 wk-4 years), and all included studies showed good long-term healing of fistulas post-MSC treatment. Therefore, we believe that fistula healing persisted after MSC treatment. Barnhoorn *et al*[17] also reported that in addition to high fistula closure rates, MSC-treated patients had a higher QoL after therapy than at baseline. Some studies have also shown that in patients receiving MSC transplantation, the PF closure rate is significantly higher and the time to closure significantly shorter than that with anti-TNF drugs and fistulotomy, and MSC transplantation yields a decreased frequency of recurrence of the disease[25-27]. Therefore, these data confirm that MSC therapy promotes the long-term healing of complex PFs and significantly improves the QoL of patients. In the future, in evaluating MSC therapy for PF, it might be useful to consider work productivity and lifestyle restrictions.

Cell therapy strategies using MSCs carried in FG have shown promising results in regenerative medicine. MSCs have angiogenic, anti-apoptotic and immunomodulatory properties. FG provides a temporary structure that favors angiogenesis, extracellular matrix deposition and cell-matrix interactions. Additionally, FG maintains the local and paracrine functions of MSCs, providing tissue regeneration through less invasive clinical procedures[28]. The use of FG has been found to be uniformly safe, with minimal adverse effects, an early return to normal activity, and no negative impact on continence. One study showed that FG had a short-term effectiveness in the treatment of PF. At week 8 of the study, more than one-third of patients had healed fistulas, and half showed clinical improvement. Most of the patients in clinical remission at week 8 maintained clinical remission at week 16[29]. There was also a study indicating that FG was effective over the long term for the treatment of PF, and nearly 2 years after the use of FG to treat PF, over half of the patients showed clinical signs of remission[30]. Therefore, in association with MSCs, the use of FG has shown promising results in the field of regenerative medicine[31]. However, there is a lack of long-term success data on the combination of FG and other treatments for complex PF. In our study, MSCs plus FG had more long-term efficacy for fistula healing than FG alone (OR = 2.30; 95%CI: 1.21 to 4.36; P = 0.01). Therefore, we believe that the stimulation of the cellular adhesion and growth action of FG and the differentiation ability of MSCs may have a synergistic effect on the healing of fistulas. In our study, all patients received cleaning surgery before MSC treatment. Deep curettage had a positive effect on fistula closure in both groups (MSC recipients and controls). However, Garcia-Arranz *et al*[16] observed an increased number of long-term recurrences among control participants. Therefore, we speculate that the inflammatory focus persists, explaining why "deep curettage" may not provide a lasting resolution. In this scenario, MSCs and their anti-inflammatory and immunomodulatory effects can promote long-term healing.

Questions persist regarding the safety of MSC treatment for PF. Although MSC therapy has not raised any major safety concerns thus far in clinical trials, it is important to evaluate the safety of cell therapy in the long term. Our study

provides evidence that MSC therapy has a good long-term safety profile as a treatment for complex PF (OR = 0.77; 95%CI: 0.27 to 2.24; P = 0.64). In our study, the surgical management was fistula tract curettage and internal opening closure before MSC therapy. Notably, this is a minimally invasive surgery (involving perioperative antibiotic use, anesthesia, antisepsis, internal fistula orifice location, de-epithelization of the fistula tract, cleaning of the cavities and fistula tracts, closure of the internal opening, stem cell handling and resuspension, and cell injection) and does not produce fecal incontinence[32]. In contrast, anti-TNF therapies used for the treatment of PFs are associated with an increased risk of opportunistic infections, and surgical procedures often result in fecal incontinence. Tumorigenicity and ectopic tissue formation are the main concerns with the use of MSCs, and the risk of these SAEs is especially high during long-term MSC treatment. To date, MSCs have not been reported to cause tumors. Nevertheless, neoplasm development may become apparent only after longer follow-up periods. In another study conducted by our group, no neoplasm development was reported over the longest follow-up period of approximately 4 years[17]. To further confirm that neoplasms are not a concern with MSC treatment, biopsies taken from the fistula region were examined in that study. However, publication of these results is still pending, and we can continue the follow-up. While MSCs have not been shown to cause tumors in existing studies, long-term follow-up should be carried out to investigate the risk of cancer development. In the future, more long-term safety data are needed to fully assess the safety aspects of local MSC treatment.

Studies included in our meta-analysis used variable definitions of fistula healing. We believe that defining a healed fistula as complete re-epithelialization of external openings is not objective or accurate, as it does not account for the inside of the entire fistula. To evaluate the efficacy of MSC treatment, we should use more accurate methods for evaluating the inside of the entire fistula. MRI is the reference standard and cornerstone of fistula imaging. It demonstrates high sensitivity and specificity for the number and location of fistula tracts, detecting complexities frequently missed on clinical examination alone[33]. Therefore, MRI plays a crucial role in the evaluation, detection and follow-up of complex PFs[34]. In our meta-analysis, 3 RCTs based fistula healing on a combination of clinical examination and MRI imaging. The results showed that the MSC group had a higher HR than the control group (OR = 2.79; 95%CI: 1.37 to 5.67; P = 0.005). The absence of MRI examinations in some of the included studies at the end of the long-term follow-up is a limitation of this meta-analysis. In the future, if possible, blood should be drawn for standard measurements, and serum should be used to comprehensively evaluate the long-term healing of MSC therapy.

In this study, we aimed to evaluate the long-term efficacy and safety of MSC therapy through a meta-analysis. However, there are some unresolved questions. In the current clinical research, there are two ways to inject stem cells: (1) Systemic (mainly intravenous) injection; and (2) local injection. In our study, all patients received local MSC treatment. We speculate that for localized digestive tract diseases, local application and delivery seems more logical because side effects can be minimized and the cells are kept in direct contact with the at-risk tissue. Therefore, local MSC therapy seems to be a more promising treatment approach for further research. In our study, all eligible patients received a fixed dose of MSCs (one-time local injection or a second dose). Unfortunately, not all of the studies have compared various doses of MSCs or the benefit of repeat injections after the initial treatment. Most patients in our study received two doses of MSCs. Some studies have indicated a relationship between cell dose—or even the number of doses and efficacy[35,36]. In addition, all eligible patients with complex PFs may have branches with multiple tracks involving an extensive area that cannot always be adequately treated with a fixed dose of cells. Perhaps the cell dosage is related to the length of the fistula tracts and cavities. Due to the limitations of studies, it is difficult to provide recommendations on the optimal dose. In future research, we should pay attention to these unresolved questions (such as MSC origin, dosage and modality of intervention) to ensure that PF patients receive optimal treatment.

Our meta-analysis is the first to evaluate the long-term efficacy and safety of MSCs for PF treatment. Inevitably, this article has some limitations: (1) The studies used MSCs of different origins (adipose tissue and bone marrow from autologous as well as allogeneic sources); (2) some included studies defined the healed fistula as re-epithelialization of the external opening of the fistula. This may cause our results to be overestimated; (3) all patients underwent surgical procedures such as deep curettage. This may be beneficial to the short-term clinical remission of the fistulas. However, whether deep curettage will benefit long-term healing remains uncertain; (4) the follow-up period of the included studies varied significantly. Indeed, some of the studies lacked long-term follow-up data. In the future, we need more patients to enter the extended follow-up period so that the long-term safety and efficacy of MSCs can be assessed; and (5) the number of included studies and the sample size were limited, and extrapolation of the meta-analysis results was limited to some extent. So, our study was limited by its multiple centers and heterogeneity in the study inclusion criteria, mesenchymal stem cell origin, dose and frequency of delivery, and definition and time point of fistula healing. In the future, more patients must be evaluated in long-term follow-ups to optimize the efficacy and safety of MSCs for PF treatment.

CONCLUSION

In summary, MSC treatment is a safe and effective method that can significantly improve the long-term healing of complex PFs, and this method confers no risk of MSC-related AEs.

ARTICLE HIGHLIGHTS

Research background

An increasing number of studies have indicated that local mesenchymal stem cell (MSC) therapy is safe and efficacious for complex perianal fistulas (PFs). But, the long-term efficacy of MSC therapy is unclear. To date, an increasing number of studies have aimed to perform long-term evaluations of MSC therapy for PFs.

Research motivation

Local MSC therapy for PFs has shown considerable promise. But, the long-term safety and efficacy of MSC therapy in complex PFs is unknown.

Research objectives

To explore the long-term effectiveness and safety of MSC therapy for complex PFs.

Research methods

PubMed, EMBASE and Cochrane Library databases were searched that reported the long-term evaluation of local MSC therapy for complex PFs. The effectiveness and safety data analysis were conducted using RevMan5.3.

Research results

After screening, 6 studies met the inclusion criteria. MSC therapy was associated with an improved long-term healing rate (HR) compared with the control condition [odds ratio (OR) = 2.13; 95% confidence interval (95%CI): 1.34 to 3.38; P = 0.001]. Compared with fibrin glue (FG) therapy alone, MSC plus FG therapy was associated with an improved long-term HR (OR = 2.30; 95%CI: 1.21 to 4.36; P = 0.01). When magnetic resonance imaging was used to evaluate fistula healing, MSC therapy was found to achieve a higher long-term HR than the control treatment (OR = 2.79; 95%CI: 1.37 to 5.67; P = 0.005). There were no significant differences in long-term safety (OR = 0.77; 95%CI: 0.27 to 2.24; P = 0.64).

Research conclusions

Our study indicated that local MSC therapy promotes long-term and sustained healing of complex PFs and that this method is safe.

Research perspectives

In complex PFs treatment, local MSC therapy should be paid more attention to. Considering that this small number may not be enough to represent the whole complex PFs population, In the future, to improve on the quality of research, future studies should be carefully designed and reported.

ACKNOWLEDGEMENTS

We appreciate the contributions of all the doctors, coworkers, and friends involved in this study and thank the editors and reviewers for their help with this manuscript.

FOOTNOTES

Author contributions: Cheng F and Zhong H developed a search strategy for each database and collected the citations; Hong Z and Li Z performed the assessment of study quality and risk of bias, the data extraction and statistical analysis; Cheng F was major contributors in writing the manuscript; and all authors read and approved the final manuscript.

Conflict-of-interest statement: All the authors report no relevant conflicts of interest for this article.

PRISMA 2009 Checklist statement: The authors have read the PRISMA 2009 Checklist, and the manuscript was prepared and revised according to the PRISMA 2009 Checklist.

Open-Access: This article is an open-access article that was selected by an in-house editor and fully peer-reviewed by external reviewers. It is distributed in accordance with the Creative Commons Attribution NonCommercial (CC BY-NC 4.0) license, which permits others to distribute, remix, adapt, build upon this work non-commercially, and license their derivative works on different terms, provided the original work is properly cited and the use is non-commercial. See: https://creativecommons.org/Licenses/by-nc/4.0/

Country/Territory of origin: China

ORCID number: Fang Cheng 0000-0003-2121-2013; Huang Zhong 0009-0003-2921-6024; Zhong Huang 0000-0002-6580-3870; Zhi Li 0000-0003-1933-0176.

S-Editor: Chen YL

L-Editor: A
P-Editor: Xu ZH

REFERENCES

1 **Zanotti C**, Martinez-Puente C, Pascual I, Pascual M, Herreros D, García-Olmo D. An assessment of the incidence of fistula-in-ano in four countries of the European Union. *Int J Colorectal Dis* 2007; **22**: 1459-1462 [PMID: 17554546 DOI: 10.1007/s00384-007-0334-7]
2 **Bubbers EJ**, Cologne KG. Management of Complex Anal Fistulas. *Clin Colon Rectal Surg* 2016; **29**: 43-49 [PMID: 26929751 DOI: 10.1055/s-0035-1570392]
3 **Park SH**, Aniwan S, Scott Harmsen W, Tremaine WJ, Lightner AL, Faubion WA, Loftus EV. Update on the Natural Course of Fistulizing Perianal Crohn's Disease in a Population-Based Cohort. *Inflamm Bowel Dis* 2019; **25**: 1054-1060 [PMID: 30346531 DOI: 10.1093/ibd/izy329]
4 **Mahadev S**, Young JM, Selby W, Solomon MJ. Quality of life in perianal Crohn's disease: what do patients consider important? *Dis Colon Rectum* 2011; **54**: 579-585 [PMID: 21471759 DOI: 10.1007/DCR.0b013e3182099d9e]
5 **Panés J**, Rimola J. Perianal fistulizing Crohn's disease: pathogenesis, diagnosis and therapy. *Nat Rev Gastroenterol Hepatol* 2017; **14**: 652-664 [PMID: 28790453 DOI: 10.1038/nrgastro.2017.104]
6 **Eglinton TW**, Barclay ML, Gearry RB, Frizelle FA. The spectrum of perianal Crohn's disease in a population-based cohort. *Dis Colon Rectum* 2012; **55**: 773-777 [PMID: 22706129 DOI: 10.1097/DCR.0b013e31825228b0]
7 **Kotze PG**, Shen B, Lightner A, Yamamoto T, Spinelli A, Ghosh S, Panaccione R. Modern management of perianal fistulas in Crohn's disease: future directions. *Gut* 2018; **67**: 1181-1194 [PMID: 29331943 DOI: 10.1136/gutjnl-2017-314918]
8 **Aguilera-Castro L**, Ferre-Aracil C, Garcia-Garcia-de-Paredes A, Rodriguez-de-Santiago E, Lopez-Sanroman A. Management of complex perianal Crohn's disease. *Ann Gastroenterol* 2017; **30**: 33-44 [PMID: 28042236 DOI: 10.20524/aog.2016.0099]
9 **Panes J**, Reinisch W, Rupniewska E, Khan S, Forns J, Khalid JM, Bojic D, Patel H. Burden and outcomes for complex perianal fistulas in Crohn's disease: Systematic review. *World J Gastroenterol* 2018; **24**: 4821-4834 [PMID: 30479468 DOI: 10.3748/wjg.v24.i42.4821]
10 **Pedersen KE**, Lightner AL. Managing Complex Perianal Fistulizing Disease. *J Laparoendosc Adv Surg Tech A* 2021; **31**: 890-897 [PMID: 34314631 DOI: 10.1089/lap.2021.0285]
11 **Sheikholeslami A**, Fazaeli H, Kalhor N, Khoshandam M, Eshagh Hoseini SJ, Sheykhhasan M. Use of Mesenchymal Stem Cells in Crohn's Disease and Perianal Fistulas: A Narrative Review. *Curr Stem Cell Res Ther* 2023; **18**: 76-92 [PMID: 34530720 DOI: 10.2174/1574888X16666210916145717]
12 **Cheng F**, Huang Z, Li Z. Efficacy and Safety of Mesenchymal Stem Cells in Treatment of Complex Perianal Fistulas: A Meta-Analysis. *Stem Cells Int* 2020; **2020**: 8816737 [PMID: 33299423 DOI: 10.1155/2020/8816737]
13 **Moher D**, Liberati A, Tetzlaff J, Altman DG; PRISMA Group. Preferred reporting items for systematic reviews and meta-analyses: the PRISMA statement. *PLoS Med* 2009; **6**: e1000097 [PMID: 19621072 DOI: 10.1371/journal.pmed.1000097]
14 **Guadalajara H**, Herreros D, De-La-Quintana P, Trebol J, Garcia-Arranz M, Garcia-Olmo D. Long-term follow-up of patients undergoing adipose-derived adult stem cell administration to treat complex perianal fistulas. *Int J Colorectal Dis* 2012; **27**: 595-600 [PMID: 22065114 DOI: 10.1007/s00384-011-1350-1]
15 **Herreros MD**, Garcia-Arranz M, Guadalajara H, De-La-Quintana P, Garcia-Olmo D; FATT Collaborative Group. Autologous expanded adipose-derived stem cells for the treatment of complex cryptoglandular perianal fistulas: a phase III randomized clinical trial (FATT 1: fistula Advanced Therapy Trial 1) and long-term evaluation. *Dis Colon Rectum* 2012; **55**: 762-772 [PMID: 22706128 DOI: 10.1097/DCR.0b013e318255364a]
16 **Garcia-Arranz M**, Garcia-Olmo D, Herreros MD, Gracia-Solana J, Guadalajara H, de la Portilla F, Baixauli J, Garcia-Garcia J, Ramirez JM, Sanchez-Guijo F, Prosper F; FISPAC Collaborative Group. Autologous adipose-derived stem cells for the treatment of complex cryptoglandular perianal fistula: A randomized clinical trial with long-term follow-up. *Stem Cells Transl Med* 2020; **9**: 295-301 [PMID: 31886629 DOI: 10.1002/sctm.19-0271]
17 **Barnhoorn MC**, Wasser MNJM, Roelofs H, Maljaars PWJ, Molendijk I, Bonsing BA, Oosten LEM, Dijkstra G, van der Woude CJ, Roelen DL, Zwaginga JJ, Verspaget HW, Fibbe WE, Hommes DW, Peeters KCMJ, van der Meulen-de Jong AE. Long-term Evaluation of Allogeneic Bone Marrow-derived Mesenchymal Stromal Cell Therapy for Crohn's Disease Perianal Fistulas. *J Crohns Colitis* 2020; **14**: 64-70 [PMID: 31197361 DOI: 10.1093/ecco-jcc/jjz116]
18 **Panés J**, Bouma G, Ferrante M, Kucharzik T, Nachury M, de la Portilla de Juan F, Reinisch W, Selvaggi F, Tschmelitsch J, Brett NR, Ladouceur M, Binek M, Hantsbarger G, Campbell-Hill S, Karki C, Buskens C. INSPECT: A Retrospective Study to Evaluate Long-term Effectiveness and Safety of Darvadstrocel in Patients With Perianal Fistulizing Crohn's Disease Treated in the ADMIRE-CD Trial. *Inflamm Bowel Dis* 2022; **28**: 1737-1745 [PMID: 35099555 DOI: 10.1093/ibd/izab361]
19 **Garcia-Olmo D**, Gilaberte I, Binek M, D Hoore AJL, Lindner D, Selvaggi F, Spinelli A, Panés J. Follow-up Study to Evaluate the Long-term Safety and Efficacy of Darvadstrocel (Mesenchymal Stem Cell Treatment) in Patients With Perianal Fistulizing Crohn's Disease: ADMIRE-CD Phase 3 Randomized Controlled Trial. *Dis Colon Rectum* 2022; **65**: 713-720 [PMID: 34890373 DOI: 10.1097/DCR.0000000000002325]
20 **Süloğlu AK**, Karacaoğlu E, Bilgic HA, Selmanoğlu G, Koçkaya EA, Karaaslan C. Osteogenic differentiation of adipose tissue-derived mesenchymal stem cells on fibrin glue- or fibronectin-coated Ceraform®. *J Biomater Appl* 2019; **34**: 375-385 [PMID: 31165664 DOI: 10.1177/0885328219853421]
21 **Trebol Lopez J**, Georgiev Hristov T, García-Arranz M, García-Olmo D. Stem cell therapy for digestive tract diseases: current state and future perspectives. *Stem Cells Dev* 2011; **20**: 1113-1129 [PMID: 21187000 DOI: 10.1089/scd.2010.0277]
22 **García-Olmo D**, García-Arranz M, García LG, Cuellar ES, Blanco IF, Prianes LA, Montes JA, Pinto FL, Marcos DH, García-Sancho L. Autologous stem cell transplantation for treatment of rectovaginal fistula in perianal Crohn's disease: a new cell-based therapy. *Int J Colorectal Dis* 2003; **18**: 451-454 [PMID: 12756590 DOI: 10.1007/s00384-003-0490-3]
23 **Spaggiari GM**, Abdelrazik H, Becchetti F, Moretta L. MSCs inhibit monocyte-derived DC maturation and function by selectively interfering with the generation of immature DCs: central role of MSC-derived prostaglandin E2. *Blood* 2009; **113**: 6576-6583 [PMID: 19398717 DOI: 10.1182/blood-2009-02-203943]
24 **Melief SM**, Schrama E, Brugman MH, Tiemessen MM, Hoogduijn MJ, Fibbe WE, Roelofs H. Multipotent stromal cells induce human

regulatory T cells through a novel pathway involving skewing of monocytes toward anti-inflammatory macrophages. *Stem Cells* 2013; **31**: 1980-1991 [PMID: 23712682 DOI: 10.1002/stem.1432]

25 **Park MY**, Yoon YS, Lee JL, Park SH, Ye BD, Yang SK, Yu CS. Comparative perianal fistula closure rates following autologous adipose tissue-derived stem cell transplantation or treatment with anti-tumor necrosis factor agents after seton placement in patients with Crohn's disease: a retrospective observational study. *Stem Cell Res Ther* 2021; **12**: 401 [PMID: 34256838 DOI: 10.1186/s13287-021-02484-6]

26 **Knyazev OV**, Fadeeva NA, Kagramanova AV, Belyakov NI, Orlova NV, Lishchinskaya AA, Konoplyannikov AG, Parfenov AI. Stem Cell Therapy for Perianal Crohn's Disease. *Ter Arkh* 2018; **90**: 60-66 [PMID: 30701858 DOI: 10.26442/terarkh201890360-66]

27 **Park MY**, Yoon YS, Kim HE, Lee JL, Park IJ, Lim SB, Yu CS, Kim JC. Surgical options for perianal fistula in patients with Crohn's disease: A comparison of seton placement, fistulotomy, and stem cell therapy. *Asian J Surg* 2021; **44**: 1383-1388 [PMID: 33966965 DOI: 10.1016/j.asjsur.2021.03.013]

28 **Ortiz AC**, Fideles SOM, Pomini KT, Reis CHB, Bueno CRS, Pereira ESBM, Rossi JO, Novais PC, Pilon JPG, Rosa Junior GM, Buchaim DV, Buchaim RL. Effects of Therapy with Fibrin Glue combined with Mesenchymal Stem Cells (MSCs) on Bone Regeneration: A Systematic Review. *Cells* 2021; **10** [PMID: 34571972 DOI: 10.3390/cells10092323]

29 **Grimaud JC**, Munoz-Bongrand N, Siproudhis L, Abramowitz L, Sénéjoux A, Vitton V, Gambiez L, Flourié B, Hébuterne X, Louis E, Coffin B, De Parades V, Savoye G, Soulé JC, Bouhnik Y, Colombel JF, Contou JF, François Y, Mary JY, Lémann M; Groupe d'Etude Thérapeutique des Affections Inflammatoires du Tube Digestif. Fibrin glue is effective healing perianal fistulas in patients with Crohn's disease. *Gastroenterology* 2010; **138**: 2275-2281, 2281.e1 [PMID: 20178792 DOI: 10.1053/j.gastro.2010.02.013]

30 **Vitton V**, Gasmi M, Barthet M, Desjeux A, Orsoni P, Grimaud JC. Long-term healing of Crohn's anal fistulas with fibrin glue injection. *Aliment Pharmacol Ther* 2005; **21**: 1453-1457 [PMID: 15948812 DOI: 10.1111/j.1365-2036.2005.02456.x]

31 **Ravari H**, Hamidi-Almadari D, Salimifar M, Bonakdaran S, Parizadeh MR, Koliakos G. Treatment of non-healing wounds with autologous bone marrow cells, platelets, fibrin glue and collagen matrix. *Cytotherapy* 2011; **13**: 705-711 [PMID: 21284564 DOI: 10.3109/14653249.2011.553594]

32 **Georgiev-Hristov T**, Guadalajara H, Herreros MD, Lightner AL, Dozois EJ, García-Arranz M, García-Olmo D. A Step-By-Step Surgical Protocol for the Treatment of Perianal Fistula with Adipose-Derived Mesenchymal Stem Cells. *J Gastrointest Surg* 2018; **22**: 2003-2012 [PMID: 30066070 DOI: 10.1007/s11605-018-3895-6]

33 **Williams G**, Williams A, Tozer P, Phillips R, Ahmad A, Jayne D, Maxwell-Armstrong C. The treatment of anal fistula: second ACPGBI Position Statement - 2018. *Colorectal Dis* 2018; **20** Suppl 3: 5-31 [PMID: 30178915 DOI: 10.1111/codi.14054]

34 **Thipphavong S**, Costa AF, Ali HA, Wang DC, Brar MS, Jhaveri KS. Structured reporting of MRI for perianal fistula. *Abdom Radiol (NY)* 2019; **44**: 1295-1305 [PMID: 30474723 DOI: 10.1007/s00261-018-1839-y]

35 **Skific M**, Golemovic M, Crkvenac-Gornik K, Vrhovac R, Golubic Cepulic B. Comparative Analysis of Biological and Functional Properties of Bone Marrow Mesenchymal Stromal Cells Expanded in Media with Different Platelet Lysate Content. *Cells Tissues Organs* 2018; **205**: 226-239 [PMID: 30223277 DOI: 10.1159/000492581]

36 **Lightner AL**, Wang Z, Zubair AC, Dozois EJ. A Systematic Review and Meta-analysis of Mesenchymal Stem Cell Injections for the Treatment of Perianal Crohn's Disease: Progress Made and Future Directions. *Dis Colon Rectum* 2018; **61**: 629-640 [PMID: 29578916 DOI: 10.1097/DCR.0000000000001093]

Published by **Baishideng Publishing Group Inc**
7041 Koll Center Parkway, Suite 160, Pleasanton, CA 94566, USA
Telephone: +1-925-3991568
E-mail: bpgoffice@wjgnet.com
Help Desk: https://www.f6publishing.com/helpdesk
https://www.wjgnet.com

© 2023 Baishideng Publishing Group Inc. All rights reserved.